Multifunctional Composites for Aerospace Applications

Matthew Collinson

A thesis submitted in partial fulfilment of the requirements for the degree of Doctor of Philosophy

The University of Sheffield
Faculty of Engineering
Department of Materials Science and Engineering

Submission Date: 1st February 2024

Abstract

This thesis investigates the development of novel multifunctional composites which primarily take advantage of the electrical conductivity of carbon fibres in high performance composites. The multifunctionalities are targeted towards use in the aerospace industry, covering manufacturing, and in-service, such as damage detection and de-icing. This work aims to increase the matureness of these and related technologies, allowing the concepts to be built on more easily, and reduce the barrier to industrial implementation.

The functionalities are Joule heating for direct electric cure (DEC), de-icing and heated tooling, and electrical self-sensing for damage detection. These utilise the electrically conductive nature of the carbon fibres in composites used in aerospace structural components. This means that little modification to the materials and structure is required, crucial for aerospace qualification and ease of use.

The low conductivity of composite matrices was identified as an initial problem to the scale up and industrialisation of multifunctional composites. Carbon Nanotubes (CNTS) resin composites were manufactured using 3 dispersion methods and tested for conductivity and piezoresistivity. Despite showing these desired properties, quick agglomeration of the particles and difficulty of manufacturing fibre reinforced composites meant that their use cases were limited to the fibre-electrode interfaces of the multifunctional demonstrators.

DEC is developed as an alternative sustainable curing method, requiring 99% less input energy when curing industrial scale components (2000 x 700 mm), using both pre-preg and vacuum assisted resin transfer moulding (VARTM). The degree of cure for VARTM was only 0.82 % lower than oven cured samples, however it was significantly lower in pre-preg samples. The main challenge was to ensure even heating over the component, which was due to the plain weave fibres used in these experiments. When the same heating technology was applied to unidirectional (UD) fibres within a representative leading-edge section of a wing, the heating performance for de-icing was more even, despite having power headroom issues due to embedded CNTs causing localised overheating.

Evidence of even heating performance of UD led it to being embedded into composite tooling, to enable the manufacture of low-cost heated tooling. The DEC style electrodes only had to be applied to the composite tooling once, rather than every part manufactured, meaning that the benefits of DEC can be achieved with an easier barrier to entry.

To further increase the benefits of these heating technologies, a cure kinetic and thermal model was assessed to reduce the energy and length of cure cycles. It predicted the exothermic energy output of composites during curing, and the heat dissipation to the environment, to be able to run close to the exothermic limits of the cure system. It accurately predicted the exothermic reaction of a commercial pre-preg system using open loop control,

leading to a degree of cure 0.14 % lower than a post cured sample, whilst saving an estimated 95 % of input energy.

A novel damage detection for composites was developed, with the aim to enable and automate damage detection without the requirement of external inspection equipment. The system monitored electrical conductivity of fibres using embedded flexible printed circuit boards (PCB) to enable implementation into a manufacturing process. Electrical self-sensing hardware and software was developed, which were tested on 360 x 360 mm components, with the aim to detect barely visible impact damage (BVID). These were then scaled up to a modular system, which monitored a 560 x 400 mm section of a leading edge. The sensing system was able to detect BVID damage in some configurations and higher impact energies in most samples.

Novelty is in both the developments to increase the scale and robustness of the components through improvements in manufacturing and testing such as with DEC and Self-sensing, but as well as identifying opportunities of applications, such as with Joule heated tooling and applied cure modelling.

The increase in maturity of these technologies has ensured that development has continued in this area. Joule heated tooling continues to be developed through funding grants with industrial partners such as Pentaxia, whereas self-sensing and Joule heating of components has attracted private funding from Tier 2 aerospace suppliers.

Declaration

I, the author, declare that this Thesis is my own work. I am aware of the University's guidance on the Use of Unfair Means (www.sheffield.ac.uk/ssid/unfair-means). This work has not been previously presented for an award at this, or any other, university. This thesis consists of the following published papers:

Published: Collinson M, Bower M, Swait TJ, Atkins C, Hayes S, Nuhiji B. *Novel composite curing methods for sustainable manufacture: A review.* Composites Part C: Open Access 2022;9:100293. https://doi.org/10.1016/j.jcomc.2022.100293.

Primarily authored and edited by Matthew Collinson, with contributions to the microwave section from Matthew Bower & Betime Nuhiji, induction section by Craig Atkins. Supervised and edited by Tim Swait, Simon Hayes and Betime Nuhiji.

Published: Collinson MG, Swait TJ, Bower MP, Nuhiji B, Hayes SA. *Development and implementation of direct electric cure of plain weave CFRP composites for aerospace.* Compos Part A Appl Sci Manuf 2023;172:107615. https://doi.org/10.1016/j.compositesa.2023.107615.

Experimental work, authorship and editing by Matthew Collinson. Experimental work was assisted by Matthew Bower, Tim Swait and Simon Hayes. Supervised and edited by Tim Swait, Simon Hayes and Betime Nuhiji.

Published: Collinson M, Hayes S, Petropoulos S. *The effect of type of mechanical processing on electrical conductivity and piezoresistive response of CNT and graphite composites.* Procedia CIRP 2019;85:314–20. https://doi.org/10.1016/J.PROCIR.2019.10.001.

Experimental work, authorship and editing by Matthew Collinson. Experimental work was assisted by Stefanos Petropoulos. Editing and supervision was by Simon Hayes.

Acknowledgements

I would like to express my deepest thanks to my supervisor Simon Hayes, who has supported me throughout my 6 years of PhD and during the MASTRO project. Your passion and expertise for all things aerospace and composites has been great to learn from over the years and will miss working with you. I am also grateful to Tim Swait who has been super helpful in bouncing ideas off and has always been happy to advise me throughout. I am indebted to Betime Nuhiji for her help throughout, particularly later with her meticulous proof reading, which improved my writing (de-yorkshirefying it) and giving valuable advice on how to get it over the line.

Many thanks to my colleagues at the AMRC, Richard Scaife and Clara Frias who allowed me to do this during my time at the composite centre in the first place, and to Matt Bower and Stefanos Petropoulos who helped me with experimentation and coordination of activities.

I'd like to also thank the partner companies in the MASTRO project such as Ricardo Reis from Embraer, and Stu Morris from Pentaxia, for their guidance and support through the projects with them. Thanks also to the funding bodies who funded the projects, including the European Commission, AMRC Board Partners and NATEP.

Thank you to my parents who have helped me through university, to get to the point where I was even ready to take this on and providing life experience and support throughout.

I'm extremely grateful to my partner Fatma, who has kept me going no end, despite the difficulties I have had on the way, and given me countless great advice on managing and finishing a PhD. No thanks to our cat Luna though, walking over my desk is no way to get a thesis written.

Table of Contents

List of Figures

List of Tables

Nomenclature

2PZ	2 Point Zone (A self-sensing technique)
4PZ	4 Point Zone (A self-sensing technique)
AE	Acoustic Emission
AFP	Automated Fibre Placement
AM	Additive Manufacturing
AMRC	Advanced Manufacturing Research Centre
ASTM	American Society for Testing Materials
BVID	Barely Visible Impact Damage
CF	Carbon Fibre
CFRP	Carbon Fibre Reinforced Plastic
CIRP	College International pour la Recherche en Productique
CNT	Carbon Nanotube
CSV	Comma Separated Values (file format)
CTE	Coefficient of Thermal Expansion
DAQ	Data Acquisition
DC	Direct Current
DEC	Direct Electric Cure
DGEBA	Bisphenol A diglycidyl ether
DMM	Digital Multimeter
DOC	Degree Of Cure
DSC	Differential Scanning Calorimetry
EIT	Electrical Impedance Tomography
EMI	Electromagnetic Interference
EV	Electric Vehicle
FE	Finite Element
FVF	Fibre Volume Fraction
FW	Filament Winding
GFRP	Glass Fibre Reinforced Plastic
GSM	Grams per Square Meter
GUI	Graphical User Interface
I2C	Inter-integrated Circuit (communications bus)
IDE	Integrated Drive Electronics (connection interface)
IO	Input Output
IR	Infrared
LAN	Local Area Network
LE	Leading Edge
LSP	Lightning Strike Protection
LVV	Lab for Verification and Validation
MASTRO	Intelligent bulk MAterials for Smart TRanspOrt industries
MFC	Macrofibre composite
MFS	Multifunctional Structure
MJ	Mega Joule
MOSFET	Metal Oxide Semiconductor Field Effect Transistor

MWCNT	Multiwall Carbon Nanotube
NACA	National Advisory Committee for Aeronautics (predates modern NASA)
NaN	Not A Number
NATEP	National Aerospace Technology Exploitation Programme
NCF	Non Crimp Fabric
NDT	Non-Destructive Testing
NI	National Instruments
OoA	Out of Autoclave
PCI	Peripheral Component Interconnect
PEI	Polyethyleneimine
PID	Proportional Integral Derivative
PS	Polystyrene
PSU	Power Supply Unit
PTFE	Polytetrafluoroethylene
PVC	Polyvinyl chloride
PVDF	polyvinylidene fluoride
PW	Plain Weave
PWM	Pulse Width Modulation
PXI	PCI eXtensions for Instrumentation
QI	Quasi Isotropic
RF	Radio Frequency
RTM	Resin Transfer Moulding
SAF	Sustainable Aviation Fuel
SCPI	Standard Commands for Programmable Instruments
SD	Standard Deviation
SHM	Structural Health Monitoring
SMA	Shape Memory Alloy
SMP	Shape Memory Polymer
SWCNT	Single Walled Carbon Nanotube
TC	Thermocouple
TFP	Tailored Fibre Placement
TRL	Technology Readiness Level
UD	Unidirectional
USB	Universal Serial Bus
VARTM	Vacuum Assisted Resin Transfer Moulding
VVF	Void Volume Fraction
XY	A self-sensing technique

1. Introduction

This work investigates the exploitation of the electrical conductivity of carbon polymer composites to enable the multifunctionalities of self-curing and self-sensing. It covers the background of these technologies, the potential benefits they could bring, including ones soon to be exploited, and investigates the development of these technologies on a larger component. Carbon fibres are an impressive material due to their extremely high tensile strength [1] and have good electrical conductivity [2]. When formed into the structures dictated by composite manufacturing processes, this also creates unique electrical networks and allows for devices to be created and these properties to be exploited [3].

1.1. Carbon Fibre Reinforced Plastic (CFRP) in Aerospace

One of the most interesting and impactful use cases for composites is in aerospace, where some of the largest benefits can come through fuel savings, leading to a reduced environmental impact of flight. Due to the size, scale and quality requirements of aerospace projects, it is where a significant investment in innovation occurs. Through this, the subsequent processes and methods are driven by, or come from, this sector.

Carbon fibres were first produced in the mid-1950s on a laboratory scale, however it wasn't until the early 1960s that the precursors of PAN (polyacrylonitrile) and Rayon enabled commercial production [4]. Its use with an epoxy matrix enabled its use as a lightweight, high strength and stiffness structural material [5]. It is commonly associated with, and was originally limited to, high performance and value applications such as sports equipment and military and commercial aircraft. This was due to its relative high cost and the expertise and equipment required to manufacture it.

The aerospace industry has historically used autoclaves and pre-preg to manufacture high quality components, that have high fibre volume fraction (FVF) and low void volume fraction (VVF). High FVF results in improved flexural properties [6], and low VVF increases fatigue resistance [7]. Producing composites this way delivers the required quality and consistency, but it is costly and time consuming. Cure cycles of these flight certified resins are long, some taking 10-12 hours, some requiring temperatures up to 180°C and pressures of 5 bar or more [8]. As resin systems and manufacturing methods have improved, there has been a desire to move away from autoclaves and these long cure cycles; to improve component throughput and deliver energy savings [9]. This is particularly important as the requirement for aircraft manufacturing rate continues to increase, as does the composite weight percentage of aircraft continues to increase.

CFRP has become standard in military aviation and motorsport applications, and in the last 20-30 years it has been used more frequently, seeing widespread use in commercial aviation. The primary driver for CFRP use in aerospace is the ability to manufacture lightweight structures with excellent fatigue life. This increase in use was also a response to saving fuel costs during the fuel crisis in the 1970's. More recently it has been driven by environmental legislation requiring reduced emissions which has led to a 24 % average reduction in fuel burn per passenger from 2005 to 2017 [10].

1.2. CFRP and Sustainability

This decrease in emissions per passenger is significant, however emissions continue to rise, as within the same period (2005-2017) passenger numbers increased by 60 %, leading to aviation accounting for 3.8 % of total global CO_2 emissions [10]. The majority of future estimated savings are through the

use of sustainable aviation fuel (SAF). However this cannot be fully relied on yet: production levels are too low, prices are higher and emissions when burnt are the same as existing fuels. Increasing efficiency and lightweighting is still a vital part of decarbonising aviation. An example of the weight and subsequent fuel savings is a vertical stabiliser on an Airbus A310, on which CFRP replaced aluminium, delivering a 400 kg reduction [5], which could result in thousands of tonnes of CO_2 savings over the aircraft's life cycle [11].

One issue when discussing the sustainability of CFRP, is that it has a large manufacturing carbon footprint given it is commonly oil derived [12,13], and the energy input for manufacture is significant, compared to other lightweight engineering materials. However given the complexity, and variability between manufacturers of the constituent materials, comparisons can be difficult. One source suggests 183-286 MJ/kg for carbon fibres, and 76-80 MJ/kg for epoxies [14], however these values should not be used in lifecycle analysis, as the underlying assumptions are likely to be different to materials used in this study. For example, there are some exceptions such as bio-based epoxies that have more sustainable material sources [15], or carbon fibres manufactured with lignin plant-based precursors [16], which would reduce these energy impact values. Aluminium is reported as 196-257 MJ/kg, which suggests on paper is worse. However these figures don't consider later manufacturing steps, or its recyclability, which is currently a significant issue with most aerospace composites. Despite this, over the lifespan of a widebody aircraft, the savings over other materials are significant, necessitating their use to achieve environmental targets [11]. Increasing the efficiency of these manufacturing methods will only make the final use cases more sustainable, which is an important target to aim for.

1.3. Direct Electric Cure

Curing of composites is an energy intensive process [17], where components and tooling are heated up to 200°C for up to 24 hours in the case of some tooling pre-pregs or thicker laminates. This has traditionally been completed in an autoclave to apply pressure and help consolidate the composite. However, as materials have developed and improved, out of autoclave (OoA) materials that can be cured in ovens have become more commonly available [9]. This still requires high capital investment, results in high energy consumption during cures. The aerospace industry is cautious about moving away or making significant changes to these manufacturing methods. Because existing methods already produce high-quality components with repeatable quality, the cost also to requalify a new process or material is difficult to justify. This high barrier to entry for new products and methods can restrict innovation in this area [18].

Direct electric cure (DEC) is a novel curing method that generates its curing heat from Joule heating of the conductive fibres, to achieve the resin's cure temperature. This direct method of heating increases the thermal efficiency of the process, only heating the component and thus reducing energy consumption by up to 99 % compared to oven cures [19,20].

DEC also provides other benefits. Given the heating is generated in the composite itself, there is evidence that it better enables voids to exit the resin than outside-in heating methods, reducing void content overall [21]. Further, the process also has a lower thermal mass, which enables higher heating rates, and enables improved response to, and control of, any exothermic reactions that may occur. The initial capital expenditure for equipment is significantly lower than that of an autoclave or oven,

only requiring a power supply and temperature data acquisition and control equipment. Another large factor is that it doesn't require a heating chamber the size of the component being cured.

1.4. Self-De-Icing and Heated tooling

DEC concentrates on the bulk heating of composites to ensure that the composite component has an isotropic degree of cure. The same heating methodologies can be repurposed for other heating requirements of composite manufacturing or final components. Joule heating can be applied to electrically insulated plies to enable heating in specific zones of a composite component [22]. This can be used for surface heating which can be used in different engineering applications, such as de-icing of aerospace 'in service' components [23] or heated tooling for composite curing [24].

Icing of aircrafts' aerodynamic surfaces is an issue primarily during take-off and landing [25]. It can cause catastrophic results if not addressed. With more aerospace components being manufactured using CFRP, there is a valuable opportunity to use Joule heating of built in carbon to heat the surface, reducing the requirement for ice removal ancillary systems. These range from inflatable boots [26], weeping wings [27], and hot bleed air systems [28,29]. These have been used successfully, however all have their drawbacks, such as system complexity, weight, or reduced efficiency. The most efficient way, theoretically, would be using the carbon fibres within the composite to heat the surface, without any extra plies or separate heating elements [30]. This would reduce the complexity of the aircraft systems and simplify both the layup sequence and subsequent manufacture. A study was completed to understand the feasibility of this system to work within a leading-edge component, and was tested in a representative icing environment.

Another area where surface heating is applicable is in heated tooling for composite manufacturing [31]. Tooling for composite manufacturing can be metallic, usually an Invar alloy, or composite, to ensure there is a low coefficient of thermal expansion (CTE) [32]. These can be used in an oven or autoclave to reduce the energy consumption of the process, whilst still obtaining the benefits of pressure, in the case of the autoclave.

Particularly in aerospace, where qualification of material processes requires extensive testing [33], it is difficult to replace these heating methods with more efficient or novel ones like self-curing. Heating the tooling directly is a way around these requirements, as the material isn't changed, and the heating methods are very similar. Existing methods use heater cartridges, heater mats [34] or heating fluid [31] to heat tools, however applying these solutions to tools can be complex or expensive. Applying direct electric cure to the composite tools themselves is a way to introduce an efficient heating method to a tooling solution with little extra expense or proprietary technology required [24,35]. The heating plies can be integrated into the layup using the same knowledge and skills, with only electrodes and insulating plies required as extra materials. The power and control system knowledge are already well established and can be applied to the tools in the same way as the self-curing.

1.5. Self-Sensing Composites

Composite materials are used in aerospace because of their high specific strength; however, they have some properties that aren't as desirable which can cause issues in service. One of these is the brittle nature of epoxy resins [36], which can lead to issues such as low impact resistance in composites [37]. Ply by ply composite structures do not absorb impact energy well, which can lead to a range of failure modes, such as microcracking, delamination of plies or fibre breakage. A specific type of impact

damage has been defined, called “Barely Visible Impact Damage”, which is named because of the undetectable visual nature of low energy impacts on the surface of composites, despite having sustained subsurface damage [38,39]. Initially these impacts may not be immediately safety critical to the structure, as they can occur in common situations, such as stones impacting during take-off and landing. However with continuous fatigue loading, they can increase in size and severity [40].

It is for this reason that a damage detection method that doesn’t rely on existing inspection techniques has been developed, titled self-sensing. By monitoring the electrical conductivity of the carbon fibre, to monitor impact induced effects such as piezoresistance and fibre breakage. To build up a dataset of the resistance changes over a surface of a laminate, resistance has to be monitored in many positions. This can be completed through the integration of flexible PCBs in the laminate which allow an array of electrodes to be integrated, whilst having minimal impact on the composite itself. This is then linked to a data acquisition system that can monitor resistance changes all over the part, then use the data to generate information on the location and severity of the damage. This method has been demonstrated multiple times on smaller scale [41,42], but this study is the first to expand the scale and consider the impact on the manufacturing of the composite.

1.6. Conductive matrixes

As these multifunctionalities increase in capability and technology readiness level, it is worth looking at the composite material as a whole. The carbon fibres themselves are very conductive [43], however the matrix, typically epoxy resin is very electrically insulative [44]. This is a prohibitive and problematic feature when trying to use CFRP as an electrical device. A solution to this could be to increase the conductivity of the matrix, by the addition of conductive nanoparticles [45,46]. This is in itself a whole area of research, as there are variations in the particle type, including carbon nanotubes (CNTs) [47,48], graphene [49,50], carbon black [46] or graphite [51]. There are also different mixing and dispersion methods [52], techniques to infuse them effectively into a composite to obtain the benefits of the novel nano materials.

An initial key part of this thesis was to understand these processes, in particular how to use a premixed CNT epoxy masterbatch to enhance the performance of the already established multifunctionalities. After the initial study on mixing and distribution of the particles, it was realised that this topic was too expansive to add to the multifunctionalities being studied. There is a short chapter, discussing where CNTs were introduced into these multifunctionalities, how they affected the processes and the resulting performance. Ultimately, they were unsuccessful in improving performance, and proved very energy intensive for the resulting savings that may have been produced from the multifunctionalities. High energy intensity isn’t a property of all conductive nanoparticles; however this study suggests areas where significant improvements are needed to consider their inclusion.

1.7. Multifunctional Composites

Incremental gains have been made that both increase the performance of composites and increase the speed and efficiency of composite manufacturing. Examples include the introduction of extreme high modulus fibres to increase laminate strength [53], or the use of novel composite layups to improve fracture toughness [54]. More recently, larger step changes have been made on fibre architecture of composites to place the fibre where is required along stress lines, through the use of tow steering of AFP [55] or tailored fibre placement (TFP) preforms [56]. All these methods are

generating significant research interest because of their substantial gains over unidirectional (UD) quasi-isotropic (QI) composite laminates. Another important opportunity is multifunctional composites that conductive carbon fibre composites enable.

Multifunctionality in composites is the ability to add additional capabilities on top of the primary functionality of composites, which would have been previously seen as mutually exclusive [57]. Because a composite is a combination of materials, it is well suited for further investigation of modifying these materials to gain additional functionality. A simple example of this could be applying metallic electromagnetic interference (EMI) shielding to an existing structure, which could be replaced by using conductive matrices within a composite structure [58]. Given the importance of light-weighting, investigations into multifunctional composites have increased significantly [59]. Other issues have increased the interest in the multifunctionalities covered here. The increasing use of CFRP for lightweighting comes with the issue on how to detect and repair impact damage of these structures, not needed in the same way before for aluminium components [39].

Increases in the number of aircraft using CFRP means that novel manufacturing methods, that improve throughput whilst reducing input energy, bring more significant benefits. Also increasing the efficiency of jet turbine engines has led to electrification of systems, meaning that systems for anti-icing such as hot air bleed are no longer viable [60].

One significant opportunity with composites is the electrically conductive nature of carbon fibres [3]. The structure of carbon fibre, comprised of graphitic planes with van der Waals bonding [61], ensures that a conductive path can occur, resulting in a conductivity of up to 10^6 S/m along the fibre. In practice, when integrated in a composite structure, this is significantly lower, around 5.88×10^4 S/m, but this is conductive enough to use as an electrical device [62]. This has enabled many multifunctionalities, such as EMI shielding [63,64], data transfer [65], lightning strike protection (LSP) [66], as well as the ones covered in this thesis, Joule heating [19,20] and structural health monitoring of impact damage.

1.8. Aims of thesis

This thesis aims to provide context on the issues of existing curing and manufacturing methods, as well as impact damage in aerospace composites. The multifunctional solutions are explained in depth in their respective papers and chapters, including the background theory, practical implementation and results compared to existing and previously trailed methods. One of the primary aims of this work is to ensure that the developments had opportunity for practical implementation and therefore were industrially relevant. This was achieved by:

- researching issues that were faced during previous implementation of these technologies,
- undertaking laboratory tests of each of the functionalities to further understand of both the opportunities these novel technologies offer and the challenges faced as they are adopted,
- incremental developing and understanding and fixing of issues that occurred, and
- discussing the results and developments with aerospace manufacturers and end users.

The technical aims of the thesis can be summarised as:

- Provide understanding and background on why these technologies are required and developments are necessary.

- Provide universal background information of the use of carbon fibre composites as multifunctional devices.
    - Investigate the possibility of using carbon based particles such as carbon nanotubes and graphite to improve the performance of these multifunctionalities
- DEC:
    - Develop a Joule heating method that can cure both pre-preg and VARTM based manufacturing methods.
    - Provide process steps on how to replicate, and suggestions for future implementations.
    - Develop and evaluate the performance of the system against existing cure methods, including properties such as:
        - Sustainability, particularly energy usage
        - Resulting degree of cure and quality of components
        - Ease of manufacture
    - Demonstrate the developments in other use cases, such as de-icing or heated tooling.
- De-icing using Joule effect:
    - Develop a leading-edge de-icing system that can match heating performance of existing similar systems.
    - Minimise the impact and modifications to the existing structural composite layup.
    - Demonstrate the heating in a relevant environment, in this case, an environmental chamber.
- Joule heated composite tooling
    - To integrate the DEC technology into composite tooling to enable heating
    - To match the heating performance of ovens used for aerospace composite curing.
- Optimise for a rapid curing system
    - Demonstrate the concept of reducing cure length and energy usage when taking into account the physics of the curing system.
    - Reduce energy further by using the exothermic energy in epoxy resins to an advantage whilst ensuring safe operation.
- Self-Sensing:
    - Provide a review and thorough testing of existing electrical sensing methods.
    - Develop existing theory into larger structures, and where modularity and manufacturability are prioritised.
    - Demonstrate the capability of a non-contact, composite damage detection system on a representative aerospace composite component.
    - Provide data on a variety of impact situations, post processing of data, and information on situations where it works well and where improvements are required.

1.9. Thesis Structure

The thesis is a combination of papers (authorship declared in section 1.10) and chapters that demonstrates the thought process of the author, mostly in the order of the development of the technologies. When including journal papers into a thesis, it may result in some loss of cohesiveness between chapters due to the way they are formatted. Therefore, this section has been added to explain the reasoning of the order of the chapters.

The work completed in this thesis was primarily under the funding of an EU Horizon 2020 project titled MASTRO (Intelligent bulk MAterials for Smart TRanspOrt industries, project ID: 760940 [67]). The main aim of the project was to develop the bulk properties of composite materials to increase conductivity and enable multifunctionalities. It involved material manufacturers such as Arkema, and end users providing feedback on developments, including Embraer.

This first investigation therefore was to research the nanocomposites manufacturing, conductivity and piezoresistive properties. As discussed later, due to the difficulties in nanocomposite development and incompatibilities with VARTM and fibre composites, the multifunctionalities of DEC, de-icing and self-sensing were developed without significant involvement of nanocomposites.

The literature review is covered over chapter 2 and chapter 3, the first chapter, covers the conductivity of composites, nano-particle modification of epoxies for conductivity, multifunctional composites, impact damage detection in composites and self-sensing of composites. It also covers the background research for the papers on Joule heating for de-icing and heated tooling, and on cure kinetic modelling in chapters of 7 & 8 respectively. The second part of the literature review is the published review paper on novel curing methods for sustainable manufacture, which reviews a variety of novel curing methods. It also gives significant information on previous implementations of direct electric cure.

Chapter 4 covers the materials and methods that were used in the later experimental chapters that weren't covered in the respective papers. Given the concise nature of journal papers, some details have been omitted, therefore this section has been added to ensure there is full coverage of the reader of the methods and materials used in the studies.

Chapter 5 is a conference proceeding on developing experimental methods to introduce conductive Carbon Nanotubes (CNT's) and graphite into epoxies to increase conductivity. The aim was to understand and develop accessible and repeatable mixing methods, which were not fully achieved. These conductive resins were to be implemented in the subsequent chapters on Joule heated composites and self-sensing composites to reduce the matrix conductivity and increase performance. Due to their incompatibility with resin infusion methods, conductive resins were not used extensively.

Chapter 6 is a published paper on direct electric cure of aerospace composites, which describes the development of the curing method, as well as experimental details and results. It details the methodology of the developments as the components being cured are scaled up, and the technical advances that were made as issues arose. It also describes Joule heating for cure on dry fibre infused composites for the first time. It compares the results of the curing method for both pre-preg and VARTM components to oven cured components, looking primarily at component quality, as well as manufacturability and sustainability.

Chapter 7 details work on other use cases for the Joule heating of composites, which includes experimental details on de-icing experiments, and the implementation of the Joule heating into CFRP tooling to enable heated tooling. These provide higher Technology Readiness Level (TRL) examples of the technologies and where they can be implemented. It also covers work on a novel cure control method, developed from first principles, which is particularly applicable to novel curing methods with rapid heating ability, such as DEC. The model was developed and tested using a heated tooling plate, as a simple use case and to demonstrate the technique on a known and controllable heating technology.

Chapter 8 is primarily an experimental paper on electrical self-sensing of aerospace composites and scaling up existing and novel techniques to detect barely visible impact damage. It reviews and tests a variety of previously published techniques, and establishes new and complementary methods, so it can be scaled up for practical implementation in representative manufacturing environments.

Conclusions on the topics covered and recommendations on areas for future development are provided in chapter 9.

1.10. Thesis Papers

This thesis consists of the following papers and papers in preparation, including CRediT author statements [68] and in which chapter they feature:

Chapter 3

Paper published: Collinson M, Bower M, Swait TJ, Atkins C, Hayes S, Nuhiji B. ***Novel composite curing methods for sustainable manufacture: A review***. Composites Part C: Open Access 2022;9:100293. https://doi.org/10.1016/j.jcomc.2022.100293.

Primarily conceptualised, authored, and edited by Matthew Collinson, with contributions to the microwave section from Matthew Bower & Betime Nuhiji, induction section by Craig Atkins. Supervised and edited by Tim Swait, Simon Hayes and Betime Nuhiji.

Chapter 5

Published: Collinson M, Hayes S, Petropoulos S. ***The effect of type of mechanical processing on electrical conductivity and piezoresistive response of CNT and graphite composites***. Procedia CIRP 2019;85:314–20. https://doi.org/10.1016/J.PROCIR.2019.10.001.

Experimental work, authorship and editing by Matthew Collinson. Experimental work was assisted by Stefanos Petropoulos. Editing and supervision was by Simon Hayes.

Chapter 6

Paper published: Collinson MG, Swait TJ, Bower MP, Nuhiji B, Hayes SA. ***Development and implementation of direct electric cure of plain weave CFRP composites for aerospace***. Compos Part A Appl Sci Manuf 2023;172:107615. https://doi.org/10.1016/j.compositesa.2023.107615.

Experimental work, authorship and editing by Matthew Collinson. Experimental work was assisted by Matthew Bower, Tim Swait and Simon Hayes. Supervised and edited by Tim Swait, Simon Hayes and Betime Nuhiji.

Chapter 7

Paper in preparation: Collinson M, Bower M, Hayes SA. ***Development of CFRP Joule heated multifunctional aerospace de-icing system.***

Experimental work, authorship and editing by Matthew Collinson. Experimental work was assisted by Matthew Bower and Simon Hayes. Supervised and edited by Simon Hayes.

Paper in preparation: Collinson M, Simpson O, Morris S, Gibbs A. ***Development of CFRP Joule heated tooling for aerospace applications.***

Experimental work, authorship and editing by Matthew Collinson. Experimental work was assisted by Matthew Bower and Simon Hayes. Supervised and edited by Simon Hayes.

Paper in preparation: Collinson M, Bower M, Swait TJ, Nuhiji B. ***Practical cure optimisation for rapid and low energy processing of thermosetting composite systems*.**

Cure model primarily authored by Tim Swait, with testing and experimentation by Matthew Collinson and Matthew Bower. Paper authored by Matthew Collinson, with supervision and editing from Tim Swait and Betime Nuhiji.

Chapter 8

Paper in preparation: Collinson MG, Swait TJ, Bower MP, Nuhiji B, Hayes SA, ***Development of large scale electrical self-sensing of CFRP composites.***

Experimental work, authorship and editing by Matthew Collinson. Experimental work assisted by Matthew Bower. Editing and supervision was by Simon Hayes, Tim Swait and Betime Nuhiji.

1.11. References

[1] Hull C, Clyne TW. An Introduction to Composite Materials. 2nd ed. Cambridge: Cambridge University Press; 1996.

[2] Owston CN. Electrical properties of single carbon fibres. J Phys D Appl Phys 1970;3:1615.

[3] Zhao Q, Zhang K, Zhu S, Xu H, Cao D, Zhao L, et al. Review on the electrical resistance/conductivity of carbon fiber reinforced polymer. Applied Sciences (Switzerland) 2019;9. https://doi.org/10.3390/app9112390.

[4] American Chemical Society. High Performance Carbon Fibers. 2003.

[5] Zhang J, Lin G, Vaidya U, Wang H. Past, present and future prospective of global carbon fibre composite developments and applications. Compos B Eng 2023;250. https://doi.org/10.1016/j.compositesb.2022.110463.

[6] He HW, Gao F. Effect of Fiber Volume Fraction on the Flexural Properties of Unidirectional Carbon Fiber/Epoxy Composites. International Journal of Polymer Analysis and Characterization 2015;20:180–9. https://doi.org/10.1080/1023666X.2015.989076.

[7] Irving P, Soutis C. Polymer Composites in the Aerospace Industry. Second Edition. Woodhead Publishing; 2020.

[8] Cytec Industries Inc. CYCOM ® 5320-1 Epoxy Resin System. vol. 324. 2015.

[9] Ekuase OA, Anjum N, Eze VO, Okoli OI. A Review on the Out-of-Autoclave Process for Composite Manufacturing. Journal of Composites Science 2022;6. https://doi.org/10.3390/jcs6060172.

[10] European Commission. Reducing emissions from aviation 2020. https://climate.ec.europa.eu/eu-action/transport/reducing-emissions-aviation_en (accessed October 2, 2023).

[11] Léonard PLY, Nylander JW. Sustainability Assessment Of Composites in Aero-Engine Components. Proceedings of the Design Society: DESIGN Conference, vol. 1, Cambridge University Press; 2020, p. 1989–98. https://doi.org/10.1017/dsd.2020.29.

[12] Suzuki T, Takahashi J. Prediction of energy intensity of carbon fiber reinforced plastics for mass-produced passenger cars. The Ninth Japan International SAMPE symposium, 2005, p. 14–9.

[13] Aldosari SM, Khan M, Rahatekar S. Manufacturing carbon fibres from pitch and polyethylene blend precursors: a review. Journal of Materials Research and Technology 2020;9:7786–806. https://doi.org/10.1016/j.jmrt.2020.05.037.

[14] Song YS, Youn JR, Gutowski TG. Life cycle energy analysis of fiber-reinforced composites. Compos Part A Appl Sci Manuf 2009;40:1257–65. https://doi.org/10.1016/j.compositesa.2009.05.020.

[15] Lu C, Bian S, Hu K, Li C, Zheng K, Sun Q. Biomass-based epoxy resin derived from resveratrol with high temperature resistance and intrinsic flame retardant properties. Ind Crops Prod 2022;187. https://doi.org/10.1016/j.indcrop.2022.115500.

[16] Biocarbon fibres made of lignin - Bioeconomy n.d. https://www.biooekonomie-bw.de/en/articles/news/biocarbon-fibres-made-of-lignin (accessed October 3, 2023).

[17] Liddell HPH, Brueske SB, Carpenter AC, Cresko JW. Manufacturing energy intensity and opportunity analysis for fiber-reinforced polymer composites and other lightweight materials. Proceedings of the American Society for Composites - 31st Technical Conference, ASC 2016, 2016.

[18] Gower MRL, Sims GD. Towards a Standard Qualification Plan (SQP) for Composite Materials-Initial Draft 2002.

[19] Collinson MG, Swait TJ, Bower MP, Nuhiji B, Hayes SA. Development and implementation of direct electric cure of plain weave CFRP composites for aerospace. Compos Part A Appl Sci Manuf 2023;172:107615. https://doi.org/10.1016/j.compositesa.2023.107615.

[20] Hayes SA, Lafferty AD, Altinkurt G, Wilson PR, Collinson M, Duchene P. Direct electrical cure of carbon fiber composites. Advanced Manufacturing: Polymer & Composites Science 2015;1:112–9. https://doi.org/10.1179/2055035915Y.0000000001.

[21] Liu S, Li Y, Shen Y, Lu Y. Mechanical performance of carbon fiber/epoxy composites cured by self-resistance electric heating method. International Journal of Advanced Manufacturing Technology 2019. https://doi.org/10.1007/s00170-019-03707-0.

[22] Kondratiev A, Píštěk V, Purhina S, Shevtsova M, Fomina A, Kučera P. Self-heating mould for composite manufacturing. Polymers (Basel) 2021;13. https://doi.org/10.3390/polym13183074.

[23] 787 integrates new composite wing deicing system | CompositesWorld n.d. https://www.compositesworld.com/articles/787-integrates-new-composite-wing-deicing-system (accessed November 9, 2023).

[24] Athanasopoulos N, Koutsoukis G, Vlachos D, Kostopoulos V. Temperature uniformity analysis and development of open lightweight composite molds using carbon fibers as heating elements. Compos B Eng 2013;50:279–89. https://doi.org/10.1016/j.compositesb.2013.02.038.

[25] Oleskiw MM. A Review of 65 Years of Aircraft In-Flight Icing Research at NRC. Canadian Aeronautics and Space Journal 2001;47.

[26] Riley JT. Investigations of Performance of Pneumatic Deicing Boots, Surface Ice Detectors, and Scaling of Intercycle Ice. 2006.

[27] Goraj Z. An overview of the deicing and antiicing technologies with prospects for the future. 24Th International Congress of the Aeronautical Sciences 2004:1–11.

[28] Yuhas AJ, Ray RJ. Effects of Bleed Air Extraction on Thrust Levels of the F404-GE-400 Turbofan Engine. California: 1992.

[29] Newman W. H., Viele M. R. Engine Bleed Air Reduction in DC-10 Aircraft. California: 1980.

[30] Idris MK, Qiu J, Melenka GW, Grau G. Printing electronics directly onto carbon fiber composites: unmanned aerial vehicle (UAV) wings with integrated heater for de-icing. Engineering Research Express 2020;2:025022. https://doi.org/10.1088/2631-8695/AB8E24.

[31] Grove SM, Progoulakis I, Searle T, Summerscales J, Healey P. Heated tooling for aerospace composites manufacture. SAMPE Journal 2005;41:36–45.

[32] Li Y, Xiao Y, Yu L, Ji K, Li D. A review on the tooling technologies for composites manufacturing of aerospace structures: materials, structures and processes. Compos Part A Appl Sci Manuf 2022;154. https://doi.org/10.1016/j.compositesa.2021.106762.

[33] Man M, Lovingfoss R, Ng Y, Lian E, Hooper E. Cytec Cycom 5320-1 T650 3K-PW Fabric Qualification Material Property Data Report - NCAMP Project Number NPN071001 2015:1–294.

[34] Maes VK, Radhakrishnan A, Lombetti D, Kratz J. Zonally heated tooling for moulding complex and highly tapered composite parts. Front Mater 2023;10. https://doi.org/10.3389/fmats.2023.1126932.

[35] Industrialisation of self heated composite tooling based on Tailored Fibre Placement Technology | GREEN-TOOLING | Project | Fact sheet | FP7 | CORDIS | European Commission n.d. https://cordis.europa.eu/project/id/605853 (accessed September 28, 2023).

[36] Argon AS, Cohen RE, Mower TM. Mechanisms of toughening brittle polymers. Materials Science and Engineering: A 1994;176:79–90. https://doi.org/10.1016/0921-5093(94)90961-X.

[37] Cantwell WJ, Morton J. The impact resistance of composite materials - a review. Composites 1991;22:347–62. https://doi.org/10.1016/0010-4361(91)90549-V.

[38] Kumar P, Rai B. Delaminations of barely visible impact damage in CFRP laminates. Compos Struct 1993;23:313–8. https://doi.org/10.1016/0263-8223(93)90231-E.

[39] Polimeno U, Meo M. Detecting barely visible impact damage detection on aircraft composites structures. Compos Struct 2009. https://doi.org/10.1016/j.compstruct.2009.04.014.

[40] Tsigkourakos G, Silberschmidt V V., Ashcroft IA. Damage assessment in CFRP laminates exposed to impact fatigue loading. J Phys Conf Ser 2011;305:12047. https://doi.org/10.1088/1742-6596/305/1/012047.

[41] Swait TJ, Jones FR, Hayes SA. A practical structural health monitoring system for carbon fibre reinforced composite based on electrical resistance. Compos Sci Technol 2012;72:1515–23. https://doi.org/10.1016/j.compscitech.2012.05.022.

[42] Alsaadi A, Meredith J, Swait T, Curiel-Sosa JL, Hayes S. Damage detection and location in woven fabric CFRP laminate panels. Compos Struct 2019;220:168–78. https://doi.org/10.1016/j.compstruct.2019.03.087.

[43] Katunin A., Krukiewiez K., Turczyn R., Sul. P, Bilewicz M. Electrically conductive carbon fibre-reinforced composite for aircraft lightning strike protection. IOP Conf Ser Mater Sci Eng 2017;201. https://doi.org/10.1088/1757-899X/201/1/012008.

[44] Dakin TW. Application of Epoxy Resins in Electrical Apparatus. IEEE TRANSACTIONS ON ELECTRICAL INSULATION 1974;9:121–8. https://doi.org/10.1109/TEI.1974.299321.

[45] Zhang Abbas A Dehghani-Sanij AE Richard S Blackburn WA. Carbon based conductive polymer composites 2007. https://doi.org/10.1007/s10853-007-1688-5.

[46] Janzen J. On the critical conductive filler loading in antistatic composites. J Appl Phys 1975;46:5536. https://doi.org/10.1063/1.321629.

[47] Tanabi H, Erdal M. Effect of CNTs dispersion on electrical, mechanical and strain sensing properties of CNT/epoxy nanocomposites. Results Phys 2019. https://doi.org/10.1016/j.rinp.2018.11.081.

[48] Vertuccio L, Guadagno L, Spinelli G, Lamberti P, Zarrelli M, Russo S, et al. Smart coatings of epoxy based CNTs designed to meet practical expectations in aeronautics. Compos B Eng 2018;147:42–6. https://doi.org/10.1016/J.COMPOSITESB.2018.04.027.

[49] Kuilla T, Bhadra S, Yao D, Kim NH, Bose S, Lee JH. Recent advances in graphene based polymer composites. Progress in Polymer Science (Oxford) 2010;35:1350–75. https://doi.org/10.1016/j.progpolymsci.2010.07.005.

[50] Kinloch IA, Suhr J, Lou J, Young RJ, Ajayan PM. Composites with carbon nanotubes and graphene: An outlook. Science (1979) 2018;362:547–53. https://doi.org/10.1126/SCIENCE.AAT7439.

[51] Gantayat S, Prusty G, Rout DR, Swain SK. Expanded graphite as a filler for epoxy matrix composites to improve their thermal, mechanical and electrical properties. Xinxing Tan Cailiao/New Carbon Materials 2015. https://doi.org/10.1016/S1872-5805(15)60200-1.

[52] Collinson M, Hayes S, Petropoulos S. The effect of type of mechanical processing on electrical conductivity and piezoresistive response of CNT and graphite composites. Procedia CIRP 2019;85:314–20. https://doi.org/10.1016/J.PROCIR.2019.10.001.

[53] Naito K, Tanaka Y, Yang JM, Kagawa Y. Tensile properties of ultrahigh strength PAN-based, ultrahigh modulus pitch-based and high ductility pitch-based carbon fibers. Carbon N Y 2008;46:189–95. https://doi.org/10.1016/J.CARBON.2007.11.001.

[54] Quan D, Alderliesten R, Dransfeld C, Murphy N, Ivanković A, Benedictus R. Enhancing the fracture toughness of carbon fibre/epoxy composites by interleaving hybrid meltable/non-meltable thermoplastic veils. Compos Struct 2020;252:112699. https://doi.org/10.1016/J.COMPSTRUCT.2020.112699.

[55] Zucco G, Rouhi M, Oliveri V, Cosentino E, O'higgins RM, Weaver PM. Continuous tow steering around an elliptical cutout in a composite panel. AIAA Journal 2021;59:5117–29. https://doi.org/10.2514/1.J060668.

[56] El-Dessouky HM, Saleh MN, Gautam M, Han G, Scaife RJ, Potluri P. Tailored fibre placement of commingled carbon-thermoplastic fibres for notch-insensitive composites. Compos Struct 2019;214:348–58. https://doi.org/10.1016/J.COMPSTRUCT.2019.02.043.

[57] Lincoln RL, Scarpa F, Ting VP, Trask RS. Multifunctional composites: a metamaterial perspective. Multifunctional Materials 2019;2. https://doi.org/10.1088/2399-7532/ab5242.

[58] Klemperer CJ von, Maharaj D. Composite electromagnetic interference shielding materials for aerospace applications. Compos Struct 2009;91:467–72. https://doi.org/10.1016/j.compstruct.2009.04.013.

[59] Ferreira ADBL, Nóvoa PRO, Marques AT. Multifunctional Material Systems: A state-of-the-art review. Compos Struct 2016;151:3–35. https://doi.org/10.1016/j.compstruct.2016.01.028.

[60] Terörde M, Lücken A, Schulz D. Weight saving in the electrical distribution systems of aircraft using innovative concepts. Int J Energy Res 2014;38:1075–82. https://doi.org/10.1002/ER.3116.

[61] Minus ML, Kumar S. The processing, properties, and structure of carbon fibers. JOM 2005;57:52–8. https://doi.org/10.1007/S11837-005-0217-8/METRICS.

[62] Yousefpour K, Lin W, Wang Y, Park C. Discharge and ground electrode design considerations for the lightning strike damage tolerance assessment of CFRP matrix composite laminates. Compos B Eng 2020;198. https://doi.org/10.1016/j.compositesb.2020.108226.

[63] Kruželák J, Kvasničáková A, Hložeková K, Hudec I. Progress in polymers and polymer composites used as efficient materials for EMI shielding. Nanoscale Adv 2021;3:123–72. https://doi.org/10.1039/D0NA00760A.

[64] Das S, Yokozeki T. A brief review of modified conductive carbon/glass fibre reinforced composites for structural applications: Lightning strike protection, electromagnetic shielding, and strain sensing. Composites Part C: Open Access 2021;5:100162. https://doi.org/10.1016/J.JCOMC.2021.100162.

[65] SurFlow™: Composite data highways for data transmission - TWI n.d. https://www.twi-global.com/media-and-events/insights/surflow-composite-data-highways-for-data-transmission (accessed October 3, 2023).

[66] Gagné M, Therriault D. Lightning strike protection of composites. Progress in Aerospace Sciences 2014;64:1–16. https://doi.org/10.1016/j.paerosci.2013.07.002.

[67] EU Horizon 2020. Intelligent bulk MAterials for Smart TRanspOrt industries. | MASTRO | Project | Fact sheet | H2020 | CORDIS | European Commission n.d. https://doi.org/https://doi.org/10.3030/760940.

[68] Allen L, O'Connell A, Kiermer V. How can we ensure visibility and diversity in research contributions? How the Contributor Role Taxonomy (CRediT) is helping the shift from authorship to contributorship. Learned Publishing 2019;32:71–4. https://doi.org/10.1002/leap.1210.

2. Literature review

This literature review covers topics not investigated in the review paper on novel composite curing methods, or in the literature sections of the included journal papers.

The aim of this review is to provide additional context and background to the topics studied in this thesis, in addition to giving a better understanding of the reasons behind the novelty and the necessity of such studies in aerospace composites and manufacturing in general.

2.1. Composites background

Composite materials are being used more frequently in structural aerospace components, particularly in commercial aerospace products, such as in the Boeing 787 and Airbus A350. This is due to their superior strength to weight ratio compared to conventional aerospace materials [1], enabling lighter aircraft, which reduces running costs and carbon emissions. Composites provide a lot of flexibility in their manufacture, allowing for novel design concepts that can enable step changes in structural properties from generation to generation. With this flexibility also comes manufacturing issues and unknowns that are not faced in metallic aerospace design. These include the expensive and long takt time during manufacture [2], the integration of existing ice prevention systems [3] and how in-service damage is detected [4] and repaired. Given to the versatility and flexibility of composite manufacture [5] and materials, it is possible to consider multifunctional composites to solve these issues.

A composite is made up to two or more other bulk materials, usually a structural reinforcement and a formable matrix, which allows the best properties from each constituent material to be realised in the final material. An example of this relevant here is one of the most commonly known composite, carbon fibre reinforced plastic (CFRP). The reinforcement, the carbon fibres, have excellent tensile properties [6], but on their own cannot hold shapes and have poor damage tolerance. When combined with a polymer matrix, such as epoxy resin, which on its own is very brittle, it becomes a versatile engineering material. The in plane tensile strength from the fibres is retained, whilst the fibres are protected and formed by the epoxy, giving overall a very stiff and light material.

The approach of combining two materials with different strengths and weaknesses to build an overall superior material allows for a huge amount of flexibility in the materials that can be chosen, and subsequently their manufacturing methods. Mud and straw used as a building material can be considered a composite, right up to a high temperature metal matrix ceramic for use in turbine fan blades. Even with a well-defined set of materials such as carbon and epoxy, there is still a huge choice of final composites that can be manufactured, along with the manufacturing method, depending on the final component requirements.

The key enabler of multifunctionality is the electrical conductivity of the carbon fibres which are the reinforcement of these composites. These multifunctionalities discussed here are Direct Electrical Cure (DEC), Self-De-Icing, Joule heated Composite Tooling and Self-Sensing. To understand how these functionalities work, it is first important to discuss the electrical properties of CFRP composites and the practicalities of using them as electrical devices. Later in this chapter, the background to multifunctional materials and composites is covered. The background to composite curing and damage detection are covered, in relation to the main multifunctionalities covered in this work, DEC and self-sensing.

2.2. Electrical conductivity in composites

There are two main methodologies when measuring the electrical resistance of a material, 2-point and 4-point. Both work for measuring the resistance of carbon-based composites, however they have differences in practicalities and accuracy, particularly when being used for electrical self-sensing. The 2-point method has electrodes attached to each end of a sample and a voltage is applied across the terminals. Using an ammeter at the same points, the induced current can be measured, therefore allowing the resistance of the sample to be derived. Using the equation below, the resistance per meter can be calculated.

$$\rho = \frac{Rwh}{l} \quad [1]$$

Where ρ is resistivity in Ω/m, R is the calculated resistance from the voltage and current readings, w, h and l are the width, height and length of the sample in meters, assuming the cross-sectional area of the sample is the same throughout the sample being tested.

The 2-point method for measuring resistance is quick and easy, as the electrodes don't require accurate positioning. However, it has not been found to be a reliable approach either when used on composites [7–9] or on other conductive and semi-conductive materials [10,11]. The 2-point method measures the entire system, which includes the wiring of the system, and the contact resistance to the material being measured. Obtaining a reliable contact with the conductive part of the composite, the carbon fibres, is a consistent difficulty which can increase the apparent overall resistance measurement and reduce reliability of these measurements.

4-point resistance testing is a more reliable and repeatable testing method, illustrated in Figure 1. Voltage is measured between the desired measurement point, and current is applied from two electrodes, further out from the measurement points. This method has been used successfully in measuring composite resistance [12,13], as well as measuring resistance change when damage has occurred [14]. It has been found that the inconsistencies with the 2-point method are primarily due to the contact resistance between the composite and the electrodes which is eliminated with the 4-point method [15]. This can also result in different values of properties such as piezoresistance between the two resistance measuring techniques [16].

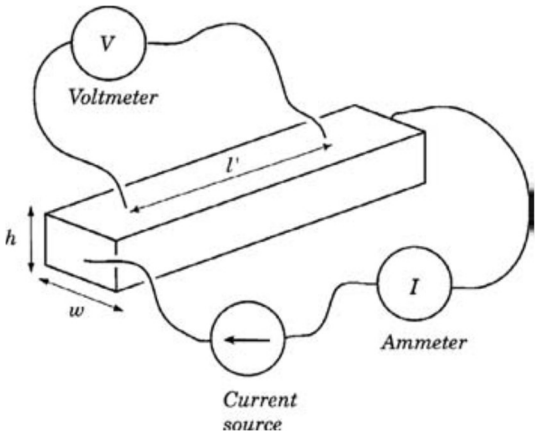

Figure 1: Experimental setup of 4-point measurement [11].

The increase in accuracy of the 4-point measurement is due to it only measuring the resistance of the

material, with the resistance of the wiring and contact resistance being cancelled out when calculating the sample, seen in the circuit diagram in Figure 2. This results in higher accuracy measurements closer to the true resistance value of the sample. This could benefit the performance and sensitivity self-sensing, as the resistance of the wires and contact resistance could be a significant percentage of the overall measured resistance.

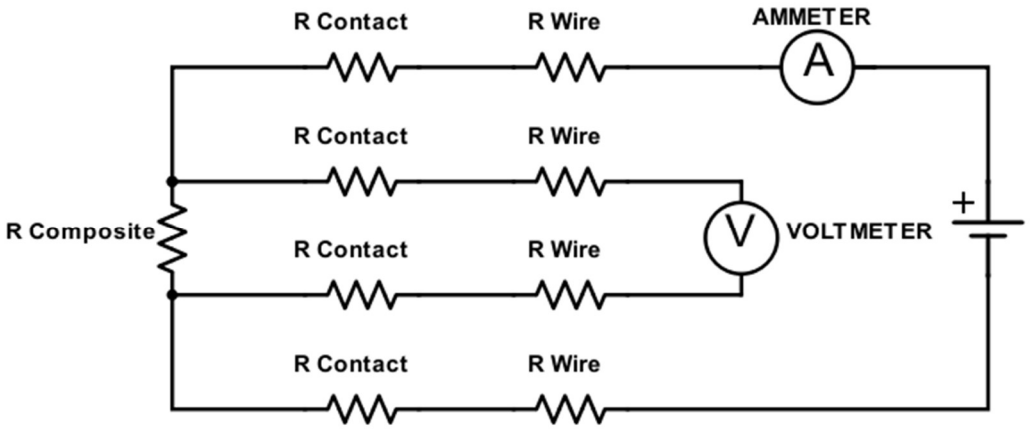

Figure 2: Circuit diagram example demonstrating the 4-point method cancels out the wire and contact resistance.

It has been observed when the current flows through a sample, as illustrated in Figure 3, that the current is non uniform through the part [17], particularly where current is introduced. This could be a reason for the variations found when using 2-point method. It also shows an example of electrode positioning during a 4-point test, and how the current in the area measurement is uniform, leading to a more repeatable testing procedure.

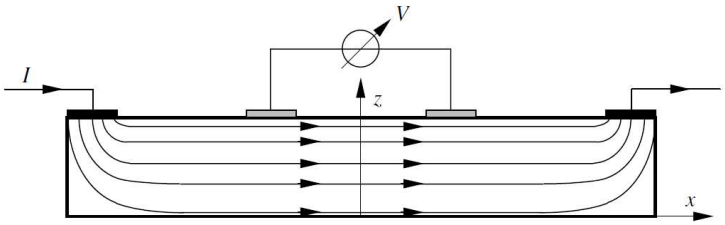

Figure 3: Current distribution through a sample during a 4-point composite resistance test [17].

Wang et al [12] investigated the setup requirements for the 4-point resistance technique, finding that it was much more sensitive to damage, giving a larger proportional change to resistance than the 2-point method. As can be seen from Figure 3, the 4-point method requires a certain minimum distance between the two electrodes of the same polarity to ensure even current distribution. For damage detection purposes, the measurable area between electrodes needs to be maximised, however this can be practically challenging to implement. One advantage of the 2-point measurement technique, is that the measurement area is maximised, and if contact resistance can be reduced, this may be a practical and accurate enough technique to measure the resistance changes due to damage induction.

2.3. Measurement and management of composite contact resistance

One practical issue that occurs with the resistance testing of composites is the ability to achieve a good electrical contact between the electrode and the sample. The resistance between the electrode

and the sample can be high, resulting in this contact resistance being a large percentage of 2-point measurements. This issue is particularly evident in composites, as the epoxy resin acts as an insulating barrier [18] to the measurement of the composite as the carbon fibres are much more conductive than the epoxy. High contact resistance will also limit the effectiveness of the multifunctionalities developed in the following studies. Therefore, it is important to consider the modification of the epoxy itself (discussed in section 5) or the modification of the surface of the composite to remove the physical barrier of the epoxy.

A common method to reduce contact resistance is to lightly sand down the CFRPs surface to expose the fibres, so that silver paint can be applied to the sample [12,16], or copper can be electroplated [8], which then gives a lower contact resistance to the fibres itself. Nanoparticle modified epoxy could be used to a similar effect, however, isn't evidenced in literature. It has been noted that removal of epoxy to expose the fibre can cause fibre damage, potentially leading to lower composite mechanical performance [7]. It may be possible to use techniques such as wet sand blasting or controlled plasma or laser polymer ablation to ensure the result is more repeatable and provide a more controlled and less aggressive method for removal of epoxy.

Another method to increase consistency of the resistance measurements was used by Swait et al [19], who embedded flexible printed circuit boards with copper contacts during the layup. The solution ensured more repeatable results, however in this case, it was still limited by the sensitivity of the 2-point measurement technique, requiring a high density of electrodes to enable damage detection.

Conductive epoxy adhesives, containing carbon based nanofillers such as CNT's and graphene have been investigated [20,21] for use in electronic devices as an alternate to lead based solder and resins highly loaded with metallics (typically silver at 70%). They have found to be a good alternative due to being lead free, processable at low temperatures, corrosion resistant and more lightweight and cost effective than silver filled adhesives. This evidence suggests that the integration of these conductive resins into a composite could be used to eliminate or significantly reduce the contact resistance issues that have limited the effectiveness of resistance measurements previously.

These conductive adhesives and epoxies have rarely been used alongside the method of exposing conductive fibres or been used as the bulk matrix in a composite. The main reason for not them in this way is due to the infusion manufacturing processes required during the research stage, which would cause issues with filtration of the particles in the fibres. Pre-pregging the nanocomposites would allow for even distribution within a composite, however require large batches of resin, and aren't commonly available at research institutions. Some studies have overcome the filtration issue to increase conductivity in glass fibre composites [22]. It is for this reason that CNT bucky papers (thin sheet of carbon nanotubes) and veils have been researched in detail for lightweight conductive composites [23], however when used with CFRP composites, would only increase the conductivity of the surface, or where the bucky paper is put in the layup.

2.4. Practical electrical conductivity of composites

Making an electrical contact to the fibres within CFRP is impractical as it is coated and encapsulated by the epoxy matrix. This difficulty in creating a reliable electrical contact is increased by the fact that conductivity is higher along the length of the fibre, opposed to through its thickness. This results in high conductivity along the fibre bundle (tow) direction and therefore in plane of the fibre direction of a composite laminate. This is due to the structure of carbon fibre being in graphitic planes in tangent

to the fibre direction, resulting in good thermal and electrical conductivity along the fibre, but not in plane [24].

In a carbon weaves or UD layups, there are inter fibre contact points between tows and plies, where current can flow into an adjacent fibre bundle. This is a weak connection due to its small contact region, and can also inhibited by the matrix, seen in Figure 4. An aligned fibre composite such as plain weave will therefore exhibit anisotropic conductivity, being conductive in the 0° and 90° and therefore limiting conducting paths in the composite.

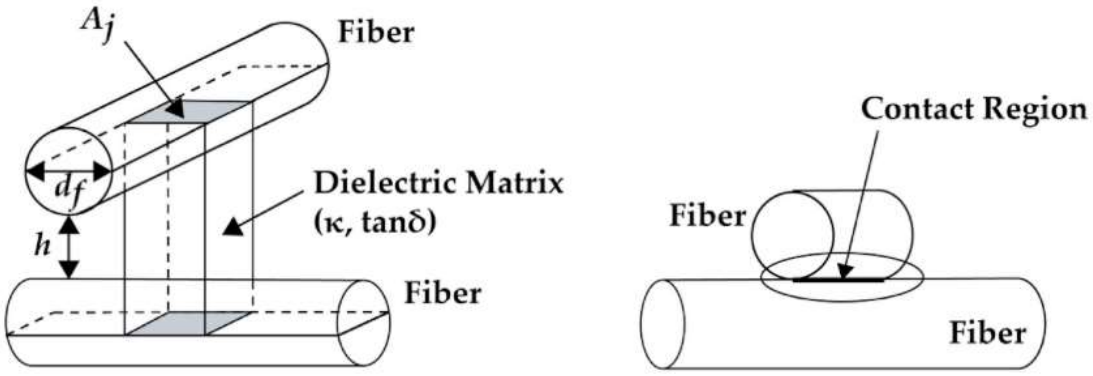

Figure 4: Examples of limitations of conductivity through thickness (left) and small contact area between fibres (right) [25].

It was observed by Abry et al [26] that the electrical resistance using the 2-point method in the longitudinal direction of a unidirectional (UD) CFRP composite was directly related to the number of conducting fibres, see Figure 5. The transverse resistivity was much higher (up to 200x) and has a linear relation to the length of the specimen being tested. The resistance of the composite in the fibre direction was given as:

$$R = \frac{\rho_f}{bhV_f} L + R_c \qquad [2]$$

where ρ_f is the fibre resistivity, L is the distance between the two electrodes, R_c is the sum of the resistance of the electrodes and wires, V_f is volume fraction and b and h are width and thickness of the sample. This is unlikely to be true for woven composites, as factors will have to be applied to take account of the transverse fibre interaction, and waviness of the fibres. Where there is a higher fibre volume fraction of conductive fibres, the conductivity of the overall composite increases.

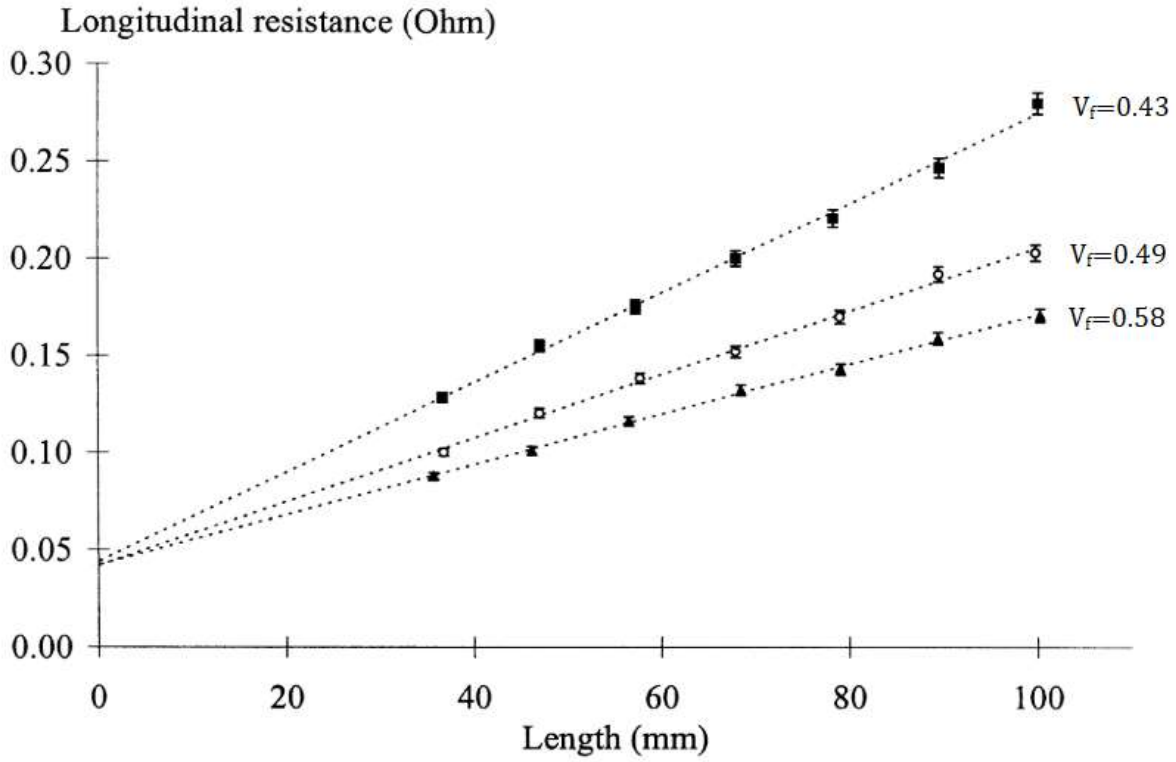

Figure 5: Longitudinal resistance of CFRP against sample length, adapted from [8].

The combination and variance of these properties seen in production parts, makes resistance measurements of composites difficult to repeat accurately, leading to variations in results of very similar samples. When testing UD composites for piezoresistivity, the results are repeatable and match predictive models [27], compared to a woven carbon architecture which are more unpredictable [14].

It is possible that this problem may be alleviated by the addition of carbon-based conductive fillers such as CNT's, which would reduce the contact resistance between the carbon fibres and the electrodes, as well as reducing the resistance between the fibres in the composite, to increase overall conductivity.

The majority of literature looks at the concept of using CFRP as a strain gauge or to allow damage detection on a small scale within a controlled environment. These environmental factors result in a strong response from the sample and report a positive outcome, however the studies rarely consider the practicalities of applying it to an end use case. This makes the results potentially difficult to scale up to a self-sensing application. Many studies test samples where the contacts equidistant from each other, as illustrated in Figure 3, which means for a sensing application only a third of the area is effective.

2.5. Practical electrical conductivity of nanocomposites

The use of nanocomposites is limited in scale, due to their difficulty in manufacture, leading to large yields required for larger scale composite manufacturing processes being prohibitively expensive. In recent years, these materials have been more commercially viable and therefore able to be purchased in larger batches. Another reason for their investigation here is that they now can be obtained pre-

dispersed in DGEBA resin, meaning that they require limited further dispersion in resins, and don't require strict health and safety controls due to being carcinogenic in their undispersed forms [28].

There is a critical weight percentage of nanofillers in the system above which there is a significant increase in the electrical conductivity, seen in Figure 6. This critical weight percentage is called the electrical percolation threshold and is dependent on many factors, such as the type and size of filler, the functionalisation and the mixing methods. The percolation threshold can also be defined as the percentage weight point where a connected electrical network is made between the conductive particles, so the whole network increases conductivity significantly.

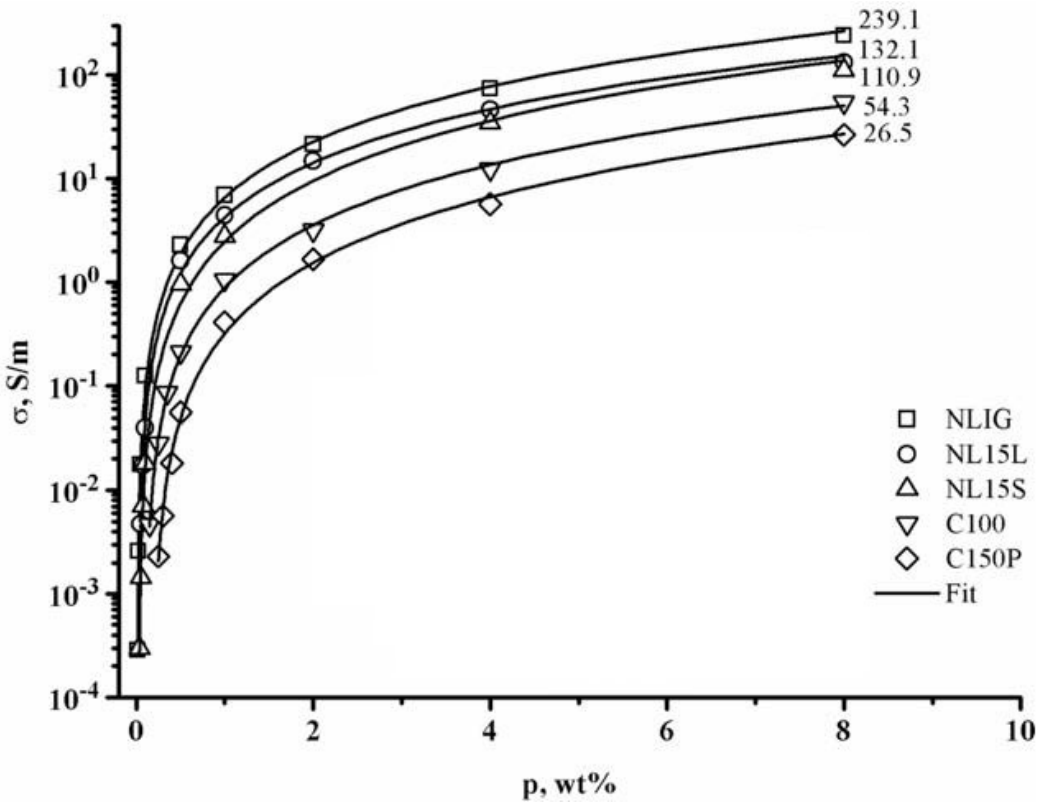

Figure 6: The figure shows conductivity per meter against weight percentage of a variety of MWCNT's [29].

One factor to consider with CNTs is that they agglomerate within the resin, meaning they are attracted together due to van der Waals forces [30] of which an extreme example can be seen in Figure 7.

The nanoparticles need to be added to and evenly distributed throughout the resin, to ensure isotropic conductivity. This can be achieved using a variety of methods, including ultrasonic dispersion (sonication), 3-roll mill or high shear mixing.

However, if perfectly distributed within a solution, the nano particles wouldn't be in contact with one another, which may be good for homogenous mechanical properties, but leads to poor electrical properties. This would result with all the conductive paths present between the nano particles being electrically isolated from each other.

Figure 7: Example of large-scale CNT agglomeration in resin manufactured at the AMRC.

Therefore, some level of agglomeration is required, so that conducting pathways can be made to achieve bulk electrical conductivity. However, if the agglomeration is too high and results in isolated agglomerates, as seen in the example in Figure 7, then both mechanical and electrical properties would be impacted.

These factors can lead to a varied range of percolation thresholds for similar materials, as seen in Table 1, taken from literature. For example, functionalisation, which is the chemical and mechanical preparation of the CNTs increases the surface energy of the nano particles. This allows a good chemical interaction between the nanofiller and the epoxy, and electrical interaction between nanoparticles. Without this, the filler is mechanically and electrically isolated from the resin. An analogy would be the sizing of carbon fibres for good compatibility between fibre and matrix to enhance the handling and mechanical properties.

Table 1: Summary of studies covering mixing methods and composite types and their percolation threshold.

Composite type	*Mixing method*	*Percolation threshold*	*Reference*
MWCNT-Polysulfone	Ultrasonic dispersion, solvent evaporated, “uniformly dispersed”	0.11%	[31]
MWCNT-Polysulfone	Ultrasonic dispersion, solvent evaporated, “agglomerated”	0.068%	[31]
MWCNT-Epoxy	Sonication	0.32%	[32]
MWCNT-Epoxy	3 Roll mill	0.0117-0.1883% depending on manufacturer (Figure 6)	[29]

MWCNT-PEI	Sonicated, solvent evaporated	0.5%	[33]
MWCNT-PS	Sonication	0.5-0.6%	[34]
MWCNT-Epoxy	Shear mixing	0.0025%	[35]
SWCNT-Epoxy	Shear mixing	0.05%	[35]
MWCNT-Epoxy	Mechanical mixing	0.0021%	[36]
MWCNT-Epoxy	Shear mixing	0.25%	[37]

The mixing method of the nanofillers into the resin is also an important factor in increasing electrical conductivity. Due to the high surface area of most carbon-based fillers, such as graphite, CNTs and graphene, it is difficult to fully wet out this area effectively, especially at high filler concentrations. From the examples seen in Table 1, there is a variation between methods, but mechanical mixing, such as shear mixing results in a lower percolation threshold.

2.6. Piezoresistance of composites

Piezoresistance is the change in electrical conductivity when the material is subject to strain. This property has been shown to occur in carbon fibres and resins modified with carbon based nano particles. To be able to monitor this property in CFRP and nano composites, it is important to investigate resistance monitoring methods and methods to reduce the contact resistance of composites.

2.7. Piezoresistance testing methodology

There have been several studies into the relationship between the strain imposed on a material and its electrical resistivity. This has the potential to be used as a structural health-monitoring tool for CFRP composites. A lot of this research is on smaller scale test coupons, with few studies increasing the scale to larger components, limiting the application of this type of work. Whilst it may not be directly applicable to the studies on scaling up self-sensing, there is a lot of information that can be gained from this research, such as mechanical and electrical testing methods, and range of expected results.

Carbon fibre's piezoresistive properties [38] have been investigated significantly in many different forms and configurations. A summary of examples of different testing methodologies can be seen in Table 2, with variations being in either the type of conductivity measurement, electrode contact method or the loading configuration.

A challenge with detecting piezoresistance is getting a consistent electrical contact with the composite. In the case of the examples given in Table 2, the electrical conductivity tests have mainly concentrated on 4-point resistivity methods, as this gives a more accurate and precise piezoresistivity measurement. 2-point resistance measurements are still considered, given it is more practical to implement into components. Gauge factor is also listed in the table which is the ratio of change of conductivity to strain.

Table 2: Summary of examples of research on CFRP piezoresistance.

Composite Type	*Electrode contact method*	*Loading configuration*	*Measurement method*	*Gauge factor*	*Reference*
CFRP	Copper plate and silver paint	Tensile	4-point	+ve, linear	[39]
CFRP strand 0.5mm diameter	Silver paint applied directly onto fibres	Bending crank arm	2-point	-ve	[40]
CFRP UD	Copper electroplating	3-point bend	2-point	+ve linear longitudinal, -ve exponential decay transverse	[26]
CFRP UD	Silver paint	Tensile, GFRP tabs	2- point	+ve, exponential increase	[41]
CFRP Quasi-isotropic	Cr/Au sputtered contacts	Tensile	4-point	+ve longitudinal, -ve transverse	[42]
CFRP Quasi-isotropic	Carbon cement	Tensile	4-point	-ve	[42]
CFRP UD	Polished surface, Silver paste	Tensile	4-point	+ve	[17]
CFRP UD	Polished surface, Silver paste	Tensile	4-point	+ve longitudinal, -ve transverse	[43]

The studies summarised in Table 2 are limited to investigating the piezoresistive property of the CFRP composite, not investigating further to understand its potential use as part of a structural health monitoring system. Some studies go as far as using it to predict fatigue damage and fibre breakage when reaching the ultimate tensile strength of the sample [14]. A significant conclusion of multiple studies was the importance of polishing the sample surface before applying an electrical contact [17,43] and ensuring that the contact material was highly conductive [42]. Whilst this mainly applies

to CFRP samples, due to the lower conductivity of the fibres, this practice can be carried forward into the testing of modified epoxy samples.

Whilst not as thoroughly researched as CFRP, key examples of studies on nanocomposite piezoresistivity are given in Table 3 below.

Table 3: Summary of composite electrode contact methods from literature.

Composite Type	*Contact method*	*Loading configuration*	*Measurement method*	*Gauge factor*	*Reference*
Epoxy-MWCNT	Silver paint, Copper tabs	Tensile	2-point	+ve	[44]
Epoxy-MWCNT-Glass	Silver paint	Tensile	2-point	+ve	[45]
Epoxy-MWCNT	Silver paint	Cantilever	2-point	+ve	[46]
Epoxy-MWCNT-Glass	Polished, silver paint	Tensile	2-point	+ve	[47]

Similar methodologies were used to the CFRP piezoresistance testing, however as nanocomposites are more electrically isotropic, they enable more consistent application of electrodes. They also have higher gauge factors, leading to a stronger resistance change in response to strain. It can also be noted that all were completed using the 2-point method, and all had a positive gauge factor, of which wasn't true with CFRP. This is likely due to the lower contact resistance between the electrode and the conducting part of the nanocomposite samples. It was noted by Vertuccio et al. [44] that the gauge factor was reduced as the nanotube percentage was increased.

The manufacture of CFRP-nanocomposites is a challenge that hasn't yet been conclusively answered by the research community. If modifying a resin, it would be normal practice to infuse the resin into carbon fibres using a vacuum assisted RTM method, which is a common way to manufacture high quality laminates. When infusing a resin in this way that contains nanoparticles, the size of the particles means that the carbon fibre fabric acts as a filter. It is common to infuse from one edge to another, and across this distance it is enough to filter the particles as well as inhibit the flow of resin completely, as seen in Figure 8. It is possible to increase the amount of flow media or ensure the length of infusion is lower, however these aren't practical as long-term solutions. Whilst this filtering effect is expected, it hasn't been reported in literature, and research into other solutions to manufacture evenly distributed fibre-nanocomposites isn't readily available or requires larger scale commercial equipment to test.

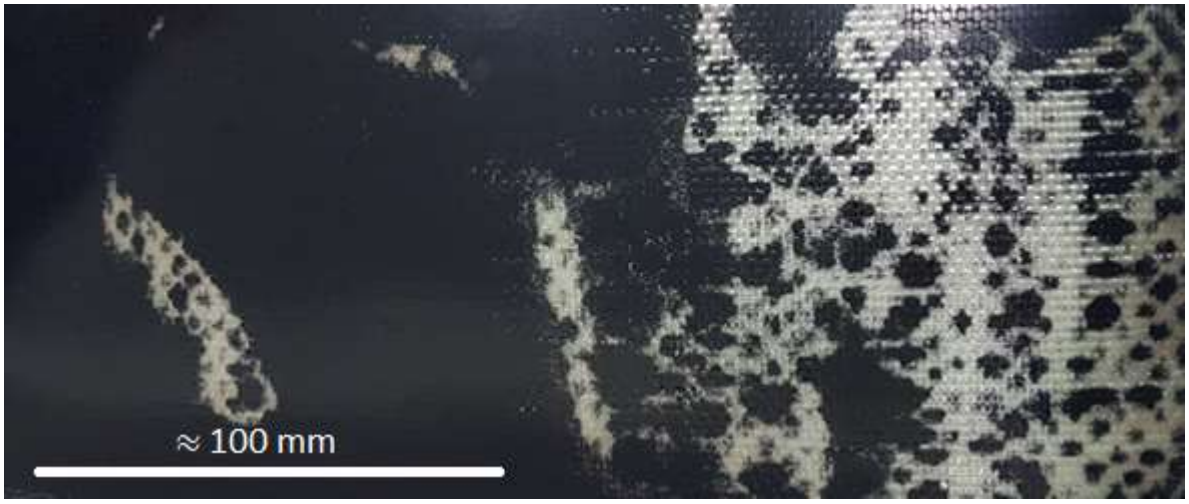

Figure 8: Example of a woven glass panel infused with CNT loaded resin, infused through plane, from left to right, manufactured at the AMRC.

To manufacture these nanocomposites, other manufacturing methods need to be investigated. One potential method is to manufacture a resin film, then use this as part of a dry fibre layup, so the resin only must infuse through thickness of the layup. This was completed by Sanli et al [46], who manufactured a CNT-epoxy film using screen printing and infused it into glass fibres. The CNT composite produced higher strain sensitivity than the metallic strain gauges, had stable responses over a 10-hour period and had low hysteresis. This combination of properties shows good promise for CNTs as an effective additive in composites to allow for structural health monitoring.

It may also be possible to evenly distribute nanoparticles during the pre-pregging stage of the materials manufacture. Resin is commonly mixed with solvent to reduce viscosity and enable consistent and even infusion into fibre tows, which could enable nanoparticles to be also evenly distributed when multiple layers are used. This hasn't been reported in many studies, due to the high cost of pre-pregging equipment, and the large quantity of materials required to test its viability.

Some commercial products have started to become available that have nano particle enhanced resins, however their ability to be used for strain measurements is not currently documented [48].

2.8. Composite curing background

The manufacture of composites is a wide topic, as there are a vast number of matrices and reinforcements available, depending on the final component requirements. All these require different processing methods, such as forming, heating, and cure temperature and pressure, further increasing complexity.

Currently in the aerospace and automotive composite industries, thermosetting matrices, specifically epoxy resins are the primary matrix material in most composite components. These applications demand medium to high mechanical property performance, requiring the use of hardeners that need external heat input to initiate the crosslinking polymerisation of the epoxy. The elevated temperature required for crosslinking results in higher mechanical performance over room temperature curing resins. This heat input can be delivered in many ways, the most common being the autoclave (Figure 9) although ovens, heated presses and heated tooling are increasingly used. The manufacturer of the

material specifies heating rates and heat source, for example using an autoclave with a 2°C/minute ramp rate to curing temperature [49].

Figure 9: Example of an autoclave at the AMRC, suitable for curing aerospace composites.

Autoclaves apply high pressures and temperature to composite layups, which reduce damage inducing voids between the plies, resulting in very consistent and high-quality parts. It is for this reason they have become industry standard [50]. However, they are very costly to purchase, setup and run, and can only manufacture a few parts at a time, leading to high part cost. Given their size, they are also very time and energy inefficient, having to heat up a whole chamber to cure a component a fraction of the chamber's volume.

Commercial composites for automotive or aerospace usually come in one of two different forms, the aerospace industry standard is to use "pre-preg", which means the fibre is pre-impregnated with resin, at the optimum weight percentage for structural performance. The resin is in a semi-solid state (B-staged) that has been through a very low energy initial cure, so that it can be easily applied in a tool and stick to other layers of pre-preg. Though the process to manufacture pre-preg is costly, it provides high precision of thickness and repeatability, ensuring the high-quality that aerospace standards demand. The layup of pre-preg is a very labour-intensive process increasing costs further. This has been automated using robotic layup techniques such as Automated Fibre Placement (AFP) [51].

The alternative method, which is seeing increased usage in industry, is resin infusion. The fibres in the form of a woven or non-crimp fabric is laid up in a tool and the resin is then infused. This can be completed under vacuum in an open mould, known as resin infusion, or vacuum assisted resin transfer moulding (VARTM), or under pressure in a closed tool, known as resin transfer moulding (RTM). The materials are lower cost, and the layup has potential to be sped up significantly as dry fibre can be deposited much quicker. RTM has more possibilities to automate processes, making it more beneficial to automotive industries, and has now started to attract the attention of the major aircraft manufacturers such as Airbus [52] and Boeing [53].

Primarily for the automotive industry, resin systems have been developed that can be cured quickly, such as some newer RTM resins, or "Snap Cure" resin systems [54], which aim to reduce the cycle time

to a couple of minutes. However, they require closed heated tooling or a heated press [54] to obtain the optimal material properties.

2.9. Stage of cure

Manufacturers of epoxy resins or pre-pregs provide a datasheet with the cure cycle, which contains a temperature time profile (and pressure when using an autoclave), which must be followed to produce a part without defects, of which an example for an out of autoclave system can be seen in Figure 10. If used in an autoclave, pressure would applied throughout the cure, typically from 5-8 bar.

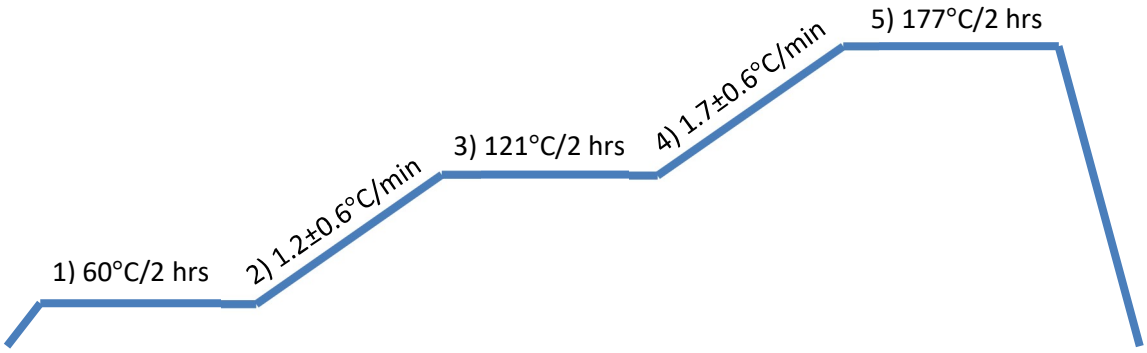

Figure 10: Example of a temperature against time graph of a cure cycle of an aerospace prepreg, Cytec Cycom 5320-1 [49].

There are typically two or three dwell or isothermal sections in a cure cycle and one to two ramp sections, which are described below (not all may be required depending on the epoxy chemistry or final use case):

1. Low temperature dwell: The slightly elevated temperature, usually 60 °C to 80 °C, decreases the viscosity of the resin, allowing it to flow between fibres more easily, allowing voids and air gaps to be closed or squeezed out of the part. The atmospheric pressure provided from applying a sealed vacuum to the part or higher with an autoclave, ensures that the composite is consolidated, and fibres are fully wetted out.
2. Ramp to cure: The ramp from the low temperature dwell to medium temperature dwell is slow, 1-2 °C a minute to reduce the chance of a runaway exothermic reaction and so the composite reaches cure temperature evenly across the part [55].
3. Medium temperature dwell: This section of the cure cycle is the section where majority of polymer crosslinking occurs, and the resin converts to a solid. By the end of this dwell, the composite is usually 70-80% cured [56]. Majority of the exothermic energy is released at this point, and therefore is important to monitor temperature carefully, especially with thick layups [57].
4. Ramp to post cure: The ramp from the main cure dwell, up to the post cure temperature. There is little crosslinking, and therefore little energy to be generated in the part.
5. High temperature dwell or post cure: This section is to complete the cure by ensuring the majority of the crosslinking has occurred and to increase and set the final glass transition temperature (T_g), which increases the service temperature of the composite and prevents the thermal properties changing during its lifetime.

It is important to consider these factors when using a high ramp rate to reduce cure cycle time, or using novel curing methods, to ensure part quality can be equalled to that produced using the recommended methods. It is common for manufacturers to overcompensate the time of the dwells and speed of the ramp rates, to ensure that there is no overheating. A thick layup will generate more exothermic energy than a thinner one, and therefore is more likely to overshoot the set temperature and could even result in a runaway exothermic reaction.

2.10. Multifunctional Structures & Composites

Multifunctional structures (MFS) are an extremely wide topic, so this review section focuses on definitions and discusses some key examples that have been proven at range of TRL's that demonstrate effectively. An MFS could be any device, material or structure that has one or more practical function in the application it is being used. This therefore brings in multiple areas of engineering and physics into a single topic area, which can be very complex.

Initial literature searches in the area indicate a huge amount of activity in MFS and individual technology developments, however this review will cover the activity themes as a whole and highlight significant technologies where required.

Definition and scope

Ferreira et al [58] investigate the definitions and nomenclature to define MFS, as well as topic areas and specific technologies that fit into this theme. An important definition to start with is the classification of multifunctional structures and materials, which can be seen in Figure 11.

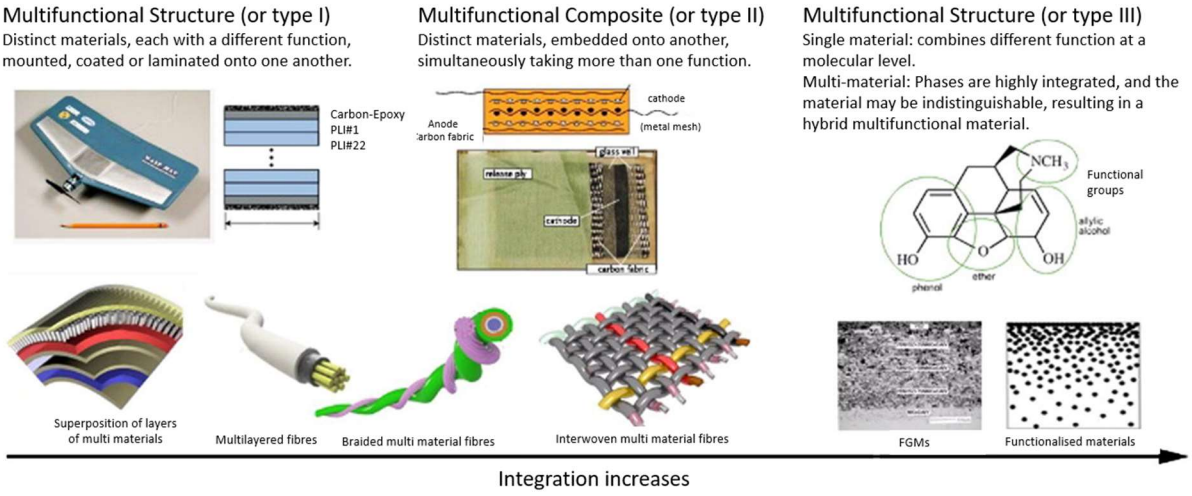

Figure 11: Stages of multifunctional research related to the scale and use of the materials, updated from [58].

It is defined on a scale of integration, which is loosely related to where and at what scale within the development cycle additional functionalities are added. It also relates the complexity of adding the multifunctionality to a structure.

Multifunctional structures are the most common in both research and industry, as the integration and development required of the product is the lowest. It involves using already functional or multifunctional materials together to make a full structure with multiple functions.

Integration of the material into a structure increases with multifunctional composites, which combines the functionality of two materials into one, and can be used as a base material in other structures. At a TRL4 or less commonly is the development of multifunctional materials, of which are more likely to combined functions. An example of this development would be conductive nano particle enhanced resins for electrical conductivity increases of the bulk material. Using this resin to manufacture a pre-preg would be an example of a multifunctional composite, then using this to protect a device from static electricity as a dissipation device would be an example of a multifunctional structure.

Another important distinction and definition to understand with multifunctional structures and systems is the autonomy and level of complexity of the resulting components/materials. These definitions will help define what level of integration would be required for some use cases, as well as the TRL levels of the technology. Definitions and examples can be seen in Table 4.

Table 4: Autonomy of multifunctional systems adapted from [59].

System	Passive geometry	Sensor	Actuator	Control	Processor	Power generation and storage
Passive	X					
Sensory/Active	X	X	X			
Adaptive	X	X	X	X		
Intelligent	X	X	X	X	X	
Autonomous	X	X	X	X	X	X
Examples						
Self-sensing CFRP		X				
Self-sensing and self-healing CFRP structure		X	X	X	X	
Fluid channels in an existing AM component	X					
DEC and de-icing composite wing		X	X			

These definitions are not without their exceptions though, for example the integration of a fluid channel into a pre-existing additive manufactured (AM) component. This provides extra passive structural functionality, however, not being an active device, therefore this just sits below an autonomous device, defined here and in Table 4 as “passive geometry”.

The final set of definitions provided by Ferreira et al was a list of specific functionalities and characteristics that a multifunctional material system should have. Examples of these specific functionalities that are relevant to aerospace composites are in Table 5.

Table 5: Summary of possible functions and individual research examples of multifunctionalities in literature where available, list adapted from Ferreira et al [60].

Functions	Example
Autonomous activation	Low level actuation such as: • Self-healing/Repairing (Self-healing epoxy resins [61], Effective electrochemical healing of structural steel [62]). • Self-Powered (Vibrational energy harvesting for aero elastic loads [63], embedded into a wing spar [64]). • Self-monitoring/diagnostic/sensing (Self-sensing composites [65] and piezoresistive epoxy [66]). • Self-assembling (Self assembly of a curved surface for use in UAVs [67], self assembly of nanostructures in epoxy for increased mechanical toughness [68]).
Highly tailorable properties	Alignment of CNTs in polymer matrices to directionally tailor mechanical, thermal and electrical properties [69].
Active sound/vibration damping	Acoustic dampening composite for aeronautic industry [70].
Actuation/shape changing	Fibre reinforced shape memory polymer composite used in a hinge application [71], Foldable high performance antennas for space deployment using elastic memory composite stiffeners [72].
Electrical/Thermal insulation/conductivity	CNT and Graphene [73], expanded graphite [74], carbon nano materials [75] modified polymers.
Heating and cooling	Cooling of windings in electric machines using 3D printed heat exchangers [76].
Electromagnetic interference (EMI) shielding	Summary of progress in polymers and polymer composites used as EMI shields [77].
Radiation protection including lightning strike protection (LSP)	Methods used for lightning strike protection of composites (carbon nanomaterials and metal meshes) [78].
Light emission	Light emitting diodes with multifunctional surface structures such as hydrophobicity and lipophobicity [79].
Energy storage	Energy storage in structural composites using electrolyte interleaves [80], structural composites for thermal energy storage [81].
Environmental remediation ability, recyclability and biodegradability	Design of Biobased Recyclable Polymers for Plastics [82], Design for Sustainability with Biodegradable Composites [83].
Bio related: bio-compatibility	Design of biocompatible and biodegradable polymers [84].
Flame retardancy	Special issue of Composites Part B dedicated to flame retardants and flame retardant polymers and composites [85]
Information storage and processing capabilities	Organic flash memory on various flexible substrates for foldable and disposable electronics [86].
Intelligence	A natively flexible 32-bit ARM microprocessor [87].

Commercially available Multifunctional materials

Multifunctional materials that can be made into multifunctional composites or structures are not yet widely commercially available, however they are not always needed to produce a complex multifunctional structure. It can be difficult to differentiate multifunctional materials and multifunctional composites, for example if a thermoplastic was modified with carbon nanotubes (CNTs) to make it conductive, it could be defined as both a thermoplastic-CNT composite or a multifunctional material to be integrated further in a later manufacturing process [88]. Even the manufacturing method can be an enabler into multifunctionalities, particularly prominent in additive manufacturing [89].

Modified base materials are available with limited extra functionalities. For example, Haydale [48] manufacture a graphene enhanced carbon fibre pre-preg with enhanced electrical and mechanical properties, already used in BAC Mono cars [90]. Formlabs [91] supply "Rebound Resin" which is a toughened elastic resin, which is used in New Balance trainers. These are functional examples of where simple multifunctional materials can be integrated into existing products with minimal product modification, whilst enhancing the engineering performance significantly. They are examples of passive geometry multifunctional structures with no automation or "smart functionalities".

Structural energy storage

This multifunctionality has mainly been seen in composites, where parts of the composite structure are multifunctional with an inbuilt battery cell or capacitor. For example, this can be achieved by simply intergrating exisiting battery cells into the layup of a composite, as reported by Ladpli et al [92], who intergrated standard lithium ion batteries into structural beams. The resulting component was able to carry structural loads without deforming the batteries and causing damage. This method is considered 1st generation multifunctional energy storage composite, or level 1 as defined by Adam et al [93], who review the topic in further detail, as seen in Figure 12.

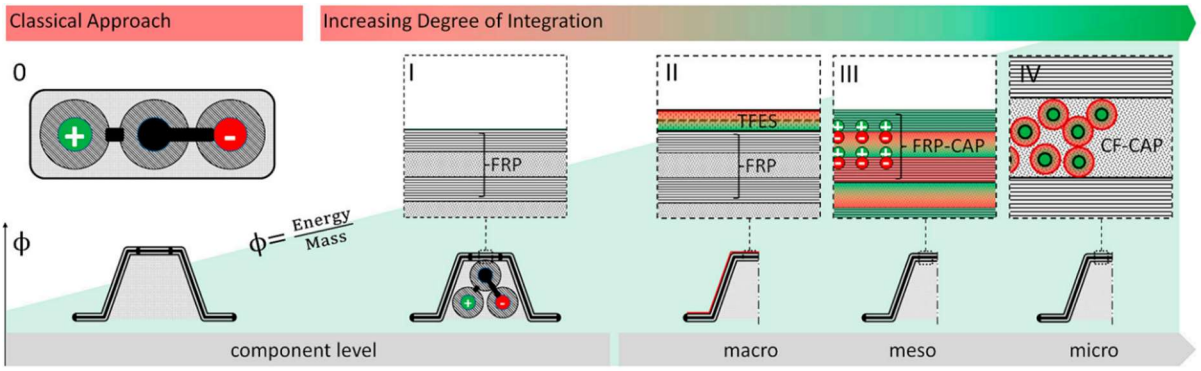

Figure 12: Degree of integration of multifunctional structural battery [146].

Further integration of structural batteries is a key research topic of the Structural Power Composites group at Imperial College London [94], where they developed car body panels that serve as an electric car battery seen in Figure 13 [95].This work has developed into project SORCERER [96] with Airbus, BAE and Qinetiq on structural energy storage, suggesting that aerospace companies are interested in this technology. In 2018, Senokos et al [80] manufactured a structural composite capacitor with the highest power (30W/kg) and energy (37.5mWh/kg) of its type so far. It was manufactured using a CNT fibre veil and polymer electrolyte interleaves, and infused with standard methods and resins, resulting in a flexural modulus of 50 GPa and flexural strength of 153 MPa. Asp et al [97] more recently reviewed the literature available on composite batteries, citing the main development challenges are the manufacture of structural positive electrodes.

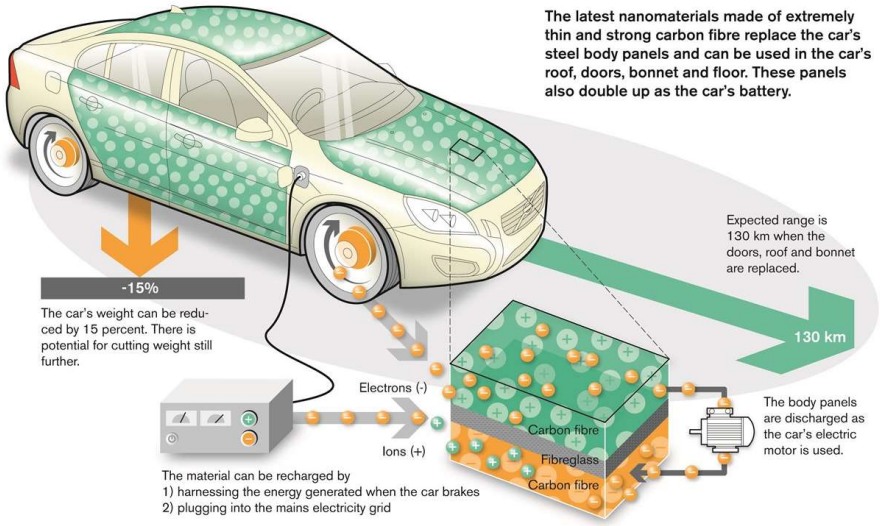

Figure 13: Example of structural battery developed with Volvo and Imperial College London [95].

Energy harvesting/generation

It is also possible to generate energy from the environment to aid in the extension of range in electric transport or power sensor systems. The energy sources are commonly vibration, thermal or solar, which can be used for a large variety of power usage scenarios. This could range from solar being used to charge EV batteries, to piezoresistive devices being used to run low-power data logging equipment.

Multilaminar polyvinylidene fluoride (PVDF) has been shown as a key piezoresistive material, able to be integrated into applications due to its flexibility and ability to be applied in thin layers. Zeng et al [98] demonstrated an all fibre ceramic piezoelectric nano generator, that could generate 0.015W at 1Hz in compression, intended for generating energy during normal human walking.

A. Alsaadi et al [99] integrated a macro-fibre composite (MFC) [100] that generated electric current through vibrational energy. This was tested with simulated vibrational data from an aircraft, a compressor motor and a suspension bridge, generating up to 0.577mWcm^{-3} from the aerospace use case, with others generating significantly lower energy. More recently Yan et al [101] used similar methods to generate power and actuate for future structural health monitoring systems. Liu et al [102] used an FE model to predict the energy generation possible using these devices on a real-world data collected from a rail vehicle. Eight locations were selected for the small (3 x 75 x 100mm) generators, which were predicted to generate 180mW, which was enough to run a hypothetical structural sensor platform.

Integrated solar cells are another way of generating electricity from the environment, Keller et al [72] integrated two types of commercially available solar cells into glass fibre polyurethane sandwich panels suited for building cladding. Flexible thin-film silicon cells performed well in mechanical and thermal testing compared to control samples, with only minor cell performance loss during mechanical loading. Maung et al [103] also integrated thin film solar cells in a similar manner, however cured it onto higher performance carbon fibre composite, with higher cure temperatures. Removal of structural film built into the commercial cells provided a weight saving of 40%. Cell performance was reduced when strain was increased over 1%.

Bishop et al [104] are developing spray coated perovskite solar cells which would allow for direct deposition of solar cells onto a surface, such as composites. The cells developed have a practical efficiency of 16-19%, depending on the size of the cells produced, however the cells have much higher theoretical efficiencies.

Damage detection

Structural health monitoring on its own is a huge area of research, however in many situations is an estimation of the damage that has occurred, taken from signals provided by acoustic monitoring or strain gauges. If the material or structure can directly respond to damage that occurred in service, then the position, type and severity of the damage could be more accurately determined. The literature related to electrical resistance monitoring, or self-sening method is not covered here, as it is covered later in chapter 8.

Lin and Chang [105] manufactured and tested a flexible printed circuit interleave that had ultrasonic sensor/actuators positioned, allowing for an integrated ultrasonic SHM system. This has been used for the localisation of impact damage [106] on a composite surface.

Giurgiutiu [107] integrated low-cost piezoelectric wafer active sensors onto a metallic plate, effectively allowing for built in phased array ultrasonic testing into the component, which typically is an external non-destructive testing method.

Self-healing

Mechanisms built into materials or structures that can self-repair, or more commonly referred to as self-heal, are able to heal cracks, delaminations or disbonds within a composite. Integration of microcapsules into the resin/polymer that have a healing agent inside is an effective method to deliver healing agent to where is required. Once a crack or damage occurs, the healing agent is released and heals the affected area. McDonald et al [108] were able to track the microcapsule activation using CT scanning during crack initiation.

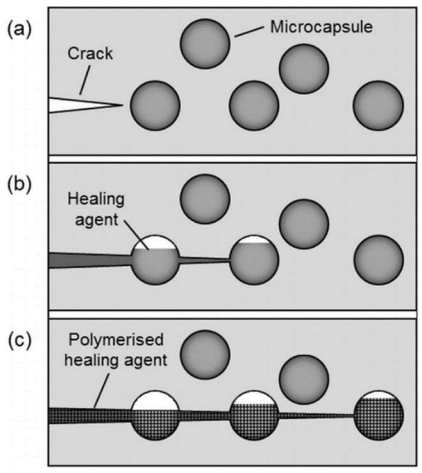

Figure 14: Self healing process using microcapsules. (a) A crack forms in the matrix; (b) the growing crack ruptures microcapsules in its path, releasing healing agent into the crack; (c) polymerisation of the healing agent occurs and the crack is closed [108].

An alternative method of delivering healing agent to an affected area is using hollow vascular networks built into the structure, which the healing agent is pumped to the affected damaged area. Chen et al [109] manufactured a sandwich panel with PVC tubing to deliver room temperature curing

epoxy to an affected area. The system has negligible effect on the baseline mechanical performance and restored the panel to 80% of the original flexural strength. A recent review by Shields et al [110] highlights that this method is still in its infancy, and low weight and high efficiency methods are still to be achieved.

Neither of these self-healing methods are suitable for aerospace, as until the healing method is required, the microcapsules and vascular channels are parasitic weight which don't provide any mechanical loading capability. Intrinsic self-healing polymers that regain strength with a heat cycle or pressure are more desirable as they don't reduce mechanical properties, however they may be more complex to manufacture. Guadagno et al [111] developed an epoxy-CNT based self-healing resin which allowed for reversable and repeatable re-healing of hydrogen bonds, enabled by the carbon nanotubes in the resin. Healing efficiencies have reached 57% using this method, however the resin viscosity increase makes this resin difficult to manufacture composites with. A method by Hayes et al [112], mixed an epoxy compatible thermoplastic into a low viscosity epoxy. The resulting composites required heat treatment to heal, providing a 70% healing efficiency, however, the viscosity increase makes this difficult to use with VARTM processes.

Morphing structures

Morphing structures which are powered by shape memory materials (Shape memory polymer, SMP or shape memory alloy, SMA), can change their form without requiring external actuation, such as servos or hydraulics. Stimulants are required for the shape memory materials, typically a thermal change. Sun et al [113] summarised the benefits of morphing structures to an aircraft, with the main benefits to typical problems in a flight envelope seen in Table 6.

Table 6: Advantages of morphing aircraft, adapted from [113].

Degree of Morphing	Morphing description	Advantages
Large	Folding wing	Increase the critical Mach number Decrease parasitic drag
	Variable sweep wing	Increase the critical Mach number Decrease high-speed drag
	Variable span wing	Increase L/D, loiter time, cruise distance Decrease engine requirements
Medium	Twisting wing	Increase maneuverability Prevent tip stall
	Flexible winglets	Increase L/D, maneuverability Decrease induced (tip vortex) drag
	Variable chord/camber	Increase low-speed airfoil performance Increase airfoil efficiency Delay separation
Small	Variable airfoil	Increase high-speed airfoil performance
	Bulging wing	Increase wing efficiency Decrease compressibility (wave) drag

Mabe et al [114] from Boeing flight tested SMA's on chevrons on a Boeing 777, to reduce noise during flights. 60-Nitinol were used as monolithic actuators, which were successfully tested to TRL 7, as seen in Figure 15. Work in this area has continued, with lots of literature available, covered most recently by Costanaza and Tata [115] who review most recent developments and key examples.

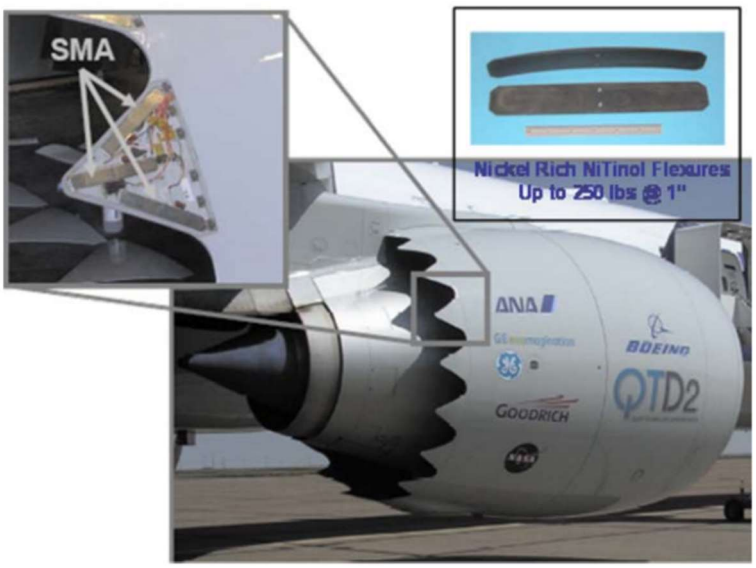

Figure 15: SMA actuated chevrons on a Boeing 777 [114].

SMP's are also commonly heat activated, and have had more research interest over SMA's, due to the shift to CFRP in aerospace and automotive. Interest has been in the space industry, for foldable satellites, where multiple experiments have been successfully deployed [116] both in microsatellites and on the international space station. In this area, particular interest is in extendable/foldable booms. An example can be seen in Figure 16 by Li et al [117], where a SMP was used in a composite to act as a potential backing structure for a space deployed solar panel where it successfully withstood space environment.

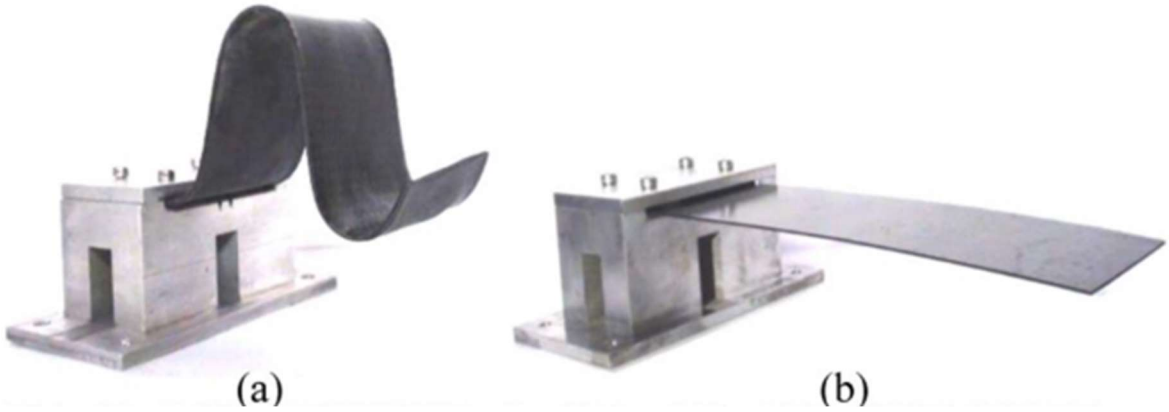

Figure 16: Configurations of experiment named Mission SMS-I [117]*, (a) packaged configuration; (b) deployed configuration.*

As these materials are heat activated, there is potential for future activation through direct electric heating of the carbon fibres themselves. Therefore, no extra resistive heating devices would be required, and would ensure that it was a more integrated as a multifunctional composite, opposed to being a multifunctional structure with two distinct components.

SHM in composites background

This section discusses the issue of damage in composites, specifically impact damage, which is a particular issue with epoxy fibre composites, due to epoxy's low fracture toughness strength. Damage modes in composites are covered and how these are related to impact damage. Barely Visible Impact

Damage (BVID) is described, its importance and difficulty in detection, due to its ability to manifest into much larger areas of damage, which can lead to catastrophic failure. Lab based and in-service damage detection and evaluation methods are described, such as Computational Tomography (CT) scan, ultrasonic C-Scan and ultrasonic Structural Health Monitoring (SHM). Finally, novel damage detection methods are reviewed, particularly efforts to monitor the electrical properties of a CFRP and CNT modified CFRP components to detect impact damages.

Damage modes of fibre composites

There are number of different types of damage that can occur in composites, given their complex micro and macro scale architectures. The damage types are all induced differently and at varying stages of loading, indicating increasing stages of severity. To be able to develop damage detection methods, it is important to understand these interconnecting damage modes.

The epoxy matrix, which transfers load to and binds the carbon fibres together, is the most brittle part of a CFRP composite, meaning it doesn't deform under stress significantly before catastrophic failure. For this reason, it is most susceptible to damage in impact and in common flexural and fatigue situations. Matrix cracking becomes a damage propagation point, leading to further damage under repeated loading, such as delaminations, which is the separation of plies.

Following on matrix damage, is the breakdown of the fibre-matrix bonding. This is mainly in the form of fibre pull out, which is where the fibre has disbonded from the matrix. This means that the load put on the matrix can no longer be transferred to the fibre, leading to an overall reduction in the strength of the composite. This can be caused by weak bonding between the fibre and the matrix during manufacture, however, usually follows on from fibre breakage in areas of the composite.

Fibre breakage is caused by localised high strain concentrations, such as a localised impact, which increases strain on the opposing face to the impact. When fibres break, the overall strength of the composite reduces, as the stress of the load is spread over fewer fibres.

Fibre breakage is the primary method used to detect damage using the electrical resistance method, as these fibres are electrically conductive, and when the electrical path is broken, the overall conductivity of the composite will reduce. It is possible to detect matrix cracking through electrical resistance method [118], however this requires many electrodes, and could be further enhanced through the use of a conductive matrix.

Barely Visible Impact Damage (BVID) and damage modes in composites

There is one type of damage that is of particular concern and interest to aerospace manufacturers is called barely visible impact damage (BVID). This type of damage is difficult to see using the naked eye during visual inspection of composites due to its size and low indentation depth. It mainly occurs in fibre laminates, where a top face, is impacted by an object, and the surface that is impacted is visibly unaffected. This usually occurs on external facing surfaces, with the many standards defining the damage as no larger than a 2.5 mm deep indent.

During the impact, the reverse side of the composite is subject to large tensile forces, which can cause significant damage such as fibre pull out, matrix cracking, fibre breakage and delamination between plies [119]. This surface sustains a large amount of damage, of which would need to be repaired, of which an example can be seen on the left of Figure 17. Due to location, the damage can't be detected

effectively without good visual access to the reverse side or by using Non-Destructive Testing (NDT) methods. Inspecting the reverse side of the composite in service is not a practical option, as for example on a leading edge of a wing, the reverse side of the surface of the wing would be at best extremely difficult to inspect effectively.

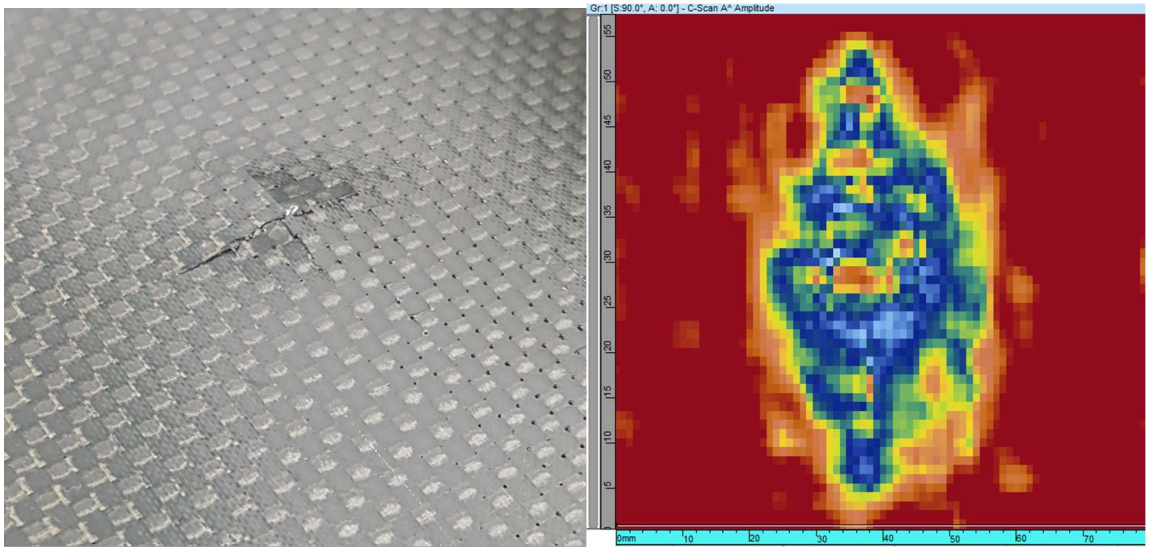

Figure 17: Example of BVID on a sample, impact size ~3mm diameter, and the C-Scan of the same damage, showing up to 55mm of delamination on the part.

Detection of this damage is particularly important as under certain fatigue loading conditions [120] the damage can continue to grow in size, whilst the impact dent size actually can decrease if the right conditions are met, and enough time is given between visual inspections [121].

It is for these reasons that aerospace manufacturers are particularly interested in a non-destructive Structural Health Monitoring (SHM) system that could automatically detect BVID in surface components, such as electrical self-sensing systems, or a detection system that could monitor primary structural components, or even bonded joints.

Damage detection in fibre reinforced composites

Because impact damage in composites can be difficult to detect visually, reliance on more complex and technical damage detection methods is required. This is achieved using Non-destructive testing (NDT), most of which require experienced operators to make informed decisions on the data from the equipment used.

One of the simplest tests that has been used in industry is using sound to determine if the structure is as intended. An example of this is the tap test, this can range from tapping a coin on a structure to see if the response sounds “sharp” or “dull” or breaking pencil lead onto the surface [122] and monitoring the response. More complex systems involve applying ultrasonic transducers and generators to a surface, to detect changes in response before, during and after damage [123]. This method is the basis behind many of the structural health monitoring (SHM) systems currently being implemented and tested on metallic and composite structures in the aerospace industry [124,125].

Ultrasonics can also be used to detect damage locally, of which the most common and suitable for detecting surface damage is C-Scan. To understand this method, the derivatives to C-scan, A-Scan and B-scan will be briefly explained.

A-Scan involves the generation and monitoring the response of an ultrasonic pulse on a single point on the surface of a composite. The pulse is emitted by a transducer, with the amplitude of response against time being plotted. The pulse will echo off any defects or back face of the composite, of which the response time can be used to measure distance, if the speed of sound of the material is known. This can be difficult in composites, as they are made up materials with different densities, therefore fibre volume fraction can vary the speed of sound of the composite. This can be used to identify the thickness of a component, bond line, or depth of defects.

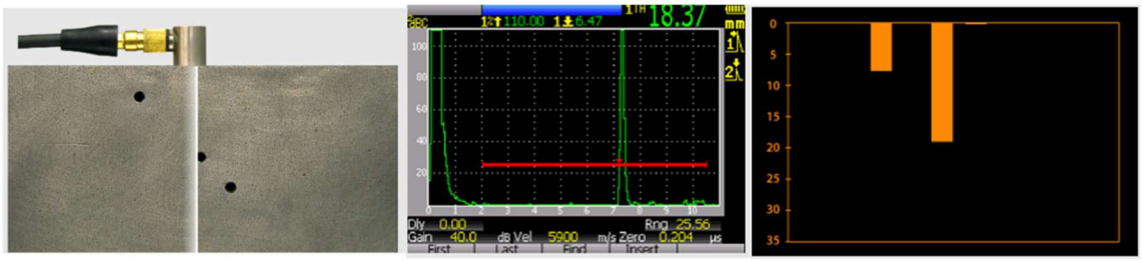

Figure 18: Images showing an ultrasonic transducer being used for flaw detection (left), showing an A-Scan(middle) and a B-Scan (right) representation of the data [126].

A B-Scan plot helps visualise the response, by taking the A-Scan data and plotting it as a function of distance over a surface, to build a 2D image slice of the surface underneath. This requires a wheel encoder or axis position information of the transducer so that it can record the information as it travels over the surface.

C-Scan further builds up the picture of under the surface by completing B-Scans in multiple planes, therefore giving a full sub-surface image of the material. Response depths in the material are represented on a colour spectrum to visualise. Responses over a certain threshold can be 'gated' to be highlighted in the processed image. An example of this can be seen in the central image in Figure 18, any response over the red line is represented in the B-Scan on the right of the figure. It is possible to build up an image using single transducer, as seen in the robotic system in Figure 19. However, it is impractical from a user's point of view to build up a C-Scan image accurately from a single point, so a few methods have been developed to generate C-Scan images.

Figure 19: Example of a robotic system with an attached water jet nozzle ultrasonic NDT head inspecting an aerospace CFRP part [127].

A user-friendly method is to use a phased array or matrix transducer, where an array or matrix of transducers is used to build up an instantaneous B-Scan or C-scan image, which is then moved across the surface to build up a larger C-Scan image, of which an example can be seen in Figure 20. Position of the transducers are fixed within the sensor, however the direction of the C-scan needs position data to define images accurately. This can be done with a transducer wheel, or by stitching multiple images together in the case of a matrix array transducer.

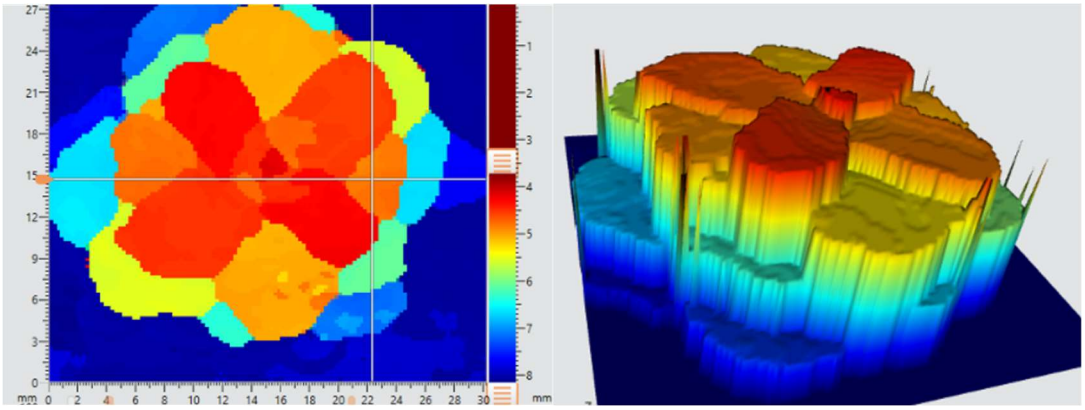

Figure 20: C-Scan images of an impacted composite, left is a standard 2D representation, right, is the same data represented in 3D. It is possible to see the delamination of the tows in both 0° and 90°.

Electrical resistance damage monitoring of composites

The piezoresistive effect of composites and nanocomposites has been studied extensively, frequently using small coupon scale samples. There are few cases where this research has been translated to larger components, to monitor strain or impact damage over a composite surface.

One challenge when applying this at larger scale components, when an impact occurs, the multiple damage modes can cause changes in resistance locally. During an impact, there is a resistance change due to the piezoresistive effect, during the peak of the deformation, but also if there is any permanent deformation. Resistance can increase when fibres are broken [128], which can occur during BVID [120]. This change in resistance is primarily due to the main conducting path being broken, but second to this would be contact between fibre bundles being broken.

A unidirectional (UD) or woven carbon fibre composite in the context of multifunctional composites can be regarded as a large array of resistors encased in an insulating epoxy matrix. If the conductivity of these carbon resistors can be monitored along the fibre direction where it is highest, in parallel along a panel, then when an impact occurs causing fibre breakage, a change in resistance can be detected. If the conductivity is measured in different segments or different axis of a woven or quasi-isotropic (QI) composite surface, then the intersection of the two axes on which damage is apparent should allow the damage to be located more accurately on the surface. This is the theory behind electrical self-sensing in its current form. A significant amount of research covers the piezoresistive nature of carbon fibres, carbon fibre composites [129] and nanocomposites [130], however only limited research looks at the materials on a larger scale, and even less at component level,[131].

Swait et al [19] investigated this by manufacturing flexible printed circuit boards (PCB) and using these as interleaves in UD Quasi-isotropic (QI) CFRP composites, that allowed precise positioning of electrodes at the edge of the panel. By recording resistance of electrode pairs in X and Y directions over the panel, a positional electrical resistivity dataset of the panel was recorded and then compared

after the panel was damaged. Where damage occurred, there would be peaks in the resistance, leading to XY coordinates of the damage location generated, and then can be linked to the physical damage position. Damage was detectable on a small scale panel with closely located electrode pairs, however as the panel scale increased, the sensitivity and the ability to detect the damage decreased. The 2-point resistivity measurement was used, allowing for quick measurements and positioning of the electrodes at the edge of the panel, only requiring PCBs to be embedded at the edge of the panel.

A. Alsaadi et al [132], used the 4-point resistivity method to accurately detect impact damage in a CFRP panel, and its location on the panel. Like Swait, a PCB was manufactured to ensure accurate placement of the electrodes. However, it was bonded to the surface of a pre-manufactured CFRP panel using low conductivity silver loaded adhesive. The 4-point method approach used allows truer conductivity values of the composite to be recorded. However due to the spacing required, the full area of the panel isn't monitored, resulting in a cross shaped area of detection, split into five segments, seen in Figure 21. Therefore, this method is suited to less accurate zonal damage detection, opposed to finding the exact position using X & Y coordinates, however within these limitations, it should be able to detect consistently and accurately.

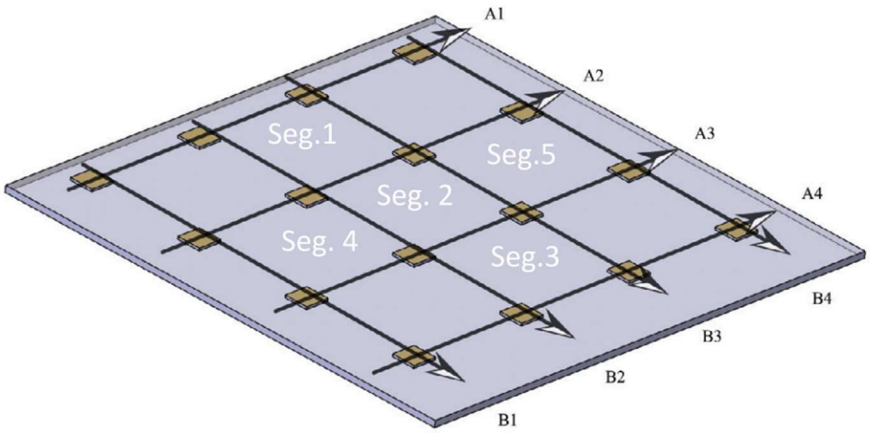

Figure 21: Damage detection area when using 4-point methodology [65].

Electrical impedance tomography (EIT) has been used by S.Nonn et al [133], R. Schueler et al [134], A. Baltopoulos et al [135][136], by taking electrical conductivity measurements across a panel from the edges then using electrical tomography to post process the data.

EIT, specifically the open-source implementation used in these cases, EIDORS [137], solves the inverse problem of resistance changes over a panel, in this case induced by damage. It uses finite element (FE) analysis to solve the expected voltage response from current introduction at the different electrodes, then is provided the data recorded before and after the impact.

Using this data, it can predict where the resistance is higher and lower in an object, in this case damage in a CFRP panel. This method was able to accurately locate the damage on panels up to 250mm^2 [133], with the potential to map the damage more accurately due to the larger number of measurements taken. This method has higher demands in computational cost, electrode input switching hardware requirements and experimental time, however, has shown the potential to be highly accurate in damage detection. An example of the electrode setup and output from the EIT solver can be seen in Figure 22.

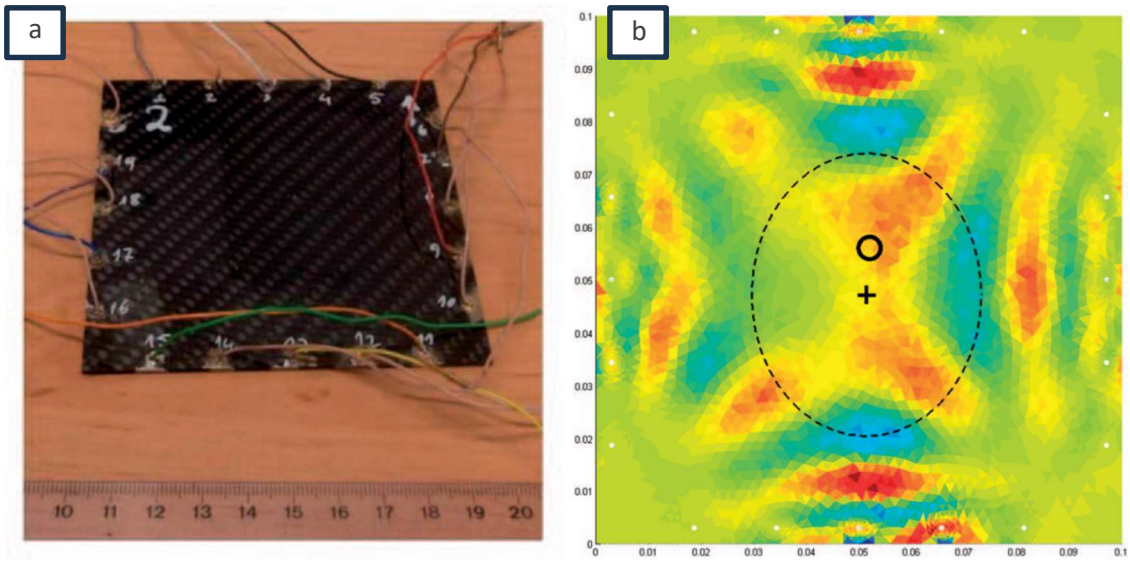

Figure 22: (a) CFRP specimen with attached electrodes and (b) resulting damage map from an impact damage, showing the impact point (+) and the software derived impact point (o) and region of interest (dotted line) [135].

2.11. References

[1] Hamerton I, Kratz J. The use of thermosets in modern aerospace applications. Thermosets: Structure, Properties, and Applications: Second Edition, Elsevier; 2018, p. 303–40. https://doi.org/10.1016/B978-0-08-101021-1.00009-5.

[2] Agius SL, Magniez KJC, Fox BL. Cure behaviour and void development within rapidly cured out-of-autoclave composites. Compos B Eng 2013;47:230–7. https://doi.org/10.1016/J.COMPOSITESB.2012.11.020.

[3] 787 integrates new composite wing deicing system | CompositesWorld n.d. https://www.compositesworld.com/articles/787-integrates-new-composite-wing-deicing-system (accessed November 9, 2023).

[4] Diamanti K, Soutis C. Structural health monitoring techniques for aircraft composite structures. Progress in Aerospace Sciences 2010;46:342–52. https://doi.org/10.1016/j.paerosci.2010.05.001.

[5] Gurit. Guide to Composites. 2022.

[6] Frank E, Hermanutz F, Buchmeiser MR. Carbon fibers: Precursors, manufacturing, and properties. Macromol Mater Eng 2012;297:493–501. https://doi.org/10.1002/mame.201100406.

[7] De Baere I, Van Paepegem W, Degrieck J. The use of rivets for electrical resistance measurement on carbon fibre-reinforced thermoplastics. Smart Mater Struct 2007;16:1821–8. https://doi.org/10.1088/0964-1726/16/5/037.

[8] Abry J, Bochard S, Chateauminois A, Salvia M, Giraud G. In situ detection of damage in CFRP laminates by electrical resistance measurements. Compos Sci Technol 1999;59:925–35. https://doi.org/10.1016/S0266-3538(98)00132-8.

[9] Hou L, Hayes SA. A resistance-based damage location sensor for carbon-fibre composites. Smart Mater Struct 2002;11:966. https://doi.org/10.1088/0964-1726/11/6/401.

[10] Lee BM, Loh KJ, Li M, Zuo T, Wang S. Analysis of variance on thickness and electrical conductivity measurements of carbon nanotube thin films Piezoresistivity of resin-impregnated carbon nanotube film at high temperatures 2016. https://doi.org/10.1088/0957-0233/27/9/095004.

[11] Webster JG. Electrical Conductivity and Resistivity. In: Webster JG, editor. Electrical measurement, signal processing, and displays, CRC Press; 2003, p. 1–14. https://doi.org/10.1201/9780203009406.

[12] Wang S, Wang D, Chung DDL, Chung JH. Method of sensing impact damage in carbon fiber polymer-matrix composite by electrical resistance measurement. J Mater Sci 2006;41:2281–9. https://doi.org/10.1007/s10853-006-7172-9.

[13] Mecklenburg M, Mizushima D, Ohtake N, Bauhofer W, Fiedler B, Schulte K. On the manufacturing and electrical and mechanical properties of ultra-high wt.% fraction aligned

MWCNT and randomly oriented CNT epoxy composites. Carbon N Y 2015;91:275–90. https://doi.org/10.1016/j.carbon.2015.04.085.

[14] Wang X, Chung DDL. Self-monitoring of fatigue damage and dynamic strain in carbon fiber polymer-matrix composite. Compos B Eng 1998;29:63–73. https://doi.org/10.1016/S1359-8368(97)00014-0.

[15] TODOROKI A, UEDA M, HIRANO Y. Strain and Damage Monitoring of CFRP Laminates by Means of Electrical Resistance Measurement. Journal of Solid Mechanics and Materials Engineering 2007;1:947–74. https://doi.org/10.1299/jmmp.1.947.

[16] Wang S, Chung DDL. Piezoresistivity in continuous carbon fiber polymer-matrix composite. Polym Compos 2000;21:13–9. https://doi.org/10.1002/pc.10160.

[17] Park JB, Okabe T, Takeda N. New concept for modeling the electromechanical behavior of unidirectional carbon-fiber-reinforced plastic under tensile loading. Smart Mater Struct 2003;12:105–14. https://doi.org/10.1088/0964-1726/12/1/312.

[18] Dakin TW. Application of Epoxy Resins in Electrical Apparatus. IEEE TRANSACTIONS ON ELECTRICAL INSULATION 1974;9:121–8. https://doi.org/10.1109/TEI.1974.299321.

[19] Swait TJ, Jones FR, Hayes SA. A practical structural health monitoring system for carbon fibre reinforced composite based on electrical resistance. Compos Sci Technol 2012;72:1515–23. https://doi.org/10.1016/j.compscitech.2012.05.022.

[20] Rosca ID, Hoa S V. Method for reducing contact resistivity of carbon nanotube-containing epoxy adhesives for aerospace applications. Compos Sci Technol 2011;71:95–100. https://doi.org/10.1016/j.compscitech.2010.10.016.

[21] Li J, Lumpp JK, Grulke E. Carbon nanotube filled conductive adhesives. 2003 International Symposium on Microelectronics 2003;5288:35–8.

[22] Domingues D, Logakis E, Skordos AA. The use of an electric field in the preparation of glass fibre/epoxy composites containing carbon nanotubes. Carbon N Y 2012;50:2493–503. https://doi.org/10.1016/j.carbon.2012.01.072.

[23] Xia Q, Zhang Z, Liu Y, Leng J. Buckypaper and its composites for aeronautic applications. Compos B Eng 2020;199. https://doi.org/10.1016/j.compositesb.2020.108231.

[24] Pop E, Varshney V, Roy AK. Thermal properties of graphene: Fundamentals and applications. MRS Bull 2012;37:1273–81. https://doi.org/10.1557/mrs.2012.203.

[25] Yarlagadda S, Kim HJ, Gillespie JW, Shevchenko NB, Fink BK. A Study on the Induction Heating of Conductive Fiber Reinforced Composites. J Compos Mater 2002;36:401–21. https://doi.org/10.1106/002199802023171.

[26] Abry JC, Bochard S, Chateauminois A, Salvia M, Giraud G. In situ detection of damage in CFRP laminates by electrical resistance measurements. Compos Sci Technol 1999;59:925–35. https://doi.org/10.1016/S0266-3538(98)00132-8.

[27] Seo D-C, Lee J-J. Damage detection of CFRP laminates using electrical resistance measurement and neural network. Compos Struct 1999;47:525–30. https://doi.org/10.1016/S0263-8223(00)00016-7.

[28] Luanpitpong S, Wang L, Rojanasakul Y. The effects of carbon nanotubes on lung and dermal cellular behaviors. Nanomedicine 2014;9:895–912. https://doi.org/10.2217/nnm.14.42.

[29] Rosca ID, Hoa S V. Highly conductive multiwall carbon nanotube and epoxy composites produced by three-roll milling. Carbon N Y 2009;47:1958–68. https://doi.org/10.1016/j.carbon.2009.03.039.

[30] Atif R, Inam F. Reasons and remedies for the agglomeration of multilayered graphene and carbon nanotubes in polymers. Beilstein Journal of Nanotechnology 2016;7:1174. https://doi.org/10.3762/BJNANO.7.109.

[31] Aguilar JO, Bautista-Quijano JR, Avilés F. Influence of carbon nanotube clustering on the electrical conductivity of polymer composite films. Express Polym Lett 2010;4:292–9. https://doi.org/10.3144/expresspolymlett.2010.37.

[32] Guadagno L, Vietri U, Raimondo M, Vertuccio L, Barra G, De Vivo B, et al. Correlation between electrical conductivity and manufacturing processes of nanofilled carbon fiber reinforced composites. Composites Part B 2015;80:7–14. https://doi.org/10.1016/j.compositesb.2015.05.025.

[33] Kumar S, Sun LL, Caceres S, Li B, Wood W, Perugini A, et al. Dynamic synergy of graphitic nanoplatelets and multi-walled carbon nanotubes in polyetherimide nanocomposites. Nanotechnology 2010;21. https://doi.org/10.1088/0957-4484/21/10/105702.

[34] Penu C, Hu G, Fernandez A, Marchal P, Choplin L. Rheological and electrical percolation thresholds of carbon nanotube/polymer nanocomposites. Polym Eng Sci 2012;52:2173–81. https://doi.org/10.1002/pen.23162.

[35] Moisala A, Li Q, Kinloch IA, Windle AH. Thermal and electrical conductivity of single-and multi-walled carbon nanotube-epoxy composites 2005. https://doi.org/10.1016/j.compscitech.2005.10.016.

[36] Martin CA, Sandler JKW, Shaffer MSP, Schwarz MK, Bauhofer W, Schulte K, et al. Formation of percolating networks in multi-wall carbon-nanotube-epoxy composites. Compos Sci Technol 2004;64:2309–16. https://doi.org/10.1016/j.compscitech.2004.01.025.

[37] Arkema. Graphistrength ® CS 1-25. n.d.

[38] Schulte K, Baron Ch. Load and Failure Alayses of CFRP Laminates by means of electrical resistivity measurements. Compos Sci Technol 1989;36:63–76. https://doi.org/10.1016/0266-3538(89)90016-X.

[39] Kupke M, Schulte K, Schüler R. Non-destructive testing of FRP by d.c. and a.c. electrical methods. Compos Sci Technol 2001;61:837–47. https://doi.org/10.1016/S0266-3538(00)00180-9.

[40] Weber I, Schwartz P. Monitoring bending fatigue in carbon-fibre/epoxy composite strands: a comparison between mechanical and resistance techniques. Compos Sci Technol 2001;61:849–53. https://doi.org/10.1016/S0266-3538(01)00028-8.

[41] Park JB, Okabe T, Takeda N, Curtin WA. Electromechanical modeling of unidirectional CFRP composites under tensile loading condition. Compos Part A Appl Sci Manuf 2002;33:267–75. https://doi.org/10.1016/S1359-835X(01)00097-5.

[42] Angelidis N, Wei CY, Irving PE. The electrical resistance response of continuous carbon fibre composite laminates to mechanical strain. Compos Part A Appl Sci Manuf 2004;35:1135–47. https://doi.org/10.1016/J.COMPOSITESA.2004.03.020.

[43] TODOROKI A, YOSHIDA J. Electrical Resistance Change of Unidirectional CFRP Due to Applied Load. JSME International Journal Series A 2004;47:357–64. https://doi.org/10.1299/jsmea.47.357.

[44] Vertuccio L, Vittoria V, Guadagno L, De Santis F. Strain and damage monitoring in carbon-nanotube-based composite under cyclic strain. COMPOSITES PART A 2015;71:9–16. https://doi.org/10.1016/j.compositesa.2015.01.001.

[45] Thostenson ET, Chou T-W. Carbon Nanotube Networks: Sensing of Distributed Strain and Damage for Life Prediction and Self Healing. Advanced Materials 2006;18:2837–41. https://doi.org/10.1002/adma.200600977.

[46] Sanli A, Benchirouf A, Müller C, Kanoun O. Piezoresistive performance characterization of strain sensitive multi-walled carbon nanotube-epoxy nanocomposites. Sens Actuators A Phys 2017;254:61–8. https://doi.org/10.1016/j.sna.2016.12.011.

[47] Bö L, Wichmann MHG, Meyer LO, Schulte K. Load and health monitoring in glass fibre reinforced composites with an electrically conductive nanocomposite epoxy matrix 2008. https://doi.org/10.1016/j.compscitech.2008.01.001.

[48] Composites – Haydale n.d. https://haydale.com/products/prepreg/ (accessed July 19, 2021).

[49] Cycom 5320-1 n.d. http://www.cytec.com/sites/default/files/datasheets/CYCOM_5320-1_031912.pdf (accessed April 28, 2015).

[50] Hull C, Clyne TW. An Introduction to Composite Materials. 2nd ed. Cambridge: Cambridge University Press; 1996.

[51] A350 & A400M wing spars: A study in contrasts : CompositesWorld n.d. http://www.compositesworld.com/articles/a350-a400m-wing-spars-a-study-in-contrasts (accessed May 9, 2015).

[52] Update: Lower wing skin, Wing of Tomorrow | CompositesWorld n.d. https://www.compositesworld.com/articles/update-lower-wing-skin-wing-of-tomorrow (accessed January 8, 2022).

[53] Boeing UK - News Release n.d. https://www.boeing.co.uk/news-media-room/news-releases/2023/july/uk-government-boeing-and-partners-announce-aerospace-manufacturing-investment.page (accessed October 20, 2023).

[54] HEXCEL. HexPly Snap-Cure 2019. https://www.hexcel.com/Products/HexPly-Snap-Cure (accessed August 26, 2019).

[55] Chairat A, Joulia X, Floquet P, Vergnes H, Ablitzer C, Fiquet O, et al. Thermal degradation kinetics of a commercial epoxy resin - Comparative analysis of parameter estimation methods. J Appl Polym Sci 2015;132:6–9. https://doi.org/10.1002/app.42201.

[56] Kratz J, Hsiao K, Fernlund G, Hubert P. Thermal models for MTM45-1 and Cycom 5320 out-of-autoclave prepreg resins. J Compos Mater 2013;47:341–52. https://doi.org/10.1177/0021998312440131.

[57] Esposito L, Sorrentino L, Penta F, Bellini C. Effect of curing overheating on interlaminar shear strength and its modelling in thick FRP laminates. International Journal of Advanced Manufacturing Technology 2016;87:2213–20. https://doi.org/10.1007/s00170-016-8613-5.

[58] Duarte Ferreira AB, Nóvoa PR, Torres Marques A. Multifunctional Material Systems: A state-of-the-art review 2016. https://doi.org/10.1016/j.compstruct.2016.01.028.

[59] Schlaich M. Future engineering structures for the urban habitat and infrastructure, International Association for Bridge and Structural Engineering (IABSE); 2004, p. 102–3. https://doi.org/10.2749/222137804796291089.

[60] Ferreira ADBL, Nóvoa PRO, Marques AT. Multifunctional Material Systems: A state-of-the-art review. Compos Struct 2016;151:3–35. https://doi.org/10.1016/j.compstruct.2016.01.028.

[61] Zhang F, Zhang L, Yaseen M, Huang K. A review on the self-healing ability of epoxy polymers. J Appl Polym Sci 2021;138. https://doi.org/10.1002/APP.50260.

[62] Hsain Z, Jiang Z, Pikul JH. Enabling effective electrochemical healing of structural steel. Multifunctional Materials 2021;4:024004. https://doi.org/10.1088/2399-7532/ABFB4F.

[63] Janak L, Singule V. Energy harvesting for aerospace: Application possibilities. Proceedings of the 16th International Conference on Mechatronics, Mechatronika 2014 2014:183–7. https://doi.org/10.1109/MECHATRONIKA.2014.7018256.

[64] Wang Y, Inman DJ. Simultaneous energy harvesting and gust alleviation for a multifunctional composite wing spar using reduced energy control via piezoceramics n.d. https://doi.org/10.1177/0021998312448677.

[65] Alsaadi A, Meredith J, Swait T, Curiel-Sosa JL, Jia Y, Hayes S. Structural health monitoring for woven fabric CFRP laminates. Compos B Eng 2019;174:107048. https://doi.org/10.1016/j.compositesb.2019.107048.

[66] Collinson M, Hayes S, Petropoulos S. The effect of type of mechanical processing on electrical conductivity and piezoresistive response of CNT and graphite composites. Procedia CIRP 2019;85:314–20. https://doi.org/10.1016/J.PROCIR.2019.10.001.

[67] Abdul Majit MR. Self Assembly of Curved Surfaces from Smart Composites for Small Unmanned Aerial Vehicles (SUAVs). UNIVERSITY OF CALIFORNIA, SAN DIEGO, 2016.

[68] Martin-Gallego M, Verdejo R, Gestos A, Lopez-Manchado MA, Guo Q. Morphology and mechanical properties of nanostructured thermoset/block copolymer blends with carbon nanoparticles. Compos Part A Appl Sci Manuf 2015;71:136–43. https://doi.org/10.1016/j.compositesa.2015.01.010.

[69] Goh PS, Ismail AF, Ng BC. Directional alignment of carbon nanotubes in polymer matrices: Contemporary approaches and future advances. Compos Part A Appl Sci Manuf 2014;56:103–26. https://doi.org/10.1016/J.COMPOSITESA.2013.10.001.

[70] Pastorino D, Lorenzo J Di, López-Romano B, Hadley P, Blanco TB. New Enhanced Acoustic Damping Composite Material for the Aeronautics Industry. I European Conference On Multifunctional Structures (EMuS2019), June, 11-12, 2019 2021. https://doi.org/10.23967/EMUS.2019.019.

[71] Lan X, Liu Y, Lv H, Wang X, Leng J, Du S. Fiber reinforced shape-memory polymer composite and its application in a deployable hinge. Smart Mater Struct 2009;18:024002. https://doi.org/10.1088/0964-1726/18/2/024002.

[72] Keller P, Lake M, Codell D, Barrett R, Taylor R, Schultz M. Development of Elastic Memory Composite Stiffeners for a Flexible Precision Reflector. 47th AIAA/ASME/ASCE/AHS/ASC Structures, Structural Dynamics, and Materials Conference, vol. 130, Reston, Virigina: American Institute of Aeronautics and Astronautics; 2006, p. 556. https://doi.org/10.2514/6.2006-2179.

[73] Kinloch IA, Suhr J, Lou J, Young RJ, Ajayan PM. Composites with carbon nanotubes and graphene: An outlook. Science (1979) 2018;362:547–53. https://doi.org/10.1126/SCIENCE.AAT7439.

[74] Gantayat S, Prusty G, Rout DR, Swain SK. Expanded graphite as a filler for epoxy matrix composites to improve their thermal, mechanical and electrical properties. New Carbon Materials 2015;30:432–7. https://doi.org/10.1016/S1872-5805(15)60200-1.

[75] Liu S, Chevali VS, Xu Z, Hui D, Wang H. A review of extending performance of epoxy resins using carbon nanomaterials. Compos B Eng 2018;136:197–214. https://doi.org/10.1016/j.compositesb.2017.08.020.

[76] Sixel W, Liu M, Nellis G, Sarlioglu B. Cooling of Windings in Electric Machines via 3-D Printed Heat Exchanger. IEEE Trans Ind Appl 2020;56:4718–26. https://doi.org/10.1109/TIA.2020.2997902.

[77] Kruželák J, Kvasničáková A, Hložeková K, Hudec I. Progress in polymers and polymer composites used as efficient materials for EMI shielding. Nanoscale Adv 2021;3:123–72. https://doi.org/10.1039/D0NA00760A.

[78] Gagné M, Therriault D. Lightning strike protection of composites. Progress in Aerospace Sciences 2014;64:1–16. https://doi.org/10.1016/j.paerosci.2013.07.002.

[79] Leem Y-C, Park JS, Kim JH, Myoung N, Yim S-Y, Jeong S, et al. Light-Emitting Diodes with Hierarchical and Multifunctional Surface Structures for High Light Extraction and an Antifouling Effect. Small 2016;12:161–8. https://doi.org/10.1002/SMLL.201502354.

[80] Senokos E, Ou Y, Torres JJ, Sket F, González C, Marcilla R, et al. Energy storage in structural composites by introducing CNT fiber/polymer electrolyte interleaves. Sci Rep 2018;8:3407. https://doi.org/10.1038/s41598-018-21829-5.

[81] Fredi G, Dorigato A, Fambri L, Pegoretti A. Multifunctional structural composites for thermal energy storage. Multifunctional Materials 2020;3:042001. https://doi.org/10.1088/2399-7532/ABC60C.

[82] Hatti-Kaul R, Nilsson LJ, Zhang B, Rehnberg N, Lundmark S. Designing Biobased Recyclable Polymers for Plastics. Trends Biotechnol 2020;38:50–67. https://doi.org/10.1016/J.TIBTECH.2019.04.011.

[83] Fouad D, Farag M. Design for Sustainability with Biodegradable Composites. Design and Manufacturing 2019. https://doi.org/10.5772/INTECHOPEN.88425.

[84] Tanaka M, Sato K, Kitakami E, Kobayashi S, Hoshiba T, Fukushima K. Design of biocompatible and biodegradable polymers based on intermediate water concept. Polym J 2015;47:114–21. https://doi.org/10.1038/pj.2014.129.

[85] Bourbigot S, Wang Y-Z, Hu Y, Song P. Preface for special issue 'Composites part B': Flame retardants and flame-retardant polymers/composites. Compos B Eng 2020;197:108191. https://doi.org/10.1016/j.compositesb.2020.108191.

[86] Lee S, Seong H, Im SG, Moon H, Yoo S. Organic flash memory on various flexible substrates for foldable and disposable electronics. Nat Commun 2017;8:725. https://doi.org/10.1038/s41467-017-00805-z.

[87] Biggs J, Myers J, Kufel J, Ozer E, Craske S, Sou A, et al. A natively flexible 32-bit Arm microprocessor. Nature 2021;595. https://doi.org/10.1038/s41586-021-03625-w.

[88] Ponnamma D, Yin Y, Salim N, Parameswaranpillai J, Thomas S, Hameed N. Recent progress and multifunctional applications of 3D printed graphene nanocomposites. Compos B Eng 2021;204:108493. https://doi.org/10.1016/J.COMPOSITESB.2020.108493.

[89] Bekas DG, Hou Y, Liu Y, Panesar A. 3D printing to enable multifunctionality in polymer-based composites: A review. Compos B Eng 2019;179:107540. https://doi.org/10.1016/J.COMPOSITESB.2019.107540.

[90] Use of Lightweight Material Technology — BAC n.d. https://www.bac-mono.com/lightweight-material-technology (accessed July 19, 2021).

[91] Rebound Resin: A Production-Ready Elastic 3D Printing Material n.d. https://formlabs.com/uk/materials/rebound/ (accessed July 19, 2021).

[92] Ladpli P, Nardari R, Kopsaftopoulos F, Wang Y, Chang F-K. Design of Multifunctional Structural Batteries with Health Monitoring Capabilities. 8th European Workshop on Structural Health Monitoring, 2016.

[93] Adam TJ, Liao G, Petersen J, Geier S, Finke B, Wierach P, et al. Multifunctional composites for future energy storage in aerospace structures. Energies (Basel) 2018;11. https://doi.org/10.3390/en11020335.

[94] Projects | Research groups | Imperial College London n.d. https://www.imperial.ac.uk/structural-power-composites/projects/ (accessed August 2, 2021).

[95] Tomorrow's Volvo car: body panels serve as the car battery - Volvo Car UK Media Newsroom n.d. https://www.media.volvocars.com/uk/en-gb/media/pressreleases/35026 (accessed August 2, 2021).

[96] SORCERER n.d. https://www.sorcerer.eu/ (accessed August 2, 2021).

[97] Asp LE, Johansson M, Lindbergh G, Xu J, Zenkert D. Structural battery composites: a review. Functional Composites and Structures 2019;1:042001. https://doi.org/10.1088/2631-6331/ab5571.

[98] Zeng W, Tao X-M, Chen S, Shang S, Lai Wah Chan H, Hong Choy S. Title: Highly durable all-fi ber nanogenerator for mechanical energy harvesting Highly durable all-fiber nanogenerator for mechanical energy harvesting †. Energy Environ Sci 2013. https://doi.org/10.1039/c3ee41063c.

[99] Alsaadi A, Shi Y, Pan L, Tao J, Jia Y. Vibration energy harvesting of multifunctional carbon fibre composite laminate structures. Compos Sci Technol 2019;178:1–10. https://doi.org/10.1016/J.COMPSCITECH.2019.04.020.

[100] MacroFiberComposite™ n.d. https://www.smart-material.com/MFC-product-mainV2.html (accessed August 4, 2021).

[101] Yan X, Courtney CR, Bowen CR, Gathercole N, Wen T, Jia Y, et al. In situ fabrication of carbon fibre–reinforced polymer composites with embedded piezoelectrics for inspection and energy harvesting applications. J Intell Mater Syst Struct 2020;31:1910–9. https://doi.org/10.1177/1045389X20942315.

[102] Liu Y, Du S, Micallef C, Jia Y, Shi Y, Hughes DJ. Optimisation and management of energy generated by a multifunctional MFC-integrated composite chassis for rail vehicles. Energies (Basel) 2020;13:1–18. https://doi.org/10.3390/en13112720.

[103] Jason Maung K, Hahn HT, Ju YS. Multifunctional integration of thin-film silicon solar cells on carbon-fiber-reinforced epoxy composites. Solar Energy 2010;84:450–8. https://doi.org/10.1016/j.solener.2010.01.002.

[104] Bishop JE, Smith JA, Lidzey DG. Development of Spray-Coated Perovskite Solar Cells. Cite This: ACS Appl Mater Interfaces 2020;12:48245. https://doi.org/10.1021/acsami.0c14540.

[105] Lin M, Chang FK. The manufacture of composite structures with a built-in network of piezoceramics. Compos Sci Technol 2002;62:919–39. https://doi.org/10.1016/S0266-3538(02)00007-6.

[106] Haywood J, Coverley PT, Staszewski WJ, Worden K. An automatic impact monitor for a composite panel employing smart sensor technology. Smart Mater Struct 2004;14:265. https://doi.org/10.1088/0964-1726/14/1/027.

[107] Giurgiutiu V. Structural Damage Detection with Piezoelectric Wafer Active Sensors. J Phys Conf Ser 2011;305:012123. https://doi.org/10.1088/1742-6596/305/1/012123.

[108] McDonald SA, Coban SB, Sottos NR, Withers PJ. Tracking capsule activation and crack healing in a microcapsule-based self-healing polymer. Sci Rep 2019;9:17773. https://doi.org/10.1038/s41598-019-54242-7.

[109] Chen C, Peters K, Li Y, Williams HR, Trask RS, Bond IP. Self-healing sandwich structures incorporating an interfacial layer with vascular network. MATERIALS AND STRUCTURES Smart Mater Struct 2007;16:1198–207. https://doi.org/10.1088/0964-1726/16/4/031.

[110] Shields Y, De Belie N, Jefferson A, Van Tittelboom K. A review of vascular networks for self-healing applications. Smart Mater Struct 2021;30:063001. https://doi.org/10.1088/1361-665X/abf41d.

[111] Guadagno L, Vertuccio L, Naddeo C, Calabrese E, Barra G, Raimondo M, et al. Self-healing epoxy nanocomposites via reversible hydrogen bonding. Compos B Eng 2019;157:1–13. https://doi.org/10.1016/J.COMPOSITESB.2018.08.082.

[112] Hayes SA, Jones FR, Marshiya K, Zhang W. A self-healing thermosetting composite material. Compos Part A Appl Sci Manuf 2007;38:1116–20. https://doi.org/10.1016/j.compositesa.2006.06.008.

[113] Sun J, Guan Q, Liu Y, Leng J. Morphing aircraft based on smart materials and structures: A state-of-the-art review. J Intell Mater Syst Struct 2016;27:2289–312. https://doi.org/10.1177/1045389X16629569.

[114] Calkins FT, Mabe JH, Butler GW. Boeing's variable geometry chevron: morphing aerospace structures for jet noise reduction. In: White E V., editor. Smart Structures and Materials 2006: Industrial and Commercial Applications of Smart Structures Technologies, vol. 6171, 2006, p. 61710O. https://doi.org/10.1117/12.659664.

[115] Costanza G, Tata ME. Shape Memory Alloys for Aerospace, Recent Developments, and New Applications: A Short Review. Materials 2020;13:1856. https://doi.org/10.3390/ma13081856.

[116] Li F, Liu Y, Leng J. Progress of shape memory polymers and their composites in aerospace applications. Smart Mater Struct 2019;28:103003. https://doi.org/10.1088/1361-665X/ab3d5f.

[117] Li F, Liu L, Lan X, Pan C, Liu Y, Leng J, et al. Ground and geostationary orbital qualification of a sunlight-stimulated substrate based on shape memory polymer composite. Smart Mater Struct 2019;28:075023. https://doi.org/10.1088/1361-665X/AB18B7.

[118] Todoroki A, Omagari K, Shimamura Y, Kobayashi H. Matrix crack detection of CFRP using electrical resistance change with integrated surface probes. Compos Sci Technol 2006;66:1539–45. https://doi.org/10.1016/j.compscitech.2005.11.029.

[119] Polimeno U, Meo M. Detecting barely visible impact damage detection on aircraft composites structures. Compos Struct 2009. https://doi.org/10.1016/j.compstruct.2009.04.014.

[120] Mitrovic M. Effect of loading parameters on the fatigue behavior of impact damaged composite laminates. Compos Sci Technol 1999;59:2059–78. https://doi.org/10.1016/S0266-3538(99)00061-5.

[121] Dubinskii S, Fedulov B, Feygenbaum Y, Gvozdev S, Metelkin E. Experimental evaluation of surface damage relaxation effect in carbon-fiber reinforced epoxy panels impacted into stringer. Compos B Eng 2019. https://doi.org/10.1016/j.compositesb.2019.107258.

[122] Sause MGR. INVESTIGATION OF PENCIL-LEAD BREAKS AS ACOUSTIC EMISSION SOURCES. J Acoustic Emission 2011;29:184.

[123] Mustapha S, Lu Y, Ng C-T, Malinowski P. Sensor Networks for Structures Health Monitoring: Placement, Implementations, and Challenges—A Review. Vibration 2021;4:551–84. https://doi.org/10.3390/vibration4030033.

[124] Qing XP, Wu Z, Yuan S. Current Aerospace Applications of Structural Health Monitoring in China. Proceedings of the 6th European Workshop on Structural Health Monitoring 2012:1–9.

[125] Güemes A, Fernandez-Lopez A, Pozo AR, Sierra-Pérez J. Structural health monitoring for advanced composite structures: A review. Journal of Composites Science 2020;4. https://doi.org/10.3390/jcs4010013.

[126] 3.5 Display Formats | Olympus IMS n.d. https://www.olympus-ims.com/en/ndt-tutorials/flaw-detection/display-formats/ (accessed October 22, 2023).

[127] Inspection of Composites - TWI n.d. https://www.twi-global.com/what-we-do/services-and-support/asset-management/inspection-of-composites (accessed October 29, 2019).

[128] Ceysson O, Salvia M, Vincent L. Damage mechanisms characterisation of carbon fibre/epoxy composite laminates by both electrical resistance measurements and acoustic emission analysis. Scr Mater 1996;34:1273–80. https://doi.org/10.1016/1359-6462(95)00638-9.

[129] Chung DDL. A review of multifunctional polymer-matrix structural composites. Compos B Eng 2019;160:644–60. https://doi.org/10.1016/j.compositesb.2018.12.117.

[130] Obitayo W, Liu T. A Review: Carbon Nanotube-Based Piezoresistive Strain Sensors. J Sens 2012;2012:15. https://doi.org/10.1155/2012/652438.

[131] Chung DDL. Damage detection using self-sensing concepts. Proc Inst Mech Eng G J Aerosp Eng 2007;221:509–20. https://doi.org/10.1243/09544100JAERO203.

[132] Alsaadi A, Meredith J, Swait T, Curiel-Sosa JL, Hayes S. Damage detection and location in woven fabric CFRP laminate panels. Compos Struct 2019;220:168–78. https://doi.org/10.1016/j.compstruct.2019.03.087.

[133] Nonn S, Schagerl M, Zhao Y, Gschossmann S, Kralovec C. Application of electrical impedance tomography to an anisotropic carbon fiber-reinforced polymer composite laminate for damage localization. Compos Sci Technol 2018;160:231–6. https://doi.org/10.1016/j.compscitech.2018.03.031.

[134] Schueler R, Joshi SP, Schulte K. Damage detection in CFRP by electrical conductivity mapping. Compos Sci Technol 2001;61:921–30. https://doi.org/10.1016/S0266-3538(00)00178-0.

[135] Baltopoulos A, Polydorides N, Pambaguian L, Vavouliotis A, Kostopoulos V. Damage identification in carbon fiber reinforced polymer plates using electrical resistance tomography mapping. J Compos Mater 2013;47:3285–301. https://doi.org/10.1177/0021998312464079.

[136] Baltopoulos A, Polydorides N, Pambaguian L, Vavouliotis A, Kostopoulos V. Exploiting carbon nanotube networks for damage assessment of fiber reinforced composites. Compos B Eng 2015;76:149–58. https://doi.org/10.1016/j.compositesb.2015.02.022.

[137] Adler A, Lionheart WRB. Uses and abuses of EIDORS: An extensible software base for EIT. n.d.

3. Novel composite curing methods for sustainable manufacture: A review

Composites Part C: Open Access

Volume 9, October 2022, 100293

https://doi.org/10.1016/j.jcomc.2022.100293

M.G. Collinson[1], M.P. Bower[1], T.Swait[1], C.P. Atkins[1], S.A. Hayes[2], B. Nuhiji[1]

[1] University of Sheffield Advanced Manufacturing Research Centre, AMP, Wallis Way, Rotherham, S60 5TZ

[2] Department of Multidisciplinary Engineering Education, University of Sheffield, 32 Leavygreave Road, Sheffield, S3 7RD

3.1. Author declaration, background and reflection

This paper is a review on novel curing methods, primarily for rapid heating and curing of composites, however as knowledge developed and attitudes changed over the period of the COVID 19 pandemic, it was realised that these methods had great benefit to the sustainability of curing composites. This was the reason it was submitted to Composites Part C: Open Access, which covers the topics of sustainable composites and multi-functional composites.

As the first author, I conceptualised, authored, and edited the paper, with particular emphasis on the Joule heating composites, whilst ensuring to provide a balanced review of the curing methods covered. Figure 1 was a concept by Tim Swait, which I then adapted and improved for the submission. Matthew Bower and Betime Nuhiji were responsible for the microwave curing section, with Matthew also contributing to the RF curing section. Craig Atkins was responsible for the section on magnetic induction for curing and bonding. Betime Nuhiji, Tim Swait and Simon Hayes provided supervision throughout and reviewed the paper before submission. I was responsible for submission and responding to the peer review process.

Composites Part C: Open Access 9 (2022) 100293

Contents lists available at ScienceDirect

Composites Part C: Open Access

journal homepage: www.sciencedirect.com/journal/composites-part-c-open-access

Novel composite curing methods for sustainable manufacture: A review

MG Collinson [a,*], MP Bower [a], T J Swait [a], CP Atkins [a], SA Hayes [b], B Nuhiji [a]

[a] University of Sheffield Advanced Manufacturing Research Centre, AMP, Wallis Way, Rotherham, S60 5TZ, United Kingdom
[b] Department of Multidisciplinary Engineering Education, University of Sheffield, 32 Leavygreave Road, Sheffield, S3 7RD, United Kingdom

ARTICLE INFO

Keywords:
Carbon fibre composites
Rapid cure
Electromagnetic radiation
Joule effect
Review
Low power

ABSTRACT

The curing of high-performance carbon fibre composites has not changed significantly since their inception, primarily using ovens and autoclaves. To reduce energy costs and continue to increase throughput, alternative novel curing methods that heat the components more directly by not relying on convection or conduction have been investigated frequently, at varying levels of success and scale. This paper critically reviews direct electric, microwave, induction, and radio frequency heating for their manufacturing and engineering applicability, overall energy consumption and evaluation of future challenges and opportunities for these methods in industry. It highlights some of the benefits such as high heating rates, ability to control exothermic reactions effectively and low power consumption, as well as some of the remaining challenges to common adoption, such as uniform degree of cure and ease of use.

1. Introduction

The use of composites in the aerospace and automotive industries is becoming increasingly prevalent, due to their high specific stiffness and strength [1]. They however are limited to high value industries due to their relatively high cost of raw materials and manufacture. International legislative measures aimed at achieving carbon neutral growth from 2020 onwards has driven the necessity of light-weighting vehicles to reduce carbon emissions [2,3]. This has led to greater utilisation and investment in composite materials, particularly in the transportation sectors of aerospace and automotive [4,5]. This increase of interest in harmful emissions has led to increased scrutiny of the emissions of the manufacturing processes associated with these weight saving materials.

Manufacture of the raw materials has the highest energy cost, with carbon fibres (CF) requiring 183-286 MJ/kg, epoxy resin 76-80 MJ/kg and pre-preg process 40 MJ/kg. This can mean in the worst-case scenario, 1 kg of CF could have an energy footprint of at least 223 MJ/kg before it has been cured [6]. Autoclave cure has been estimated to be around 20-22 MJ/kg [7], which accounts for less than 10 % of the total energy consumed in the manufacturing process up until this point. However, it is still important to remove energy intensive processes from the supply chain where possible.

Despite the through-life energy savings of a lightweight component [8], the total embodied energy can have a costly environmental impact [9,10], and significantly reduce the previously gained in-service benefits.

To improve the energy efficiency during composites manufacturing, alternative cure methods that can deliver power directly to the composite need to be considered. Example methods that are covered in this study include microwave (MW), magnetic induction, radio frequency (RF) and direct electric cure (EC) [11]. Novel curing methods are experimental and have challenges to overcome before implementation [12,13]. Many of these methods rely on the composite exhibiting electrically conductive and Electromagnetic (EM) susceptible properties to generate heat within the part. This method of heating from inside of the composite can be described as volumetric heating or inverse thermal gradient curing. Carbon fibre reinforced polymers (CFRP) exhibit non-isotropic electrical performance due to the contrast in conductivity between the conductive CFs and an insulating matrix. This can cause uneven heating patterns using these methods [14–16]. These properties can contribute to uncontrolled heating modes and therefore uneven degree of cure (DoC) across a component. Other issues include the difficulty of setup over existing methods, not being universally compatible with all geometries due to lower technology readiness level (TRL) [17] and are not yet turnkey solutions.

All these heating methods have challenges to their implementation, which if these can be overcome, can provide significant benefits over existing manufacturing methods. These benefits include lower power requirements, higher heating rates for reduced cure times, and the flexibility to deliver energy to a targeted location in the component [14].

* Corresponding author.
E-mail address: m.collinson@amrc.co.uk (M. Collinson).

https://doi.org/10.1016/j.jcomc.2022.100293
Received 25 April 2022; Received in revised form 27 June 2022; Accepted 27 June 2022
Available online 3 July 2022

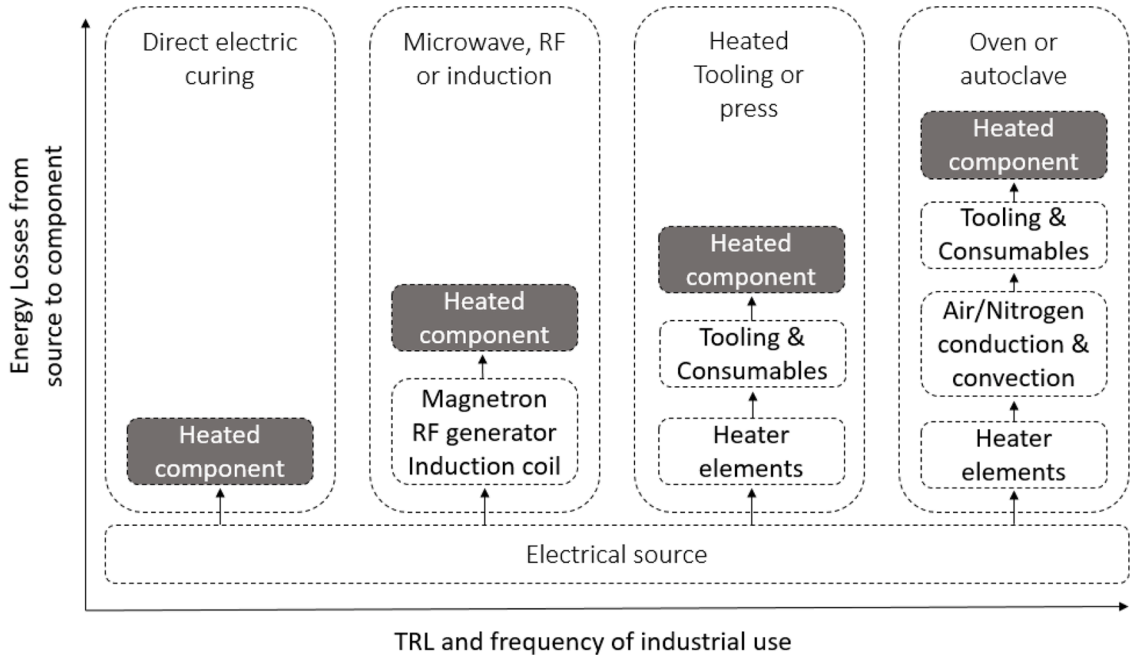

Fig. 1. Diagram to illustrate the energy flow in existing and new composite manufacturing processes, demonstrating the high losses in existing processes and the opportunity provided by novel cure methods.

This is in comparison to autoclaves and ovens that have large thermal masses and slow ramp rates, which add to energy consumption, time and cost during production [18].

This paper reviews the state-of-the-art for novel composite heating and curing methods, outlining their heating performance, practical considerations for manufacturing and overall energy efficiency. Current performance, challenges and potential future opportunities for implementing these curing methods are reviewed, considering existing manufacturing methods, materials and specific end-use cases.

1.1. Curing of composites

To compare novel heating and curing systems, the heating response of the composites being manufactured needs to be understood. Epoxy resins are the primary system covered in this review, as high temperature and/or pressure processes are required to achieve high mechanical performance. External thermal input is necessary to:

- Reduce viscosity of the resin;
  - to ensure full wet-out and adhesion to reinforcement
  - to allow voids to exit
  - to allow the resin to flow out of the part and increase the fibre volume fraction
- Ensure crosslinking occurs and the gel point is reached
- Accelerate crosslinking and therefore reduce cure duration
- Raise the glass transition temperature to the level required [19]

Conventional heating is supplied by convection in an oven or autoclave, which has the advantage of applying homogenous temperature to the component. Most composite matrices, from polyester resins for low cost and performance composites, to epoxy resins for higher performance, cure in an exothermic manner [20].

The primary matrix material discussed in this review is epoxy resin, which can have a wide variety of properties depending on the use case, before and after cure. If formulated for an adhesive, it can come as a film, or as a paste with a viscosity as high as 700 Pa/s. As a matrix for carbon and glass fibre composites, it can range from 20,000 Pa/s for vacuum assisted resin transfer moulding resins, or 1200 Pa/s for use in filament winding applications [21]. Glass transition and service temperatures of these resins depend on the final use case requirements, automotive resins can reach up to 130°C, with aerospace resins reaching up to 200°C.

In minor cases of exothermic reactions, local areas can be overheated, leading to residual stresses within the part [22–24]. Failure to control the heating rates, and thus achieve the required structural performance can lead to premature part failure [25]. In extreme cases, the resin can self-ignite, damaging the component, and potentially the tooling and associated curing equipment, in addition to releasing toxic smoke [26].

To ensure that uncontrollable exothermic reactions do not occur, reducing ramp rates up to the final cure temperature, and increasing dwell times are common strategies. If a composite is made thicker or has a reactive resin, then the heating rates will need to be reduced further and dwells made longer [27], to reduce the exothermic peak. Resin and pre-preg manufacturers have to therefore account for a large range of composite geometries consisting of thick ply composites, thicker than 12 mm, in less-than-optimal cure environments (i.e. tooling with low heat transfer coefficient, and convective heating hotspots).

A homogenous DoC is desirable to achieve consistent mechanical properties but to maintain costs manufacturers require this to be achieved in the shortest time possible [28], which works against the desire to avoid exothermic reactions. An issue for ovens and autoclaves is that even if the air temperature is controlled from the component temperature, due to the high thermal mass of the internal cavities, the component temperature cannot be controlled quickly enough to stop an exothermic reaction [29]. With these novel curing technologies, the power input to the reaction can be instantaneously switched off, leading to a greater degree of control over the cure. This allows increased protection against exothermic reactions and enables greater control for reactive or predictive control cure cycles to be used.

1.2. Introduction to novel curing methods

Cure cycles defined by resin and pre-impregnated composite manufacturers are significantly longer than is required for many components, resulting in energy inefficiencies [30]. Fig. 1 illustrates the method by

Table 1
Overview of cure methods reviewed here, their pros and cons, and references to previous studies on these heating methods.

Heating type	Advantages	Challenges	Reference
MW	• Energy efficient heating process • Non-contact method • Heat generated within the component	• Arcing, localised heating and burning can occur • Particular health and safety requirements • Requires compatible consumables • Potential high capital cost of commercial MWs	[15,16,31, 33–36, 53–74]
Electric Cure	• Energy efficient heating process • Lower void content and higher flexural modulus components	• Requires electrode contact on, or within the component • Electrically insulated tooling required • Specific component setup required • Localised heating and burning can occur	[14,32,37, 38,75–89]
RF	• High energy efficiency	• Large knowledge gap concerning composites	[49,90,91]
Induction	• High heating rates • Not RF based so low health and safety requirements	• Specific coil design required for each heating pattern/ component geometry • Inductor coil must be close to the heating area	[51, 92–103]

which electrical energy is converted to thermal energy for a variety of traditional, emerging and novel composite manufacturing techniques. Oven and autoclave are the least direct methods, with heated presses improving on these, with respect to energy efficiency per part. The stage of development of these technologies is also reflected in the TRL used to determine a technologies state of development and use in manufacturing environments.

Novel curing methods can be characterised as using heating methods that bypass, or significantly reduce, convective and conductive heating. These methods have the potential to achieve greater manufacturing energy efficiency, a higher degree of control and therefore the ability to cure composite components quicker leading to further energy savings. Other specific benefits can include;

- MW cure - the ability to only cure certain areas on a part [31],
- Direct electric cure - to produce overall lower void content composites [14] and
- Induction cure - the ability to heat at hundreds of degrees per minute [32]

These technologies can have unique advantages over conductive heating methods, resulting in substantial research in this area [11,14,15, 31–39], (summarised in Table 1). Widespread adoption within industry is limited due to significant technical challenges that have not yet been solved, where turnkey solutions are required. A summary of the advantages over cure methods and current challenges for each heating method can be found in Table 1.

Other heating technologies can provide some of the previously described benefits to composite manufacturing, such as Infra-red (IR) [40,41], laser [42] and flash lamp systems. These technologies only heat a very specific area and need to be combined with other automated technologies such as Automated Fibre Placement (AFP) [43] or filament winding [44] to realise their potential. They are used as a preheating technology for single plies as they are only able to heat the surface. In the cases of laser and flash lamp systems, they are only able to heat in a very localised area, i.e. not the bulk component, and can be prohibitively expensive to acquire.

Other bulk curing technologies have also been discounted as a part of this review, such as Ultraviolet (UV) curing and frontal polymerisation. UV curing requires specific resins that can be polymerised by UV radiation. For this reason, they can be cured at low temperatures and be cured rapidly under the correct conditions. Common use cases in the composites industry are filament winding and gel coats, due to UV requiring line of sight and having limited depth penetration [45] Frontal polymerisation is a very promising technology, as there is an opportunity to cure large volumes of composites with very little initial energy input, however there is little literature available on composite

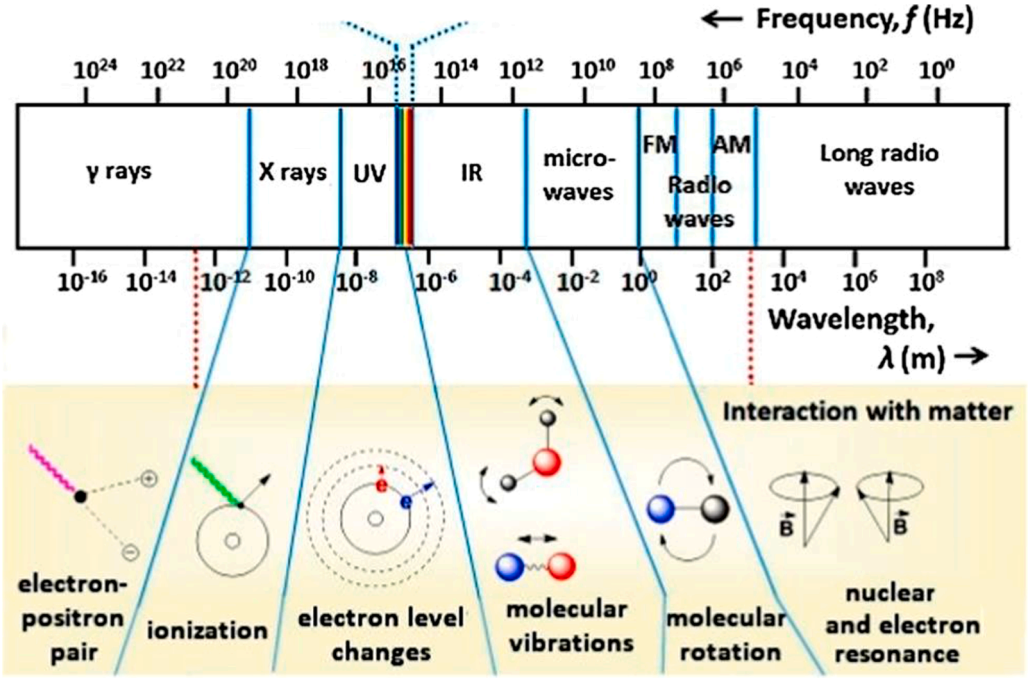

Fig. 2. - EM spectrum [52]

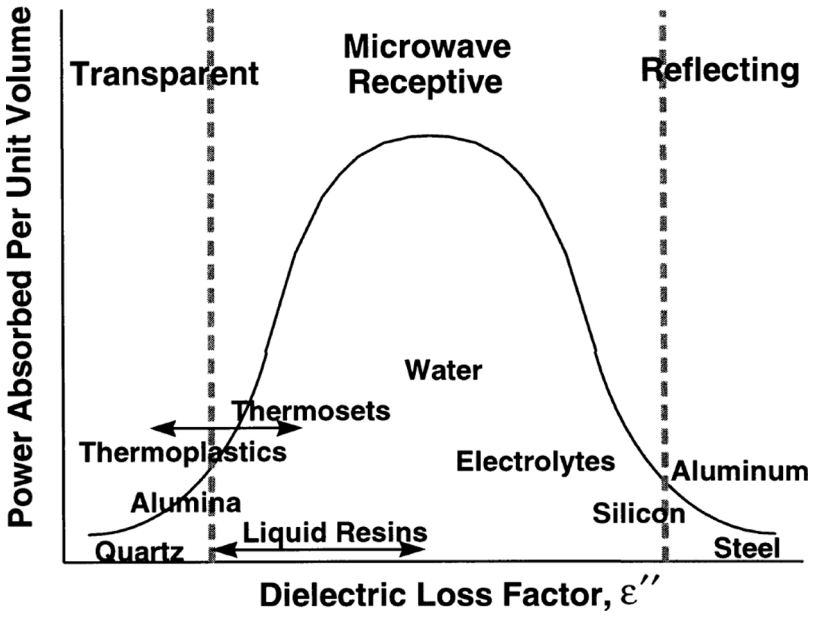

Fig. 3-. MW receptivity: The variation of power absorption as a function of dielectric loss factor (2.45 GHz) from the figure in Thostenson & Chou [69]

applications. Robertson et al [46] demonstrated resins suitable for frontal polymerisation in 3D printing and CF curing applications. With very little energy input, less than 20 W, it was possible to cure a 100 × 200 mm panel in less than 5 minutes with a polymerisation rate of 98 mm/min. Goli et al [47] modelled the frontal polymerisation effect on unidirectional (UD) composites, finding that increased fibre volume fraction increased the speed of the polymerisation front, also observed by Robertson et al. This was due to the thermal conductivity of the fibres assisting heat transfer over the composite. This research shows that frontal polymerisation is a promising curing technology, suited for composites, however, isn't yet commonly available.

1.3. Novel cure methods overview

There are two main ways that novel cure methods generate heat within a composite:

1 by the absorption of EM radiation - MW, RF and IR energy are all on the EM spectrum (Fig. 2) and are generated by passing alternating current along a conductive material, which can be in the form of a magnetron for MW [48], field applicator for RF [49] or lamp for IR [50].
2 by generating electron movement to induce the joule effect - Induction heating uses an alternating current to generate a local EM field which induces a flow of electrons in a material [51]. Like induction, direct electric cure relies on the movement of electrons to generate heat, although it is applied directly through contact electrodes. This movement of electrons induces the Ohmic heating effect, or Joule effect within the fibres, allowing for the composite to be cured.

An overview of all the cure methods covered in this paper is outlined in Table 1, summarising their advantages and disadvantages with respect to their practical implementation in industry, TRL and part quality.

2. Novel cure methods review

In the following sections is an in-depth review of the novel cure methods identified in Table 1.

2.1. MW curing

2.1.1. Background to MW processing

MW curing of polymer matrix composites is a method of heating composite materials using EM radiation in the MW spectrum [53,104]. The early research into curing composite materials using EM radiation found that cure cycles could be reduced and optimised for MW curing applications [54,55,104]. The reduction in cycle time was attributed to the volumetric nature of MW heating. Lee and Springer [53] particularly focused on creating a model of the curing process which captures the temperature distribution, resin viscosity and fibres. Using these inputs, the DoC of the resin, the void content and residual stresses were calculated and experimentally validated. The study uses an experimental methodology to validate these findings. This early work shows the importance of understanding material properties when MW processing materials. Lee and Springer list several key parameters: Dielectric constants, thermal conductivity and DoC as a function of temperature.

Thostenson and Chou [69] presented a detailed review of previous MW processing literature. They state that the MW field and dielectric response of a material is critical to the ability to heat using MW power. Therefore, understanding the dielectric response of materials is required to optimise the heating process [65]. The key points highlighted by the authors include:

1 When materials are incident to MW radiation but have different dielectric properties. The MWs will selectively couple with the higher loss material.
2 Non-uniformity within the EM field will result in non-uniform heating. This point is important for closed-cavity systems where standing waves are generated due to constructive and destructive interference.
3 Dielectric properties change with temperature, therefore the ability of MW's to generate heat varies during the curing process.

Fig. 3 is a graphic representation of how the dielectric loss factor affects power absorption. It shows how power is absorbed in a material as a function of the dielectric loss factor at a particular frequency. The dielectric loss factor forms an upper and lower bound on power absorption in a material through two different mechanisms: transparency and reflectance. A material is transparent when incident EM radiation passes through the material with little to no absorption which occurs in

materials with a low dielectric loss factor. Conversely, a material is reflective when incident EM radiation is reflected off the surface of the material before being absorbed. This phenomenon is most prominent in materials with high dielectric loss factors.

The authors also detail an equation for power absorption per unit volume [69]:

$$P = 2\pi f \varepsilon'' E^2 \quad (1)$$

where P is the power (W), f is the frequency (Hz) of the EM radiation, ε'' is the dielectric constant and E is the EM field strength (V/m).

However, as the energy is absorbed into the material, the electrical field strength reduces. Therefore, a penetration depth can be defined, which is linked to a reduction in power in the material by 1/e (Euler's number) compared to the surface power [69]:

$$d = \frac{c\varepsilon^0}{2\pi f \varepsilon''} \quad (2)$$

where d is the penetration depth (m), c is the speed of light in a vacuum (m/s) and ε^0 is the dielectric constant of free space. Power absorption is also affected by penetration depth, exponentially decaying via the following relationship [105]

$$P(x) = P_0 e^{-2\alpha x} \quad (3)$$

Where P(x) is power dissipated at depth x, P_0 is the power at the surface and α is the attenuation constant, which is a function of wavelength (m), loss tangent and relative dielectric constant. It is noted that Eqs. 1-3 do not include magnetic losses.

These two equations highlight the importance of understanding the material properties of the composite, as the power absorption and penetration of the MWs are heavily dependent on the dielectric loss factor.

2.1.2. MW processing of composite materials

A summary of some of the key experimental MW studies covered in this review are in Table 1. This review mainly covers thermosets, however a review and comparisons of thermoplastic and thermoset MW processing was published by Naik et al [106].

Mishra and Sharma [109] conducted a detailed review of the MW heating phenomena in a variety of materials including polymer composites. The authors highlighted the difference in heating mechanics relating to the fibre type. In low conductivity fibres (such as glass or aramids), the heating mechanism is dominated by the resin system. However, many resin systems have low dielectric loss factors meaning the heating rate of the cure will be reduced. Alternatively, fibres with high conductivity (such as CFs) absorb the MW radiation rapidly and heat quickly. This phenomenon is less understood, but the authors speculate that the alternating EM field induces an electric current into the fibres. The fibres then heat due to the Joule heating effect.

Kwak et al [56–58] detail the potential advantages of MW curing of composites: rapid heating, volumetric heating, selective heating, self-limiting properties, and reduction in non-conforming parts. The authors discuss the main issues of MW processing including inhomogeneous energy distribution, arcing, tooling design and understanding of the 'MW effect' that improves interfacial bonding and glass transition temperatures. Kwak emphasises the importance of the dielectric properties on the MW curing process and reviews how the dielectric material response is dependent on several variables:

- Dielectrics as a function of frequency: The dielectric response varies as a function of frequency [110]. Materials peak at a dielectric resonance at a specific frequency. Therefore, to maximise MW heating the appropriate frequency should be selected (i.e. water resonance at 2.45 GHz).
- Dielectrics as a function of the DoC [111]: As the resin system begins to cure, the dipolar molecules are restricted, and this can reduce the dielectric heating effect of the MW.

The key aspects of MW curing that need to be explored further are: characterisation and material properties, specific tooling, process control and simulation.

Xuehong et al [60,61] conducted two cross-platform studies into MW versus thermal curing. The study [60] found a reduction in the cycle time of 63 % using MW curing optimising the process by adjusting input power (W) and radiation time (s). The final void content and ILSS properties were also found to be equivalent between each platform. Xuehong et al [61] also found a significant increase in compressive strength of composites cured using MWs compared to autoclave cured equivalents. The improvement in compressive strength was attributed to the superior interfacial adhesion between fibres and resin, which was attributed to the volumetric heating, despite the higher porosity of these samples.

Papargyris and Day [62] used MW assisted RTM to achieve a 50% reduction in cycle time compared to the conventional curing process. The study found both processes produced similar flexural moduli and strength, with the ILSS of the MW cured composite outperforming the autoclave process by 5 MPa (9 % increase). However, Nightingale and Day [59] found a reduction in ILSS and flexural properties of MW produced composites. This finding was attributed to the high void content of MW cured composites (ranging from 9 – 19 %). The authors stated this was caused by a lack of consolidation and the void forming a crack initiation site.

Yusoff et al [63], compared MW RTM to conventional RTM. They found a reduction in cure cycle time (between 30 – 60 %) using the MW process however composites exhibited much higher void content. These findings suggest that the rapid curing process has reduced the time to allow volatiles to escape the resin, leading to voids being trapped.

Li et al [64] investigated the induced strains associated with thermal and MW curing on 'L-shaped' CF bismaleimide composites. The MW curing process led to reductions in cycle times and the DoC between the two platforms were equivalent. The MW cured composites recorded a low strain throughout the cure and therefore had less spring-back of the 'L-shape' once cured. Li et al associated this with CFs' high dielectric loss, indicating that the MW process heated the fibres directly. The surrounding resin is then heated through conduction leading to a coefficient of thermal expansion mismatch.

The literature relating to suitable tooling materials can be separated into laboratory and industrial scale materials. On the laboratory scale, glass quartz [65] and Polytetrafluoroethylene (PTFE) [53,62] are commonly used due to their low dielectric properties. By using low dielectric tooling, the MW can be absorbed by the polymer matrix composites thereby improving the curing efficiency. Although glass and PTFE are suitable for the laboratory scale, the materials cannot be used on the industrial scale due to their brittleness, poor machinability, and cost. The studies where large tools have been used are predominately flat plates of quartz glass in a highly controlled environment [66]. Metal tooling [56,57] has also been used for more complex tools but has the disadvantage of reflecting MW energy which can cause arcing. The metal tooling can also act as a heat sink that limits the heating of the composite component.

The literature about MW cured composites generally finds that properties are equivalent to conventional curing processes. However, it is difficult to compare as very few of the studies encompass all aspects of composite characterisation. Void content has been highlighted as critical to the performance of MW cured composites. For out-of-autoclave processes such as MW heating, void content is linked to the quality of the vacuum on the part. Hence, developing a consistent process is vital for the efficacy of the MW process.

Energy consumption of the microwaving of composites for curing has not been characterised fully yet. Many of the previous studies have

Fig. 4. - Vötsch MW system at the AMRC [112]

Fig. 5. - Robotic MW cell at AIMPLAS pilot plant developed during the WAVECOM project [71]

highlighted the opportunities to reduce the length of the cure cycle but have not yet linked directly to benefits in reduced energy consumption. Many papers indicate the maximum power of the magnetrons and indicate what power percentage levels they were used at during the cures, however, do not indicate total power usage. Thostenson and Chou [65] do briefly discuss power usage during a 3-hour cure, which is estimated to be 1.13 kW/hr. However, the dimensions of the component are not fully specified, which makes it difficult to compare against other curing methods.

2.1.3. MW curing methodologies and use cases

Numerous scientific publications have investigated MW curing of composites closed cavity magnetron systems, as discussed in section 2.1.2 [15,31,56,57,67,68]. The closed cavity MW systems consist of a sealed metallic chamber that contains any MW energy that is emitted into the chamber. The MWs are reflected off the cavity walls until they are either absorbed by the component or attenuated in the cavity. The MWs are generated using magnetrons and then transmitted towards the cavity using waveguides.

A commercially available industrial MW heating platform used throughout the field is the Vötsch HEPHAISTOS system (Fig. 4). The MW consists of a large closed hexagonal cavity and operates using a magnetron/ waveguide system [68].

Nuhiji et al and Green et al [15,31,67] used a Vötsch system to explore the control and temperature monitoring of MW processes. They modelled the MW system heating process and investigated novel tooling materials suited to MW processing. Of this research, the main highlight is the effectiveness of the MW curing processes and the potential energy savings available when upscaling the technology to within TRL 5 or 6.

Kwak et al [56,57] developed a dedicated composite manufacturing process using the Vötsch system and have created a consistent process method for manufacturing composites. The methodology developed enabled the measurement of MW penetration depth and the characterisation of composite properties. The composites produced were of equivalent quality to that expected of autoclave produced composites.

Kwak et al [58] also developed a closed cavity MW which included a pressure vessel. The system has 96 magnetrons supplying MWs at 2.45 GHz, however, limited information is published on this technology. Hang et al [70] developed a bespoke closed cavity octagonal MW to process polymer composites with a maximum power of 5 kW.

To summarise, the closed cavity MW systems reviewed present several limitations challenging the technology:

1 Fixed frequency and ‘closed cavity’ design: Despite the unique cavity designs, the MW system is still susceptible to the generation of standing waves. This causes inhomogeneous heating during the curing process, which can lead to poor part quality. This phenomenon is complex and based on the interaction between the MW frequency, composite materials, tooling, consumables, metallic trolley, and magnetron phase.
2 Cavity size: This can limit the part size and lead to batch processing, although is mitigated by the improved cycle times.
3 Arcing: Exposing the edges of conductive fibres to MW energy within the cavity can lead to issues with electrical discharge. This has the potential to damage the vacuum bag or component leading to scrapping of the part.

Concentrated efforts by industrial and academic consortiums have been made on the mounting of MW heating systems onto robotic arms

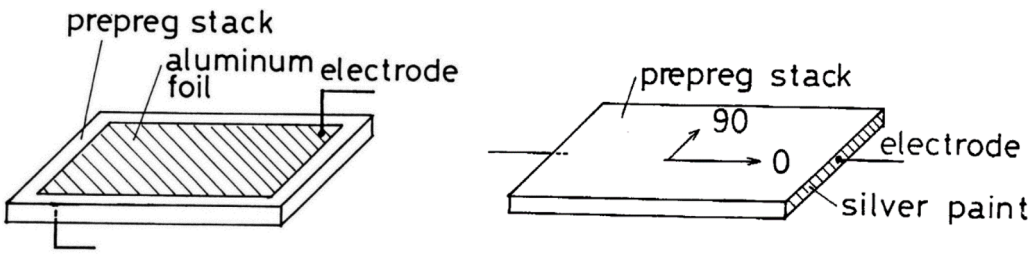

Fig. 6. Initial electrode positions identified by H. Fukuda [76] suitable for electric cure.

for localised heating of composites. Rudolf et al [113,114] developed a robotic arm MW system, alongside a resin functionalised suitable for MW energy absorption.

It reports that the MW system led to 'a strong improvement of degree of polymerisation' as tested using Differential scanning calorimetry (DSC) and highlights how a lightweight antenna system was developed to enable complex geometries of components.

E. Díaz et al investigated the use of MWs to cure composites with an integrated robotic system as part of the WAVECOM project [115]. They investigated susceptors to enhance absorption of MW radiation and monitored residual stresses and distortion using FBG during curing.

Trials were conducted using the robotic arm and a 2000 W magnetron (2.45 GHz). A cylindrical type antenna was used inside an isolated cell (Fig. 5), where susceptors improved the curing process and enhanced the degree of polymerisation [71]. Borrás et al. [116] highlight the improvements in heating efficiency by adding 1 % carbon nanotubes and identify how the dispersion of the nanotubes is vital to homogenising the heating pattern.

Zhou et al [107,108] used frequency-selective absorption films to generate heat in localised areas to enable easy to control zonal heating of composites. Films with absorption of 915 MHz and 2.45 GHz were used, alongside their respective MW sources at the same frequencies. This enabled the thermal control of two independent zones, allowing even temperature distribution in standard, or non-uniform thickness laminates.

Researchers have implemented MW heating in an RTM closed mould process [72]. The resin system is preheated (using MW heating) and injected into the mould cavity, the injected resin is then heated via a secondary MW source, to assist with issues with achieving homogenous heating in the tooling.

MW curing has the opportunity to be applied in a high range of applications that are currently served by autoclaves or ovens. The controllability of high heating rates shown in most studies allow for significant cycle time reduction and an increase in mechanical properties. Naik et al [106] discuss that these properties ensures that it is economically viable, particularly in aerospace. It will likely take industry a lot longer to adopt over existing methods due to cost and required technical know-how to ensure high quality parts are produced.

2.2. Direct electric curing

Direct electric cure uses the low electrical resistance of CF composites as the heating element through the exploitation of the Joule effect. In literature, this method has also been called Joule effect cure, electric heating and self-resistance curing. By running current through the fibres and inducing the Joule effect, the component itself acts as a heating element to cure the matrix. Epoxy matrices used in most studies reviewed are insulators [117], which therefore inhibits Joule heating by increasing the contact resistance between an electrode and the composite. Electrically conductive resins modified with nanoparticles to increase electrical conductivity are of interest in this area of research, discussed more generally in Section 3.3.

2.2.1. Background to Joule heating composites

When using CF, or a single tow bundle as a heating element, the fibre can act as a continuous resistor, and therefore heat is generated evenly along the length [77,80]. PolyAcryloNitrile (PAN) fibres have low electrical resistance due to the graphitic nature of the fibres, with a 12K tow having a resistance value of around 18 μΩ.m at 25°C. A reduction in resistance of 3.2 % can be observed as the temperature increases to 150°C [77]. This introduces a time dependency to the power requirements of this cure system.

In any long fibre carbon composite, conductivity is lower in-plane (along fibres), compared to through thickness [92]. Electron transfer is primarily in the fibre direction, 200x more than across the thickness of the fibre, and increases with fibre volume fraction [118]. Any fibre-to-fibre crossover has a very small contact area and will have matrix around it which is commonly dielectric [92], leading to high electrical resistance between fibre plies. Current applied through an electrode will only primarily heat the plies in direct contact, with the resistance between plies limiting electrode transfer and subsequent heating [119]. Contact resistance between the electrical source and the composite needs to be lower than the resistivity of the composite, or the electrical contacts will heat up at a higher rate than the composite itself. This limitation restricts electrode layouts for electric curing and further complicates Joule effect heating patterns.

Table 3 contains a summary of studies on direct electric cure, covering a range of manufacturing scenarios and applications specific to heating the manufactured component. Key electric curing parameters such as material type, electrode configuration and resulting heating performance are highlighted. As there is a large range of testing methods, material types and geometries, a summary of key results of the studies is presented, with respect to being a viable future manufacturing method.

2.2.2. Direct electric cure of composite materials

H Fukuda [76] was one of the first to introduce current into CF pre-preg stacks (TORAYCA P3060) to reach a curing temperature of 180°C. Through thickness and edge to edge were identified as electrode positions, seen in Fig. 6, which set out a standard and repeatable method for electric cure.

Heating of plies with through thickness electrodes provided poor temperature uniformity, of which an example can be seen in Fig. 9 (e). It was not used further in their study and has only been a suitable way to Joule heat in very specific cases, as demonstrated by Reese et al. in a modified industrial composite press on 3D woven architectures that had specific through thickness fibres [82].

Edge to edge curing of 150 mm x 50 mm, 16 ply stacks was more successful, reaching the desired cure temperature, however it was only monitored and controlled from one foil type thermocouple. These were compared to autoclave-manufactured samples, achieving around 78-90 % of the bending strength. It was observed that due to the low resistance of the fibres, the current required to reach 180°C was significant (~100 A) and the voltage less than 10 V, leading to a requirement of high current, low voltage power supply units for electric curing large geometry components.

C. Joseph et al [75] modified the edge-to-edge curing method, by

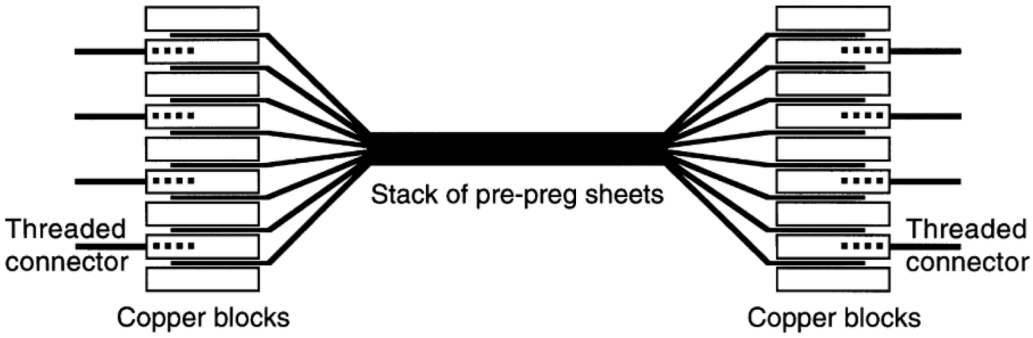

Fig. 7. Example setup used by C. Joseph et al [75], with individual ply pairs having dedicated electrodes.

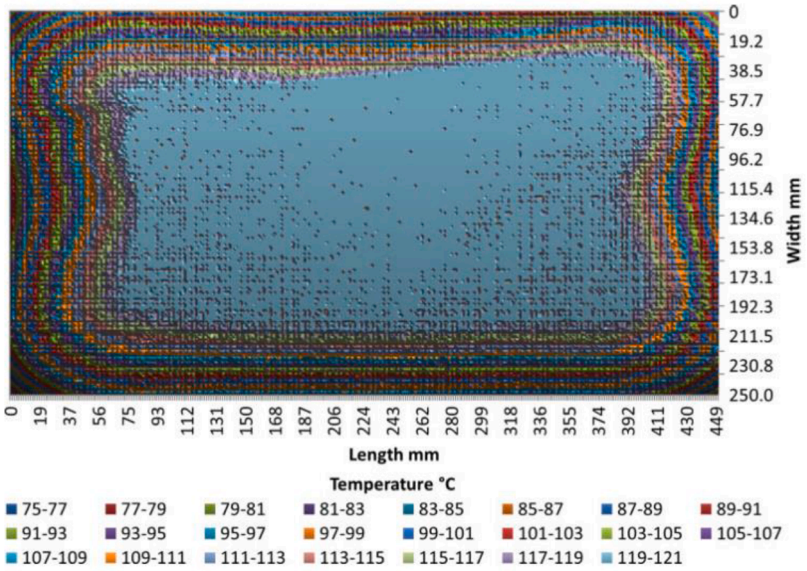

Fig. 8. Temperature distribution over a 450 × 250mm CFRP panel cured at 120°C [37]

consolidating the main curing area, whilst separating the 8 individual plies between copper blocks to reduce contact resistance, as seen in Fig. 7.

This experimental setup is impractical to repeat due to the complexity of applying electrodes to each ply and the cured sample size was comparatively small (60 mm x 30 mm). Tensile strain to break, and energy to break were higher than oven cured samples, 4.1% to 2.2% and 0.57 MJ^{-3} to 0.43 MJ^{-3}, respectively, suggesting the electrode setup could provide even heating and additional structural benefits to the composite.

Wellekotter and Bonten [83] investigated the effect of various electrical contact setups for the Joule heating of thermoplastic composites. A design of experiments (DOE) was completed, that found a larger contact area increased the performance of the heating process and part quality. Increasing contact force was also determined as a positive factor in the DOE, which is not possible without of autoclave methods, however, could be applied in specific cases, such as a mechanical press. Resistance welding of thermoplastic composites is more established and will have transferable methods to electric curing of composites [120], however, these are limited in scope and have moved towards metal mesh and nanocomposite heating elements providing better reproducibility and scaling [121].

2.2.3. *Evaluation against existing curing methods*

Y. Gu et al [38] investigated vacuum assisted resin infusion moulding heating methods, comparing oven, heated tooling, and internal resistive heating. Internal resistive heating provided the fastest heating rate (30°C/min), but also the highest temperature delta over the component (13°C) in comparison to heated tooling at 25°C/min with a 4°C difference and oven at 2°C/min and 0°C deltas. The importance of tooling materials was highlighted, and those manufactured with applicable thermal properties would assist in the temperature distribution of resistive heating. Athanasopoulos et al. [78] also compared electric cures in dry carbon infusion, pre-preg and oven samples, able to produce samples with the same DoC or more (±0.5%), and matching tensile properties. The tooling used was also specific for the process, being a thermally insulating glass fibre reinforced plastic (GFRP) on top of an aluminium plate, which assisted in the low temperature delta over the component.

Hayes et al. [37] investigated the effect of the geometry of the CFRP, the connector geometry and connector position on the heating homogeneity, the final mechanical properties and the cure percentage of the part. Flexural modulus and strength matched oven and autoclave samples, with the DoC between oven and autoclave at 97.2%. When applying current from edge to edge, the power requirement increased linearly to the distance between the connectors, whereas when increasing thickness by 2 plies, the average increase in power was 5%. This suggests that electric cure could be suited to highly energy efficient cures of thick ply composites.

Temperature distribution data over the panel was recorded, as seen in Fig. 8. It shows that when electrically curing a CFRP panel, most of the centre of the panel is at the desired cure temperature. The temperature

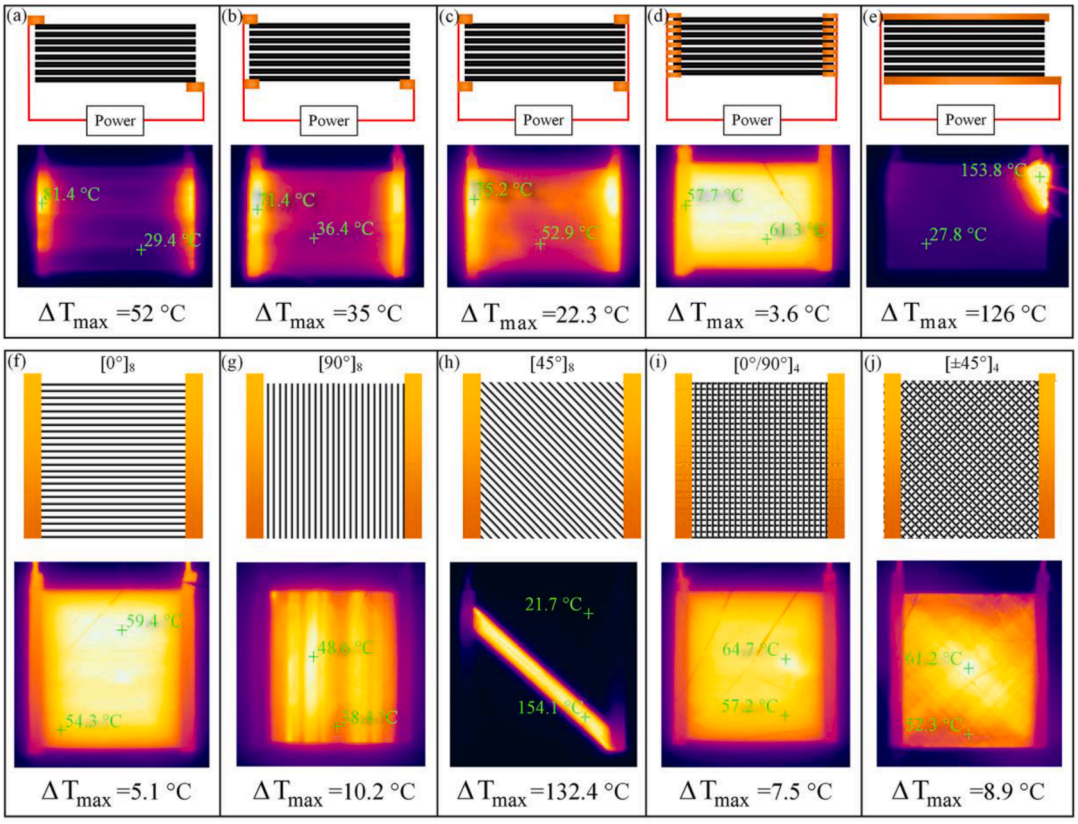

Fig. 9. Thermal images of different contact (a-e) and layup sequences (f-j) [14].

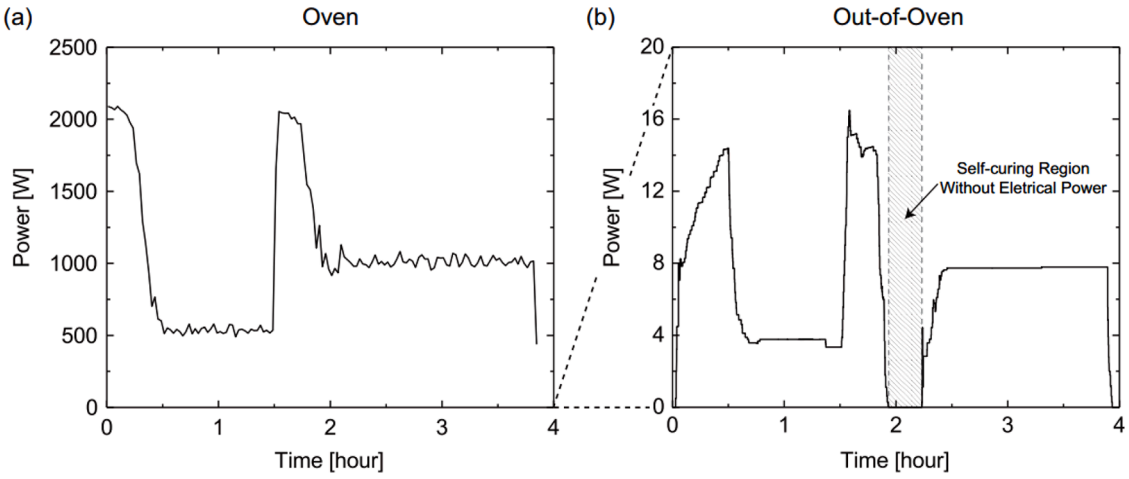

Fig. 10. Comparison of power consumption of a 160 ply (20 mm thick), 50 mm x 60 mm laminate via (a) oven curing and (b) direct electric curing. Note the differences in scale between the axes.[123]

starts to drop from around 20 mm from the edge, leading to around a 10°C reduction at the edges, which would lead to under cured areas.

Liu et al [14] investigated the electrical contact arrangements and positions, different fibre orientations and UD ply layups. Obtaining an even temperature distribution over the CFRP component is a crucial step in implementing this technology as a replacement for oven or autoclave. Edge to edge contact position within the ply layup was investigated (Fig. 9, a-e), and having the copper contacts placed between every ply reduced the contact resistance enough to not have a significant increase in temperature around these points.

Significantly the void content in the electrically cured components was consistently lower than the equivalent oven cured samples, as well as improved tensile strength and modulus. Comparisons were also made between different heating rates possible with this technology, namely 1, 3, 5, and 10°C/min, which showed if heated and therefore cured too quickly, the void content will increase significantly, as well as significant decreases in compressive strength.

2.2.4. *Specific manufacturing applications*

S.A. Sarles and D.J. Leo [81] investigated the possibility of using a continuous carbon tow to cure an inflatable structure, suitable for space applications. The cure temperature was consistent along the length (1.1°C root mean square), using thermocouples and a PI controller, which overcomes a significant challenge in joule heating of composites.

Optimised cure cycles were developed in this study, which achieved higher heating rates and shorter cure times, however, they did not consider the potential of uncontrolled exothermic reactions in thicker composites.

S.Liu et al [84] also developed a rapid composite repair system using the Joule effect to cure pre-preg patches onto CFRP components, removing the requirement for heated blankets. This had the advantage of being able to heat uniformly through the thickness of the patch, rather than conduction from the outer face of the component. The repair cure temperature was within ±5°C of the desired temperature, with void content being comparable to heater blanket repairs.

Robert et al [122] developed a novel towpregging line, using copper rollers as electrodes to Joule heat carbon tow to melt powder epoxy into the fibre. Power consumption was significantly lower than the equivalent IR lamp, whilst heating more uniformly. The resulting laminates manufactured matched or outperformed commercially available towpreg systems.

The sustainability of this method has been considered in more detail than other methods, as it is easier to monitor the power going directly into the cure, as it is commonly displayed using the power supplies used. Hayes et al detailed the effect of thickness and length increases on the power usage, which were both linear, with thickness having a lower impact on power usage than length. Jeonyoon Lee et al [79,123] directly compared a 160 ply, 50 mm x 60 mm panel cured in an oven and a joule heated CNT film which can be seen in Fig. 10.

This comparison is not completely representative, as it is heating a CNT film next to the component, and is deliberately a thick ply laminate, which appears to have exothermic runaway after the second ramp in the cure cycle, and exothermic results in no external power is required. C. Viney [75] noted the power requirement of the electric cure method compared to an oven was significantly reduced from 500 W maximum for an oven and 96 W for the electric cure method, with an 82% overall energy consumption reduction.

Joule effect curing has been shown to produce high quality composites at low cost, however, still has technical barriers to overcome to become widely adopted. The requirement of electrodes in a part means they have to be removed post cure, increasing costs, as well as the requirement of UD plies in the layup to obtain optimal temperature distribution. As mentioned in this section, there are some specific use cases where it very well suited such as patch repair, inflatable structures and low power curing. To be implemented more universally, the curing method needs to be more universally compatible with more composite types. This may be possible with future developments with CNT interleaves or joule effect heated tooling.

2.3. RF Curing

RF heating is similar to MW heating; however, it has a few key differences that have restricted widespread adoption in curing composites, of which there is little recent literature. A report by the Electric Power Research Institute considers RF heating for plastics processing and drying, although it does not mention it for CFRP manufacture [124]. This report also lists similar disadvantages to many EM cure methods:

- “Highly irregular shapes may heat non-uniformly in certain applications”
- “Certain products will not heat in a dielectric heating field”

Sweeney et al [49] focused on doping composites with multi-walled CNTs, mostly for joining processes rather than full-component curing. Lap-shear bonding of 0.25% CNT-epoxy resin was conducted at 44 MHz applying up to 100 W, achieving a shorter cycle time compared to oven cured samples. The CNT-epoxy composites were processed at 200°C and held at that temperature for two and three minutes. The samples were then loaded in shear per ASTM D1002 with the samples held at temperature for three minutes passing the testing.

Li and Dickie [90] bonded thermoset sheet moulding compound (SMC) and thermoplastic to steel sheet to produce lap shear coupons. The steel was used as the RF antenna, with the press head as the other electrode. Cycle time for the SMC was reduced from 20-30 minutes down to 20-30 seconds, with a high degree of crosslinking achieved, matching the bond strength achieved by using oven cure.

Vashisth et al [91] conducted a parametric study with various RF power levels and composite types. They trialled CF/epoxy (UD), CF/epoxy (plain weave) and CNT/epoxy composite materials at a variety of radio frequencies to determine which led to an increased rate of heating. Heating rates of 8°C/min were observed indicating the potential of RF heating. They also experimented with the RF power to observe how the heating rate was affected. As expected, the higher the power, the higher the subsequent heating rate. To validate the experimentation, they developed a COMSOL multi-physics model to evaluate the heating of CF/epoxy materials with RF power. The model showed good agreement in terms of heating rates with the physical experiments and future models will be used as a predictive tool.

2.4. Magnetic Induction

2.4.1. Background to magnetic induction heating

Electrically conductive materials can be heated when exposed to a magnetic field that is generated by an alternating current (AC) passing through a coil of wire –referred to as an induction coil, or inductor [125]. When applied to CFs, heating occurs primarily via resistive heating (from Joule losses) caused by the induced eddy currents [126]. This in turn can heat surrounding materials via conduction [93,94]. Junction heating and hysteresis loss have also been identified as potential heating mechanisms, particularly for ferromagnetic materials [95–97]. The effectiveness of the technique is directly related to the electrical properties of the material (which must form an electrically closed-loop, to allow the formation of eddy currents), the inductor coil design and the input power and current frequency [127].

The advantages of magnetic induction heating include the ability to rapidly transfer energy to a component, and the power input can be instantly adjusted as required to maintain or increase temperatures to match a programmed set point and can be a contactless heating method.

The heat generated by magnetic induction can be harnessed for various purposes as opposed to only curing, for example, a coil can be held in a fixed position or mounted to a robotic arm to allow for a continuous heating process, as is often seen with induction welding of thermoplastic composites. Typical applications have focused on the areas of thermoplastic forming and consolidation, fusion bonding, and rapid cure of adhesives [95,128]. In the case of heating CFRP components, magnetic induction can be used to directly heat the CFs. This requires the use of woven or non-crimp fabrics. UD material can be heated using magnetic induction when used in a quasi-isotropic layup sequence, so there are conductive pathways between fibres at each layer through thickness. A study by Khan et.al [129] showed that the heating response of a quasi-isotropic layup subjected to magnetic induction is more isotropic than if the plies were stacked in purely UD configuration which showed an anisotropic heating response. In both cases, it was shown that the fibres could be heated to 177°C which would allow the curing of most aerospace epoxies.

An alternative to directly heating the CF is to use an electrically closed loop susceptor, such as a metal mesh or conductive particles, placed at the location where heating is required. Heat is then transferred to the local area via conduction [98]. The technique is therefore versatile and can be used to deliver heat locally and through thickness without the challenges and drawbacks associated with methods such as ovens and autoclaves. Table 4 summarises some of the key studies covered in this review.

2.4.2. Magnetic induction for processing thermoset composites

The use of magnetic induction heating to cure a thermoset composite

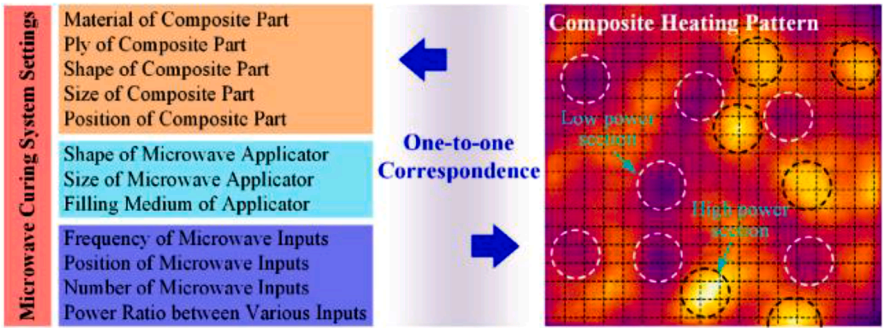

Fig. 11. Overview of MW curing system settings. IR image with highlighted hot/cold spots [36].

Table 2
Table summarising the key experimental studies and their outcomes covered in this review of MW processing of composites.

Author	Material	MW setup	Heating specifications	Significant outcomes
Kwak et al [57]	Gurit WE91-2 CFRP prepreg.	Vötsch Hephaistos MW.	10°C/min to 90, 100, 110 and 120°C dwells.	Industrial MW designed for composites. 10% increase in tensile strength.
Xuehong et al [60]	Bismaleimide (BMI) UD T700 CF, 170 × 90 mm, 22 plies.	WZD1S-03 Nanjing Sanle MW Technology Development Co.	Power based cured cycles, up to 220°C.	63 % reduction in cycle times, comparable void, and interlaminar shear stress (ILSS) to autoclave, slight reductions in flexural and fibre volume fraction.
Xuehong et al [61]	UD epoxy prepreg, T800 CFs, 175 × 90 mm, 14 plies	WZD1S-03 Nanjing Sanle MW Technology Development Co	Power based cured cycles, up to 220°C.	39 % reduction in cycle time, 22 % increase in compression strength, despire increased porosity. Evidence of increased interfacial adhesion of fibre to resin.
Li et al [64]	BMI UD CF, 100 × 100 mm, 1.5 mm thickness.	Custom design by Nanjing University. Fibre Bragg Gratings (FBG) used for strain monitoring.	1.5°C/min up to 200°C.	95% reduction in residual cure-induced strain, 64 % reduction in cycle time. Lower spring back in L-shaped components, by up to 1.2 °.
Lee and Springer[53]	Hercules AS/3501-6 carbon and Fiberite S2/9134B glass prepregs, 203 × 203 mm, 32 plies.	Commercial 700 W MW oven.	177°C, ramp rate not specified.	90 % reduction in gel time. Agreement between modelling and experimental.
Papargyris et al [62]	Araldite LY5052/HY5052 epoxy, satin weave T300 CFs, 200 × 300 × 3 mm.	Custom MW resin transfer moulding (RTM) setup, variable frequency, up to 250 W.	100°C cure.	50 % cycle time reduction. Equal flexural strength and void content, 9 % higher ILSS compared to oven cured RTM.
Thostenson and Chou [65]	E glass, Epon 862/ Epi-Cure W epoxy resin, 44 plies.	6 kW of MW power at 2.45 Ghz.	5°C/min up to 165°C.	Reduction in processing time, inside out MW processing reduced matrix cracking compared to autoclave cured samples.
Nuhiji et al [15]	Cycom 5320-1 T650 plain weave prepreg, 190 × 190 mm, 8 plies.	Vötsch HEPHAISTOS VHM 180/200.	3°C/min up to 177°C, manufacturers recommended cure cycle.	Investigated alternate tooling materials for MW cure, CFRP tooling performed best.
Green et al [31]	Cycom 5320-1 T650 plain weave prepreg, 200 × 200 mm, 1.5 mm thick.	Modified domestic MW, Panasonic NN-CF778.	3°C/min up to 177°C, manufacturers recommended cure cycle.	Conversion of domestic MW to cure composites with accurate multiphysics modelling.
Kwak et al [56]	Gurit Sparpreg UD CFs, 300 × 300 mm, up to 60 mm thick.	Vötsch Hephaistos MW 100/100 system.	2°C/min up to 120°C, manufacturers recommended cure cycle.	Highlights if the process setup is correct then high quality laminates can be manufactured. Practical method for MW penetration depth demonstrated.
Nuhiji et al [67]	Cycom 5320-1 T650 plain weave prepreg, 600 × 600 mm, 14 plies.	Vötsch HEPHAISTOS VHM 180/200.	3°C/min up to 177°C, manufacturers recommended cure cycle.	Multiphysics model of MW field, showing effect of frequency on field homogeneity and temperature distribution, experimentally validated.
Feher and Thumm [68]	LY556 infusion resin, CF plain weave, up to 450 × 300 mm.	DLR custom HEPHAISTOS-SA/CA.	20°C/min up to 130°C.	Details the process on developing industrial MW system suitable for composite processing at pressure.
Zhou et al [36]	Short fibre CFRP composite (T300 fibres), 200 × 200 × 2 mm	Custom design by Nanjing University, 2.45 GHz, 20 KW.	3°C/min up to 120°C. Active temperature compensation through selective magnetron activation.	Significant reduction in temperature difference (<10°C) over the panel, a 67 % improvement over single pattern and 58 % improvement over random pattern heating modes. Methodology can be transferred to other heating technologies.
Zhou et al [107]	UD CFRP, epoxy matrix, T800 fibres. 300 × 300 × 2 mm. Copper/polyaimide resonance structure-insulator (RSI) films.	Custom design by Nanjing University, multimode, high pressure, 2.45 GHz.	CFRP uniformly up to 120°C at 1 and 5°C/min.	CFRP/RSI film enabled high MW absorption and heating of CFRP to cure temperature. Less than 10°C range of temperature over the panel.
Zhou et al [108]	UD CFRP, epoxy matrix, T800 fibres. 600 × 300 × 2 mm. Copper/polyaimide RSI films.	Custom design by Nanjing University, multimode, high pressure, 2.45 GHz at 1500 W and 915 MHz at 1000 W.	Multi zone heating of CFRP uniformly up to 120°C.	Able to independently zonally heat CFRP with multimode RSI films. Allows for MW curing of components with non-uniform thickness.

Table 3
A summary of studies on the direct electric curing method, overviewing the materials used, electrode configuration, heating performance and significant outcomes

Author	Material	Electrode configuration	Heating specifications	Significant outcomes
Chien et al. [80]	Carbon nanotube (CNT) modified PAN fibres	Electrodes clamped at tow ends	1000°C on 2 mm fibres 300°C on 76 mm fibres at low current, 0-6 mA	Conductivity increase with temperature CNT doped PAN fibres
Naskar and Edie [77]	Pitch (2K) and PAN (12K) based fibre tows Ultem® powder (polyetherimide)	Silver paste and copper wires	0-400°C within 50 seconds, 150 mm tows	Conductivity increase with temperature Successful rigidisation, however, flaws in final composites
S.A. Sarles & D.J. Leo [81]	U-Nyte epoxy coated tow	Crocodile clips	Up to 200°C following the cure cycle. 50°C/min ramp rate.	Proving the technology for alternate curing situations such as inflatable space structures
H Fukuda [76]	Torayca P3060 pre-preg	Aluminium foil. Edge to edge & through the thickness (Fig. 6)	Proportional integral derivative (PID) control to cure cycle. Up to 180°C.	Electrode layouts reviewed. Power reduction observed.
C. Joseph [75]	Hexcel 914c pre-preg Unidirectional	Copper blocks on each ply, edge to edge (Fig. 7)	Followed cure cycle up to 175°C	Increased mechanical properties. Power reduction.
Y. Gu et al. [38]	T700SC unidirectional (UD) Carbon, DGEBA E51 resin	Copper foil, stacked between plies	Followed cure cycle up to 120°C, 30°C/min ramp rate. 13°C Δ over panel.	Dry fibre infusion experimental process. Rapid heating rates, however poor temperature distribution. Highlighted issues with tooling.
N. Athanasopoulos et al (2008) [78]	CF preform/Epocast52 epoxy, UD sigrafil E022 pre-preg	Copper electrodes	Followed cure cycle, up to 130°C	Matching mechanical properties to oven cured. Comparison between pre-preg and infusion samples. Accurate power data
S. Hayes et al. [37]	Cycom 950-1 plain weave pre-preg	Copper foil or Copper/ flexible printed circuit board (PCB)	Followed cure cycle, up to 160°C	Understanding of scalability and practical implementation. Highlighting temperature distribution issues.
S. Liu et al [14]	UIN10000/T800 UD pre-preg	Copper strips, 10mm wide	Followed cure cycle, up to 120°C	Detailed experimental procedure, layup/electrode arrangement on temperature distribution, mechanical properties comparison.
Reese et al.[82]	Recycled carbon, Nylon 6, custom weave	Press plates as electrodes, 900-2500mm^2. Through thickness.	222°C (T^{melt}) within 15 seconds	Combination of press and joule heating to reduce cycle time

component, through heating the CFs or an embedded susceptor, is limited. Investigations of induction curing through heating the fibres, have only been proven on lab scale components at TRL 3 or lower. Pitchumani and Johnson used induction to heat a composite preform [99] to control the flow of epoxy resin in a VARTM process. A woven fibreglass mat was used with a layer of woven CF embedded in the preform to act as the susceptor, eliminating the need for metallic inclusions and reducing weight and corrosion concerns. The inductor coil is moved as determined by the active control program to facilitate resin flow and preform fill. The induction system was not used to facilitate the final cure of the component; however, directly heating the fibres to induce volumetric cure would require a coil that was at least as large as the part to be cured.

2.4.3. *Magnetic induction for processing thermoplastics*

The use of magnetic induction heating for the processing of thermoplastics has been focused on thermoforming and fusion bonding processes, driven by the advantages of the technique that include rapid processing times, low energy consumption and the ability to volumetrically heat a substrate or tool.

The heating of thermoplastics for thermoforming processes can be completed without conductive fillers [128] if part of the component is electrically conductive or indirectly by heating a metallic tool or forming plates. In the Induction Diaphragm Forming (IFD) process, thermoplastic sheets are held between two sheets of aluminium. The aluminium is heated by induction that then heats the thermoplastic via conduction, with the molten stack then formed over a die.

Ramulu et al. [103] performed a comparison of autoclave and induction joining for processing CF/ PEEK, CF/PIXA-M [130] and Hybrid Titanium Composite Laminates (HTCL) panels. Induction heating presents a potential processing solution to autoclave, enabling rapid heating and reducing cycle time and costs. Micrographs showed CF/PEEK panels consolidated using induction heating and autoclave both showed high quality laminates. Induction processed CF/PIXA-M panel showed increased levels of void formation and fibre distortion, and the HTCL panel showed poor quality consolidation compared to autoclave processing.

Rudolf et al [94] investigated the effect of various induction heating process parameters on the temperature distribution and heating rate for Polyphenylene Sulfide (PPS) and Polyamide (PA) reinforced CF composite. There was a direct correlation between heating rate and coil separation distance, with a quadratic growth associated with increased separation. The authors also found that heating time is reduced by increasing the input power and that heat generation was found to be driven by Joule losses.

2.4.4. *Magnetic induction for curing adhesives*

Magnetic induction technology has been investigated to cure adhesives, in the context of in-situ repairs or rapid joint formation with reduced cycle times. For applications involving GFRP composites, adhesive curing via induction is only possible with the use of a susceptor. Tay et al. [98] investigated the accelerated curing of room temperature paste adhesive bonded GFRP single lap-shear (SLS) specimens, with and without a copper mesh susceptor in the bond line. The magnetic induction heating was successful, with shear strength results comparable to, or better than, oven cured specimens. Mahdi et. al. [97] performed a similar investigation using a stainless-steel mesh and comparing two different types of epoxy paste adhesive. It was found that the shear strengths of the induction cured specimens were within 10 % of the results obtained when oven cured. Severijns et. al. [93] used varying levels of iron particles as a susceptor for curing adhesive in GFRP SLS samples. Samples, where the adhesive was induction, cured had up to 6 % higher shear strengths than their oven counterparts that also had iron filled bond lines. The introduction of iron particles reduced the shear strength of all samples, compared to the unmodified adhesive samples, as well as adding weight to the assembly.

Studies have been carried out to investigate whether heating CFRP adherends directly, without a susceptor, could cure adhesive bond lines via conductive heat transfer. Frauenhofer et. al. [100] investigated woven and UD CF architectures and how that influenced heating rates on CFRP-to-CFRP and CFRP-to-Aluminium SLS components. Lower frequencies resulted in more homogeneous heating than higher frequencies, and rapid curing via magnetic induction led to better bulk adhesive properties and DoC compared with samples cured with longer

Table 4
Summary of key studies of induction heating of composites for curing and adhesive curing.

Author	Material	Experimental setup	Processing specification	Significant outcomes
Pitchumani and Johnson [99]	Woven CF mat, 305 × 305 mm (BFG Industries), Epon 815C epoxy resin.	32 × 68 mm coil size, mounted to motion stage for active RTM.	Not directly observed. Feedback control based off flow front.	Localised heating for active flow front control of vacuum assisted resin transfer moulding (VARTM).
Ramulu et al [103]	Polyether ether ketone (PEEK), PIXA-M, Hybrid titanium composite laminate.	Comparison of induction and autoclave processing of thermoplastic laminates.	Forced cooling on the induction samples. No data on temperature.	Less than 10% difference in in flexural and tensile properties. Significantly quicker processing time.
Rudolf et al [94]	Process parameter setup on CF-PPS, 2mm thick, laminate structure tests on CF polyamide 66.	Understanding coil setup parameters on heating performance. Continuous induction welding process.	Investigated different coil geometries, frequency, power, distance from laminate.	Heat only generated in closed fibre loops, i.e UD fibres. Maximum temperature is limited by power. Through thickness temperature distribution is even.
Tay et al [98]	Hysol EA9394 epoxy paste adhesive, GFRP substrate, 34 plies, 3 mm.	Curing of paste adhesive for composite repair to reduce cycle time, tested with single lap shears.	Copper susceptor introduced in adhesive.	Copper susceptor reduced strength slightly, but reduced scatter of data. Reduced cycle time from 120 hrs to 15 minutes.
Severijns et al [93]	EC9323 epoxy paste adhesive, GFRP substrates, 8 plies.	One-turn and pancake coils tested. Tested with single lap shear bonding.	Iron particles introduced into adhesive as susceptor. Varying process parameters for heating performance.	Iron particles reduced shear strength by 15-20 % in all samples, but induction cured samples were 6 % higher than oven cured samples.
Frauenhofer et al [100]	HexPly 913 CF-epoxy laminates, UD and woven. Henkel Loctite EA 9394 adhesive.	Testing consolidation of laminates and subsequent ILSS and flexural strength. SLS test of adhesive bonded parts.	Varying frequencies tested to determine heating performance, 120°C cure.	Penetration depth higher than metals. Able to heat both side of SLS and cure adhesive effectively.
Sánchez Cebrián et al [101]	Huntsman ME 10049-4/LMB 6687-2 epoxy adhesive, Cytec MTM 44-1 CFRP.	2 part heating method to reduce volatiles and voids being created.	Stepped cure cycle, up to 140-180°C, at 25°C/min.	Cure time reduced from 4 h to 30 min without increase in void content.
Kim et al [102]	3M F-163-2 K adhesive film, AL-6061-T6 aluminium.	Carbon patched double lap aluminium joints for use in repairs. Compared oven and induction.	120°C for 90 minutes for direct comparison to oven cured samples.	Induction samples matched oven cured samples bond strength.

cycle times using an oven. Higher shear strength values were obtained in all cases where the adhesive was cured via induction, compared to the oven baseline. This proved the possibility of heating the composite to conductively cure the adhesive and could do so from one side and rapidly.

Cebrián et al. [101] used magnetic induction to heat CFRP laminates to cure adhesive via conduction alongside a model simulating and predicting the DoC. The model was validated using SLS specimens that were monitored for temperature and DoC, and the results showed a good correlation between predictive and actual values.

Kim et. al. [102] investigated CFRP patch repairs of aluminium double lap-shear joints using either oven cure or induction heating. Two types of patches, bonded to the aluminium via a single layer of film adhesive, were investigated: pre-cured and co-cured UD composite. Additional samples were prepared with 0.5 %wt. CNTs in a resin mix was applied to the bonding surfaces before adhesive application. The authors found that the co-curing of CFRP patches and film adhesive yielded higher shear strengths than bonding with pre-cured patches. No difference in shear strength was found between the oven and induction heating when bonding pre-cured patches, although oven co-curing presented 8% higher shear strengths compared to induction co-cured. The inclusion of CNTs at the bond interface increased shear strengths in all cases. For patch repair applications, this is advantageous because it would remove the need for IR heaters, heated blankets/mats, or transferring large sections to an autoclave or oven to complete the repair – provided a means of applying sufficient consolidation was implemented. This saves on process time, energy, floor space and storage requirements. There is a need for further research to validate the technique on larger components and to develop the process.

3. Future challenges

The research presented shows some of the challenges and solutions to a range of EM curing methods, however in the following section are three main themes that have occurred frequently and will need further research as the methods become more industrially relevant and frequent in use.

3.1. Sustainability and economics of novel curing methods

One of the most significant benefits of many of these novel cure methods is the low energy consumption when compared to oven or autoclave methods. This is due to the direct heating nature of these techniques described in Fig. 1, meaning that the energy going into the curing system is only heating the component. The cost has always been a strong driver in any manufacturing situation, however with sustainability now reaching similar importance, it is expected that the energy consumption is given more scrutiny. Reduction in energy usage will lead to lower costs of a process as well as improve the sustainability of existing processes, particularly in aerospace where changes to materials and processes can take years due to the high cost of qualification.

Sustainability as a topic has increased in prevalence around the pandemic, which has meant that the overall sustainability as a benefit is not discussed in detail in papers reviewed before this date. The primary focus of the papers has been the resulting composite mechanical properties, with authors assuming or not accounting for sustainability or being cost effective at the lab scale. Another issue that is considered in few cases is the effects of scaling up will have on not only the composite mechanical properties but on the economic practicality of it for composite manufacturers.

3.2. Control systems

An aspect of novel curing methods is the control systems that accompany them. Closed loop PID control algorithms have traditionally controlled oven, autoclave and press plattern temperatures. These controllers are suitable when longer time intervals are used and when temperature overshoots need to be avoided. When ramp rates in cure cycles increase from 2-3°C/minute to 10-20°C/minute, closed loop PID controllers would have to be tuned accordingly to optimise for each component [131]. These controllers are commonly Single Input Single Output (SISO) or Multiple Input Single Output (MISO) and are unsuitable for accommodating the uneven heating of a variety of cure methods or controlling heating in multiple and specific areas, which require more complex Multiple Input Multiple Output (MIMO) controllers [31].

There is an opportunity to use enhanced temperature and cure monitoring tools alongside these cure methods, as well as predictive cure models that can account for the highly controllable power inputs [85].

Non-conventional heating methods provide a new challenge to heating controllers to overcome some of the disadvantages, particularly localised or uneven heating patterns. Rapid heating would require updated or faster controllers, alongside predictive cure which could allow for more consistent quality cures. Because of these reasons, increased monitoring of the cure is required, which can increase setup cost, however, a key trend of Industry 4.0 is data collection [132,133], suggesting existing manufacturing methods will require this level of data collection in the future.

MIMO control systems have been suggested as a solution to ensure even bulk heating of large composites, regardless of geometry [31]. These difficult control system problems are complex to implement, therefore systems based on pattern detection and understanding of the underlying physics have been developed. Zhou et al [36] developed a real-time thermal imaging monitoring system to improve the MW curing process. A database of heating patterns from different magnetron activations and therefore different standing waves are recorded in a database. The composite is heated, and the heating pattern is fed back to the control system which calls on the database for an inverse pattern and alters control parameters to homogenise the heat pattern. The controller can adjust which magnetrons are activated, the frequency of the MW inputs and the power ratio Fig. 11.

Pitchumani and Johnson [99] developed an active controller that moved an induction coil to the position in an X-Y plane of a composite to assist in heating resin to reduce viscosity and ensure there was an even flow front during the VARTM process. A method like this could be applied to local MW, induction, or IR transmitters to cure components locally.

D. Kim et al. [111] produced a cure kinetic model of out-of-autoclave prepreg to control the cure of the prepreg at different lengths of outlife with high accuracy, however, stated that the model could be used to gain further efficiencies from existing manufacturing processes.

3.3. Matrix modification for enhanced susceptibility

Modifying polymers with fillers to improve material properties is a practice that has existed for decades, one of the most common examples being carbon black in tyre rubber to increase wear resistance [134]. More recently research has focused dispersion of graphene or carbon nanotubes in matrices, which enhances a variety of properties, including fracture toughness and tuning of electrical conductivity [135], which affects the susceptibility of many of the curing methods mentioned in this paper.

Conductive resins, and therefore composites can increase the effectiveness of novel curing methods [136] which commonly heavily rely on conductive fibres. Nanocomposites without reinforcing fibres have been cured using MWs [73,74], RF [49], direct electric [80,86–88] and induction [102] successfully.

An electrically conductive matrix in a CFRP composite would be more isotopically electrically conductive, therefore potentially more isotropic heating within novel curing methods. Mas et al [89] highlighted three examples of how CNT loaded epoxy could be used with electric cure, for composite fabrication, composite repair, and as electronic adhesive/solder. In all situations, it was possible to cure the epoxy, without the requirement of CFs as a conducting element.

3.4. Modelling of heating methods

Modelling of curing is vital for the acceleration of development of these methods, as experimentation is time consuming and costly. The majority of the methods mentioned require multi-physics modelling to provide effective and accurate results and due to the low TRL of this area of research, it is more accessible to do so on these less complex systems. Tertrais et al [137,138] have published initial modelling of a Vötsch MW cavity. The publications detailed the mathematical equation necessary to calculate in-plane and out-of-plane thermo-chemical analysis but included no results.

Kim et al [139] successfully modelled the representative volume element of an electrically cured chopped strand CF composite, characterising the heating behaviour dependent on fibre volume fraction.

Nuhiji et al [67] successfully modelled and simulated an industrial scale MW using COMSOL Multiphysics. A quarter-scale model of the Votsch MW system was generated and a parametric study of heating a composite panel using a variety of frequencies and magnetron configurations. The analysis showed that as frequency increased from 500 MHz to 2.45 GHz, the heat distribution within the panel became less homogeneous. The authors' findings indicated that by altering the frequency or the number of magnetrons, the heat distribution changed. This could then be used to inform future control algorithms to improve the composite curing process.

Mitschang and Neitzel [140] used a predictive Finite Element model to generate parameters for use in a Continuous Induction Welding (CIW) process. The model aimed to reduce the quantity of physical testing required to validate the process parameters, reducing overall effort, time, and costs. The outputs were validated using a limited set of single-lap welded panels, using PPS reinforced with either plain weave or 5-Harness Satin.

4. Conclusion

Existing composite curing methods produce consistently high-quality components; however, this is one of their few advantages. The research covered in this paper shows that novel curing methods can produce equivalently high, or higher quality composites, and using considerably less energy. Depending on the method used there are also other significant advantages apart from the component quality, for example, increased heating rates, safer operation in thicker layups, and lower capital expenditure equipment.

The low TRL of these curing methods means that the expertise, equipment, and time required to produce components of the same quality as existing methods are not feasible currently. As these methods are developed, standardisation will follow, allowing further research at higher TRLs and implementation in components in small specific cases.

After the review of a wide range of novel curing methods, it is

expected that the themes of future research in these areas will be:

- Environmental impact: One of the most significant benefits of these novel cure methods is their energy efficiency compared to standard cure methods, however, this is explored in very little detail by most of the papers reviewed. As more scrutiny is put on the energy efficiency of the composite supply chain,
- Modelling of the novel cure methods: A Complex multiphysics methodology is required and has not been explored for many curing scenarios. For example, it has been investigated in detail for MW curing, however very little for electric cure.
- Industrialisation and compatibility with existing methods: A lot of the research covered rarely considers how the process will work in industry, or how this transition can be made. This is expected in with low TRL research, however as these cure methods are developed, industrialisation needs to be considered in more detail.
- Characterisation on component level: Significant research has been completed on the thermal and mechanical characterisation of components manufactured using novel cure methods, which allows for easy comparison to existing cure methods. The next step for these comparisons is the component level comparisons, including the practicality and capital expenditure over a production series of a component.

Research needs to continue in these areas to overcome these challenges to ensure the benefits start to outweigh the issues that still occur. Once these are solved, they can start to be tested in service and data collected with prolonged use, which will help wider adoption in high value industries such as automotive or aerospace. These future curing methods can solve the future requirements of these industries for quality and quantity, as well as meeting future energy saving requirements.

Funding sources

Funding: This work was supported by the European Union's Horizon 2020 research programme under grant agreement No 760940, under the project titled MASTRO.

Declaration of Competing Interest

The authors declare that they have no known competing financial interests or personal relationships that could have appeared to influence the work reported in this paper.

References

[1] PE Irving, C Soutis, Polymer Composites in the Aerospace Industry, Elsevier, 2020, https://doi.org/10.1016/c2017-0-03502-4.
[2] ICAO. 2. What is CORSIA and how does it work? 2020. https://www.icao.int/environmental-protection/Pages/A39_CORSIA_FAQ2.aspx (accessed September 11, 2020).
[3] JR Duflou, J de Moor, I Verpoest, W. Dewulf, Environmental impact analysis of composite use in car manufacturing, CIRP Ann. - Manuf. Technol. 58 (2009) 9–12, https://doi.org/10.1016/j.cirp.2009.03.077.
[4] Aerospace Technology Institute, Composites UK. Composite material applications in Aerospace, Insight, ATI, 2018.https://www.ati.org.uk/wp-content/uploads/2021/08/insight_9-composites_amended-2018-09-20.pdf (accessed December 21, 2021)
[5] T Ishikawa, K Amaoka, Y Masubuchi, T Yamamoto, A Yamanaka, M Arai, et al., Overview of automotive structural composites technology developments in Japan, Compos. Sci. Technol. 155 (2018) 221–246, https://doi.org/10.1016/j.compscitech.2017.09.015.
[6] YS Song, JR Youn, TG. Gutowski, Life cycle energy analysis of fiber-reinforced composites, Compos. Part A: Appl. Sci. Manuf. 40 (2009) 1257–1265, https://doi.org/10.1016/j.compositesa.2009.05.020.
[7] Liddell HPH, Brueske SB, Carpenter AC, Cresko JW. Manufacturing energy intensity and opportunity analysis for fiber-reinforced polymer composites and other lightweight materials. Proceedings of the American Society for Composites - 31st Technical Conference, ASC 2016, 2016.
[8] Marino M, Sabatini R. Advanced lightweight aircraft design configurations for green operations, 2014. 10.13140/2.1.4231.8405.
[9] Timmis AJ, Hodzic A, Koh L, Bonner M, Soutis C, Schäfer AW, et al. Environmental impact assessment of aviation emission reduction through the implementation of composite materials n.d. 10.1007/s11367-014-0824-0.
[10] JR Duflou, J De Moor, I Verpoest, W. Dewulf, Environmental impact analysis of composite use in car manufacturing, CIRP Ann. Manuf. Technol. 58 (2009) 9–12, https://doi.org/10.1016/j.cirp.2009.03.077.
[11] D Abliz, Y Duan, L Steuernagel, L Xie, D Li, G. Ziegmann, Curing methods for advanced polymer composites - a review, Polym. Polym. Compos. 21 (2013) 341–348, https://doi.org/10.1177/096739111302100602.
[12] SL Agius, KJC Magniez, BL. Fox, Cure behaviour and void development within rapidly cured out-of-autoclave composites, Compos. Part B: Eng. 47 (2013) 230–237, https://doi.org/10.1016/j.compositesb.2012.11.020.
[13] DA Lakho, D Yao, K Cho, M Ishaq, Y. Wang, Study of the curing kinetics toward development of fast-curing epoxy resins, Polym. Plastics Technol. Eng. 56 (2017) 161–170, https://doi.org/10.1080/03602559.2016.1185623.
[14] S Liu, Y Li, Y Shen, Y. Lu, Mechanical performance of carbon fiber/epoxy composites cured by self-resistance electric heating method, Int. J. Adv. Manuf. Technol. (2019), https://doi.org/10.1007/s00170-019-03707-0.
[15] B Nuhiji, T J Swait, MP Bower, JE Green, RJ Day, RJ. Scaife, Tooling materials compatible with carbon fibre composites in a microwave environment, Compos. Part B: Eng. (2019), https://doi.org/10.1016/j.compositesb.2019.01.047.
[16] CO Mgbemena, D Li, MF Lin, PD Liddel, KB Katnam, VT Kumar, et al., Accelerated microwave curing of fibre-reinforced thermoset polymer composites for structural applications: A review of scientific challenges, Compos. Part A: Appl. Sci. Manuf. 115 (2018) 88–103, https://doi.org/10.1016/j.compositesa.2018.09.012.
[17] M. Héder, From NASA to EU: the evolution of the TRL scale in public sector innovation, The Innovation J.: The Public Sector Innovation J. n.d 22 (2017) 3.
[18] T Centea, LK Grunenfelder, SR. Nutt, A review of out-of-autoclave prepregs - Material properties, process phenomena, and manufacturing considerations, Compos. Part A: Appl. Sci. Manuf. 70 (2015) 132–154, https://doi.org/10.1016/j.compositesa.2014.09.029.
[19] C Hull, TW. Clyne, An Introduction to Composite Materials, 2nd ed., Cambridge University Press, Cambridge, 1996.
[20] B Ellis, WR Ashcroft, SJ Shaw, WJ Cantwell, HH Kausch, GP Johari, et al., Chemistry of Epoxy Resins, Springer-Sci.+Bus. Media, B.V. (1993).
[21] Huntsman, High Performance Components Selector Guide n.d (2018).
[22] HT. Hahn, Residual stresses in polymer matrix composite laminates, J. Compos. Mater. 10 (1976) 266–278, https://doi.org/10.1177/002199837601000401.
[23] TE Twardowski, SE Lin, PH. Geil, Curing in thick composite laminates: experiment and simulation, J. Compos. Mater. 27 (1991) 216–250, https://doi.org/10.1177/002199839302700301.
[24] TA Bogetti, JW. Gillespie, Process-induced stress and deformation in thick-section thermoset composite laminates, Jo. Compos. Mater. 26 (2016) 626–660, https://doi.org/10.1177/002199839202600502.
[25] G Struzziero, JJE. Teuwen, Effect of convection coefficient and thickness on optimal cure cycles for the manufacturing of wind turbine components using VARTM, Compos. Part A: Appl. Sci. Manuf. 123 (2019) 25–36, https://doi.org/10.1016/j.compositesa.2019.04.024.
[26] A. P. Mouritz AGG. Health Hazards of Composites in Fire. Fire Properties of Polymer Composite Materials, Springer Netherlands; 2007, p. 359–84. 10.1007/978-1-4020-5356-6_12.
[27] ZL. Yang, Optimized curing of thick section composite laminates, Mater. Manuf. Processes 16 (2001) 541–560, https://doi.org/10.1081/AMP-100108526.
[28] Young W bin, Compacting pressure and cure cycle for processing of thick composite laminates, Compos. Sci. Technol. 54 (1995) 299–306, https://doi.org/10.1016/0266-3538(95)00067-4.
[29] N Slesinger, T Shimizu, ARA Arafath, A. Poursartip, Heat transfer coefficient distribution inside an autoclave, ICCM17 Edinburgh (2017).
[30] L Nele, A Caggiano, R. Teti, Autoclave cycle optimization for high performance composite parts manufacturing, Procedia CIRP 57 (2016), https://doi.org/10.1016/j.procir.2016.11.042, 241–6.
[31] Green JE, Nuhiji B, Zivtins K, Bower MP, Grainger R v., Day RJ, et al. Internal model control of a domestic microwave for carbon composite curing. IEEE Trans. Microwave Theory and Techniques 2017;65:4335–46. 10.1109/TMTT.2017.2693145.
[32] S Enoki, K Iwamoto, R Harada, K Tanaka, T. Katayama, Heating properties of carbon fibers by using direct resistance heating, WIT Trans. The Built Environ. n.d (2012) 124, 10.2495/HPSM120211.
[33] Y Li, X Hang, N Li, X. Hao, A temperature distribution prediction model of carbon fiber reinforced composites during microwave cure, J. Mater. Processing Technol. 230 (2015), https://doi.org/10.1016/j.jmatprotec.2015.12.001, 280–7.
[34] Y Li, N Li, J. Gao, Tooling design and microwave curing technologies for the manufacturing of fiber-reinforced polymer composites in aerospace applications, The Int. J. Adv. Manuf. Technol. 70 (2014) 591–606, https://doi.org/10.1007/s00170-013-5268-3.
[35] N Li, Y Li, X Wu, X. Hao, Tool-part interaction in composites microwave curing: Experimental investigation and analysis, J. Compos. Mater. 51 (2017), https://doi.org/10.1177/0021998317693674, 3719–30.
[36] J Zhou, Y Li, N Li, S Liu, L Cheng, S Sui, et al., A multi-pattern compensation method to ensure even temperature in composite materials during microwave curing process, Compos. Part A: Appl. Sci. Manuf. (2018), 107:10–20. 10.1016/j.compositesa.2017.12.017.
[37] SA Hayes, AD Lafferty, G Altinkurt, PR Wilson, M Collinson, P. Duchene, Direct electrical cure of carbon fiber composites, Adv. Manuf.: Polym. Compos. Sci. 1 (2015) 112–119, https://doi.org/10.1179/2055035915Y.0000000001.

[38] Y Gu, X Qin, M Li, K Zhang, Z. Zhang, Temperature distribution and curing behaviour of carbon fibre/epoxy composite during vacuum assisted resin infusion moulding using rapid heating methods, Polym. Polym. Compos. 23 (2015) 11–20, https://doi.org/10.1177/096739111502300102.

[39] PK Bajpai, I. Singh, Reinforced Polymer Composites, 1st ed., Wiley-VCH, 2020.

[40] I Zhilyaev, C Brauner, S Queloz, H Jordi, R Lüscher, S Conti, et al., Controlled curing of thermoset composite components using infrared radiation and mathematical modelling, Compos. Structures (2021) 259, https://doi.org/10.1016/j.compstruct.2020.113224.

[41] M Uday, P. Kirankumar, Heat transfer studies for infrared radiation assisted curing in polymer composites, J. Phys.: Conference Series 1473 (2020), https://doi.org/10.1088/1742-6596/1473/1/012027. Institute of Physics Publishing12027.

[42] R Weber, C Freitag, T v. Kononenko, M Hafner, V Onuseit, P Berger, et al., Short-pulse laser processing of CFRP, Phys.Procedia 39 (2012) 137–146, https://doi.org/10.1016/j.phpro.2012.10.023. Elsevier B.V.

[43] P Monnot, D Williams, M. di Francesco, Power Control of a Flashlamp-Based Heating Solution For Automated Dry Fibre Placement, 18, ECCM, Athens, 2018, 24–8.

[44] S.T. Peters, Composite Filament Winding, ASM International, 2011.

[45] A. Endruweit, M.S Johnson, ACL, Curing of Composite Components by Ultraviolet Radiation: A Review, Polym. Compos. 27 (2006) 119–128, https://doi.org/10.1002/pc.

[46] ID Robertson, M Yourdkhani, PJ Centellas, J En Aw, DG Ivanoff, E Goli, et al., Rapid energy-efficient manufacturing of polymers and composites via frontal polymerization, Nature 557 (2018), https://doi.org/10.1038/s41586-018-0054-x, 223–7.

[47] E Goli, SR Peterson, PH. Geubelle, Instabilities driven by frontal polymerization in thermosetting polymers and composites, Compos. Part B: Eng. 199 (2020), 108306, https://doi.org/10.1016/j.compositesb.2020.108306.

[48] AC Metaxas, RJ. Meredith, Industrial microwave heating, IET (1988), https://doi.org/10.1049/pbpo004e.

[49] CB Sweeney, AG Moran, JT Gruener, AM Strasser, MJ Pospisil, MA Saed, et al., Radio frequency heating of carbon nanotube composite materials, ACS Appl. Mater. Interfaces 10 (2018), 27252–910.1021/acsami.8b06268.

[50] GJ Sweeney, PF Monaghan, MT Brogan, SF. Cassidy, Reduction of infra-red heating cycle time in processing of thermoplastic composites using computer modelling, Compos. Manuf. 6 (1995) 255–262, https://doi.org/10.1016/0956-7143(95)95018-T.

[51] O Lucia, P Maussion, EJ Dede, JM. Burdio, Induction heating technology and its applications: Past developments, current technology, and future challenges, IEEE Trans. Ind. Electron. 61 (2014), https://doi.org/10.1109/TIE.2013.2281162, 2509–20.

[52] WT. Hill, Electromagnetic Radiation. digital Encyclopedia of Applied Physics, Wiley-VCH Verlag GmbH & Co. KGaA, Weinheim, Germany, 2009, pp. 1–26, https://doi.org/10.1002/3527600434.eap112.pub3.

[53] Woo Il Lee, Springer GS, Microwave curing of composites, J. Compos. Mater. 18 (1984) 387–409, https://doi.org/10.1177/002199838401800405.

[54] FYC Boey, CY. Yue, Interfacial strength of a microwave-cured epoxy-glass composite, J. Mater. Sci. Lett. 10 (1991), https://doi.org/10.1007/BF00722652, 1333–4.

[55] F Boey, I Gosling, SW. Lye, High-pressure microwave curing process for an epoxy-matrix/glass-fibre composite, J. Mater. Processing Technol. 29 (1992), https://doi.org/10.1016/0924-0136(92)90445-X, 311–9.

[56] M Kwak, P Robinson, A Bismarck, R. Wise, Microwave curing of carbon–epoxy composites: Penetration depth and material characterisation, Compos. Part A: Appl. Sci. Manuf. 75 (2015) 18–27, https://doi.org/10.1016/j.compositesa.2015.04.007.

[57] Kwak M, Robinson P, Bismarck A, Wise R. Curing of composite materials using the recently developed hephaistos microwave. 18th Int. Conference on Compos. Mater., 2011, p. 21–6.

[58] M. Kwak, Microwave Curing of Carbon-Epoxy Composites: Process Development and Material Evaluation, Imperial College London, 2016.

[59] C Nightingale, RJ. Day, Flexural and interlaminar shear strength properties of carbon fibre/epoxy composites cured thermally and with microwave radiation, Compos. - Part A: Appl. Sci. Manuf. 33 (2002), https://doi.org/10.1016/S1359-835X(02)00031-3, 1021–30.

[60] X Xu, X Wang, R Wei, S. Du, Effect of microwave curing process on the flexural strength and interlaminar shear strength of carbon fiber/bismaleimide composites, Compos. Sci. Technol. 123 (2016), https://doi.org/10.1016/J.COMPSCITECH.2015.11.030, 10–6.

[61] X Xu, X Wang, Q Cai, X Wang, R Wei, S. Du, Improvement of the compressive strength of carbon fiber/epoxy composites via microwave curing, J. Mater. Sci. Technol. 32 (2016), https://doi.org/10.1016/J.JMST.2015.10.006, 226–32.

[62] DA Papargyris, RJ Day, A Nesbitt, D. Bakavos, Comparison of the mechanical and physical properties of a carbon fibre epoxy composite manufactured by resin transfer moulding using conventional and microwave heating, Compos. Sci. Technol. 68 (2008), https://doi.org/10.1016/J.COMPSCITECH.2008.01.010, 1854–61.

[63] R Yusoff, M Aroua, N A, RJ Day, Curing of polymeric composites using microwave resin transfer moulding (RTM), Eng. Sci. Technol. 2 (2007) 151–163.

[64] N Li, Y Li, X Hao, J. Gao, A comparative experiment for the analysis of microwave and thermal process induced strains of carbon fiber/bismaleimide composite materials, Compos. Sci. Technol. 106 (2015) 15–19, https://doi.org/10.1016/j.compscitech.2014.10.008.

[65] ET Thostenson, TW. Chou, Microwave and conventional curing of thick-section thermoset composite laminates: Experiment and simulation, Polymer Compos. 22 (2001) 197–212, https://doi.org/10.1002/PC.10531.

[66] N Li, Y Li, J Jelonnek, G Link, J. Gao, A new process control method for microwave curing of carbon fibre reinforced composites in aerospace applications, Compos. Part B: Eng. 122 (2017) 61–70, https://doi.org/10.1016/j.compositesb.2017.04.009.

[67] B Nuhiji, MP Bower, T Swait, V Phadnis, RJ Day, RJ. Scaife, Simulation of carbon fibre composites in an industrial microwave, Mater. Today: Proceedings 34 (2021) 82–92, https://doi.org/10.1016/j.matpr.2020.01.284.

[68] LE Feher, MK. Thumm, Microwave innovation for industrial composite fabrication - The HEPHAISTOS technology, IEEE Trans. Plasma Sci. (2004), https://doi.org/10.1109/TPS.2004.823983.

[69] ET Thostenson, T-W. Chou, Microwave processing: fundamentals and applications, Compos. Part A: Appl. Sci. Manuf. 30 (1999) 1055–1071, https://doi.org/10.1016/S1359-835X(99)00020-2.

[70] X Hang, Y Li, X Hao, N Li, Y. Wen, Effects of temperature profiles of microwave curing processes on mechanical properties of carbon fibre–reinforced composites, Proceedings of the Institution of Mech. Eng., Part B: Jo. Eng. Manuf. 231 (2017), https://doi.org/10.1177/0954405415596142, 1332–40.

[71] E Díaz, R Emmerich, M Graf, C Ress, I Roig, L. Chamudis, Microwave Curing of Long Fiber Reinforced Composites in an Open Antenna System, 15, ECCM, Venice, 2012.

[72] N Pantelelis, E Bistekos, R Emmerich, P Gerard, A Zoller, RR. Gallardo, Compression RTM of reactive thermoplastic composites using microwaves and cure monitoring, Procedia CIRP 85 (2020) 246–251, https://doi.org/10.1016/j.procir.2019.10.005. Elsevier B.V.

[73] VK Rangari, MS Bhuyan, S. Jeelani, Microwave curing of CNFs/EPON-862 nanocomposites and their thermal and mechanical properties, Compos. Part A: Appl. Sci. Manuf. (2011), https://doi.org/10.1016/j.compositesa.2011.03.014.

[74] N Uyanık, AR Erdem, MF Can, MS. Çelik, Epoxy nanocomposites curing by microwaves, Polym. Eng. Sci. 46 (2006), 1104–10. 10.1002/pen.20574.

[75] C Joseph, C. Viney, Electrical resistance curing of carbon-fibre/epoxy composites, Compos. Sci. Technol. 60 (2000) 315–319, https://doi.org/10.1016/S0266-3538(99)00112-8.

[76] H. Fukuda, Processing of carbon fiber reinforced plastics by means of Joule heating, Adv. Compos. Mater. (1993), https://doi.org/10.1163/156855194X00015.

[77] Naskar AK, Edie DD. Consolidation of reactive ultem powder-coated carbon fiber tow for space structure composites by resistive heating n.d. 10.1177/0021998306061300, 2005.

[78] Athanasopoulos N, Sotiriadis G, Kostopoulos V. A study on the effect of Joule-heating during the liquid composite molding (LCM) process and on the curing of CFRP composite laminates. The 10th International Conference on Flow Processes in Composite Materials (FPCM10), 2010, p. p5.

[79] J Lee, X Ni, F Daso, X Xiao, D King, JS Gómez, et al., Advanced carbon fiber composite out-of-autoclave laminate manufacture via nanostructured out-of-oven conductive curing, Compos. Sci. Technol. (2018), https://doi.org/10.1016/j.compscitech.2018.02.031.

[80] A-T Chien, S Cho, Y Joshi, S. Kumar, Electrical conductivity and Joule heating of polyacrylonitrile/carbon nanotube composite fibers, Polymer (Guildf) (2014) 55, https://doi.org/10.1016/j.polymer.2014.10.064.

[81] SA Sarles, DJ. Leo, Consolidation of U-Nyte epoxy-coated carbon-fiber composites via temperature-controlled resistive heating, J. Compos. Mater. 42 (2008) 2551–2566, https://doi.org/10.1177/0021998308097197.

[82] J Reese, M Vorhof, G Hoffmann, K Böhme, C. Cherif, Joule heating of dry textiles made of recycled carbon fibers and PA6 for the series production of thermoplastic composites, J. Eng. Fibers and Fabrics 15 (2020), 155892502090582, https://doi.org/10.1177/1558925020905828.

[83] J Wellekötter, C. Bonten, Influence of the contacting on the resistance heating of carbon fiber reinforced thermoplastics, AIP Conference Proceedings (2020), https://doi.org/10.1063/5.0029567, 2289:20063.

[84] S Liu, Y Li, S Xiao, T. Wu, Self-resistive electrical heating for rapid repairing of carbon fiber reinforced composite parts, J. Reinforced Plastics and Compos. 38 (2019) 495–505, https://doi.org/10.1177/0731684419832793.

[85] JS Weiland, MP Hartmann, RM. Hinterhölzl, Cure simulation with resistively in situ heated CFRP molds: Implementation and validation, Compos. Part A: Appl. Sci. Manuf. 80 (2016) 171–181, https://doi.org/10.1016/j.compositesa.2015.10.020.

[86] FS Xoan, A Sans, A Jim, M Campo, A Ureña, SG. Prolongo, Highly multifunctional GNP /epoxy nanocomposites : from strain-sensing to joule heating applications, Nanomaterials 10 (2020), https://doi.org/10.3390/nano10122431.

[87] T Xia, D Zeng, Z Li, RJ Young, C Vallés, IA. Kinloch, Electrically conductive GNP/epoxy composites for out-of-autoclave thermoset curing through Joule heating, Compos. Sci. Technol. 164 (2018) 304–312, https://doi.org/10.1016/j.compscitech.2018.05.053.

[88] X Xu, Y Zhang, J Jiang, H Wang, X Zhao, Q Li, et al., In-situ curing of glass fiber reinforced polymer composites via resistive heating of carbon nanotube films, Compos. Sci. Technol. 149 (2017), https://doi.org/10.1016/j.compscitech.2017.06.001, 20–7.

[89] B Mas, JP Fernández-Blázquez, J Duval, H Bunyan, JJ. Vilatela, Thermoset curing through Joule heating of nanocarbons for composite manufacture, repair and soldering, Carbon N Y 63 (2013), https://doi.org/10.1016/j.carbon.2013.07.029, 523–9.

[90] C Li, RA. Dickie, Bonding adhesive joints with radio-frequency dielectric heating, Int. J. Adhes. Adhesives 11 (1991), https://doi.org/10.1016/0143-7496(91)90007-5, 241–6.

[91] A Vashisth, RE Healey, MJ Pospisil, JH Oh, MJ. Green, Continuous processing of pre-pregs using radio frequency heating, Compos. Sci. Technol. 195 (2020), 108211, https://doi.org/10.1016/j.compscitech.2020.108211.

[92] S Yarlagadda, HJ Kim, JW Gillespie, NB Shevchenko, BK. Fink, A study on the induction heating of conductive fiber reinforced composites, J. Compos. Mater. 36 (2002), https://doi.org/10.1106/002199802023171, 401–21.

[93] C Severijns, ST de Freitas, JA. Poulis, Susceptor-assisted induction curing behaviour of a two component epoxy paste adhesive for aerospace applications, Int. J. Adhes. Adhesives 75 (2017) 155–164, https://doi.org/10.1016/j.ijadhadh.2017.03.005.

[94] R Rudolf, P Mitschang, M. Neitzel, Induction heating of continuous carbon-fibre-reinforced thermoplastics, Compos. Part A: Appl. Sci. Manuf. 31 (2000) 1191–1202, https://doi.org/10.1016/S1359-835X(00)00094-4.

[95] TJ Ahmed, D Stavrov, HEN Bersee, A. Beukers, Induction welding of thermoplastic composites-an overview, Compos. Part A: Appl. Sci. Manuf. 37 (2006), https://doi.org/10.1016/j.compositesa.2005.10.009, 1638–51.

[96] T Bayerl, M Duhovic, P Mitschang, D. Bhattacharyya, The heating of polymer composites by electromagnetic induction - a review, Compos. Part A: Appl. Sci. Manuf. 57 (2014) 27–40, https://doi.org/10.1016/j.compositesa.2013.10.024.

[97] S Mahdi, H-J Kim, BA Gama, S Yarlagadda, JW. Gillespie, A comparison of oven-cured and induction-cured adhesively bonded composite joints, J. Compos. Mater. 37 (2003) 519–542, https://doi.org/10.1177/0021998303037006776.

[98] TE Tay, BK Fink, SH McKnight, S Yarlagadda, JW. Gillespie, Accelerated curing of adhesives in bonded joints by induction heating, J. Compos. Mater. 33 (1999), https://doi.org/10.1177/002199839903301704, 1643–64.

[99] Johnson RJ, Pitchumani R. Active control of reactive resin flow in a vacuum assisted resin transfer molding (VARTM) process n.d. 10.1177/0021998308091264, 2008.

[100] M Frauenhofer, H Kunz, Dilger, Fast curing of adhesives in the field of CFRP, The J. Adhes. 88 (2012) 406–417, https://doi.org/10.1080/00218464.2012.660386.

[101] A Sánchez Cebrián, R Basler, F Klunker, M. Zogg, Acceleration of the curing process of a paste adhesive for aerospace applications considering cure dependent void formations, Int. J. Adhes. Adhesives 48 (2014), https://doi.org/10.1016/j.ijadhadh.2013.09.029, 51–8.

[102] M Kim, H Kim, W. Lee, Repair of aircraft structures using composite patches bonded through induction heating, Adv. Compos. Mater. 24 (2015) 307–323, https://doi.org/10.1080/09243046.2014.899553.

[103] M Ramulu, PB Stickler, NS McDevitt, IP Datar, D Kim, MG. Jenkins, Influence of processing methods on the tensile and flexure properties of high temperature composites, Compos. Sci. Technol. 64 (2004), https://doi.org/10.1016/j.compscitech.2003.12.008, 1763–72.

[104] FYC Boey, TH. Lee, Electromagnetic radiation curing of an epoxy/fibre glass reinforced composite, Int. J. Radiation Appl. Instrumentation Part C Radiation Phys. Chem. 38 (1991) 419–423, https://doi.org/10.1016/1359-0197(91)90118-L.

[105] S Chandrasekaran, S Ramanathan, T. Basak, Microwave material processing-a review, AIChE J. 58 (2012) 330–363, https://doi.org/10.1002/AIC.12766.

[106] TP Naik, I Singh, AK. Sharma, Processing of polymer matrix composites using microwave energy: A review, Compos. Part A: Appl. Sci. Manuf. 156 (2022), 106870, https://doi.org/10.1016/J.COMPOSITESA.2022.106870.

[107] J Zhou, Y Li, Z Zhu, E Xu, S Li, S. Sui, Microwave heating and curing of metal-like CFRP laminates through ultrathin and flexible resonance structures, Compos. Sci. Technol. (2022) 218, https://doi.org/10.1016/J.COMPSCITECH.2021.109200.

[108] J Zhou, Y Li, S Liu, Y Zhang, P Wang, S. Sui, Zone-regulated microwave heating of CFRP laminates via ultrathin and flexible resonance structures with different working frequencies, Compos. Commun. 29 (2022), 101016, https://doi.org/10.1016/J.COCO.2021.101016.

[109] RR Mishra, AK. Sharma, Microwave-material interaction phenomena: Heating mechanisms, challenges and opportunities in material processing, Compos. Part A: Appl. Sci. Manuf. 81 (2016) 78–97, https://doi.org/10.1016/j.compositesa.2015.10.035.

[110] AJ. Bur, Dielectric properties of polymers at microwave frequencies: a review, Polymer (Guildf) 26 (1985) 963–977, https://doi.org/10.1016/0032-3861(85)90216-2.

[111] D Kim, T Centea, SR. Nutt, Out-time effects on cure kinetics and viscosity for an out-of-autoclave (OOA) prepreg: Modelling and monitoring, Compos. Sci. Technol. 100 (2014) 63–69, https://doi.org/10.1016/j.compscitech.2014.05.027.

[112] AMRC. Monitoring thermal distribution optris IR camera. n.d, 2015.

[113] E Rudolf, Final report summary - CODE (Curing polyester resins on demand, CORDIS - EU Commision (2007).

[114] Inma Roig Asensi, Rudolf Dr, Emmerich, Liliana Chamudis Varan. EP2062930A1 - Method and resin system for producing plastics mouldings having a cured plastics matrix -, Google Patents (2009).

[115] AIMPLAS, WAVECOM summary report. (2014).

[116] Borrás AB, Galindo B, Ramos F. Microwave heating of polymers: Influence of carbon nanotubes and graphene dispersion on the microwave susceptor effectiveness. 6th International Conference on Carbon Nanoparticle Based Composites, Dresden, Germany: 2013.

[117] Tuncer E, Sauers I, James R. Electrical properties of epoxy resin based nano-composites 2007. 10.1088/0957-4484/18/2/025703.

[118] JC Abry, S Bochard, A Chateauminois, M Salvia, G Giraud, In situ detection of damage in CFRP laminates by electrical resistance measurements, Compos. Sci. Technol. 59 (1999) 925–935, https://doi.org/10.1016/S0266-3538(98)00132-8.

[119] JB Park, T Okabe, N. Takeda, New concept for modeling the electromechanical behavior of unidirectional carbon-fiber-reinforced plastic under tensile loading, Smart Mater. Structures 12 (2003) 105–114, https://doi.org/10.1088/0964-1726/12/1/312.

[120] D Stavrov, HEN. Bersee, Resistance welding of thermoplastic composites-an overview, Compos. Part A: Appl. Sci. Manuf. 36 (2005) 39–54, https://doi.org/10.1016/j.compositesa.2004.06.030.

[121] D Brassard, M Dubé, JR. Tavares, Resistance welding of thermoplastic composites with a nanocomposite heating element, Compos. Part B: Eng. 165 (2019) 779–784, https://doi.org/10.1016/j.compositesb.2019.02.038.

[122] C Robert, T Pecur, JM Maguire, AD Lafferty, ED McCarthy, Brádaigh CMÓ, A novel powder-epoxy towpregging line for wind and tidal turbine blades, Compos. Part B: Eng. 203 (2020) 1359–8368, https://doi.org/10.1016/j.compositesb.2020.108443.

[123] J Lee, X Ni, F Daso, X Xiao, D King, J Sánchez Gómez, et al., Supplementary materials: advanced carbon fiber composite out-of-autoclave laminate manufacture via nanostructured out-of-oven conductive curing, Compos. Sci. Technol. 166 (2018), https://doi.org/10.1016/j.compscitech.2018.02.031, 150–9.

[124] Thermo Energy Corporation. EPRl Radio-Frequency Dielectric Heating in Industry. California: 1987.

[125] A Riccio, A Russo, A Raimondo, P Cirillo, A. Caraviello, A numerical/experimental study on the induction heating of adhesives for composite materials bonding, Mater. Today Commun. 15 (2018) 203–213, https://doi.org/10.1016/j.mtcomm.2018.03.008.

[126] Rudnev V, Loveless D, Cook R. Handbook of induction heating valery. 2017. 10.1201/9781315117485-3.

[127] T Segreto, A Bottillo, B Palmieri, L Nele, R. Teti, Ultrasonic evaluation of induction heat treatment applied to thermoplastic matrix CFRP, Procedia CIRP 88 (2020) 467–472, https://doi.org/10.1016/j.procir.2020.05.081. Elsevier B.V.

[128] DA McCarville, HA. Schaefer, Processing and Joining of Thermoplastic Composites, Compos. ASM Int.; (2001) 633–645, https://doi.org/10.31399/asm.hb.v21.a0003425.

[129] JB Khan, AC Smith, PM Tuohy, M Gresil, C. Soutis, Three-dimensional finite-element analysis multiphysics modelling of electromagnetic Joule heating in carbon fibre composites, IET Electr. Power Appl. 14 (2020), https://doi.org/10.1049/iet-epa.2019.0963, 1966–73.

[130] Kim D, Ramulu M, Doan AX. Influence of consolidation process on the drilling performance and machinability of PIXA-M and PEEK thermoplastic composites. J. Thermoplastic Compos. Mater. 2005;18. 10.1177/0892705705044556.

[131] KJ Åström, T. Hägglund, PID controllers: theory, design, and tuning 2 (1995).

[132] Vaidya S, Ambad P, Bhosle S. Industry 4.0 - A glimpse. Procedia Manuf., vol. 20, Elsevier B.V.; 2018, p. 233–8. 10.1016/j.promfg.2018.02.034.

[133] V Alcácer, V. Cruz-Machado, Scanning the industry 4.0: a literature review on technologies for manufacturing systems. engineering science and technology, An Int. J. 22 (2019) 899–919, https://doi.org/10.1016/j.jestch.2019.01.006.

[134] JL. Koenig, Spectroscopy of Polymers, Second Edition, American Chemical Society, 1999.

[135] S Liu, VS Chevali, Z Xu, D Hui, H. Wang, A review of extending performance of epoxy resins using carbon nanomaterials, Compos. Part B: Eng. 136 (2018) 197–214, https://doi.org/10.1016/j.compositesb.2017.08.020.

[136] V Kostopoulos, A Masouras, A Baltopoulos, A Vavouliotis, G Sotiriadis, L. Pambaguian, A critical review of nanotechnologies for composite aerospace structures, CEAS Space J. 9 (2017) 35–57, https://doi.org/10.1007/s12567-016-0123-7.

[137] H Tertrais, A Barasinski, F. Chinesta, Simulation of the propagation of an electromagnetic field in a laminated composite part: Application to microwave heating, AIP Conference Proceedings 1769 (2016), 170037, https://doi.org/10.1063/1.4963593.

[138] H Tertrais, R Ibanez, A Barasinski, C Ghnatios, F. Chinesta, Simulation of microwave heating of a composite part in an oven cavity, AIP Conference Proceedings (2017), https://doi.org/10.1063/1.5008005, 1896:30018.

[139] M Kim, DH Sung, K Kong, N Kim, BJ Kim, HW Park, et al., Characterization of resistive heating and thermoelectric behavior of discontinuous carbon fiber-epoxy composites, Compos. Part B: Eng. 90 (2016) 37–44, https://doi.org/10.1016/j.compositesb.2015.11.037.

[140] P Mitschang, R Rudolf, M. Neitzel, Continuous induction welding process, modelling and realisation, J. Thermoplastic Compos. Mater. 15 (2002) 127–153, https://doi.org/10.1106/089270502021451.

4. Materials and methods

This section covers in more depth the materials and methods used in the studies covered throughout the thesis. The section further demonstrates the potential applicability of the methods to aerospace applications.

4.1. Joule heating and self-sensing equipment

The methods developed for Joule heating and electrical resistance monitoring for self-sensing are discussed in further detail below.

4.1.1. Hardware selection:

National Instruments equipment was primarily used throughout for both Joule heating and electrical self-sensing, mainly due to the wide range of data acquisition and control hardware that was available at the time within one chassis. A PXI (PCI eXtensions for Instrumentation) system was used, which integrated a controller for LabVIEW programming, with the following modules installed, categorised by their use cases:

- Electrical self-sensing:
    - PXIe-4080 Digital Multimeter (DMM) – Enabling resistance monitoring in 2-point and 4-point modes, with automatic adjustment of input current depending on resistance [1].
    - PXI-2530B 128-Channel 4-wire multiplexer module – This enables a 4 wire connection to be switched over 32 resistance monitoring points, or a 2-wire connection over 64 resistance monitoring points [2]. This enabled a single DMM to scan and measure a large number of resistances in a short period.
- Direct electric cure:
    - PXI-6229 Multifunction IO [3]: This equipment's digital output was used to control relays to switch off the PSU in case of a system failure and provided the potential for future modulation of relays. It also monitored the safety controls such as emergency stop.
    - PXIe-4353 Temperature input module – This is a 32-channel thermocouple input module, with cold junction compensation [4]. The number of channels allowed for large amount of data to be monitored in areas of components being cured.
    - NI RMX-4124 programmable power supply unit (PSU) – This PSU provided high current limit to ensure it could provide enough power to the low resistance loads of the CFRP components [5]. It was also had drivers for LabVIEW, ensuring easy development of software.

The DMM module was also reused for monitoring the resistance during piezoresistance testing of nanocomposites in chapter 8.

4.1.2. Self-curing hardware and software setup

A block diagram of the setup described in the previous section can be seen in Figure 23.

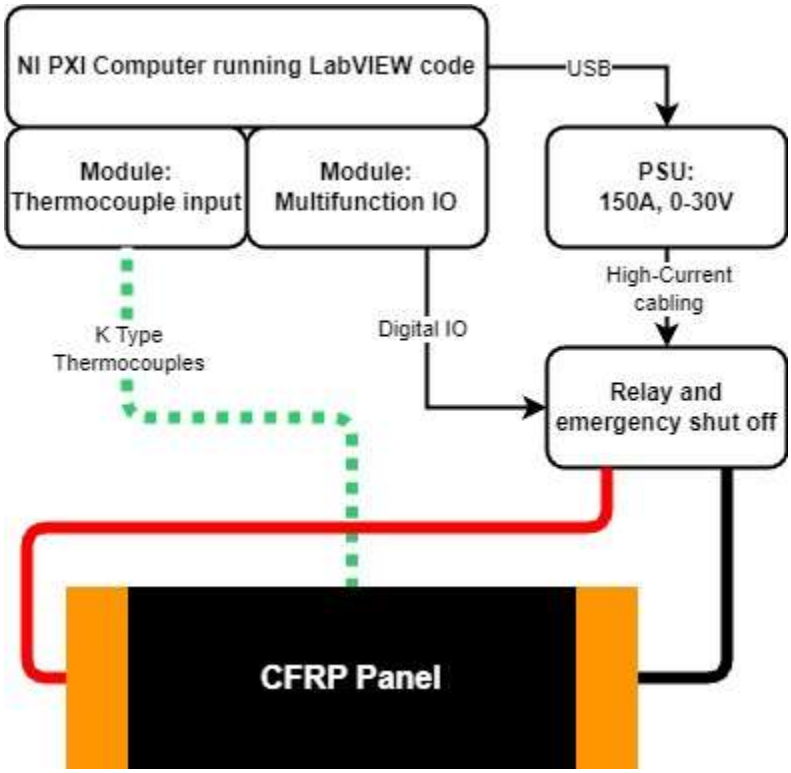

Figure 23: A block diagram of the direct electric cure setup, including NI PXI modules, power supplies and custom-made hardware.

The relay and emergency switch off equipment was originally designed to be able to switch on and off multiple heating zones within the CFRP panel. This was to enable zonal heating, which would result in a more uniform temperature over the CFRP surface if modulated correctly. However, due to time constraints it wasn't possible to implement and test this approach. Nevertheless, it was used as an extra safety measure. The switching was utilised during the de-icing testing, where it was used to power two zones at different power levels.

The thermocouple module had the capacity to monitor up to 32 thermocouples simultaneously, however the maximum used on the larger components was around 12.

The LabVIEW code is too complex to fully cover in this section and is only a supporting feature. However, some of its highlights are detailed here. A screenshot of the final graphical user interface (GUI) can be seen in Figure 24.

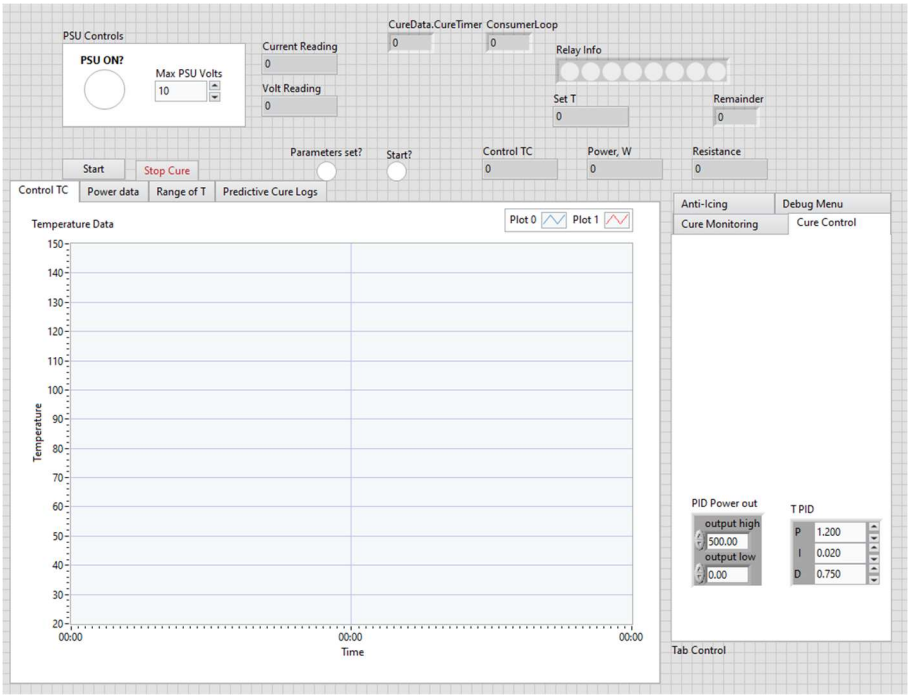

Figure 24: A screenshot of the user interface of the direct electric cure LabVIEW software.

The code was written as a producer consumer architecture, which worked effectively for this use case as there was data collected from many sources at varying sample rates. This architecture also allowed for accurate cycle timing, cycling every second. The program had the following features:

- Generation of complex temperature cure cycles though a graphical user interface.
- Simple PID temperature and power control, of which parameters could be adjusted during a cure cycle.
- Calculation and adjustment of calculated power (using a secondary PID loop), allowing the PSU to be power controlled. The PSU was only controllable in constant current mode, some of the safety implications are discussed in the DEC paper in section 8.
- Ability to control from any thermocouple, or the thermocouple showing the highest or lowest reading.
- Logging metadata of the component, such as thermocouple positions over a panel, panel size, electrode setup, time & date.
- Debug controls to adjust parameters during cure, such as PSU output and current limits.
- Automatic CSV logging of all cure and control parameters.
- Visual GUI for setting up cure parameters, such as thermocouple position.
- Thorough error logging to assist with debugging.
- Algorithm for the switching for de-icing modes, discussed further in section 5 de-icing work.

4.1.3. Self-sensing hardware and software setup

A block diagram of the self-sensing hardware setup can be seen in Figure 25.

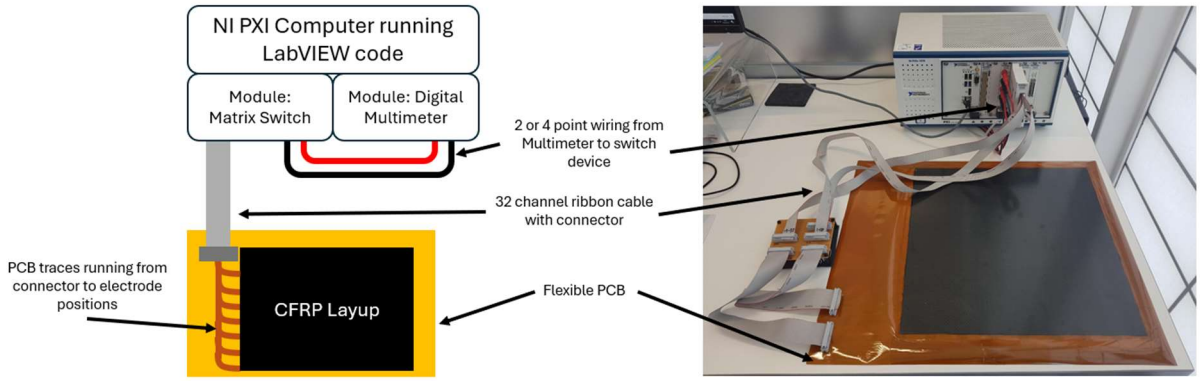

Figure 25: A block diagram of the self-sensing setup, including NI PXI modules.

Due to the limitation of the number switching inputs on the matrix module, there were multiple sets of ribbon cables, depending on the setup or electrodes that needed to be monitored. There were two sets for the panel PCB setup, one addressing only the electrodes on the perimeter of the panel (used by XY scan pattern), and one that addressed the electrodes in the centre of the panel and alternating the perimeter electrodes (used by the 2PZ & 4PZ scan patterns, effectively half density of all electrodes available), therefore only some electrodes being used in both use cases. In the case of the modular scanning setup, the ribbon cable could connect to 4 modular PCBs at the same time. For an area covered by more than 4 PCBs, it would allow for a set of 4 to be scanned, then move the ribbon cable from the 1st to the 5th PCB, then rescan. This could be repeated as many times as required depending on the size of the scan area. Further details on this setup are described in chapter 8.

The software was written in multiple stages and different programs were written for different panel and PCB configurations. However, they followed the main reoccurring design pattern, namely:

- Input the exact number of electrodes in the set configuration to the GUI.
- Software calculates the electrode positions and numbering.
- A scan pattern based on the PCB and scan mode used is generated.
- This is converted to NI proprietary code for switching driver to run.
- Collect data and log resistance values into a CSV.
- Interrogate data manually, or
- Convert datapoints into a matrix, interpolate and generate a heat map.

Because the electrode positions and resulting switch connection were so different between methods, a separate program was created for each method for logging the data and automatic interpretation. For trials on the panel PCB setups, such as XY and 4-point zone, the results could be interpreted within Excel. Larger data sets such as 2-point zone, or data collected with the modular PCB's were processed automatically in LabVIEW. This enabled the removal or replacement of Not a Number (NaN) readings, interpolation between values and generation of heat maps.

4.2. Other methods and equipment

4.2.1. Impact tower setup

For the self-sensing development in chapter 8, impact damage was generated in samples using a Imatek IM1C impact testing machine, seen in Figure 26. It has a maximum drop height of 1.5 metres, with an impact energy range from 1 J to 98 J. This equipment is specifically designed to impact samples according to ASTM D7136, with a composite specific frame for 200 x 100 mm samples to be secured. It has features such as a second impact protection system, where the impactor is lifted away from the sample after the first impact, so further damage doesn't occur. It also has force measurement transducer in the impactor head, however this data was only used to verify the impact was successful.

Figure 26: Imatek IM1C impact tower installed at the AMRC.

To determine the energy required to generate barely visible impact damage, 200 x 100 mm clamped samples of the same layup and materials as the panel PCB samples were used (8-plies of Cycom 5320-1) except without the PCB interleave. This was done by impacting a set of samples with increasingly higher impact energy and visually inspecting the damage that occurred. The impact tower's clamping system was configured for 200 x 100 mm samples, therefore it had to be modified for the larger PCB panel samples.

4.2.2. Differential Scanning Calorimetry (DSC) for degree of cure monitoring

For all DoC monitoring in the studies in this thesis, a Perkin Elmer DSC 4000 with an intracooler was used. Any analysis was completed using the software supplied with the hardware (Pyris), which enables calculation of the energy generated per gram. Samples were weighed with a 4-point scale prior to testing.

Figure 27: Perkin Elmer DSC 4000 [6].

This Differential Scanning Calorimetry (DSC) equipment was used to provide estimates of degree of cure of the components manufactured using direct electric cure and the cure modelling algorithm. DSC works by comparing the heat (calorific) output of a sample to an empty reference sample, hence the differential in the name. It monitors the heat output over time, which is commonly completed with a temperature scan, in this study from 30 °C to 300 °C. The total heat output per gram of sample can provide an indication of the degree of cure, as the crosslinking process in epoxy cure is an exothermic process. There are multiple ways to interpret these results, as degree of cure is not well defined, and this can cause the results to seem better than they are.

One way to interpret it is on a scale of 0-100 %, where 0 % DoC is the sample state when the energy in the sample after the initial epoxy-hardener mixing, or 0 hours out life if pre-preg (despite being b-staged during manufacture), and 100 % cured has J of energy released/remaining from the sample during testing. This will give a good indication of the remaining percentage of molecules that remain to crosslink. However, it is very rare for cure cycles for commercial resin systems to designed to achieve 100 % DoC after a cure and post cure, despite the high temperature and lengths of some of these cycles. The resulting DoC using this measurement can be anywhere from 85 to 97 %, which could be misinterpreted as all results being under cured, or not completing a cure cycle correctly. However, this under curing is intentional, as it allows for refinement of the material properties of the end component, particularly allowing desirable reduction in the flexural stiffness of the resulting resin or component.

Another approach is to define 100 % cure as the energy remaining after completion of the manufacturer's recommended cure cycle. This again can be confusing, as it allows for results of over 100 % DoC to occur.

4.2.3. C-scan equipment

An Olympus Omniscan MX-1 unit with a phased array ultrasonic module was available to verify impact damage in composite samples. An encoder wheel was used to enable C-scan data to be collected.

Figure 28: Olympus Omniscan MX [7].

It is relatively simple to setup the unit to detect different the ultrasonics characteristics and flaw sizes within composites. However it is complex to setup effective reporting, and the file format does not enable copying for later post-processing using a PC. Given these limitations this older unit was used for BVID verification only.

The details on how ultrasonics can be used to detect damage in composites can be found in chapter 2.

4.3. References

[1] PXIe-4080 Specifications - NI n.d. https://www.ni.com/docs/en-US/bundle/pxie-4080-specs/page/specs.html (accessed November 13, 2023).

[2] PXI-2530B Specifications - NI n.d. https://www.ni.com/docs/en-US/bundle/pxi-2530b-specs/page/specs.html (accessed November 13, 2023).

[3] PCI/PXI/USB-6229 Specifications - NI n.d. https://www.ni.com/docs/en-US/bundle/pci-pxi-usb-6229-specs/page/specs.html (accessed November 13, 2023).

[4] PXIe-4353 Specifications - NI n.d. https://www.ni.com/docs/en-US/bundle/pxie-4353-specs/resource/375508c.pdf (accessed November 13, 2023).

[5] RMX Programmable Power Supplies (RMX-412x) User Manual - NI n.d. https://www.ni.com/docs/en-US/bundle/rmx-412x-features/resource/375744c.pdf (accessed November 13, 2023).

[6] PerkinElmer, Inc. A WORLD OF OPPORTUNITY IN THERMAL ANALYSIS DSC 4000/6000/8000/8500 Comprehensive Solutions for Differential Scanning Calorimetry. n.d.

[7] Olympus. OmniScan ® MX with ECA/ECT Modules Discover Eddy Current Color Imaging OmniScan MX. 2018.

5. The effect of type of mechanical processing on electrical conductivity and piezoresistive response of CNT and graphite composites

Procedia CIRP

Volume 85, December 2019, Pages 314-320,

https://doi.org/10.1016/j.procir.2019.10.001.

M.G.Collinson[1], S.Petropoulos[1], S. Hayes[2]

[1] Advanced Manufacturing Research Centre, University of Sheffield, Wallis Way, Catcliffe, Rotherham, S60 5TZ UK

[2] Department of Multidisciplinary Engineering Education, University of Sheffield, 32 Leavygreave Road, Sheffield, S3 7RD

5.1. Author declaration, background and reflection

This conference proceeding was conceptualised, investigated, authored, edited and presented by Matthew Collinson for the 2nd CIRP conference on composite material parts manufacturing in 2019. Simon Hayes assisted with the conceptualisation, supervision and reviewing of the paper. Stefanos Petropoulos assisted with the experimental work and post processing of the data generated.

This work was early during my PhD studies, where previous literature had indicated that increasing the conductivity of the matrix could improve the performance the DEC and self-sensing technologies, which I was developing in parallel. Working with nanoparticles in this study led to the realisation that the method is not robust or repeatable to increase conductivity, nor was it compatible or easily applicable to pre-preg or VARTM manufacturing processes. The resulting nanocomposites were tested in de-icing and self-sensing experiments as electrode-carbon fibre interface, however there was little or no system conductivity increase. In many cases, it increased the range of the conductivity readings due to the low homogeny of the nanocomposites, or led to conductivity decreases, resulting in hotspots, and burning during the Joule heating experiments. I believe that CNTs are unlikely to find commercial success in composite matrix systems, due to the complexity of processing [1], the occupational health risk they pose [2], and their current enormous energy input required to manufacture [3].

5.2. Amendments and clarifications

In Section 3.2, paragraph 1 and 2, it is stated the conductivity of the graphite mixed samples doesn't change between mixing methods. This is incorrect, as it can be seen in Table 2, that when hand mixed, both batches of graphite have significant increases in conductivity, compared to mechanical methods. This discussed later in section 3.4.

In the conclusion, it is stated that there is no significant change in gauge factor in respect to manufacturing methods and loading percentage of the nano particles. This is meant to conclude that there are limited conclusions and trends that can be taken from the gauge factor data. The gauge factors of hand mixed samples are lower on average compared to mechanical methods. The gauge

factor of shear mixed samples appears to rise with loading percentage, however not enough samples were tested to confidently conclude this.

References

[1] Collinson M, Hayes S, Petropoulos S. The effect of type of mechanical processing on electrical conductivity and piezoresistive response of CNT and graphite composites. Procedia CIRP 2019;85:314–20. https://doi.org/10.1016/J.PROCIR.2019.10.001.

[2] Luanpitpong S, Wang L, Rojanasakul Y. The effects of carbon nanotubes on lung and dermal cellular behaviors. Nanomedicine 2014;9:895–912. https://doi.org/10.2217/nnm.14.42.

[3] Gutowski TG, Liow JYH, Sekulic DP. Minimum exergy requirements for the manufacturing of carbon nanotubes. Proceedings of the 2010 IEEE International Symposium on Sustainable Systems and Technology, IEEE; 2010, p. 1–6. https://doi.org/10.1109/ISSST.2010.5507687.

Available online at www.sciencedirect.com

ScienceDirect

Procedia CIRP 85 (2019) 314–320

www.elsevier.com/locate/procedia

2nd CIRP Conference on Composite Material Parts Manufacturing (CIRP-CCMPM 2019)

The effect of type of mechanical processing on electrical conductivity and piezoresistive response of CNT and graphite composites

Matthew Collinson[a]*, Simon Hayes[b], Stefanos Petropoulos[a]

[a]*Advanced Manufacturing Research Centre, Advanced Manufacturing Park, Wallis Way, Catcliffe, Rotherham, S60 5TZ*
[b]*Department of Multidisciplinary Engineering Education, The University Of Sheffield, 32 Leavygreave Road, Sheffield, S3 7RD*

* Corresponding author. Tel.: +44 (0)144-215-8032. *E-mail address:* m.collinson@amrc.co.uk

Abstract

Nanocomposite materials are attracting significant interest as matrices for conventional composite materials, where their increased electrical conductivity present the possibility of multi-functional properties, such as embedded heating and electromagnetic shielding. One problem facing the increased use of the nanocomposites is their rapid and efficient production. Three different mixing methods: 3-roll mill, shear mixing and hand mixing were tested to mix carbon nanotubes (CNTs) and graphite into epoxy resin. The electrical conductivity and piezoresistive response of the resulting nanocomposites were measured and compared to the relative rate of nanocomposite could be produced. Maximisation of the functional properties is important, but speed of throughput is also essential, thus enabling larger and production ready components to take advantage of the additional functionality. Because of health and safety concerns during material handling of nanoparticles, this study employed a premixed CNT masterbatch (Arkema) and graphite powders (Superior Graphite), as these do not require specialised health and safety equipment to process, making industrial application more viable. It was found that the 3-roll provided the largest increase in conductivity out of the three mixing methods, and hand mixing and shear mixing performed similarly. Piezoresistivity was seen in all modified samples, however gauge factors were difficult to determine due to underdeveloped sample contact and preparation methods.

Keywords: composites; nanocomposites; CNT; carbon nanotubes; graphite; piezoresisitve; conductivity; 3-roll mill; shear mixing

1. Introduction

Nanocomposites, the combination of a polymer matrix and a nanoscale reinforcement, have attracted significant research interest, particularly with the increased commercial availability of carbon-based nanostructures such as carbon nanotubes, graphene and graphite. Combining polymer matrices such as thermoplastics or epoxy resins, which are all electrically insulating, with these nanofillers has shown increased material properties. In particular fracture toughness and thermal conductivity, and also enhancing the material with new properties, such as conductivity and piezoresistance. The realisation of these properties allows for exciting developments in design of composite materials, in particular, multifunctional composites. These include, but are not limited to: piezoresistive sensors, antistatic protection, localised joule effect heating and increased heat dispersion, meaning extra external devices on the part are not required.

Benefits like these are of interest to the aerospace and automotive industries, where light weighting is of significant importance due to legislation limiting emissions, which leads to reducing fuel usage, resulting in increased profitability.

Manufacturing of nanocomposites is a difficult process for most standard composite part manufacturers. Unprocessed carbon nanotubes and graphene need functionalisation, which is the enabling chemical compatibility between the filler and the matrix. This requires a strong knowledge of the nanofillers and the resin, as well as specialised chemical processes. These

10.1016/j.procir.2019.10.001

nanoparticles also in their raw form require strict and costly health and safety controls, due to their comparison to asbestos and potential carcinogenic nature [1].

Once these issues are resolved, for nanocomposites to be effectively integrated into a component to enable smart functionalities, they need to be able to be processed using a medium to high throughput processes. Many previous studies have used a variety of mixing and dispersion methods, such as sonication [2], solvent evaporation [3], ball milling, dissolver disk mixing [4], shear mixing and 3-roll mill [5]. These all have varying levels of success at dispersing the nanoparticles evenly in a matrix, but have not been considered for manufacture beyond laboratory scale. Whilst it is important to obtain a high level of dispersion and therefore improvements in material properties, in this case primarily electrical conductivity, the ability to manufacture at a higher rate needs to be taken into account.

For this study, processability and practicality have been prioritised, from the material selection to the equipment used to manufacture the nanocomposites, in view to manufacture fibre based composites in the future. This means that conductivity vs filler content needs to be scrutinised, as manufacturing a composite with a high percentage of nanofillers is difficult due to the filtering effect when infusing. This can be alleviated with different manufacturing techniques such as pre-pregging, however are costly and prohibitive in a development environment, and also not relevant to industries such as automotive. Keeping the nanofiller weight percentage low will allow for the resin to retain its low viscosity, whilst having fewer nanoparticles to be filtered out when manufacturing along the length larger scale fibre composites.

The materials selected are either pre-functionalised in a DGEBA-CNT masterbatch (Arkema), or do not require any functionalisation, namely super expanded graphite flake (Superior Graphite) which will be mixed directly into resin. The CNTs used are Multi Walled CNTs, having 10-15 walls of 10-15nm in diameter, with an aspect ratio of 600-700. The graphite used is a super expanded graphite flake, with 90% of the particles being 17.6μm or smaller.

The mixing methods have been selected based on effectiveness, market availability, time to process and cost. The 3-roll mill was selected as it was a recommended method by the CNT masterbatch manufacturer (Arkema) as the optimal dispersion method and therefore the method has also been replicated for graphite. Another industrial method suggested by the literature and the manufacturer is a high shear mixer, which is seen more commonly in industry for efficient mixing and dispersion of solutions. The final method used in this study is hand mixing of the materials into the resin, which is used as a low effort comparative baseline, to show what conductivity can be achieved with little equipment expenditure.

CNTs were primarily investigated in this study due to their higher conductivity to weight ratio compared to graphite, and therefore more dispersions at different percentages were manufactured. Future consideration needs to be taken into account when these nanocomposites are to be used as matrices in fibre composites, where it is important that low as possible percentages of filler are used so that they can be infused and distributed between fibres evenly. When high percentages of larger particles are used, filtration occurs between and through fibres when infusing along a fabric, and on a smaller scale, through thickness, which leads to uneven distribution, and inhomogeneous material properties [6]. Another reason to use lower percentage weight of nanoparticles is to limit the change in mechanical properties, whilst they are commonly reported as an increase, in some cases they can reduce some mechanical properties.

The piezoresistive mechanism of these nanocomposites is a complex one and not yet fully understood. It is know that there is high contact resistance between the nanoparticles in the polymer matrix, also known as the tunneling effect, of which when strained increases this contact resistance. This tunneling effect is influenced by the makeup of the internal percolation conductive network, such as weight % loading, particle conductivity, cross sectional area and particle alignment [7].

2. Experimental

2.1. Resin preparation and dispersion method

An toughened epoxy system (Gurit Prime 180 [8]) suitable for RTM and infusion was selected as the matrix for the nanocomposites, due to its low ambient viscosity and overall high processability. Two types of nanocomposites were manufactured, at different percentage loadings, to evaluate conductivity and piezoresistivity depending on the dispersion method used. The base materials for the two mixtures were MWCNTs pre-dispersed at 25% by weight in a DGEBA resin, supplied by Arkema (CS1-25), and super expanded graphite flake, supplied by Superior Graphite (FormulaBT LBG8010).

The CNT masterbatch requires mixing and coarsely dispersing into the resin, before any further mechanical mixing or processing. This was done by hand mixing the pellet style masterbatch into the resin at 80 °C, leaving overnight at temperature, then mixing by hand periodically until the pellets had visibly dispersed into the resin. CNT samples were prepared at 0.1, 0.25, 0.5 0.75 and 1% by weight, recommended by the manufacturer and previous studies on MWCNTs [9] .

The graphite nanocomposites were processed in a similar way, with the graphite being hand mixed in, then left over night and mixed periodically until visible dispersion had been achieved. Graphite samples were prepared at 5.3% and 6.5% by weight [10].

Table 1 : Summary of materials used, processing method and weight percentages tested.

Material	Processing method	Wt. %
CNT	Shear mixed 3-Roll milled Hand mixed	0.1, 0.25, 0.5 0.75 and 1%
Graphite	Shear mixed 3-Roll milled Hand mixed	5.3% and 6.5%

A batch of 500 ml resin and filler was prepared for each dispersion and mixing type, then the mixtures were dispersed further in the three different ways (Table 1). All these processes

were completed with the resin at 80 °C at the start of the mixing processes.

A 3-Roll mill (Exakt) was used to then further disperse the fillers into the resin. The resins were processed twice, from 90 microns to 30, and then from 15 to 5 microns, which was the minimum gap possible with this equipment.

Shear mixing (Greaves) was used on the pre-mixed batches at 1500 RPM for 60 minutes, using a stator mixer head.

Hand mixing was completed as per the preparation for the two mechanical dispersion methods. Heating was instead completed on a hotplate, and hand mixing was done for 30 minutes continuously, ensuring that the pellets were dispersed in the case of the CNTs

2.2. Sample manufacture

Once the nanocomposite blends had been prepared, hardener was added at 50% of the original resin weight used, which was mechanically mixed in with a stirrer. Immediately after stirring they were cast in dog bone style silicone moulds, at 6 casts per sample, with the sample geometry conforming to ASTM D638 [11], and placed in a curing oven at 120 °C. Particularly in the case of the CNTs, agglomeration starts immediately, which can reduce the electrical and mechanical properties of the samples. Some agglomeration is required so that a connected electrical network is made, however if allowed to develop further, the agglomerations become so large that the electrical network is lost. This is further discussed in Section 0. After curing, the meniscus of the samples was removed using a water assisted polishing wheel, which also ensured correct sample thickness was achieved.

2.3. Measurement of conductivity

The 4-probe resistivity method was used, which has previously been used successfully to measure conductivity of composites and nanocomposites accurately. This method can be practically applied in a composite part design situation as it doesn't require significant design changes to the composite [12].

The polishing of the samples during manufacture also provided adequate surface preparation for applying highly loaded silver epoxy adhesive (RS Components). This ensured contact resistance was minimized during conductance and piezoresistance testing. A National Instruments PXI 4080 digital multimeter was used for the 4 point conductivity measurement, which was recorded values every 100 ms during the piezoresistive testing. Resistance was automatically calculated by the National Instruments drivers, with using a current injection value depending on the resistance of the sample being tested. This allowed a large range of sample conductivities can be accounted for, whilst still providing accurate resistivity values.

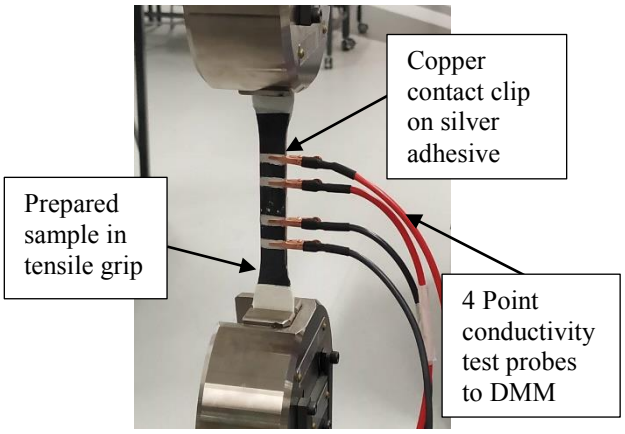

Fig. 1. Experimental setup for piezoresistive testing of dog bone samples, with the 4-point method attached to the sample whilst in the grips of the tensile testing machine.

The resistance value is then corrected for cross section of the sample, and the length between the electrodes for measuring voltage, seen in Equation 1.

$$R = \frac{V}{I}\frac{wt}{L}\Omega.cm \qquad (1)$$

Where V is voltage, I is current, w & t are width and thickness of the sample, and L is the distance between the electrodes for measuring voltage.

Flat, crocodile style clips were used to clamp onto the sample, with the side not prepared with silver epoxy being insulated from the clip, of which can be seen in Fig.1. The sample was insulated from the tensile test clamp to ensure no electrical interference.

Piezoresistance is a change in a materials resistance in response to mechanical strain. Gauge factor (GF) is a way of quantifying this response, as seen in the equation below.

$$GF = \frac{\Delta R/R_0}{\varepsilon} \qquad (2)$$

Where R is the resistance of the sample, ΔR is the change in resistance and ε is the strain of the sample. This allows for characterisation of the response of the material, depending on the sample tested. If a material's conductivity change can be measured in service, and the gauge factor is known, then the strain can be estimated.

2.4. Measurement of strain

Tensile testing was completed with a Shimadzu EZ Test machine, run at 2 mm/min as per the ASTM specification.

Machine compliance was tested using an unloaded epoxy sample with a strain gauge applied. Clip gauges were tested as a possible re-usable strain sensor, however these short circuited the resistance measurement and proved unreliable when insulated, hence the use of calibrated machine measured strain.

Strain was therefore assumed to be the change in length of the sample against the original length of the sample, as described in Equation 3 below.

$$\varepsilon = \frac{l_T - l_0}{l_0} \quad (3)$$

Where ε is strain, l is the length of the unloaded sample, and δl is the change in length in respect to the unloaded sample. These restrictions will mean that sample slippage in the grips will not be accounted for, which would be if a strain gauge was used for example.

3. Results and discussion

3.1. Manufacturing observations and considerations

As seen in previous studies [13] and in practice, the manufacture of high quality dog bone samples in epoxy resin is a challenging process. Issues included manufacturing a void free sample, with defect free edges, without a meniscus, which could lead to premature sample failure. In unmodified epoxy samples, voids were visible, however in modified opaque samples, potential voids were no longer visible, particularly in highly loaded samples. For the opaque samples, manufacturing methods were improved where the voids were visible, then were eventually eliminated through improvements in procedure.

The polishing of the samples also proved to have the benefits of removing the meniscus, bringing the thickness of the samples to specification, and providing repeatable surface preparation conditions for the application of the silver epoxy adhesive.

3.2. Sample conductivity

Of all the samples, the 3-roll mill proved to be a more consistent dispersion method compared to the shear mixer and the hand mixing for CNT composites, providing higher conductivities at equivalent percentage loading of fillers, summarised in Table 2 and Fig.2. Not enough data was collected to determine if this effect was experienced in the graphite mixtures, with little variance in conductivity between the manufacturing methods. Shear mixing did not provide an increase in conductivity over hand mixing in CNT samples, which would have been expected for it being a high shear process. With all mixing methods the percolation threshold was 0.25-0.5% for CNTs, with this being much closer to 0.25% for the 3-roll mill processed samples. It wasn't possible to determine the percolation threshold for the graphite nanocomposites with the data available.

The CNT masterbatch requires high shear forces to break up the pellets and coarsely disperse into the resin, whereas it appears the graphite in powder forms require only basic mixing to disperse effectively. This is highlighted when comparing the increase in conductivity from hand mixed to the 3-roll mill for both fillers: CNTs have a large increase, whereas graphite powders do not change.

The increases between mixing methods for the CNTs may be due to the heavily loaded masterbatch requiring high shear to be broken apart properly, which the shear mixer cannot provide. Another reason, suggested by the manufacturer, is that shear mixing can on occasion damage the CNTs, breaking the walls or making them shorter. This would damage the connections within a percolation network, however there is little evidence of this in any previous studies that suggest that shear mixing doesn't have the energy density to damage CNTs [14].

Another reason for the lower conductivity of the shear mixed samples could be due to the way that the mixer head sits in a batch of epoxy-nanoparticle mixture. With this configuration, it is not always guaranteed that all the resin is processed evenly, or is passed through the mixer head an equal amount of time. Full processing of the mixture is more guaranteed with a 3-roll mill, which would be more suitable for a continuous process.

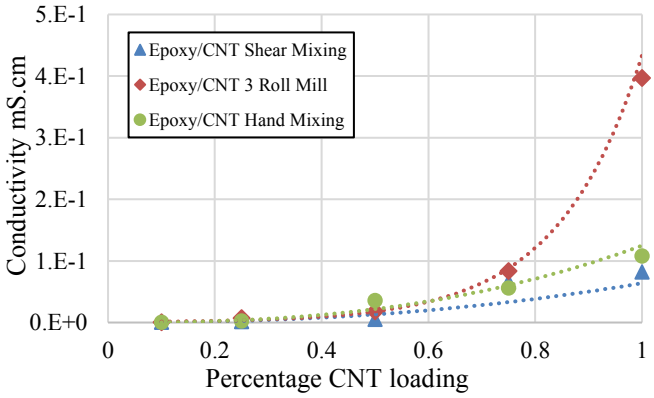

Fig. 2. Conductivity of the CNT dispersions, comparing 3-roll mill to shear mixing and hand mixing.

Table 2 : Mean conductivities for CNT and graphite, for hand mixing, shear mixing and 3-roll mill

Material & loading wt. %	Conductivity 3-roll mill mS.cm	SD	Conductivity shear mixing mS.cm	SD	Conductivity hand mixing mS.cm	SD
0.1% CNT	7.71E-04	±4.57E-04	5.85E-04	±4.00E-04	2.29E-04	±1.11E-04
0.25% CNT	7.51E-03	±1.29E-03	1.48E-03	±5.19E-04	2.66E-03	±2.52E-03
0.5% CNT	1.82E-02	±8.53E-03	5.44E-03	±3.02E-03	3.60E-02	±7.71E-03
0.75% CNT	8.35E-02	±7.11E-03	6.62E-02	±3.64E-03	5.61E-02	±1.42E-02
1% CNT	3.97E-01	±3.62E-02	8.21E-02	±8.61E-03	1.08E-01	±4.40E-02
5.3% Graphite	8.75E-04	±1.86E-05	9.19E-04	±1.36E-04	1.25E-01	±2.19E-02
7.5% Graphite	1.66E-03	±6.02E-04	2.41E-03	±1.41E-03	3.09E-01	±3.85E-03

Re-agglomeration of the nanoparticles is a crucial process that occurs enabling the conductivity of samples. A theoretically 100% distributed epoxy-particle mixture would result in no particles touching one another, which would give a homogeneous mixture, however would give the mixture electrical conductivity equivalent of the matrix, resulting in an insulator. Van der Waals forces are present between the conductive particles, leading to the particles to bunch together in groups, also known as agglomeration. The interaction of these particles leads to the conductivity of the resin increasing due to the percolation network growing, allowing more paths for the current to flow.

The agglomeration of the particles is something that continues to happen over time, leading to larger agglomerates. If left over a long period, the agglomerates continue to increase in size up to the point they become large enough so the percolation network becomes disconnected. The agglomerates no longer have links between them, therefore the conductivity is reduced, leading to a similar problem to perfectly distributed particles.

Agglomeration of CNTs in epoxy resin was investigated by Inam and Peijs [15], looking at average agglomerate size over time in epoxy resin, hardener and after mixture of the two. Agglomeration size stays low over time when mixed with just the epoxy for all variations of CNTs. Once CNTs were mixed with hardener, they agglomerated very quickly, leading to agglomerations four times larger than was observed in the epoxy after 200 minutes. This is in line with many studies that explicitly initially always mix the CNTs with the resin as opposed to the hardener component, and with what was observed by the naked eye in this study (Fig.3). CNT-Epoxy mixture was stored for days with no visual agglomerations, whereas when mixed with the hardener, agglomerations were visible if left to cure at room temperature, seen in Fig.3.

Agglomeration of the graphites were not seen visually, most likely due to the larger particle size, of which Van der Waals forces do not affect in the same way. This is also confirmed by the little difference in conductivities between mixing methods. This effect may have been further helped by the low viscosity of the resin used in this study, which would have enabled accelerated movement of particles, and therefore quicker agglomeration.

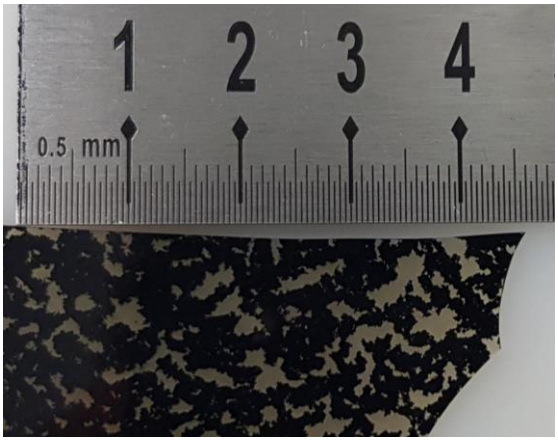

Fig. 3. Example of extreme visual CNT agglomeration in epoxy resin at 0.5% wt.

3.3. Sample piezoresistivity

All the epoxy samples that were modified with either CNTs or graphite showed a piezoresistive response. All graphite samples had a higher gauge factor than the CNT samples, however when corrected for their higher loading percentages, the loading efficiency was lower than the CNTs. When correcting for the wt.% loading of the filler in each sample, it appears that the lower the CNT loading, the more efficient the gauge factor response is.

One of the largest factors in obtaining a good quality piezoresistive signal was the quality of the connection between the DMM and the sample, with clip connectors seen in Fig.1. Poor connections and electrical interference from the conducting grips on the tensile testing machine led to noisy results, which were inconclusive. Tighter grips and insulating the part from the grips led to more consistent results, of which an example can be seen in Fig.4. These responses were consistently in line with the axial strain when normalised. The change in resistance and the axial stress were normalised in respect to axial strain, of which the response of the resistance change is directly related to the stress. Whilst there were only a few of these samples that showed this positive response, showing good replication of the samples, the overall method had poor repeatability.

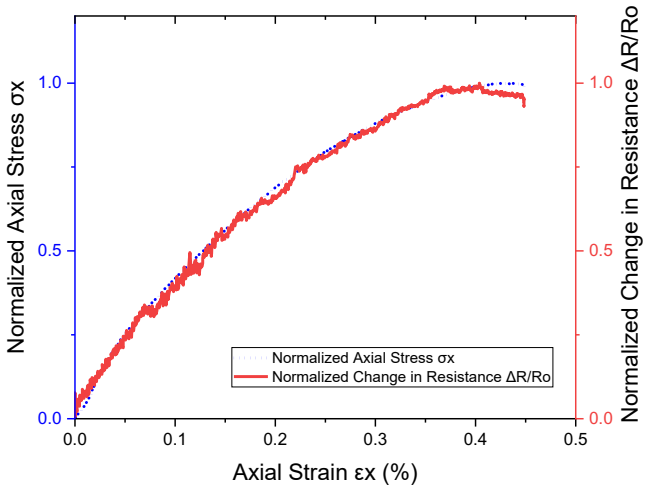

Fig. 4. Example of a piezoresistive response from a 0.25% by wt. CNT epoxy sample processed in the 3-roll mill.

Gauge factor was determined for each concentration and manufacturing method, which ranged from 0.5 to 3.1 for CNT composites, and from 7.8 to 33.4 for graphite composites, as summarised in Table 3.

Even though there were 6 samples manufactured per method and concentration, there were only one or two good results per set. This led to large variability and inconsistency in the results, which have been presented in Table 3. Where results aren't presented, it wasn't possible to get a piezoresistive response.

Table 3 : Mean gauge factors for all samples tested.

Material & loading	Gauge factor 3-roll mill	Gauge factor shear mixing	Gauge factor hand mixing
0.1% CNT	0.49	N/A	N/A
0.25% CNT	2.85	1.37	1.10
0.5% CNT	3.09	0.72	2.10
0.75% CNT	2.39	2.62	1.88
1% CNT	0.89	2.94	1.87
5.3% Graphite	7.84	8.81	13.6
7.5% Graphite	27.75	33.39	7.40

For the graphite samples, an increase in gauge factor was seen in the mechanically mixed samples when loading was increased, however this same pattern did not occur for the hand mixed samples. It seems that when using high shear mixing methods on the graphite samples, the gauge factors are similar, however see a large change, for better or worse when hand mixing is used. This may be due to lack of consistency of the hand mixing method, of which is significantly less controlled than the mechanical mixing methods.

The noise issues and variances in gauge factor may have also been affected by the resistivity and therefore gauge factor of the connection method, which could have dominated the response. Whilst attempts to reduce contact resistance were taken, it is possible that the negative gauge factors of the contacts were interfering with the results. This is more frequently seen in the measurement of CFRP piezoresistive samples [16], but still could be possible in the testing completed here.

It would be recommended to directly bond on the wires to the samples with conductive adhesive, rather than using clips, to ensure that the connection is more repeatable and consistent. On in service parts, the connectors are likely to be integrated into the part during manufacture and therefore be more durable, however there is limited research in this area and therefore wasn't pursued during this study.

The responses and gauge factors seen in the samples allows for potential composite smart functionalities, if these resins were to be integrated into or applied to the surface of composites. The gauge factors seen in this study would allow for smart sensors, replacing strain gauges at low cost, where typically a gauge factor of a Constantan or nickel-chromium strain gauge is around 2 [17]. The quality of the response, when a good connection was available was high, giving a very consistent and high quality response, comparable to a strain gauge. This case, and other investigations on nanocomposites consistently get within this gauge factor range [18]. This could allow lower cost and less sensitive equipment to detect strain, and eventually damage in composites, without having to apply a strain gauge to the structure, which is a time consuming and expensive operation.

Consistency of the measuring of composite samples is still an issue, of which a standard test method needs to be developed and agreed upon. Even when taking in to account recommendations from previous studies, it is still a challenge to get consistent contact resistance when applying electrodes to a sample.

3.4. Manufacturing rate

3-Roll mill, high shear mixing and hand mixing were selected as mixing methods as they vary largely in initial cost, ease of use and processing time. 3-roll mill and shear mixing are commonly used techniques for particle dispersion in mixtures, with hand mixing used as example of minimum effort and cost of what can be achieved.

To compare the methods, literature was examined to ensure the highest level of dispersion was achieved using each method, taking into account the low viscosity resin being used, as described in section 2.1.

The 3-roll mill was the most time consuming and hands on method for dispersion, as the resin mixture has to be fed through slowly, and requires careful cleanup after use. To feed through 500 ml of resin containing fillers takes around 20 minutes, which increases in duration as the gap between the rollers is reduced. This process has to be repeated more than once and requires user supervision throughout. The pouring of the resin from old containers to new, to not contaminate samples, leads to resin waste, as does resin that is stuck on rollers and not processed. This process could be adapted to be run continuously, which would not require cleaning as often, and would reduce wastage.

High shear mixing is easier to run when working with batches, as the mixture can be left to run without supervision. The samples for this study were mixed for 60 minutes, but were left unsupervised during this time, making it more suitable as an industrial process. Mixers of this type are also available that convert the method from a batch process to a continuous one.

Hand mixing was the most simple, however most labour intensive, and operator dependent on the final dispersion. In small batches this method is a useful comparison, but unlike the other methods, it isn't suitable for scaling up to large manufacturing rates.

In the case of the CNTs, the high shear methods were the only ones that provided the higher conductivities and therefore more even distribution. This is partly due to the highly loaded masterbatch format they are provided in, requiring force and heat to break them apart.

Graphite mixtures did not benefit from the mechanical dispersion methods as shown by the conductivities seen in Table 2.

3.5. Future use cases

With all the research activity around nanocomposites, particularly around their benefits to increasing material properties, it is important to know how to process and test the resulting nanocomposites to ensure that they are being manufactured optimally and obtaining the expected final properties. This study was completed to understand these dispersion methods and the factors that affect the final

conductivities of the samples, particularly the interface method between the sensing equipment and the nanocomposites.

Being able to measure the conductivity and piezoresistivity of a composite, or nanocomposite accurately opens up opportunities for multifunctional composites, beyond a structural material. The primary additional function would be integrated structural health monitoring (SHM) systems, being able measure strain in a structure, as well as impact damages. Other uses for conductive composites could be for other electrical interfaces, such as effective static dissipation and joule heating applications such as direct electric cure.

4. Conclusion

The processing and mixing methods of fillers in epoxies are critical to getting the required performance, in this case electrical conductivity, and subsequently piezoresistivity. CNT-epoxy composites had higher conductivities compared to graphite-epoxy composites for a much higher loading content. Significantly higher conductivities were found when mixing in CNT masterbatch when using the 3-roll mill, compared to the shear mixer and hand mixing, which performed similarly.

Piezoresistivity was found in all composite samples, with there being no significant change in gauge factor between manufacturing methods and loading percentage.

Measuring conductivity whilst loading the sample proved difficult, with signals dropping out, and giving consistently different gauge factors within the same set of samples, even when conductive paint and copper clips were used to achieve a high conductivity connection. More research is required to enable consistent piezoresistive testing, so that studies can be compared more easily, and results within studies are more consistent.

This study has shown that it is possible to manufacture and process nanoparticle modified resins with high conductivities, without requiring high expenditure equipment or health and safety controls or processes, enabling more accessible research and product development into multifunctional materials.

5. Acknowledgements

This work was funded by the European Union's Horizon 2020 research programme under grant agreement No 760940, under the project titled MASTRO.

References

[1] C.A. Poland, et al., Carbon nanotubes introduced into the abdominal cavity of mice show asbestos-like pathogenicity in a pilot study, *Nat. Nanotechnol.* 3 (2008) 423–428. doi:10.1038/nnano.2008.111.

[2] P.C. Ma, et al., Dispersion, interfacial interaction and re-agglomeration of functionalized carbon nanotubes in epoxy composites, *Carbon N. Y.* 48 (2010) 1824–1834. doi:10.1016/j.carbon.2010.01.028.

[3] S. Kim, et al., Assessment of carbon nanotube dispersion and mechanical property of epoxy nanocomposites by curing reaction heat measurement, *J. Reinf. Plast. Compos.* 35 (2016) 71–80. doi:10.1177/0731684415613704.

[4] J.K.W. Sandler, et al., Ultra-low electrical percolation threshold in carbon-nanotube-epoxy composites, *Polymer (Guildf).* 44 (2003) 5893–5899. doi:10.1016/S0032-3861(03)00539-1.

[5] I.D. Rosca, S. V. Hoa, Highly conductive multiwall carbon nanotube and epoxy composites produced by three-roll milling, *Carbon N. Y.* 47 (2009) 1958–1968. doi:10.1016/j.carbon.2009.03.039.

[6] S.G. Miller, et al., Mionitoring nanoparticle filtration in a RTM processed epoxy/carbon fiber composite, 2011. https://ntrs.nasa.gov/search.jsp?R=20110014529 (accessed June 27, 2019).

[7] Alamusi, et al., Piezoresistive strain sensors made from carbon nanotubes based polymer nanocomposites, *Sensors*. 11 (2011) 10691–10723. doi:10.3390/s111110691.

[8] G.H. AG, Prime^{TM} 180, (n.d.) 1–4. http://www.gurit.com/-/media/Gurit/Datasheets/PRIME_180.pdf.

[9] R. Khare, S. Bose, Carbon nanotube-based composites - A Review, *J. Miner. Mater. Charact. Eng.* 4 (2005) 31–46. doi:10.1016/B978-0-12-803581-8.10313-3.

[10] S. Gantayat, et al., Expanded graphite as a filler for epoxy matrix composites to improve their thermal, mechanical and electrical properties, *New Carbon Mater.* 30 (2015) 432–437. doi:10.1016/S1872-5805(15)60200-1.

[11] ASTM D638, Standard test method for tensile properties of plastics, *ASTM Int.* 08 (2015) 46–58. doi:10.1520/D0638-14.1.

[12] K.T. Ikikardaslar, F. Delale, Self-sensing damage in CNT infused epoxy panels with and without glass-fibre reinforcement, *Strain*. 54 (2018). doi:10.1111/str.12268.

[13] T.T. Chiao, et al., Fabrication and testing of epoxide resin tensile specimens, *Composites*. 3 (1972) 10–15. doi:10.1016/0010-4361(72)90465-X.

[14] Y.Y. Huang, et al., Dispersion of Carbon Nanotubes: Mixing, Sonication, Stabilization, and Composite Properties, *Polymers (Basel).* 4 (2012) 275–295. doi:10.3390/polym4010275.

[15] F. Inam, T. Peijs, Re-agglomeration of Carbon nanotubes in two-part epoxy system ; Influence of the concentration, 2007. http://nrl.northumbria.ac.uk/12712/1/IBCAST_Proc._May_2007.pdf (accessed August 14, 2018).

[16] G. Georgousis, et al., Piezoresistivity of conductive polymer nanocomposites: Experiment and modeling, *J. Reinf. Plast. Compos.* 37 (2018) 1085–1098. doi:10.1177/0731684418783051.

[17] A. Technologies, Practical Strain Gage Measurements, 1999. https://www.omega.co.uk/techref/pdf/StrainGage_Measurement.pdf (accessed June 11, 2019).

[18] A. Sanli, et al., Piezoresistive performance characterization of strain sensitive multi-walled carbon nanotube-epoxy nanocomposites, *Sensors Actuators A Phys.* 254 (2017) 61–68. doi:10.1016/j.sna.2016.12.011.

6. Development and implementation of direct electric cure of plain weave CFRP composites for aerospace

Composites Part A: Applied Science and Manufacturing,

Volume 172, January 2023, 107615,

https://doi.org/10.1016/j.compositesa.2023.107615.

M.G.Collinson[1], T.J.Swait[1], M.P.Bower[1], B.Nuhiji[1] S.A. Hayes[2]

[1] Advanced Manufacturing Research Centre, University of Sheffield, Wallis Way, Catcliffe, Rotherham, S60 5TZ UK

[2] Department of Multidisciplinary Engineering Education, University of Sheffield, 32 Leavygreave Road, Sheffield, S3 7RD

6.1. Author declaration, background and reflection

As the first author, I authored, developed the methodology, completed experimentation and edited the paper. The concept was developed by Simon Hayes, built on earlier work he authored, and I developed the experimental work [1]. Over the 3 years of developing the technology, all authors assisted in the experimental work, particularly Matthew Bower when it came to the larger more complex layups. Tim Swait, Betime Nuhiji and Simon Hayes provided supervision throughout, and helped with the final paper editing. I was responsible for submission and responding to the peer review process.

The larger leading-edge components were used in section 7.1 for de-icing, as they also contained the plies near the surface that enabled Joule heating. The performance and potential of the de-icing components, led to further grant funding for the Joule heated composite tooling in section 7.2.

6.2. Amendments and clarifications

In section 3.2, paragraph 5, it describes that edge trimming is used in many component manufacturing situations. If DEC isn't able to heat the edge of the component fully, as seen in Figure 4, this trimming operation could be used to trim areas that are not fully cured. If this is considered during the design phase, additional material or insulation could be added in these areas to assist the cure and ensure that the final trimmed part is fully cured.

In the same paragraph it also describes the patterns seen in figure 4, which show that average temperatures are lower at the end of the dwell, than the start. To clarify, it is expected that the higher power inputs seen during the ramp phase can ensure more even heating.

The description of figure 5 isn't clear, it should read "Summary of DSC results of 575 × 575 mm pre-preg panel, comparing relative DoC from oven cured to DEC cured."

The Nomex core described in section 3.5 was 5 mm thick.

In section 3.6, BigHead fasteners are described as electrodes, however they are only part of the electrode setup. The fasteners used were steel, with no mechanical connection to the copper sheets used as the main contact electrode, which would reduce robustness. The materials used within the

composite would induce galvanic corrosion if not removed. This isn't an issue if the electrodes are removed after DEC, however it may be an issue in later Joule heating technologies where they are left in the product.

References

[1] Hayes SA, Lafferty AD, Altinkurt G, Wilson PR, Collinson M, Duchene P. Direct electrical cure of carbon fiber composites. Advanced Manufacturing: Polymer & Composites Science 2015;1:112–9. https://doi.org/10.1179/2055035915Y.0000000001.

Composites: Part A 172 (2023) 107615

Contents lists available at ScienceDirect

Composites Part A

journal homepage: www.elsevier.com/locate/compositesa

Development and implementation of direct electric cure of plain weave CFRP composites for aerospace

M.G. Collinson [a,*], T.J. Swait [a], M.P. Bower [a], B. Nuhiji [a], S.A. Hayes [b]

[a] Advanced Manufacturing Research Centre, University of Sheffield, Wallis Way, Catcliffe, Rotherham S60 5TZ, UK
[b] Department of Multidisciplinary Engineering Education, University of Sheffield, 32 Leavygreave Road, Sheffield S3 7RD, UK

ARTICLE INFO

Keywords:
Composite curing
Out of autoclave
Low power curing
VARTM pre-preg
Sustainable curing
Joule heating

ABSTRACT

Curing aerospace composites is time-consuming with high energy requirements, particularly when using methods such as autoclaves, ovens and heated presses. This study investigates direct electric cure (DEC), which uses the Joule effect to directly heat carbon fibre composites to their cure temperature. Its benefits include a significant increase in energy efficiency, control over the cure temperature and low void content compared to oven curing. Samples were manufactured with vacuum-assisted resin transfer moulding (VARTM) and prepreg, as well as curing a two-meter-long leading-edge component, to demonstrate and evaluate the curing method at scale. The average void content for VARTM DEC samples was lower by 0.82 % compared to the oven-cured panel, however, the average degree of cure (DoC) decreased by 6.25 %. Normalised energy consumption for the cure was significantly reduced for all DEC cures, with VARTM cures using 99 % less energy than oven-cured components.

1. Introduction

High-performance carbon fibre reinforced polymer (CFRP) composites for aerospace are traditionally cured in high-pressure autoclaves or ovens. This equipment can be prohibitively expensive, energy inefficient, time-intensive to operate and the components manufactured are limited by the size of the chamber [1]. However, they consistently produce parts with a void volume fraction (VVF) below 0.5% which is the critical VVF for high performance epoxy composites [2]. The rate of manufacture also needs to be addressed, with Boeing predicting that 171 aircraft a month will be manufactured from 2022 to 2041 [3]. To enable this throughput whilst minimising environmental impact, capital expenditure and energy consumption of current manufacturing methods needs to be reduced, or new materials and methods need to be introduced.

Direct electric cure (DEC) is the application of a current through conductive carbon fibres in a CFRP component, to heat the component to its cure temperature via the Joule effect. This has been used to cure panels on a small scale, showing the benefits in improvements to DoC, VVF, cure energy and time to cure [4–6]. It has significant energy-saving advantages over convection-based methods, up to 99 % [7,8]. These advantages show promise for DEC to be a future heating or curing method for composite materials [9].

Autoclave curing is the preferred method of manufacture of primary aerospace structures, as high pressure (6–20 bar) ensures voids are compressed or eliminated. Out of Autoclave (OoA) pre-preg systems have been developed to provide low VVF whilst using atmospheric pressures, allowing ovens or heated tools to be used. This reduces initial equipment and running costs, such as energy consumption. It is also possible to heat these material systems at rates of 10 °C/min or higher without degradation of final cure properties. This aligns well with novel cure methods such as DEC that are capable of reaching these heating rates [9].

A significant limitation of autoclave or oven curing is the that the cured component can't be larger than the heating chamber, limiting large component manufacture to those who can afford the high capital equipment expenditure. DEC has the potential to cure large components using comparatively low-cost power supplies, control equipment and consumables, significantly reducing the cost of increasing the manufacture rate of large CFRP components.

The resistivity of carbon fibres is low, with a 3 k tow being less than 25 Ω/m [10]. The matrix, commonly epoxy resin, is electrically insulating and used in high voltage applications with a breakdown voltage of 400 V/mm [11]. This contrast in conductivities results in issues when

* Corresponding author.
E-mail address: m.collinson@amrc.co.uk (M.G. Collinson).

https://doi.org/10.1016/j.compositesa.2023.107615
Received 16 January 2023; Received in revised form 15 March 2023; Accepted 7 May 2023
Available online 10 May 2023

trying to electrically interface with the composite, with areas of high resistance causing excessive heat generation and uneven cure temperatures [12].

Copper electrodes have commonly been used to introduce current for DEC, either through copper clamps [13] or copper sheets [4,5,14–16] introduced in a vacuum bag. Previous investigations have shown the cure carbon tows [17,18] and pre-preg components, made up of unidirectional (UD) [5,14,15] and plain weave (PW) [4] plies. DoC has been shown to match or improve properties over oven-cured samples and be close to autoclave. VVF has also been compared, in some cases showing that it can be reduced over oven and autoclave cured samples, theorised to be enabled by the inside-out heating mode, as opposed to outside-in with conduction [15]. Power requirements for DEC are extremely low as there are very few losses in the process, compared to oven curing. As the component is the heating element, it can also be locally insulated for further energy efficiency gains, not possible in other curing methods.

In addition to component curing, Joule heating of composites has been previously researched in a wide variety of use cases and industries. Examples include it being used for foldable space applications [17,19], patch repairs [20], curing of multiple-zoned irregular shapes [14], heated tooling [21,22], preheating [12], anti-icing [23]and controlled curing of thick laminates [15]. The methods developed in this study will have multiple use cases and provide important data for future Joule heated composites. All of these studies share common characteristics and issues, such as contact resistance, temperature uniformity and control systems.

To cure a composite effectively, the temperature distribution needs to be uniform over the surface and through the thickness, which is a challenge with DEC [14]. UD plies can improve the uniformity of heating, however, it is important to consider universal compatibility with components, and not restrict the layup of a component to a certain curing method. As the scale of the component is increased, the temperature differentials can become larger and harder to control. Little research has been completed on compatibility with manufacturing methods and materials, such as dry fibre infusion, ply breaks, thickness changes and core materials.

This study builds on the pre-preg processes established in previous literature [4,5] of curing components with the DEC method and obtaining increased manufacturing and component characteristics. It develops the process for dry fibre vacuum-assisted resin transfer moulding (VARTM), and for larger laminates, up to 2 m in length. It also investigates other standard composite features such as ply breaks and core materials, increasing the methods compatibility with aerospace composite requirements. With these changes to the method, issues in laminate quality are encountered, however, suggestions for future research and development are suggested. If these were implemented, DEC would enable future large aerospace structures to be cured using this low power method, whilst retaining the benefits such as low void content and higher controllability over temperature and DoC.

2. Methods and materials

2.1. Materials and composite layup

Pre-preg experiments used Cycom 5320–1 plain weave which contained 3 K Toray T650 fibres. The cure cycle used in this study is the recommended cycle from the manufacturer as follows: Ramp from room temperature (RT) at 3 °C min^{-1} up to 120 °C min^{-1}, hold for 2 h, then 2 °C min^{-1} ramp up to 180 °C, hold for 2 h and then ramp down to RT at 2 °C min^{-1}.

For the VARTM experiments, Chomarat plain weave 3 K fabric was used, containing Toray T300 fibres, matching the plain weave pattern used in the Cycom 5320–1 pre-preg material. This should ensure the conducting fibres should act similarly. The infusion resin system was Huntsman Araldite CY 179/ Aradur 917, which has a cure cycle defined as 100 °C for 2 h, and 160 °C for 6 h, with no defined ramp rates. The layup sequences used were $[0/90]_s$ for 4 ply, and $[0/90/0/90]_s$ for 8 plies.

2.2. Tooling and ancillary materials

For all cures, vacuum was applied to the composite using vacuum bagging (Tygavac). For pre-preg cures breather fabric and release films were applied, and for VARTM peel ply and resin transfer mesh were applied (all obtained from Tygavac). During initial experimentation, the composites were cured on a ceramic tile covered in Polytetrafluoroethylene (PTFE). Later in development, glass fibre reinforced plastic (GRFP) tooling was used to ensure the composite was electrically insulated. Two layers of ¼ inch thick rock wool insulation (Morgan Advanced Materials) was used in experiments where thermal insulation is described.

2.3. Power supply, control, and data acquisition systems

An RMX-4124 (NI) power supply unit (PSU) was used to deliver power to the composite, at 0–30 V and up to 150 A, with a maximum power output of 1500 W. This was controlled by an PXI computer (NI) running a software PID controller programmed in LabVIEW. Up to 12 K-type thermocouples (TC Direct) were used to monitor and control the cure using a PXIe 4353 (NI). A FLIR AC655 (Teledyne) was used to monitor the temperature of the surface of the vacuum bag, to provide a reading of the temperature distribution over the panel during initial experimentation.

2.4. Component electric curing setup

A 0.035 mm thick copper sheet (CCI Eurolam) was used as the electrode material, which was laminated between plies at the edge of the composite. An overlap of the copper was left at the edge of the composite, which was hole-punched and bolted to crimped power cables, as seen on the left of Fig. 1. For VARTM, flat-ended bolts were used with penny washers and tacky tape to provide a vacuum seal, as seen in the right of Fig. 1. This was to ensure that air was not introduced into the bag through the multicore copper cable used.

2.5. Energy consumption measurements

The power output from the DEC power system was directly recorded for each component from the LabVIEW interface. Power usage data for oven curing was collected using a CUBE 400 (ND Metering Solutions) on a composite curing oven (Caltherm), measuring 3000 × 3000 × 3000 mm, with a 95 kW power output, and a smaller curing oven (Hedinair), measuring 1000 × 1000 × 1000 mm, with a 12 kW power output.

2.6. Characterisation

A Perkin Elmer DSC 4000 was used to determine the DoC. Sample weights were 20 μg, and followed the heating cycle from 30 °C up to 300 °C at 10 °C min^{-1}.

To determine fibre volume fraction (FVF) and VVF, samples were cut and cast in a potting resin, then polished (Struers). The samples were then imaged with a Zeiss LSM 800, then automatically processed using image recognition software to find VVF.

3. Results and discussion

3.1. Development methodology

The aim of this work was to increase the scale of the components cured, whilst maintaining the benefits of electric cure such as low power requirements, high heating rates, high DoC and low VVF. The safety of the curing method, difficulty of setup, compatibility with common

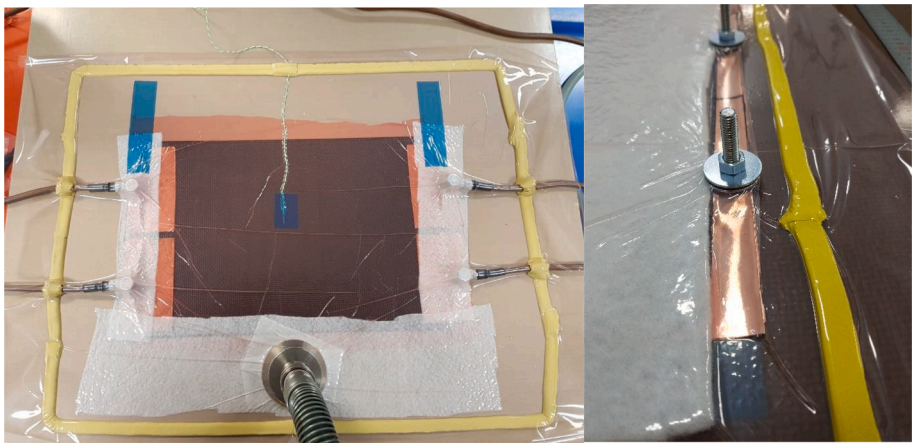

Fig. 1. Left: Example of a simple direct electric cure setup with reduced breather material to show layup sequence, Right: Example of through bag electrode setup, showing penny washers and tape fastened to the bag to ensure vacuum integrity of the bag.

composite layup techniques such as ply overlaps and the inclusion of core materials were also considered.

The initial work completed in this study was completed on pre-preg materials, building on previous literature, covered in sections 3.2 to 3.5. Once the fundamentals of the process had been understood, they were transferred and adapted for VARTM and to larger components, covered in sections 3.7 to 3.9. The culmination of these developments was demonstrated and tested with 2-meter-long leading-edge sections, manufactured with both pre-preg and VARTM, described in section 4.

3.2. Temperature distribution assessment

Achieving even temperature distribution over a CFRP component is a crucial step to implementing this technology as it directly correlates to DoC and the final mechanical properties. Previous research with woven CFRP produced an uneven temperature over the composite and with the optimal use of UD CFRP this temperature delta was improved, however the results were not fully optimal. These temperature differentials were expected to scale with the size of the component, so temperature distribution of the curing process was monitored.

A thermal imaging camera was used on a 200 × 300 mm pre-preg panel being heated to 90 °C, as seen in Fig. 2. The heating appears in a band in the centre of the composite, with the edges of the composite being considerably cooler, primarily due to higher thermal losses at the edges. This may be exacerbated by the negative resistance to temperature gradient of CFRP tows [24] Excessive heating is also observed around the electrodes, which is further discussed in section 3.6. Thermally insulating the tooling and surface of the composite reduces overall temperature differential. When using thermal insulation, line of sight is blocked to a thermal imaging camera, limiting the usefulness of this tool in this investigation. Therefore, in subsequent cures, an array of thermocouples was used to monitor temperature, particularly at edges and at the electrodes, monitoring for lower and higher temperatures respectively.

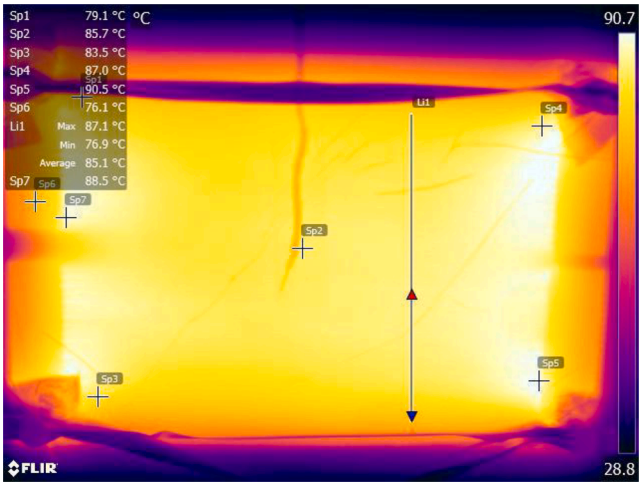

Fig. 2. Thermal image of a 200 × 300 mm panel, showing the temperature differences over the panel. Set points (Sp) show temperature points over the surface, whereas the line (Li) shows the hottest and coolest part, which are the centre and the edge, indicated by up and down triangles respectively.

To investigate the cooling edge effect further, a 200 × 300 mm pre-preg panel was cured. A line of thermocouples was spaced 10 mm apart, from the centre to the edge, as seen in Fig. 3.

The central thermocouple was used as PID control input and was set to dwell temperatures of 120 °C and 180 °C, as seen in Fig. 4, without thermal insulation.

The temperature reduction from centre to edge for 120 °C and 180 °C set temperatures at the end of the dwell are 50 °C and 77 °C respectively. There is an increase in the temperature differential at the edge of the panel, meaning that the temperature is within 20 °C for 70 % of the width. For most components there is an edge trimming operation, which if designed carefully could allow for the under-cured sections to be removed. Temperatures at the start of the dwell are higher than at the end of the dwell end at both temperatures, which is immediately after a high-power input in order to raise the temperature.

Low frequency pulse width modulation (PWM) of the DC supply therefore could potentially provide more uniform heating. Zonal heating of UD CFRP sections has been used to uniformly heat complex geometries [25], which could also be applied to uniformly heat other layup scenarios, such as PW layups, or thickness changes. Selective insulation of the edges may be another means to improve temperature uniformity.

3.3. Degree of cure

Considering the temperature differentials seen in heating PW composites, seen in section 3.2, it is important to evaluate the DoC at different points on a component. A 575 × 575 mm, 8 ply pre-preg panel was cured, of which the temperature profile can be seen in Fig. 11. Samples were taken in the centre and edge of the panel, and a point between the two, of which the results can be seen in Fig. 5.

These results align closely with the temperature trends seen in Fig. 4, the temperature reduction at the edge of the panel has directly resulted in a significant drop in DoC of approximately 36 %. This percentage drop is less than the temperature drop, due to this cure being thermally insulated, however it is unacceptable at present and requires further

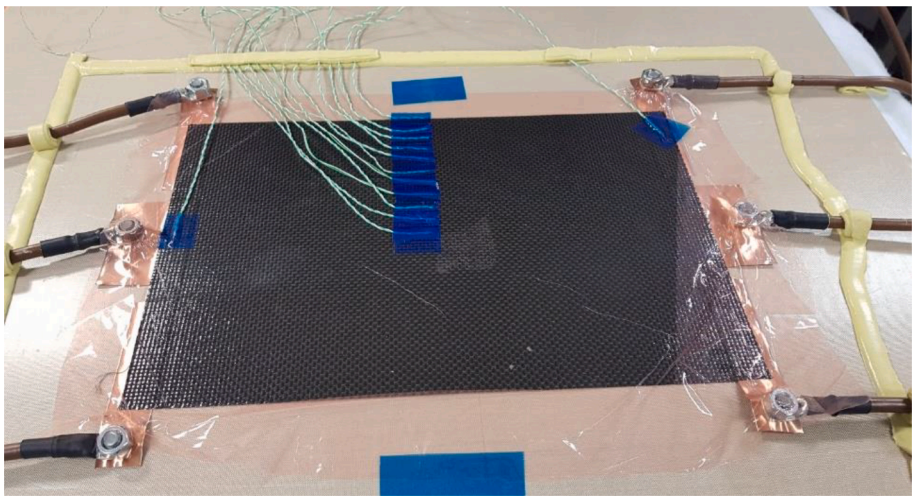

Fig. 3. Electric cured panel, showing the setup to monitor temperature drop off from centre to the edge.

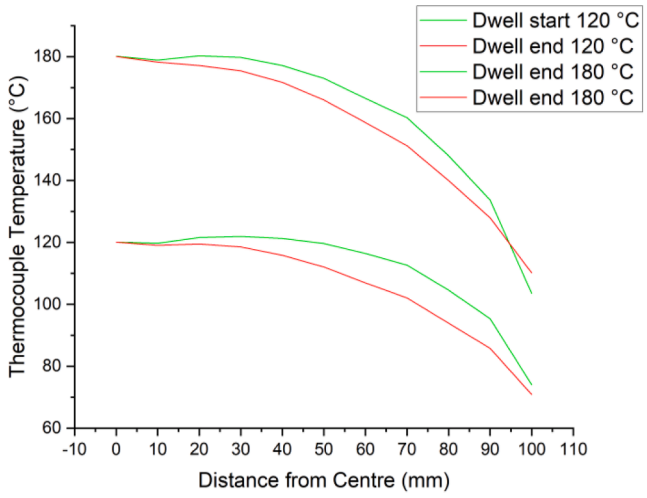

Fig. 4. Temperature reduction from centre of a panel to the edge at 120 °C and 180 °C set temperatures. Note that this is without thermal insulation, so the reduction is exaggerated compared to other experiments detailed in this study.

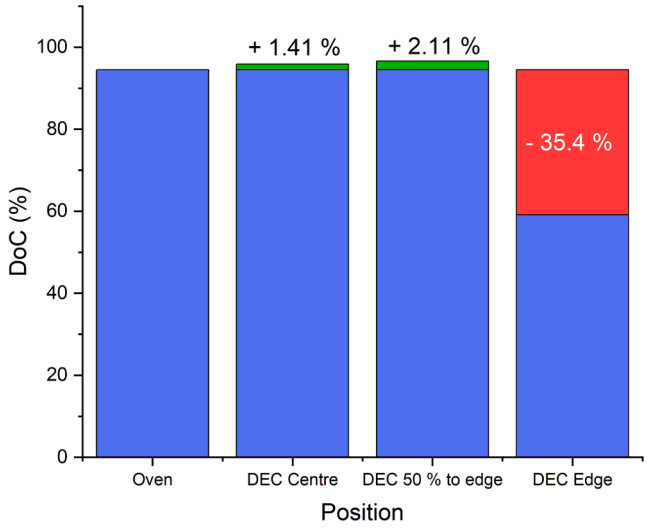

Fig. 5. Summary of DSC results of 575 × 575 mm pre-preg panel which has been electrically cured.

development to address. Previous literature states that when using UD plies, temperature and therefore DoC over the surface is more uniform, therefore being similar to oven or autoclave cure, if the same cure cycle is used [5]. This assumption, however, is not possible when using plain weave plies as the main heating elements in the composite.

3.4. Safety considerations

There are multiple safety considerations to be made when using this method, due to the way high current is used to heat the component, and the associated risks with potential burning, and interactions that could occur with the tooling and consumables. Fig. 6 shows the current and voltages used to cure for various geometry samples.

The PSU used in this study was controlled in constant current mode. In this mode, there were slight setup inconsistencies with the electrodes, causing localised high resistance, resulting in hotspots around the electrodes. In rare cases, this would develop into burning when higher ramp rates were used, as the temperature increased beyond the thermal breakdown temperature of the epoxy. During a cure, these were identified by the user and the system powered down, to avoid further damage. Burning led to an increase in resistance of the component, and in constant current mode, would lead to spikes in power input to the panel seen in the left of Fig. 7. This power increase would compound the

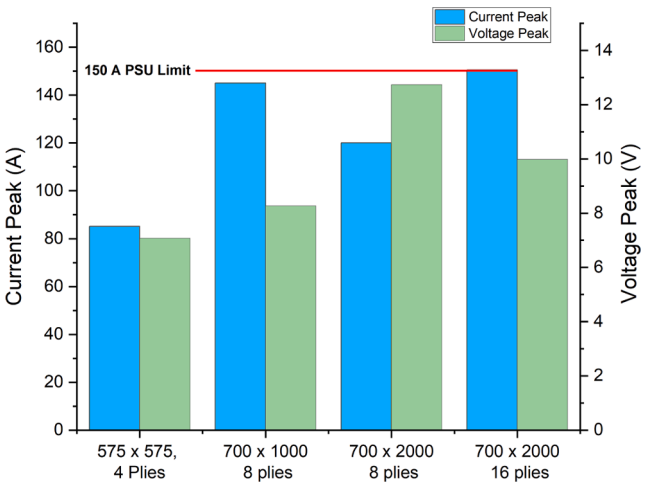

Fig. 6. Bar chart showing the current and voltage peaks of various pre-preg panels manufactured using DEC. The peaks were all recorded during the ramp up to their set temperature.

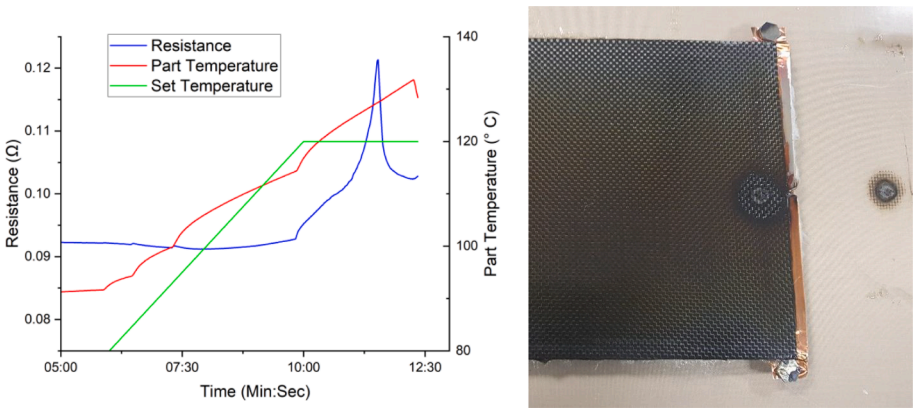

Fig. 7. Left: Graph showing the temperature runaway during a burning event. The behaviour of the part temperature is due to manual limits being applied to the output current. Note the sharp increase in resistance, leading to a 200 W spike in power input at the peak. Right: Component and PTFE plate burn damage after curing.

burning, which could lead to a dangerous runaway situation, as seen in the right of Fig. 7.

The control system was changed to control the calculated power reported by the PSU, which will reduce the severity of burning and allow for more time to intervene.

3.5. Ply breaks and core materials

The use of core materials and ply breaks are common in composite manufacturing, to increase component stiffness [26] and to change the thickness or join large sections together. Both features were tested for compatibility with the electric cure method. The following layup was used to test if core materials were compatible with DEC: $[0/90/0/90]_s$[GFRP/Nomex/GFRP] $[0/90/0/90]_s$. The carbon plies were heated to cure temperature, which through conduction cured the adhesive ply, bonding the Nomex to the adhesive ply. This was then repeated with GFRP ply laid up on top of the Nomex, then 8 plies joule heated, to form a sandwich structure. The cure cycle was completed as expected, and through visual inspection, the Nomex was successfully bonded within the sandwich structure.

Ply breaks were tested on a 2000 × 700 mm, 8-ply pre-preg panel that had a single 10 mm overlap, alternating directions every ply. There was a slight increase in temperature of 2–5 °C on the overlap where resistance increased. This overlap is too small to provide optimal mechanical strength [27], therefore could be increased to reduce temperature difference further. It was observed that the temperature increase was maintained along the width of the ply drop, rather than reducing in temperature towards the edge of the laminate, as seen in previous experiments in section 3.2.

3.6. Contact arrangement

The electrodes were copper sheets applied along the full length of opposite edges of the uncured carbon fibre, or dry fibre for VARTM. Previous literature suggested that placing electrodes on the short edges of higher aspect ratio geometry had the best heating performance and efficiency [4] so this approach was adopted. As seen in Fig. 2, localised heating can occur at the electrode contact, caused by the contact resistance from the epoxy between the conductive copper and carbon fibres, as noted by Çelik et al [12]. If not controlled carefully, overheating can lead to damage to the component and its tooling, as seen in Fig. 7. Therefore, various layouts of electrodes were tested to reduce this effect, as seen in Fig. 8.

The main observations on the variation of contacts on temperature are:

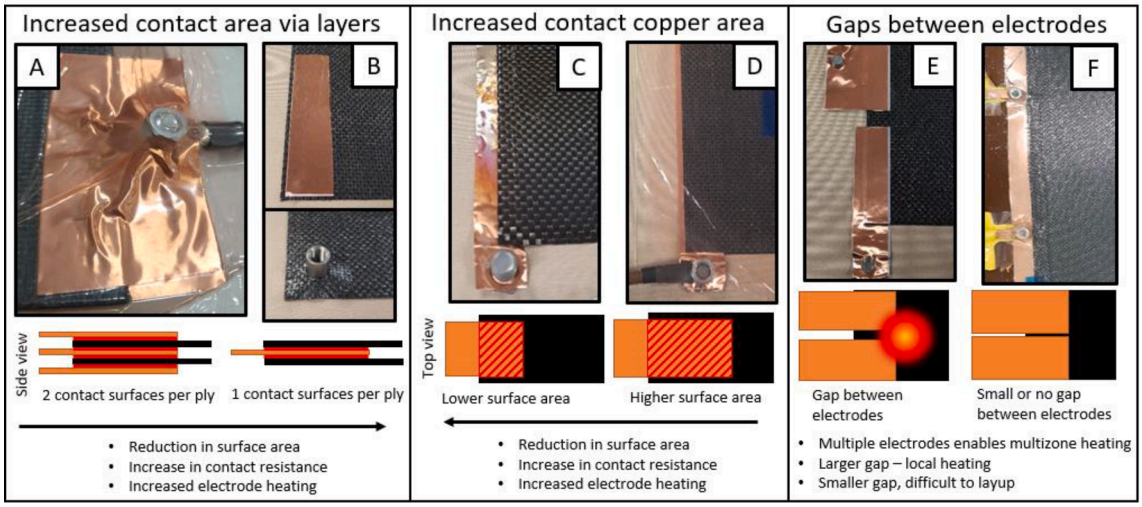

Fig. 8. Examples of copper electrodes used in electric cure: A & B: Demonstrating the use of more layers to sandwich a composite to increase contact area, C & D: Demonstrating the depth of the electrode within the composite to change contact area, E & F: Demonstrating the gaps between multiple electrodes and how these can cause unwanted localised heating.

- Efficient use of surface area in contact with the composite. Fig. 8A shows two electrodes with 2 contact surfaces, whereas Fig. 8B shows one contact with 2 contact surfaces, reducing contact resistance by half.
- Increasing depth into the composite from the edge, increasing the contact area. Fig. 8E generates more local heating compared to Fig. 8D. If the electrode is placed too deep into the layup, the current does not flow at the edge of the composite and is left unheated.
- Reducing gaps between multiple electrodes. When electrodes are placed with a gap between them as in Fig. 8E, the gap between the electrodes becomes a significant hotspot. Reducing this eliminates the hotspot as in Fig. 8F, however, this makes layup more difficult, particularly when this method is adapted for more complex geometries. Multiple electrodes will be essential for zonal heating, to be explored in future studies.

The peak power requirement during the cure cycle is the ramp, meaning heat is also generated at the electrode interface. Therefore, if the ramp rate was increased or lowered, there would be overheating of the electrodes or under-curing of the edges of the component respectively. Therefore, the electrode size and position need to be carefully considered for each cure of a different component geometry.

Full-length, single-piece electrodes were tested to enable a simpler layup, Fig. 8F and G. Multiple electrodes on the same edge had also been tested to enable current to be run through certain sections of the composite, to enable zonal heating. This was not compatible with PW causing excessive heating around the electrodes, however, which will be investigated in future work to modify the heating profile.

BigHead composite fasteners were used as electrodes, enabling the electrode to be fully integrated into the layup as seen in Fig. 8B, which gives composite fasteners dual use post-curing. Integrating a robust electrode within the surface, rather than at the edge, which allows for other joule heating use cases, such as anti-icing or heated composite tooling.

3.7. Infusion development

Adaptations to the process were made to ensure that DEC was compatible with dry fibre, vacuum-assisted resin transfer moulding. The procedure for VARTM is as follows:

1. Apply the electrodes to the dry fibres and secure them with high-temperature tape.
2. Apply vacuum and do a vacuum drop test on the bag. Any leak can lead to significant localised heating around the electrodes.
3. Infuse the resin into the component. Once the infusion is complete, then start the cure cycle and apply current to the composite.

Multicore cable cannot be sufficiently vacuum-sealed, allowing air into the bag when the cable was passed through into the bag, using tacky tape to seal the insulation. The interface was replaced with a bolt, that provided a mechanical lock, power transfer and vacuum seal and enabled a quicker setup. This setup was used on all cures afterwards, including the large-scale components.

Using this method, it is possible to preheat the fibres and the tooling before infusion (heating the fibres without resin), which would decrease the viscosity of the resin during infusion. This may enable the infusion of high viscosity resins with thermoplastic hardeners or fillers to be infused using VARTM methods.

3.8. Cure kinetics and power delivery

DEC has high controllability of the power going into the component, compared to closed cavity curing, which offers novel opportunities for temperature control.

The first is to increase the ramp rates beyond 1–3 °C/min which is standard for many pre-preg systems, including the ones used in this study. To test the potential of higher ramp rates, a small 200 × 300 mm, 6 ply panel of pre-preg was laid up with the electrode arrangement of Fig. 8.

C was cured at 120 °C with a 10 °C/min ramp. The cure system was able to maintain the set temperature at this ramp rate, as seen in Fig. 9.

The peak power output of this ramp was 608 W, meaning that for curing larger components, the control system used in this study wouldn't be suitable for this heating rate. With increased power limits on the power supply, it would be possible to ramp cures at 10 °C/min or more.

Another opportunity is the low thermal mass of the system and how this can be used to further reduce the cure power consumption of the cure. Heat generated in the exothermic reaction of the epoxy can be controlled to further heat the part, without the danger of a runaway reaction. To test this, an infusion resin with a low activation and cure temperature (Gurit T-Prime 130) was infused into a 4-ply, 1000 × 350 mm preform. To ensure a safe, self-sustaining exothermic reaction takes place, the temperature was raised up to 60 °C at 3 °C/min, which can be seen in Fig. 10.

The initial temperature increase set off the exothermic reaction, which continued beyond the cure temperature up to 66 °C, after the control system turned off the power. This exotherm lasted for 1 h in duration, ensuring that the composite was at the cure temperature without any external power input. With a more carefully controlled initial power input, the overshoot could have been reduced and time at zero power input increased. The average power after this section was 37 W, with the entire 2-hour 15-minute cure requiring 85.8 Wh.

The increased control over the temperature of components would allow for more custom cure cycles to be developed, which would be controlled by the cure kinetics of the resin. If the heat losses from the cure to the environment and resin cure kinetics could be calculated, then cure cycle time and energy could be minimised, whilst not having a runaway exothermic reaction. Unfortunately this is out of scope of this study, however, it provides another way of energy and cycle time reduction.

3.9. Resistance observations during cure

In Fig. 11, the resistance of the component can be compared to the cure temperature, at the start and throughout the cure. The resistance could be used to detect irregularities in the layup, i.e., if there was a ply missing or an irregularity in the electrode setup. In this case it shows changes to the component during the cure, with electrical resistance increasing in respect to component temperature.

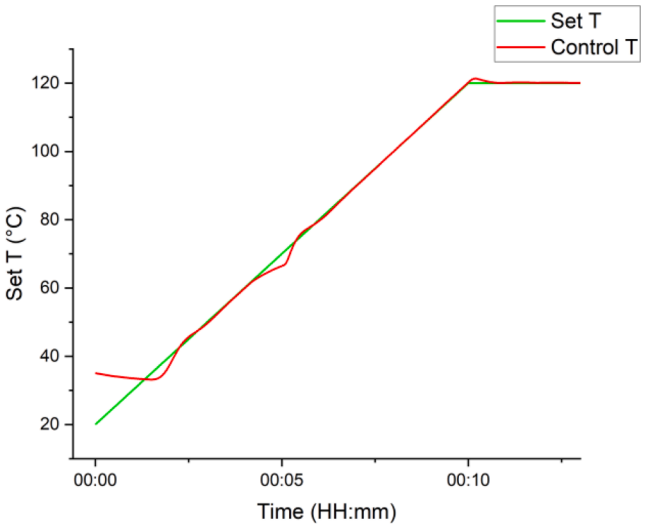

Fig. 9. Example of a sample being heated using DEC at 10 °C/min.

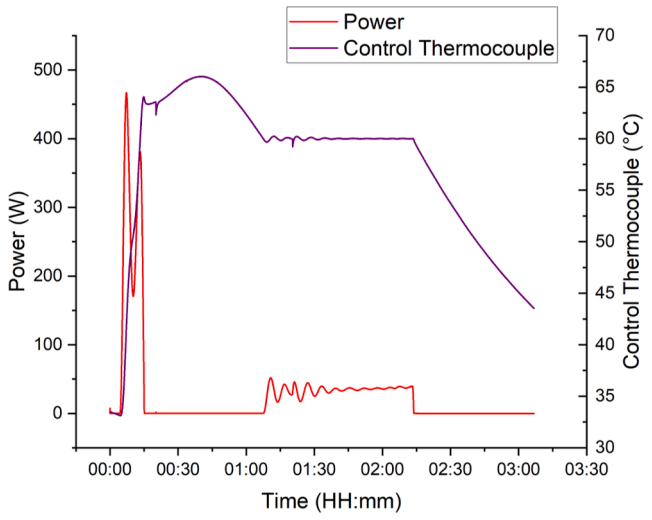

Fig. 10. Graph showing power and temperature of a panel cured partially using exothermic energy.

Thermal expansion during heating induces the piezoresistive effect, increasing the electrical resistance of the panel. A combination of these effects leads to an increase in resistance (0.0804 Ω to 0.0977 Ω, 18 % increase) from 120 °C to 180 °C. It is unlikely that this could be used as an accurate temperature measurement method, however, it could be used to monitor when the component reaches excessive temperatures. This could be useful to detect when sections of a component are over the glass transition (T_g) or thermal degradation temperature.

There is also an increase in resistance during the first isothermal dwell at 120 °C, where there is an increase from 0.0772 Ω to 0.0804 Ω, a 4 % increase. This also occurs at the beginning of the second dwell at 180 °C, from 0.0910 Ω to 0.0977 Ω, a 7 % increase. This trend is also seen in other pre-preg and VARTM panels. A physical change that occurs during the cure is the degree of polymerisation of the epoxy, which could account for the increase in the resistance. DC cure monitoring is a method to monitor the electrical resistance of epoxy resin, which can increase by a factor of 10^4 MΩ during a cure [28]. These resistance changes are also affected by the average temperature over the panel, (Right of Fig. 10) which shows a combination of these effects. During both dwells, the average temperature decreases by around 2–3 °C, whereas resistance increases during the first dwell, where the majority of the cure takes place, approximately 75 % [29]. During the second dwell, there is a downtrend in resistance, which matches the average temperature trend, and the smaller amount of curing that happens in the post cure. In future experiments, this could be matched to the degree of cure more closely, and resistance changes to be used as an indicator to move to the post-cure.

4. Large component manufacturing and cure evaluation

The research and results described in the previous sections were used as the basis for the trial manufacture of two large scale components. Their cured material properties, energy efficiency and ease of manufacture were all evaluated. The two parts' geometries were identical, with one being manufactured with pre-preg and the other VARTM. The plies were 2000 × 700 mm, including a Nomex core mid-ply of a 16-ply layup. This was cured in a GFRP tool that had the geometry of a NACA 2412 aerofoil, as seen in Fig. 12. The pre-preg cure was completed in one cure, whereas the VARTM cure had to be completed in multiple steps to ensure the Nomex core was not filled with resin during the infusion.

4.1. Heating uniformity and degree of cure

Curing effectiveness was evaluated by comparing the temperature uniformity and DoC with oven cured samples (following the manufacturers recommended cure cycle). This was done at six different positions on the component, as seen in Fig. 12. Based on previous work on DEC methods [5], it was assumed that if the temperature was matched to an oven cure, the DoC and consolidation of the component would also be the same. DoC for VARTM and pre-preg samples can be seen in Fig. 13.

For VARTM, the average DoC for the six locations is within 6.25 % of the oven cured samples. This includes sample position 2 which is almost 17 % under cured compared to the oven sample. Position 2 is edge of the part having the lowest temperature during the 3 cure stages, which is a result of the non-uniform temperature during the cures. The average is very close to the oven cured samples and shows the potential of the curing method to provide uniform DoC over a component. The range of thermocouple temperatures can be seen against the set temperature for the final cure stage, seen in Fig. 14.

After the ramp to dwell temperature, and the subsequent control system settling, the average range of temperatures is approximately 20 °C. A common standard for curing in aerospace ovens (SAE AMS 2750F Class 2 [30]) requires no more than ± 6 °C temperature uniformity tolerance. Whilst that has not been achieved in this work, ± 20 °C has been achieved with sub optimal materials and setup, at a significantly larger scale than that has been observed previously.

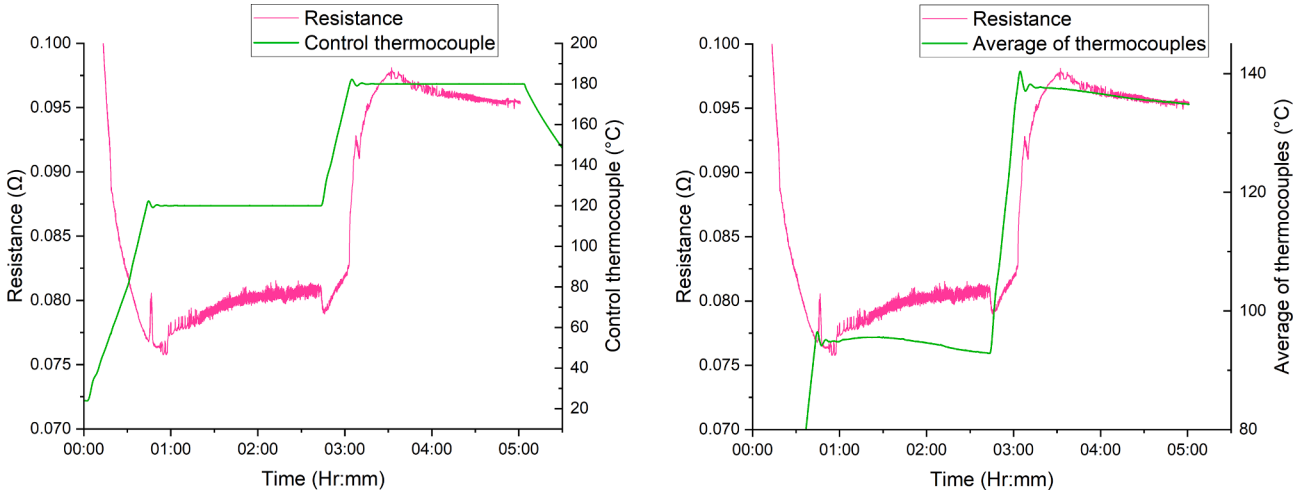

Fig. 11. Left: Graph showing a comparison of temperature and resistance over time during a cure of Cycom 5320–1, Right: Average of temperatures recorded and resistance over the same cure period.

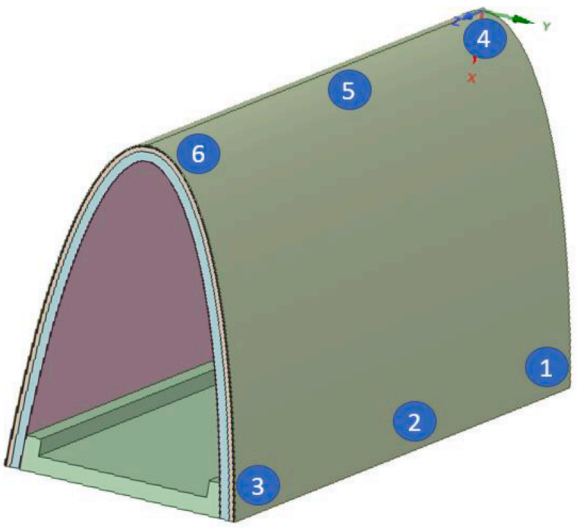

Fig. 12. Leading edge geometry used for large-scale cure evaluation, with numbers indicating sample positions for DoC and VVF evaluations.

For the pre-preg cure, due to power limitations of the PSU, the full 180 °C post-cure temperature was not possible, therefore a 160 °C post cure was used, see the 700 × 2000 mm 16 ply sample in Fig. 6. During the cure, the temperature range was over 30 °C, meaning some areas reached only 90 °C during the cure and 130 °C during the post cure. These are significantly under the desired set temperatures leading to sections of the component being up to 35.77 % under-cured, compared to the 180 °C oven post-cured samples.

4.2. Void volume fraction

VVF was tested for electric cure samples and compared to oven cured samples to assess if the cure method had any detrimental effect. The results can be found in Fig. 13.

The VARTM component followed the cure cycle ensuring a DoC 6.25 % lower than oven, therefore it is expected the VVF would be similar. However, is it significantly lower, averaging 0.55 %, which is closer to that expected of autoclave cured samples. It is significant that the VVF is lower in the VARTM electric cured components, considering they were prepared similarly and followed the same cure cycles. If this is a consistent trend with DEC, it would be of interest to compare DEC components against autoclave cured ones.

The pre-preg VVF average and standard deviation were significantly higher than the oven cured samples, suggesting whist it is possible to achieve low VVF, it is not as consistent. This is likely due to the uneven temperature profiles being applied leading to void formation, of which examples can be seen in microscopy in Fig. 15.

4.3. Energy consumption analysis

One of the key opportunities with DEC is the increases in energy efficiency of the process, compared to ovens and autoclaves. Energy consumption was compared by normalizing the energy used per hour of cure cycle, which gives an estimation of the efficiency of the curing methods for high temperature cures. Most significantly, the average normalised power usage was reduced by at least 99.15 %, as seen in Fig. 16.

It would be possible to cure more than one of these components in an oven at a time, increasing the efficiency as more are added. In the case of this comparison, even if 25 components could be cured in an oven, using DEC would still results in energy saving of greater than 95%.

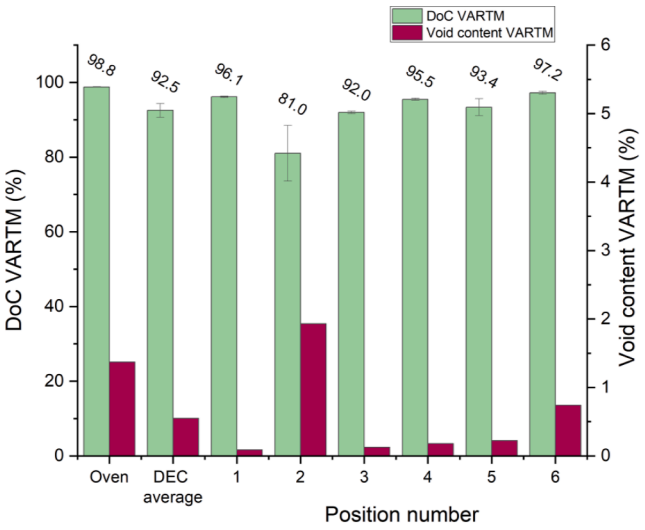

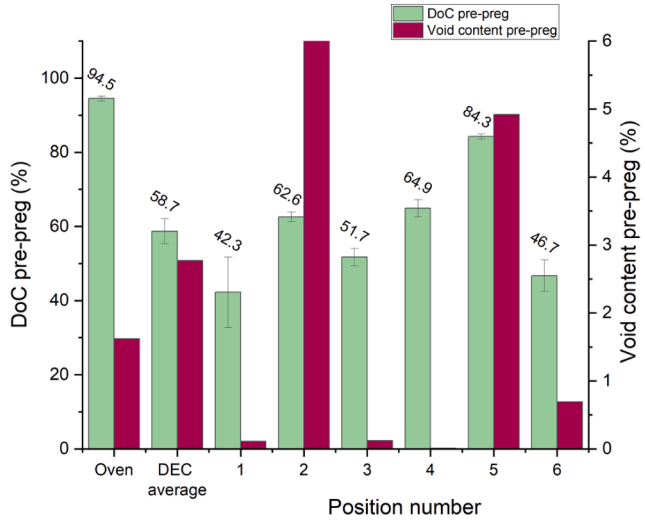

Fig. 13. DoC and void content for both VARTM (left) and pre-preg (right) large scale components.

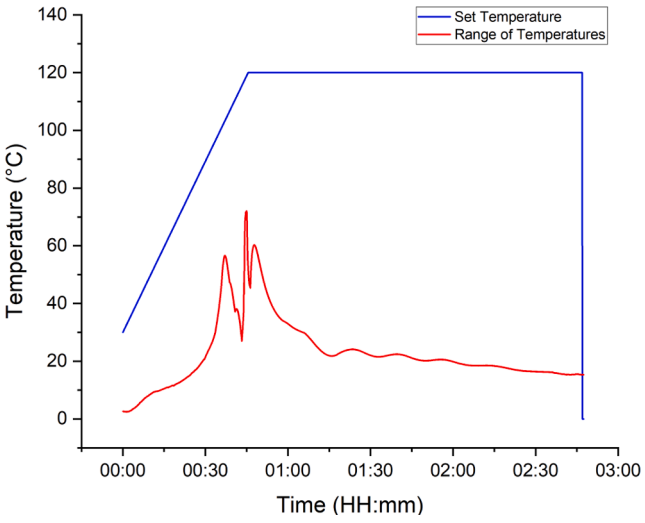

Fig. 14. Range in temperatures on the last stage of cure against set temperature for VARTM component.

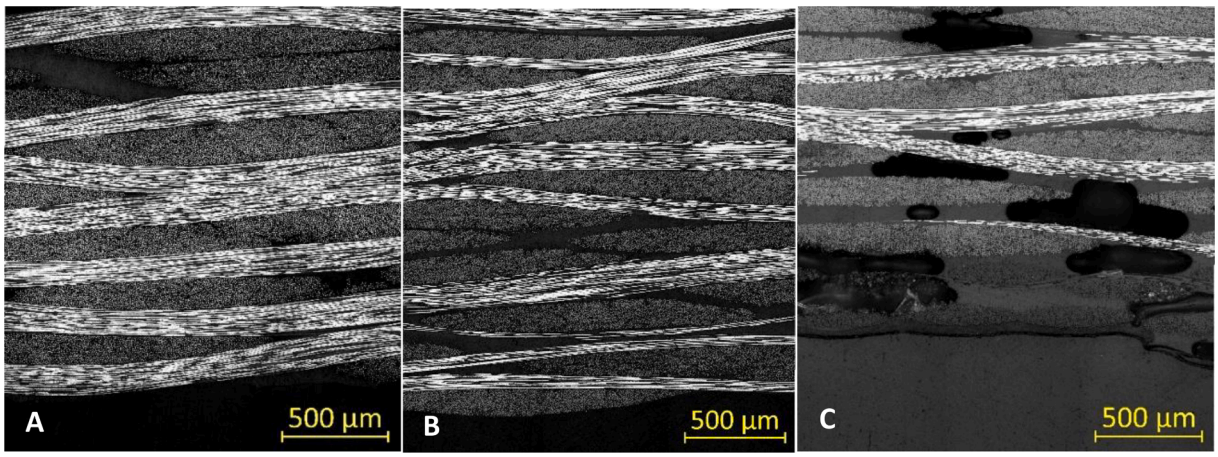

Fig. 15. Microscopy of cross section of final electrically cured components, A) VARTM with 0.09 % VVF, B) Pre-preg with 0.01 % VVF, C) Pre-preg with large voids, 10.81 % VVF.

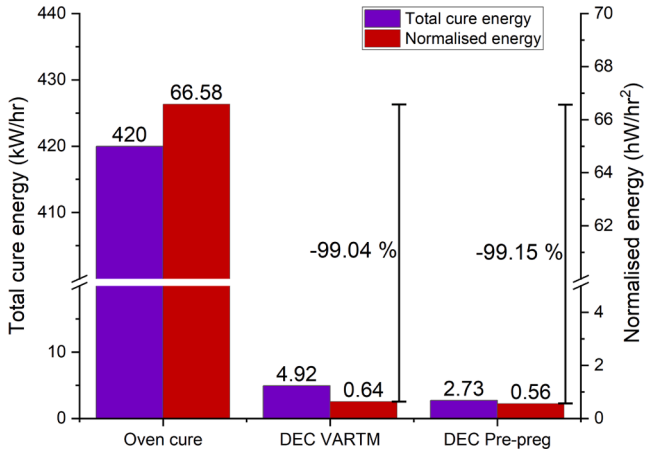

Fig. 16. Summary of cure energy and normalised cure energy of Oven, DEC VARTM and DEC Pre-preg, accounting for different cure lengths.

5. Conclusion

This paper outlines the development of the DEC method, culminating in the manufacture of large-scale aerospace inspired components with plain weave VARTM and pre-preg materials. Safety and part quality was improved compared to previous trials through modifications to the control systems employed. Modifications to the electrodes were made to reduce hotspots, VARTM manufacturing was introduced and practicality of the setup was increased. Energy efficiency was significantly higher than oven curing, with 99 % less energy used when curing large components using the same cure cycle.

Pre-preg samples produced a lower DoC and higher void content, partially due to PW pre-preg composites performing poorer in producing uniform heating, as well as problems in reaching the 180 °C post cure temperature due to limitations in the available PSU.

The use of PW reduced the heating uniformity compared to studies that used UD, however in the case of VARTM, it produced samples within an average DoC within 6.25 % of an oven cured part, and 0.82 % lower void content. This shows that it is possible to cure components using DEC, achieving a DoC close to oven-cured samples with comparable or improved void content, whilst achieving a significant energy saving.

Through testing the limits of PW cured with DEC, it increases the knowledgebase on what range of materials it is compatible with, and how best to apply it to new and existing layups.

Future research must address the temperature uniformity and resulting DoC, which is essential to application in curing aerospace structures. Another significant boundary to adoption is the added complexity of the layup to enable DEC. For small structures, the benefits of this method may not outweigh the time and cost required to apply electrodes. For larger structures, like the ones demonstrated in the last section of this study, the benefits start to outweigh the negatives. When these issues related to the cure are resolved, the cost reduction in manufacturing large structures will be significant, whilst reducing overall environmental impact. There are also opportunities to use a cure kinetic modelling system coupled with the ability to rapidly heat and closely control the temperature and exotherms to reduce cure times and input energies further. In the meantime research will be of use to other Joule heating applications such as anti-icing or heated tooling, which can be exploited in a shorter timeframe.

Funding sources

Funding: This work was supported by the European Union's Horizon 2020 research programme under grant agreement No 760940, under the project titled MASTRO.

CRediT authorship contribution statement

M.G. Collinson: Conceptualization, Methodology, Software, Investigation, Writing – original draft. **T.J. Swait:** Conceptualization, Methodology, Writing – review & editing, Supervision, Funding acquisition. **M.P. Bower:** Methodology, Investigation, Writing – review & editing. **B. Nuhiji:** Writing – review & editing, Supervision, Project administration. **S.A. Hayes:** Conceptualization, Methodology, Investigation, Writing – review & editing, Supervision, Funding acquisition.

Declaration of Competing Interest

The authors declare that they have no known competing financial interests or personal relationships that could have appeared to influence the work reported in this paper.

Data availability

Data will be made available on request.

References

[1] Liddell HPH, Brueske SB, Carpenter AC, Cresko JW. Manufacturing energy intensity and opportunity analysis for fiber-reinforced polymer composites and other lightweight materials. In: Proceedings of the American Society for Composites - 31st Technical Conference, ASC 2016; 2016.

[2] Yoshida H, Ogasa T, Hayashi R. Statistical approach to the relationship between ILSS and void content of CFRP. Compos Sci Technol 1986;25:3–18. https://doi.org/10.1016/0266-3538(86)90018-7.
[3] Boeing. Commercial Market Outlook. 2022.
[4] Hayes SA, Lafferty AD, Altinkurt G, Wilson PR, Collinson M, Duchene P. Direct electrical cure of carbon fiber composites. Adv Manuf Polym Compos Sci 2015;1:112–9. https://doi.org/10.1179/2055035915Y.0000000001.
[5] Liu S, Li Y, Shen Y, Lu Y. Mechanical performance of carbon fiber/epoxy composites cured by self-resistance electric heating method. Int J Adv Manuf Technol 2019;103(9-12):3479–93.
[6] Yue C, Zhang Y, Lu W, Zhang Y, Wang P, Li Y, et al. Realizing the curing of polymer composite materials by using electrical resistance heating: a review. Compos Part A Appl Sci Manuf 2022;163:107181.
[7] Lee J, Ni X, Daso F, Xiao X, King D, Gómez JS, et al. Advanced carbon fiber composite out-of-autoclave laminate manufacture via nanostructured out-of-oven conductive curing. Compos Sci Technol 2018;166:150–9.
[8] Lee J, Ni X, Daso F, Xiao X, King D, Gómez JS, et al. Supplementary materials: advanced carbon fiber composite out-of-autoclave laminate manufacture via nanostructured out-of-oven conductive curing. Composite Sci Technol 2018;166:150–9.
[9] Collinson M, Bower M, Swait TJ, Atkins C, Hayes S, Nuhiji B. Novel composite curing methods for sustainable manufacture: a review. Composites Part C: Open Access 2022;9:100293. https://doi.org/10.1016/j.jcomc.2022.100293.
[10] Wentzel D, Sevostianov I. Electrical conductivity of unidirectional carbon fiber composites with epoxy-graphene matrix. Int J Eng Sci 2018;130:129–35.
[11] Dakin TW. Application of epoxy resins in electrical apparatus. IEEE Trans Electr Insul 1974;9:121–8. https://doi.org/10.1109/TEI.1974.299321.
[12] Çelik M, Noble T, Haseeb A, Maguire J, Robert C, Conchúr, et al. Contact resistance heating of unidirectional carbon fibre tows in a powder-epoxy towpregging line. Plastics Rubber Composites 2022:1–10. doi: 10.1080/14658011.2022.2108982.
[13] Joseph C, Viney C. Electrical resistance curing of carbon-fibre/epoxy composites. Compos Sci Technol 2000;60(2):315–9.
[14] Liu S, Li Y, Shen Y, Goh YM. A multi-zoned self-resistance electric heating method for curing irregular fiber reinforced composite parts. vol. 0, 2021, p. 1–6. doi: 10.3233/ATDE210028.
[15] Zhang B, Li Y, Liu S, Shen Y, Hao X. Layered self-resistance electric heating to cure thick carbon fiber reinforced epoxy laminates. Polym Compos 2021;42:2469–83. https://doi.org/10.1002/PC.25992.
[16] Fukuda H. Processing of carbon fiber reinforced plastics by means of Joule heating. Adv Compos Mater 1994;3(3):153–61.
[17] Naskar AK, Edie DD. Consolidation of reactive Ultem®Powder-coated carbon fiber tow for space structure composites by resistive heating. J Compos Mater 2006;40(20):1871–83.
[18] Sarles SA. Controlled resistive heating of carbon fiber composites. Virgin Tech 2006:18–60.
[19] Smith BP, Tuttle ME, Devasia S. Investigation of embedded resistive heating for high strength adhesive bonding of modular space structures 2017. doi: 10.2514/6.2017-5228.
[20] Liu S, Li Y, Xiao S, Wu T. Self-resistive electrical heating for rapid repairing of carbon fiber reinforced composite parts. J Reinf Plast Compos 2019;38:495–505. https://doi.org/10.1177/0731684419832793.
[21] Weiland JS, Hartmann MP, Hinterhölzl RM. Cure simulation with resistively in situ heated CFRP molds: implementation and validation. Compos Part A Appl Sci Manuf 2016;80:171–81. https://doi.org/10.1016/j.compositesa.2015.10.020.
[22] Athanasopoulos N, Koutsoukis G, Vlachos D, Kostopoulos V. Temperature uniformity analysis and development of open lightweight composite molds using carbon fibers as heating elements. Compos B Eng 2013;50:279–89. https://doi.org/10.1016/j.compositesb.2013.02.038.
[23] Idris MK, Qiu J, Melenka GW, Grau G. Printing electronics directly onto carbon fiber composites: unmanned aerial vehicle (UAV) wings with integrated heater for de-icing. Eng Res Express 2020;2:025022. https://doi.org/10.1088/2631-8695/AB8E24.
[24] Forintos N, Czigany T. Reinforcing carbon fibers as sensors: the effect of temperature and humidity. Compos Part A Appl Sci Manuf 2020;131:105819. https://doi.org/10.1016/J.COMPOSITESA.2020.105819.
[25] Shen Y, Lu Y, Liu S, Liu Q, Tao S, Hao X. Self-resistance electric heating of shaped CFRP laminates: temperature distribution optimization and validation. Int J Adv Manuf Technol 2022;121(3-4):1755–68.
[26] Vinson JR. The Behavior of Sandwich Structures of Isotropic and Composite Materials. The Behavior of Sandwich Structures of Isotropic and Composite Materials 2018. doi: 10.1201/9780203737101.
[27] Jin H, Nelson K, Werner B, Briggs T. Mechanical strength of composites with different overlap lengths. Livermore, CA; 2018.
[28] Pantelelis NG, Efthymios Bistekos. Process monitoring and control for the production of CFRP components. In: Proceedings of Conference SAMPE'10; 2010.
[29] Kratz J, Hsiao K, Fernlund G, Hubert P. Thermal models for MTM45-1 and Cycom 5320 out-of-autoclave prepreg resins. J Compos Mater 2013;47:341–52. https://doi.org/10.1177/0021998312440131.
[30] SAE International. AMS2750F - Aerospace Material Specification - Pyrometry. 2020.

7. Joule heating composites for de-icing and heated tooling applications.

7.1. Development of CFRP Joule heated multifunctional aerospace de-icing system

The background to this study was to aim to develop multifunctional composites for uses in aerospace. Early on in the conceptualisation phase, it was evident that Joule heating could have dual use cases, to cure a leading-edge section, and heat the section for de-icing. The development of Joule heated composites was completed for DEC, which was then transferred to the de-icing, which is why there is less extensive experimental detail in this section. Experimental work in this section was assisted by Matthew Bower, who assisted in the layup of the components, and setup of the components in the climate chamber. The climate chamber was run by the University of Sheffield's Lab for Verification and Validation.

7.1.1. Introduction

Regulatory requirements for more sustainable aircraft and lower CO_2 emissions are driving two major trends in the commercial aerospace industry. The first is the light weighting of aerospace structures, using CFRP and other composite materials. This has been increasing for the last 40 years [1], continues to ramp up and increasingly forms a major proportion of new commercial airframes. The second, electrification of aircraft systems, is increasing the efficiency of existing jet turbine engines and to develop powertrains for battery and hydrogen power sources [2].

One system that is significantly affected by electrification is the ice removal systems on flight control surfaces of aircraft. On jet turbine aircraft, it is common to heat the wings to remove or prevent ice buildup, by bleeding hot air from the turbine and feeding it through channels along the wing's leading edge. This is a simple and effective method, however, it reduces the efficiency of the engine during operation, and without a jet turbine engine, this method isn't feasible.

Manufacturers are therefore introducing electrothermal anti-icing systems as an alternative. An example of this already in production is in the Boeing 787 where a metallic resistive heater mat was embedded in the leading-edge layup.

This study takes a multifunctional materials approach, attempting to use existing manufacturing methods and materials to develop a Joule heated de-icing system, with the carbon fibres themselves as the heating element. The conductive carbon fibres within the composite enable the use of the Joule effect in unidirectional plies, to heat sections of a component. This has previously been successfully used to cure composites [3], however, hasn't been investigated for this specific use case which utilises the UD fibres.

In this study two components were tested in a climatic chamber for their ability to remove ice from their surfaces using the in-built Joule heating. The first was a 500 x 500 mm flat CFRP panel, and the second was a representative aerospace component with the geometry of a leading edge (LE) section. Both were manufactured using pre-preg materials.

7.1.2. Aerospace ice removal methods

Icing on aircraft refers to the build-up of ice on aerodynamic surfaces, typically when flying through clouds at temperatures below 0 °C. It was first identified in the 1920's and became a more frequent problem in the 1940's as aircraft reached higher altitudes to enable longer distance routes [4].

Simple systems were developed using engine exhaust heat to control ice build-up, or freezing point depressant liquid was delivered to the wing surface to prevent build up. These preventative measures that stop build up in the first place are called anti-icing methods, where ice is prevented from building up in icing conditions. Other novel anti-icing methods include icephobic surfaces, which allow for rapid removal of water before freezing, or less ice to be accumulated overall. An example of this by Yang used PTFE particles in epoxy to achieve this effect, reducing ice accumulation [5]. However, this approach is not yet common in aviation.

Other systems developed involve inflatable bladders on the leading edges of wings, called boots, which change geometry to remove, or de-ice the surfaces [6,7]. This system is classed as a de-icing system, as it removes ice that builds up on an aerodynamic surface, and continues this cycle as long as is required. These are common on smaller aircraft due to their simplicity and effectiveness, not impacting performance or being costly to install aftermarket.

Electro-thermal heating systems can be run in both anti and de-icing modes, but are primarily used for the former as this is deemed more reliable and a safer mode of running. They consist of metallic heater elements embedded in, or attached to, the critical aerodynamic surfaces. Like the metallic meshes that are added to aerospace composites to protect from lightning strikes [8] these are unlikely to provide any structural benefit to the composite.

There are many examples of Joule heating of nanocomposites with the aim of ice removal, such as embedded bucky paper [9], graphite [10], carbon nanotubes [11] and graphene [12,13]. These perform well on smaller scales but will likely face issues when scaling up to component scale, such as manufacturability, weight, cost and environmental impact.

There are few examples of using CFRP as the heating element for Joule heating for the purposes of anti-icing. Martinez-Diaz et al [14] manufactured a chopped strand carbon fibre coating and bulk material from recycled carbon fibres. The resulting materials had a low conductivity and were able to be heated to high temperatures quickly. However, the preparation of the chopped strands required an extra sonication mixing step.

Idris et al [15] directly printed silver inks onto cured CFRP substrates, which were used as electrodes to induce the Joule effect. Pairs of electrodes were printed onto a complex surface, measuring 20 x 5 mm, with 100 mm distance from each other, using a Voltera PCB printer. A variety of substrates were tested which had different weave patterns. It was found that 3K twill fabric gave the most uniform heating performance opposed to 6K twill and unidirectional carbon.

7.1.3. Methodology and component design

The Joule heating system suitable for CFRP was adapted from the method developed by M. Collinson [3], which were used previously to Joule heat composites to their cure temperature. This study applied this method to unidirectional fibres with the aim to heating performance and uniformity in a related, but different end use case.

Two components were manufactured and tested. The first was a flat panel, 500 x 500 mm, to test the concept and its functionality outside of the icing testing. Once the concept had been proven out, the manufacturing method and any improvements could be applied on the second component, a larger leading-edge section, 2000 mm long with a surface ply width of 700 mm.

Both LE and flat panel components had the following layup:

- 200 GSM epoxy resin film (SHD)
- Copper electrodes (0.035 mm copper sheet)
- UD CFRP (Cycom 5320-1)
- Copper electrodes
- 200 GSM epoxy resin film (SHD)
- 8 Plies of PW CFRP (Cycom 5320-1)
- 5 mm Nomex core
- 8 Plies of PW CFRP (Cycom 5320-1)

Both components were cured using the direct electric cure method, of which more details can be found in the paper on direct electric cure in chapter 7.

Each component used CNT modified epoxy resin between the copper electrodes and the UD CFRP, which can be seen in the right image in Figure 2. This was prepared at 10 % by weight from a 25 % masterbatch of CS1-25 MWCNTs (Arkema), using a high shear mixer (Silverson).

The smaller flat panel component was manufactured and tested first in a lab environment to ensure the UD plies heated on the surface as intended, as seen on the left of Figure 1.

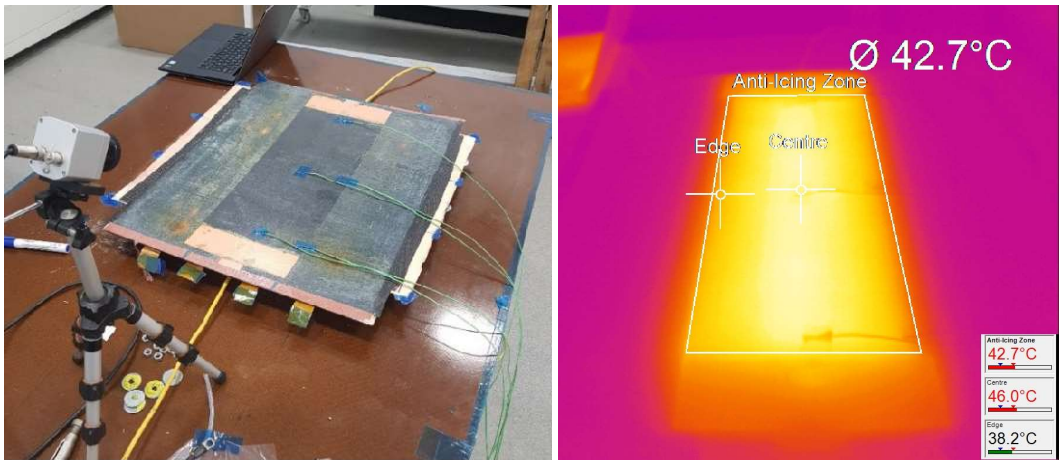

Figure 1: Left; Flat panel static dry heating test, Right; Thermal image showing even temperature distribution.

On the right of Figure 1 shows a thermal image of the component when heated, which was primarily to evaluate the temperature difference over the surface, rather than absolute temperature, as this camera was not calibrated to the emissivity of the sample. The heating was controlled from the central thermocouple, which reached the set temperature of 40 °C for this test. The temperature difference measured with thermocouples and IR camera is estimated to be lower than 5 °C. This is a positive result, as Joule heating for electric cure has significant issues with temperature distribution. It was the results from this test that suggested this method may be suitable for Joule heated composite tooling, seen later in this chapter.

7.1.4. Manufacture of test components

The LE demonstrator was designed to have 3 heating zones for de-icing, one primary zone at the leading edge, measuring 200 mm wide, and two secondary heaters on the top and bottom of the leading edge, 100 mm wide each. In a real de-icing scenario, the area at the front of the wing will have the most surface area facing into the oncoming airflow and will be subject to highest heat transfer. The secondary heaters are required to ensure that the recently melted ice from the leading edge does not refreeze further down the surface of the component, which can be common in an airstream in icing conditions.

A mix of rollers and hard PFTE hand tools were used to apply the plies, which is standard practice for the layup of composite components. Copper sheet was cut into T-shapes and then laid up for the de-icing electrodes. The tab at the end meant that there was a good contact between the copper electrodes on each side of the de-icing UD carbon ply, which is the de-icing heating connector. The CNT resin was applied to the contacts using a paintbrush, seen in Figure 2. On top of these copper electrodes, bighead connectors were placed, and narrow cuts were made in the plies above to allow the thread through the thickness of the component. The base of the bighead thread was insulated with PTFE tape so that the de-icing circuit was not in contact with any other carbon in the layup to avoid a short circuit. A thin gauge thermocouple was placed in the centre of the component, to be used to monitor the temperature of the de-icing operation.

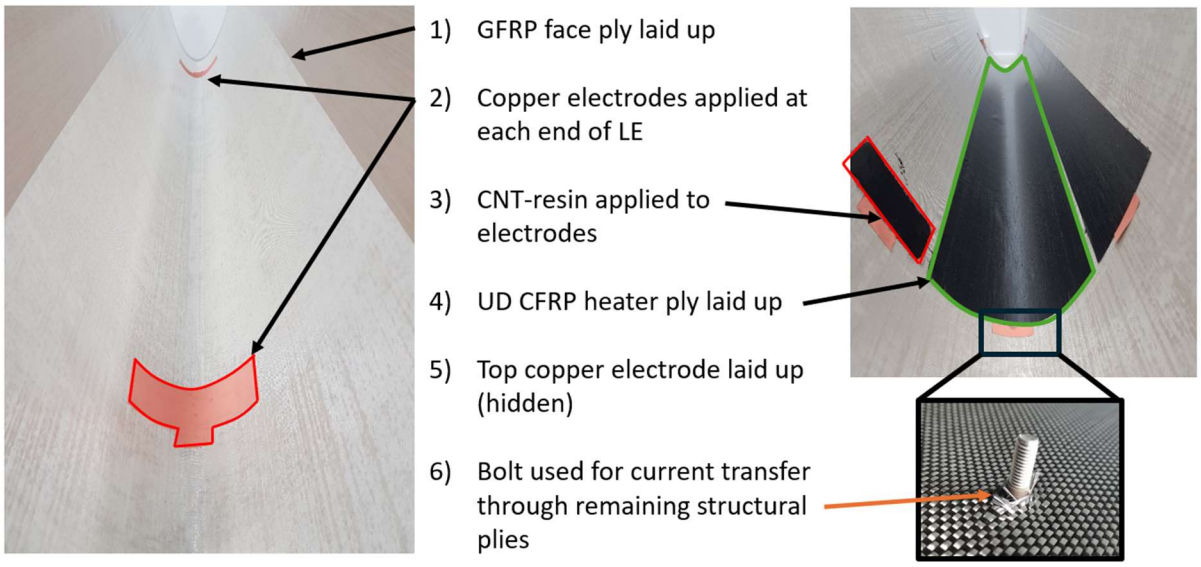

Figure 2: Stages of laying up the de-icing electrodes.

After the second glass ply, 8 plies of pre-preg were laid up directly on top one by one, with electrodes being applied at each carbon layer. Every 4 plies, a vacuum bag was applied to the layup and vacuum applied to debulk the ply stack.

The Nomex plies were directly laid up onto the pre-preg, no adhesive layer was required as the pre-preg can provide this adhesion without filling the Nomex cells with resin. After this, another set of 8 carbon pre-preg plies was laid up directly onto the Nomex.

The cure followed was Room Temperature (RT) to 120 °C at 2 °C/min, dwell for 2 hours, 120 °C to 160 °C at 2 °C/min, dwell for 2 hours, ramp down to RT.

The surface finish can be seen in Figure 3. Issues with tooling manufacture resulted in some bubbling on the surface of the component, however this was away from the heating zones, and only slightly effected the area around the electrodes. The surface finish was deemed smooth enough for ice accretion to occur, and for semi melted ice to slide from the surface effectively.

Figure 3: Leading edge component after demoulding and trimming of the DEC electrodes.

7.1.5. Ice build-up test environment

Testing was completed in a large environmental chamber at the University of Sheffield Lab for Verification and Validation (LVV), approximately 6 x 3 x 3 m in size. It was possible to change the air temperature from -20 °C up to room temperature. Ice build-up was completed by using compressed air through an atomiser nozzle, which drew through de-ionised water. A series of these were setup next to each other to evenly spray over the length of the demonstrators, show in Figure 4. Only one nozzle was used for the test panel. These nozzles were not able to be restarted during the test otherwise they would freeze up, therefore were started at room temperature, and then the chamber was reduced to -10 °C to ensure ice build-up would occur.

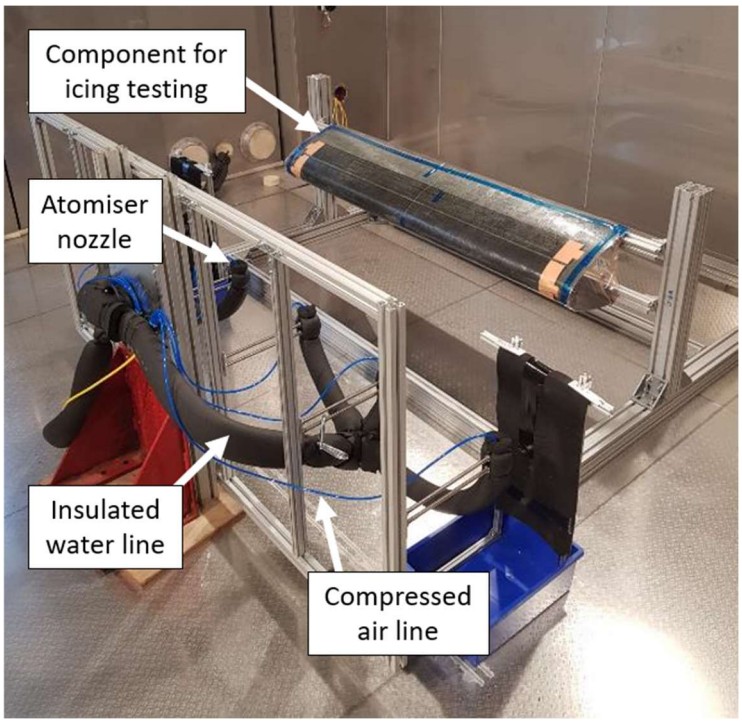

Figure 4: Nozzle setup used to spray water onto the components to build up ice.

Once the climatic chamber had reduced the ambient air temperature to -10 °C, the water that sprayed onto the components becomes super-cooled and instantly freezes when it hits the surface. This rime ice build-up is typical in ice accretion during inflight icing situations, and is characterized by its rough and crystalline appearance, with an opaque white colour, of which an example can be seen in Figure 5. The system was run for a set amount of time for both use cases to build up a set thickness of ice. Due to the uneven ice deposition, it is difficult to determine the thickness, but it was estimated to be a minimum thickness of 5 mm, and a maximum of 10 mm.

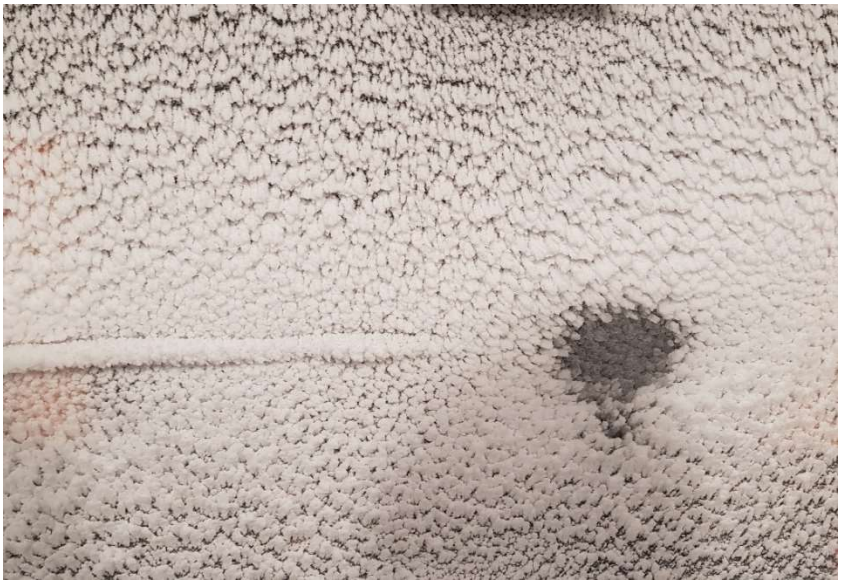

Figure 5: Ice build-up on the test panel, showing typical rime ice build-up.

A GoPro camera was used to monitor the ice removal on the surface. A thermocouple was taped to the centre of the panel to be used for PID control if required. A FLIR thermal camera was also used to

evaluate surface temperatures. As seen later, this was sometimes ineffective, as surface ice blocked the view, giving little data on the component temperature.

The LE was mounted onto a Bosch Rexroth frame, allowing it to be suspended into the air, around 300 mm from the chamber floor. The sample was powered and heated prior to being tested in the climatic chamber and was found to have small hotspots on the surface around the electrodes, where the CNT resin had been applied. These limited the power that heating system could be run at, as otherwise localised burning would occur. The hottest of these were repaired by the removal of material local to the heat generation with a diamond tipped rotary tool, then using quick dry epoxy to ensure the area was electrically insulated, circled in red in Figure 6. It was also for this reason that no ice prevention tests were completed, only de-icing tests were completed.

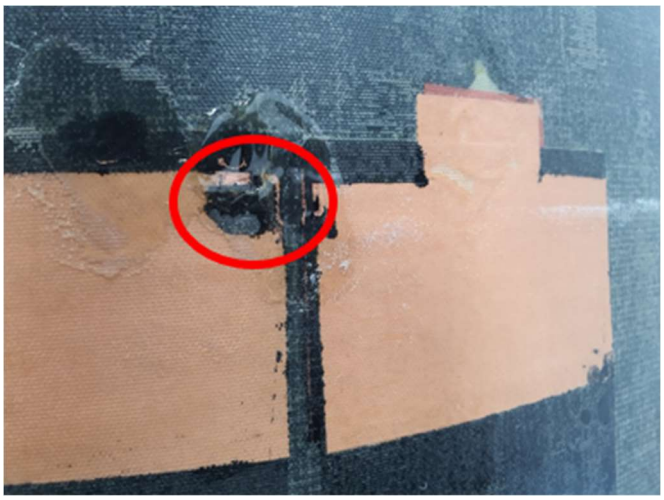

Figure 6: Image of an area of overheating that required removal and temporary repair, circled in red.

The panel demonstrator had a single thermocouple monitoring the temperature in the centre of the heating zone. The LE had four thermocouples, three were placed on the centre point of each of the heating zones, and the fourth was attached near the frame, away from the demonstrator to record the ambient temperature of the chamber, as seen in Figure 7.

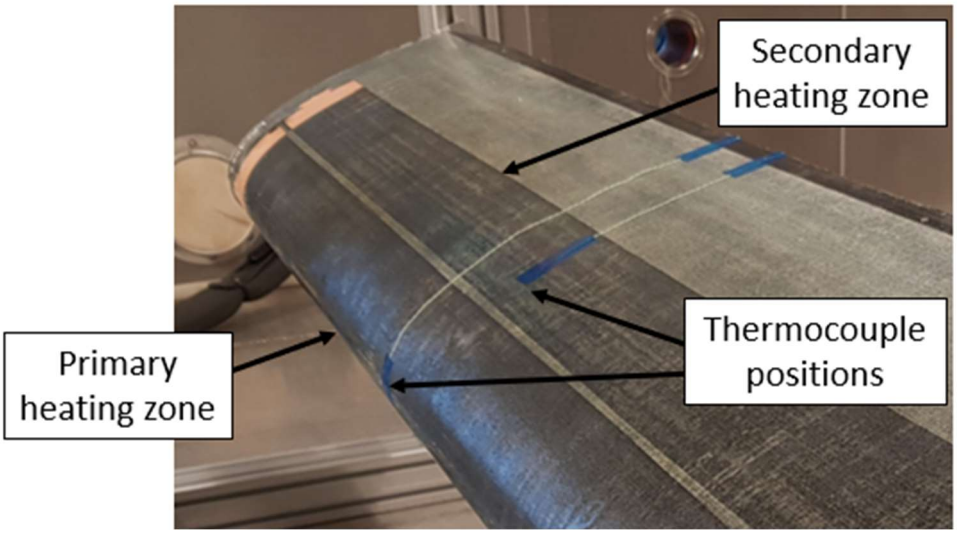

Figure 7: Image showing thermocouple position of two of the heater zones in view on the LE. The other half of the secondary heating zone is on the reverse side of the LE, out of view.

The thermocouples were threaded through a hole in the wall (top of Figure 7) as well as the power cables for powering the heating zones. Due to the extreme conditions, it was only possible to photograph the test at short intervals. GoPro cameras were used to record the ice melt and shedding, and a FLIR AC655sc IR camera was used to record the surface temperature.

7.1.6. Results for the test panel demonstrator

Images from the GoPro timelapse can be seen in the storyboard in Table 1. Visually, the ice is removed in 17 minutes from the start of the power being turned on. Due to the panel being in the upright position, it is difficult to tell how much of the ice is being supported by the un-melted ice directly below. As close observation was not possible during the test whilst it was running, there is a chance that the ice directly on the surface of the heater was melted, however was still visually covered with ice. When observed in real time on the video, the first sections on melting occurred gradually (top left of heating zone) whereas the last sections dropped off in large sections right at the end, suggesting the ice was being supported elsewhere.

Table 1: Timelapse images showing the de-icing process, with an image every 2 minutes until the ice has been removed.

00:00 - Start	2:00	4:00	6:00
			
8:00	10:00	12:00	14:00
			
16:00	18:00 - End		
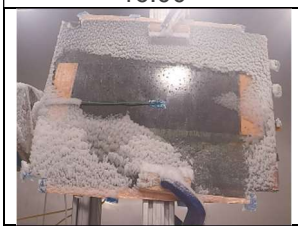			

The thermocouple log and power output to the de-icing zone can be seen in Figure 8. Power was controlled in a combination of automatic and manual modes, as it was difficult to predict the power requirements of this use case. Power was increased quickly to 170 W within 5 minutes to ensure melting could occur as quickly as possible and to test the power density of the system. The sharp rise in temperature around the 10-minute mark could be due to the ice locally moving away from the thermocouple being monitored. Ice was melting quickest at the top of the panel, moving down. This heated water could have assisted this rapid rise in temperature, which occurred with very little additional power at this time.

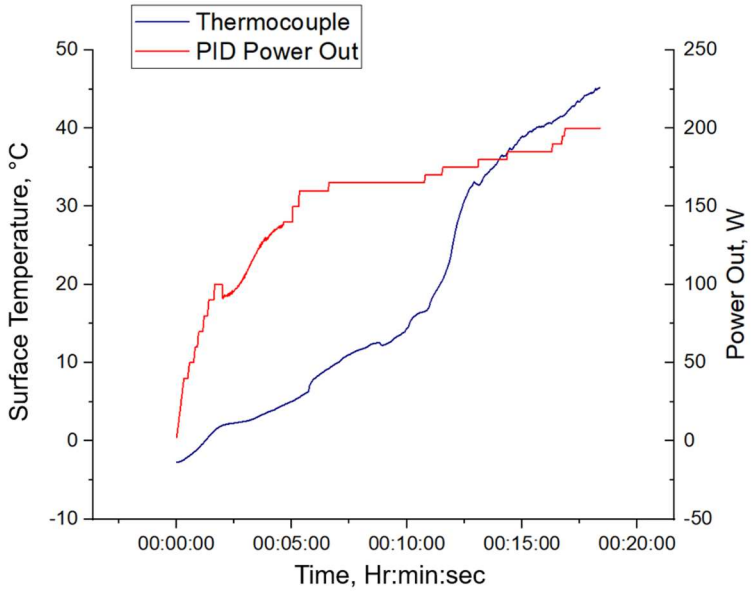

Figure 8: Part temperature and power out to the heating zone on the panel demonstrator.

It is noted that the thermocouple is reading -3 °C at the start of the experiment in Figure 8, opposed to being nearer -10 °C, which is the temperature of the air in the chamber. Figure 9 shows an IR image with a minimum temperature of -7.6 °C, it is expected that these discrepancies are due to the experiment starting shortly after minimum air temperature was reached, opposed to part temperature.

Thermal images were taken throughout the heating cycle, a sample image mid-way (10 minutes) through the testing can be seen in Figure 9.

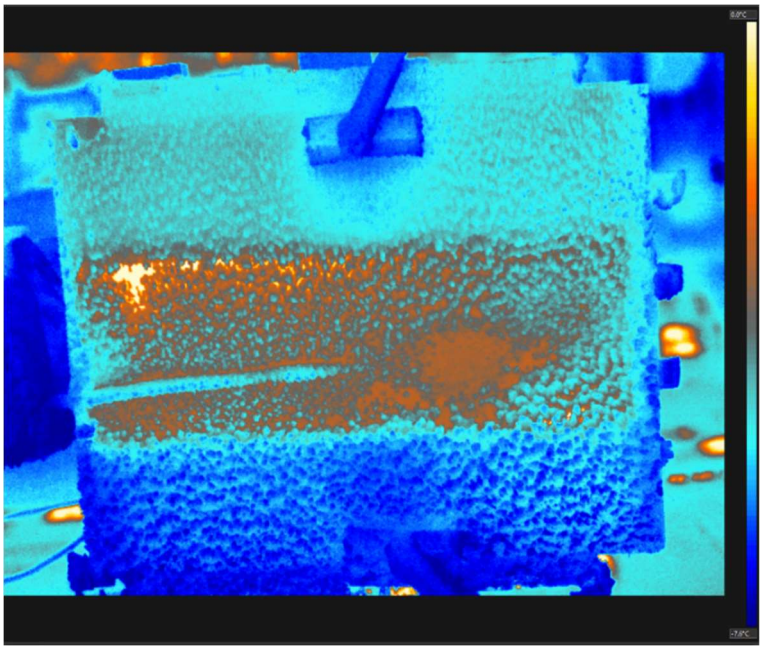

Figure 9: IR image showing the heating during the panel icing test. Coldest temperature shown in blue is -7.6 °C and warmest in yellow is 0.0 °C

7.1.7. Results for the LE

Given the limitations of the maximum power due to the hotspots identified during the test, the focus was turned to finding the power limits of the heater zones and to better understanding the test setup. Figure 10 shows a close up of the ice build-up immediately after the nozzles have been shut off prior to de-icing testing. The chamber was kept at -10 °C during the testing.

Figure 10: A closeup image of the ice build-up on the LE demonstrator leading edge, prior to de-icing testing.

Once the power limits were understood (due to hot spots), the LE was then covered in ice, after which the zones were run near their maximum possible power. This was ~80 W for the primary zone and ~150 W for the secondary zones. As the power supply and control system was unable to control the heaters simultaneously at different power levels, they were switched every 3 seconds, with the power changing independently on the relay switch. Throughout the de-icing test the timing and ratio of this switching was changed to attain optimal performance of the system, and ensure the zones were heating at a similar rate. Similar to the panel sample, a timelapse was created, seen in Table 2, which shows the de-icing process at 5-minute intervals.

Table 2: Timelapse images showing the de-icing process of the leading edge, with an image every 5 minutes until the ice has been removed.

00:00 - Start	5:00
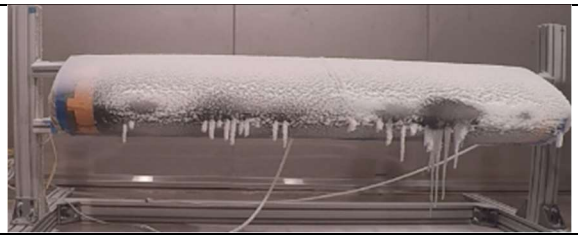	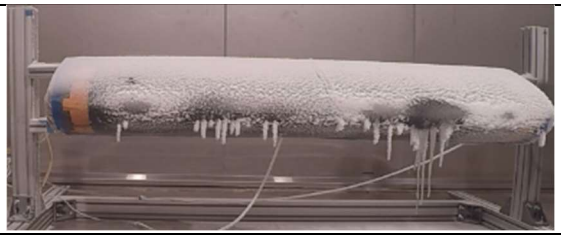
10:00	15:00
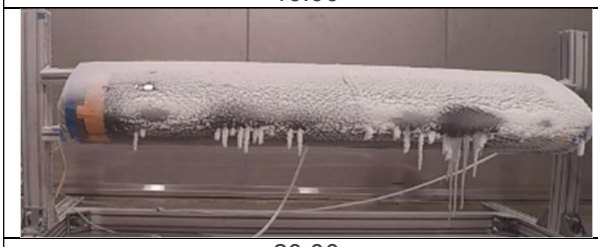	
20:00	25:00
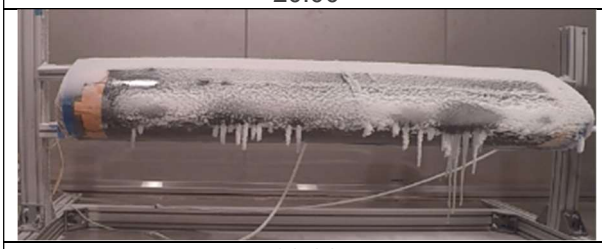	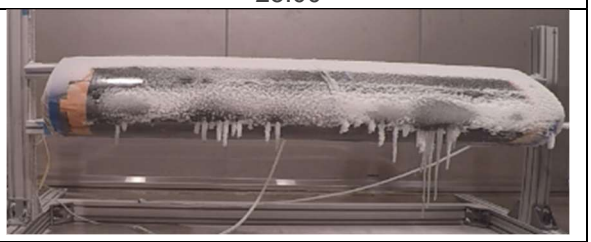
30:00	35:00
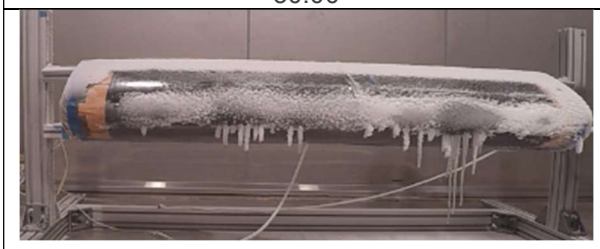	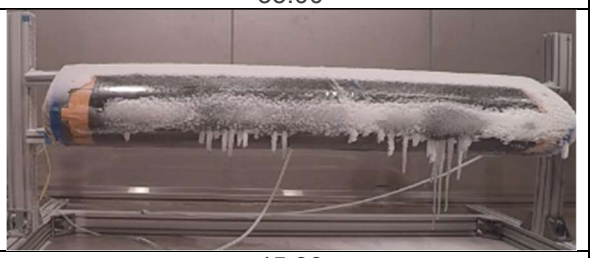
40:00	45:00
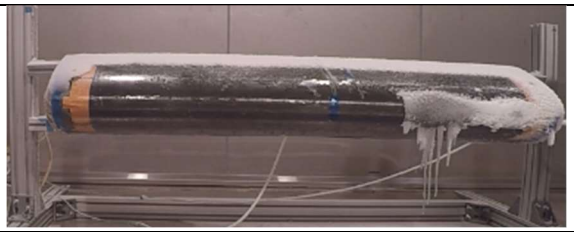	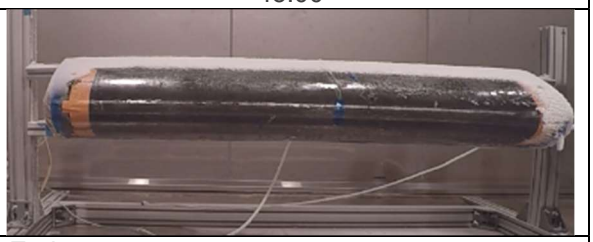
50:00 - End	
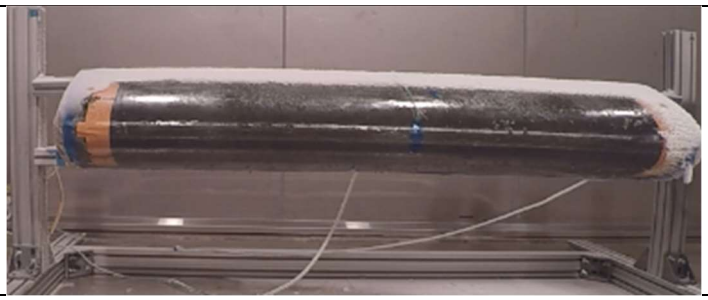	

These were adjusted throughout in response to the hotspots, seen in the power and temperature traces in Figure 11 and Figure 12. Note the differences in scale, particularly for power, which is significantly higher for the secondary heaters.

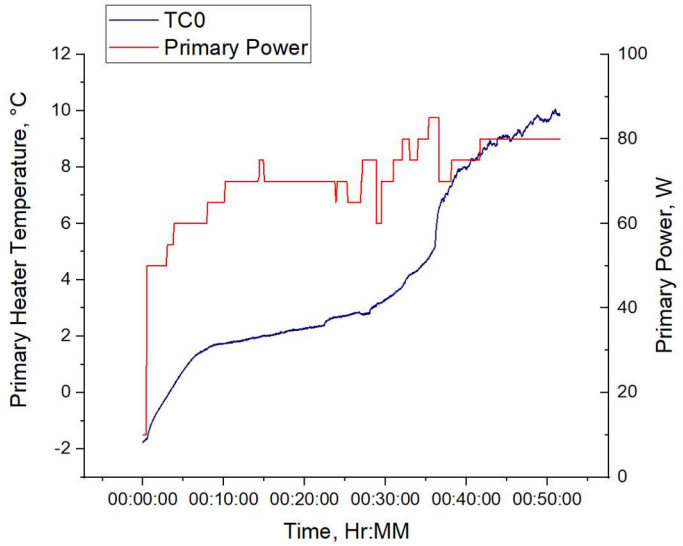

Figure 11: Graph showing the power and temperature to the primary heater during the de-icing process for the LE.

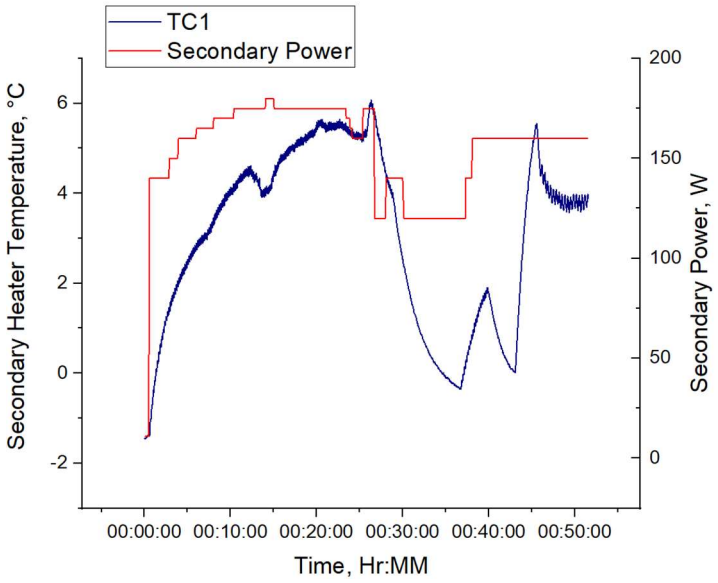

Figure 12: Graph showing the power and temperature to the secondary heater during the de-icing process for the LE.

IR images were also taken during the icing test, of which an example can be seen in Figure 13.

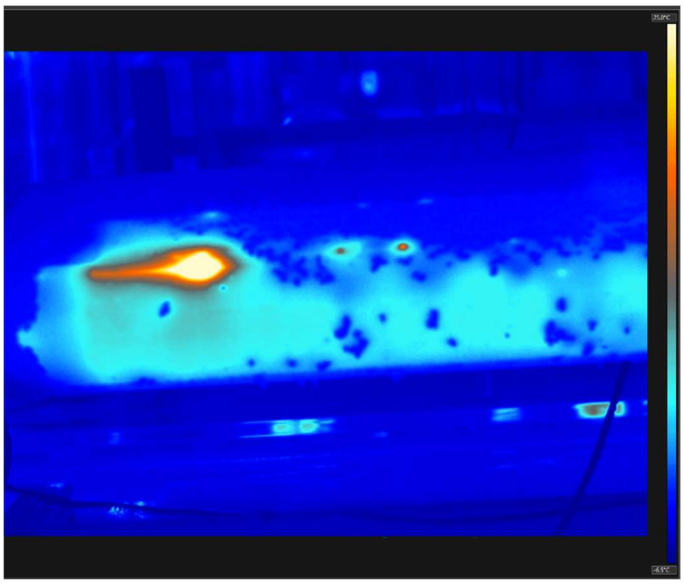

Figure 13: IR image showing the heating during the LE de-icing test. Coldest temperature shown in blue is -6.5 °C and warmest in yellow is 25.0 °C.

The main hotspot that limited the power going into the primary heater can be seen in Figure 13 on the left side. Two further smaller hot spots can be seen in the centre of the image.

7.1.8. Discussion

The panel component enabled a high-power test of the de-icing systems. The heating zone was 200 x 400 mm, with a maximum power of 200 W used, meaning the ice was fully shed in a 17 minute period. This raised the surface temperature to 45 °C by the end of the test. There were no hotpots recorded during lab testing or icing testing.

The IR image shown in Figure 9 shows a very even temperature distribution over the heating area, even behind the larger pieces of ice. It appears that there is a hot spot in the top left of the heater zone, however this is where there is a slight gap in where the ice has formed. The even spread of heating is a good indicator for the capability of a high-performance heating mode.

When reviewing the timelapse of the leading edge in Table 2, the higher power of the secondary heaters is evident, as the ice on the top heaters away from the leading edge melt the ice much sooner than on the leading edge. The ice appears to mechanically hold on to the leading edge for around 40 minutes, after which the majority of the ice falls together. The surface roughness of the LE could be improved as it retained the pattern of the PTFE from the tool, resulting in ice sticking more readily. If this system was running in airflow, the ice would have shed sooner due to the mechanical assistance. The aim of this test was to evaluate the heating mode, not whether the surface roughness would improve the de-icing performance, but this could easily be improved in future work.

When collating information from the time/temperature/power graphs in Figure 11 and Figure 12, it can be seen that the secondary heaters had de-iced their sections by the 25–30-minute mark. At this point, the power was reduced and more time and power was allocated to the primary heater to remove the rest of the ice. This is the reason that the temperature of the primary heater increased after 30 minutes, and from the timelapse the ice in the primary zone was removed after this point.

The peak power densities for the primary and secondary heater zones of the LE were 0.025 W/cm^2 and 0.053 W/cm^2 which are significantly lower than the 0.25 W/cm^2 achieved on the test panel. It was not possible deliver higher power levels, as the IR camera indicated that the material was over 100 °C at the hot spot locations and would have likely been higher sub surface. If the power had been extrapolated to the level used in the test panel, it would have used 800 W. If the full power of the PSU had been used (1500 W) and extrapolating these results would have resulted in the wing having been cleared of ice in around 8 minutes or sooner.

7.1.9. Future work

Understanding of the power requirements for use in commercial aircraft is still required, as it needs to be compatible with alternating current at higher voltages, such as 240V. The resistance of the heaters used in this study ranged from 0.35 to 1.5 Ω which isn't compatible with these range of voltages currently. The use of transformers is not desired for a system like this, therefore modifications to the carbon layout to modify the resistance would be required. There are a few ways to achieve this, through the use of Tailored Fibre Placement (TFP) or Automated Filament Placement (AFP), longer thinner traces of carbon tow could be placed on a wing to increase the resistance of the system.

If the issues with localised burning were not present, and the power requirements were tuned closer to what is required by aerospace, this method could be a viable method for lightweight electrothermal de-icing or anti-icing. The testing here showcases the potential, however, needs to be evaluated in a full icing wind tunnel to understand if this method would be suitable for aerospace in the future.

It does highlight some of the significant disadvantages of the use of CNT's in composites, where they limited the maximum performance of the demonstrators, particularly with the LE, where the hot spots were generated. There are a few reasons why they could have changed characteristics between the panel and LE tests. The application of resins to the surfaces wasn't optimal and would be difficult to recreate. It is significant that there were no hot spots on the test panel, showing it is possible to use them effectively, however the LE shows that this is not consistently achievable. As discussed in chapter 5, the processing and preparation of CNT-epoxy blends is important, as is the amount of time they are stored after processing.

7.2. Development of CFRP Joule heated tooling for aerospace applications

Following the application of UD fibres in a composite layup for de-icing applications, the technology was developed further to enable low-cost Joule heated tooling. The project was conceptualised by Matthew Collinson, with help from Dr Stu Morris, Director of Engineering at Pentaxia, which was successful in obtaining grant funding from NATEP. This work covers the first stage of this "EcoTool" project, covering adaptations to the process to enable compatibility with composite tooling, and the curing of a small-scale wing skin section. This work is still ongoing; however, it is highlighted to show further use cases for this technology, that have real world applications.

7.2.1. Abstract

The previously developed direct electric cure (DEC) technology for Joule heating of CFRP was adapted and implemented to manufacture a heated tool and subsequently heat and cure CFRP components. Unidirectional carbon fibre pre-preg was laid up as a heater element in the middle of a standard 1-8-1 tooling layup, which was then used to cure the tooling pre-preg itself, as well as components on the tool after this initial cure. Electrical connectors and adhesive film were used to pass the electrical connection through the resulting carbon tooling plies, to ensure even temperature distribution and safe operation in a manufacturing environment. A custom power distribution setup and custom software to heat multiple heating zones equally was developed. A demonstrator tools were developed with the shape of a generic wing skin, to test the technique on larger components, as well as testing more complex geometries with tapers with multiple heating zones.

7.2.2. Introduction

The composite manufacturing industry is continuously looking for novel manufacturing solutions that achieve increased manufacturing rates, reduce energy consumption and reduce manufacturing costs. This is happening across many sectors, particularly in aerospace, automotive and energy.

Direct electric cure has previously been developed and discussed as a potential way of achieving these improvements. It would be challenging to introduce to the aerospace industry, given the certification requirements for a novel curing method which introduces fundamental changes to materials and process. Recertification of novel cure methods reviewed in chapter 3 would require significant investment as most fundamentally change how heat is delivered to the component. Heated composite tooling is used in some aerospace applications to manufacture parts already. Therefore, there is an opportunity to use the technology and developments for DEC and apply them to composite tooling to get similar benefits, but with lower certification requirements.

Heated tooling for composite manufacturing has been used for the curing of composites since their inception, using technologies such as heater mats, heated fluid, heater lamps and resistive heating to provide heat [16]. Common heating methods for metallic tooling comes in the form of fluid heating channels within the tool, embedded heater cartridges or having the tool within a heated press. All of these methods are effective for curing of pre-pregs and resins, helping increase throughput, however they have limited benefits in energy efficiency and cost to run.

The heating of composite tooling using Joule effect heating has been explored in a small number of previous studies using UD plies [17,18] or tailored fibre placement (TFP) [19]. In the area of TFP heater

elements, it is clear that there are many private operations heating carbon in this way, however there aren't any identified instances of technical publications.

Weiland et al [18] simulated a CFRP mould with inbuilt resistive heaters to study the effects of non-uniform heating of resistive heating methods, which could be caused by the low thermal conductivity of CFRP compared to metallic tooling. It was possible to predict the temperatures up to thermocouple accuracy, however this was only completed on very simple geometry. Athanasopoulos et al [20] manufactured a top hat geometry resin transfer moulding (RTM) tool that used the embedded carbon fibres as heating elements, in particular to assist resin flow during the infusion process. The carbon fibre heating elements were embedded near to the A surface, using a gel coat to ensure a high-quality surface finish as well as electrically insulating the fibres. Degree of Cure (DoC) was found to be within < 1 % of components cured in the oven, however there were thermal gradients on the tool surface, which were attributed to the heat transfer at the edges of the part to the environment.

7.2.3. Objectives

This study used previous knowledge from Joule heating of CFRP and understanding of composite tooling for aerospace components, to manufacture and test a Joule heated CFRP tool. Modulated MOSFETs were used to control power output to multiple zones of a tool, to enable even temperatures to be reached over the surface of a more complex tool geometry. This method was previously demonstrated as effective for improving temperature distribution over multiple complex heating zones when joule heating composites by Liu et al [21]. The curing performance was verified using a thermal survey and DSC testing of components cured on it.

The manufacturability of the tool is also of importance, as many commercial or custom heated tooling solutions are cost prohibitive, negating the positives of low energy consumption and shorter cycle times. This study aims to use standardised composite materials and methods to ensure that the resulting heated tooling has a minimal impact to the overall cost.

The larger tools demonstrated in this study were cured in an oven, however, it will be of interest to cure the tooling pre-preg itself using the Joule effect heating so that an oven or autoclave isn't required at all as part of the processes. This not only lowers the cost barrier to composite manufacturing, but it also presents the opportunity to manufacture components larger than the constraints of the size of heating chamber that is available, such as oven or autoclave. This could enable large monolithic composite structures for aerospace, such as wing skins, without the requirement of extremely large autoclaves.

7.2.4. Methods and hardware

The experimental hardware from previous experiments in CFRP Joule heating [3] was updated to ensure that was easier to program, now in Python, and subsequently using more open-source hardware. The National Instruments (NI) and TDK power supply units (PSU) were controlled using the standard command for programmable instruments (SCPI) commands over a local area network (LAN) connection. Off the shelf thermocouple amplifiers and PWM controllers from Adafruit were used to log temperature data and modulate the MOSFETs respectively. The control software was written in Python and provided a PID loop of equivalent energy to each zone as required based on the temperature feedback. A user interface was written in Plotly Dash.

The layup, including the copper electrodes, UD plies, glass insulation and bolts for the power pass through, can be seen in Figure 14. Bolts were used to easily pass through the remaining bulk and surface plies in the tooling layup, as well as being easy to attach onto power cables post cure. The base of the bolts were insulated to ensure that they are electrically isolated from the other carbon plies.

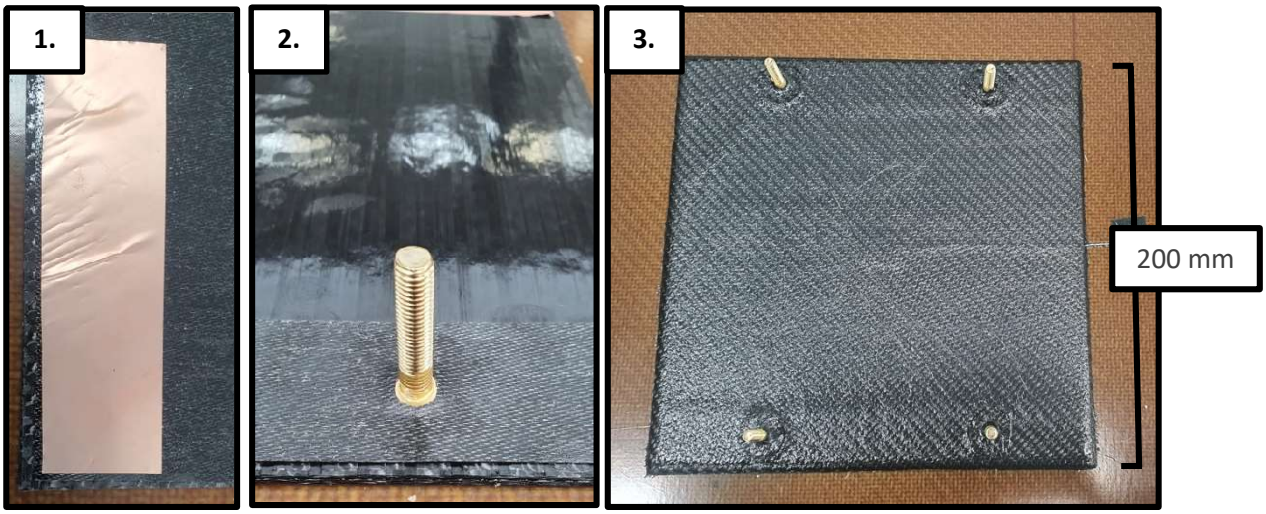

Figure 14: Photos of the process of laying electrodes in tool. 1. Layup of copper electrode, 2. GFRP used to hold in place bolts to allow for passthrough 3. Final layup with bolts through the thickness of the remaining ply layups.

The electrical insulation was required to ensure that Joule heating wasn't occurring in any other plies, and to ensure that the tooling would be safe for a user to touch whilst it is operational. To verify this had been achieved, a Megger insulation tester was used to test the insulation between the electrodes and the surface of the tool, as seen in Figure 15.

Figure 15: Megger insulation tester attached to a tool.

The clamp was attached to the surface of the tool and then each electrode was probed to test the insulation. 50 V was first tested, as this is within the operating voltage range of the tool during cure. Additionally, higher voltages were also tested in case any overload situations occurred. As the primary area for current to enter the bulk plies was around the bolt. The electrical insulation was improved until the tools passed the 1 kV test. This was achieved through additional debulking steps, occurring after every GFRP ply, and improved insulation of the brass bolts at their base, where there is possible contact with bulk carbon plies. After these improvements, complete electrical insulation from the heating plies to the external surfaces was demonstrated.

Two geometries were tested. The first was a 300 x 300 mm flat plate with the UD carbon heater plies laid up to within 5 mm of the edges of the plate. The second was based on an aerospace component, which was a top wing skin of a NACA 2412 aerofoil, which has been tapered from a chord of 340 mm to 250mm. These two tooling designs can be seen in Figure 16.

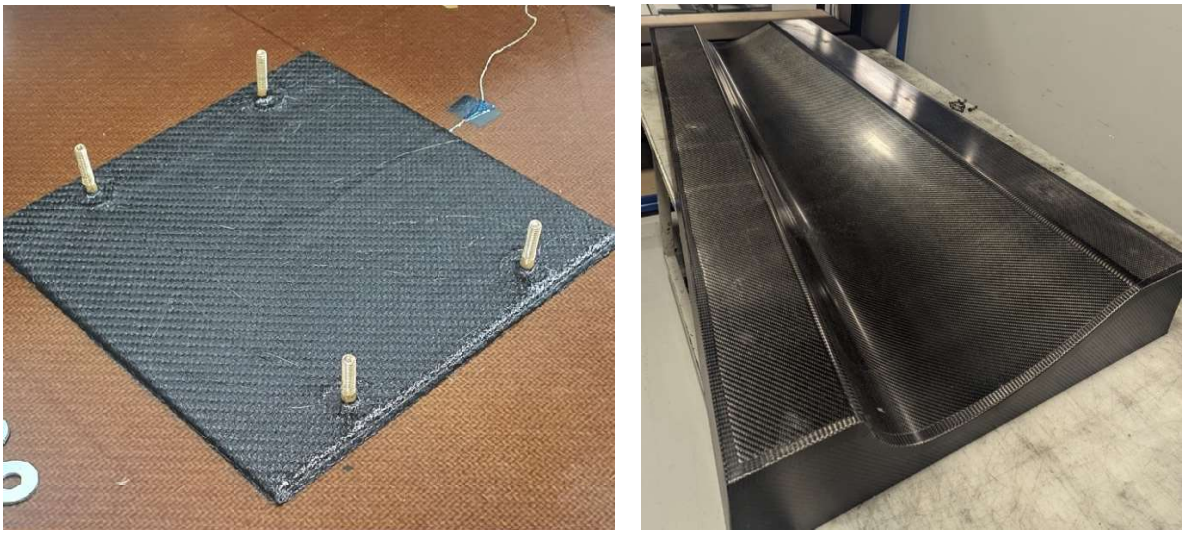

Figure 16: Left: Small flat plate tool, Right: Example of a cured tool with embedded electrodes (sub-surface).

Components being cured on the tools are made of SHD VTC410, which cures at 120 °C and post cure at 180 °C. The smaller tool was cured using the Joule effect itself, whereas the larger wing skin geometry was cured in an oven, as the heating elements were only placed where the component was to be cured.

7.2.5. Experimental

The small flat plate tool was used to do initial assessment of the Joule heating to cure the tooling pre-preg, and of curing components using the heated tool itself. Two 200 x 200 mm panels of 8 plies thick UD SHD VTC 410 pre-preg were cured, one using the Joule heated tooling and the other cured in an oven to compare the curing methods. Both followed the same recommended cure cycle of 1 hour at 120 °C. Samples were taken from two opposite corners and the centre of the panels and tested in a DSC. The results can be seen in Figure 17. ΔH is the energy released by the sample after the cure when raised to 300 °C, then adjusted for the samples mass. ΔH is directly related to the DoC, a low ΔH would indicate a higher DoC.

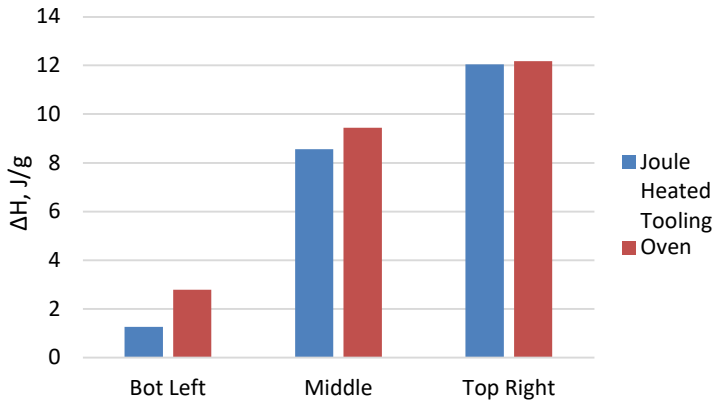

DSC curve peak temperature (T_g)		
	Oven (°C)	Joule heated tooling (°C)
Bot Left	181.45	181.85
Middle	170.43	174.26
Top Right	163.11	162.30

Figure 17: Graph: Data showing ΔH (J/g), Table: Temperature peak from ΔH curve.

As it can be seen from the DSC data, the degree of cure is very similar between the Joule heated tooling and the oven cure when following the same cure cycle, with the heated tooling performing slightly better than the oven cure. The DoC's both follow a similar pattern, with the bottom left of both samples being significantly more cured than the other areas. This position on the heated tooling is

nearer the electrodes, which can heat up more than the rest of the panel, as seen in Figure 18. It is unclear as to why this same pattern has occurred with the oven cured components. It could be due to the position of the part being not being central to the caul plate, leading to uneven heat transfer, leading to hot spots on the component.

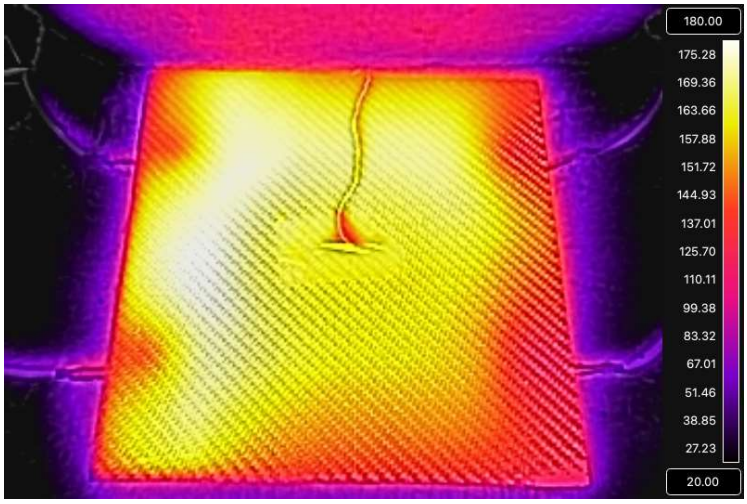

Figure 18: Thermal image showing that additional heating can occur around the electrodes, see the left side of the panel.

When scaling up, the excess heating around the electrodes can be reduced to acceptable level by increasing the electrode area, reducing the contact resistance. Composite tooling commonly has excess material around the edge of where the component is being cured, therefore the area required for the electrode can potentially be accommodated in the tooling design.

The small flat plate tool was cured using the in-built heater plies, however the larger tool with the aerofoil geometry was cured in an oven, as there was no current way to fully cure the flanges/stiffening structure using the Joule effect curing method. Future developments aim to cure the whole tool using this method, to reduce reliance on ovens, and allow for larger components to be manufactured. Due to the tapered complex geometry, the tool was split into 3 separate heating zones to ensure that an even temperature could be achieved. Once the tool was cured, the zones were tested individually to ensure that they were working as expected with no shorting or major temperature changes, of which thermal images can be seen in Figure 19.

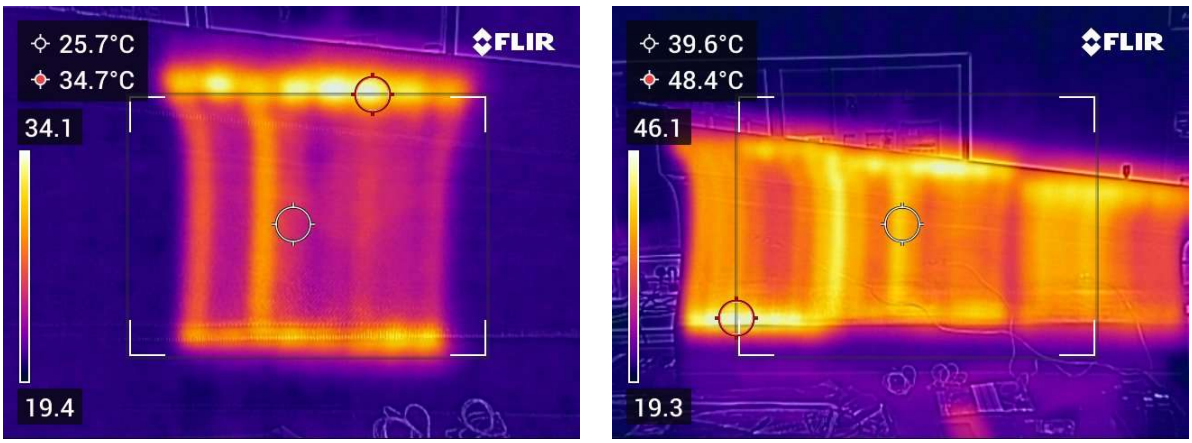

Figure 19: Thermal images showing the temperature distribution over one zone (left image) and all three zones (right image).

The zones heat up at slightly different rates, however this isn't expected to affect the overall heating performance during cures. The addition of the component plies (to be cured) and thermal insulation is expected to significantly reduce this effect and provide more even heating. Compared to previous Joule heating completed on plain weave composites (see direct electric cure), here the heating occurs at edge of the composite, rather than reducing as it gets closer to the edge. This previously resulted in under-cured components, however as seen in the previous section, this appears to no longer be the case.

To test the aerofoil geometry tool, 8 plies of pre-preg were laid up onto the tool, leaving a 50 mm gap to the edge of the tool at each end. A cure cycle at 120 °C was completed, for which the time and temperature trace at thermocouple 1 can be seen in Figure 20. During this cure, the tool was insulated using rock wool, over 100 mm in thickness.

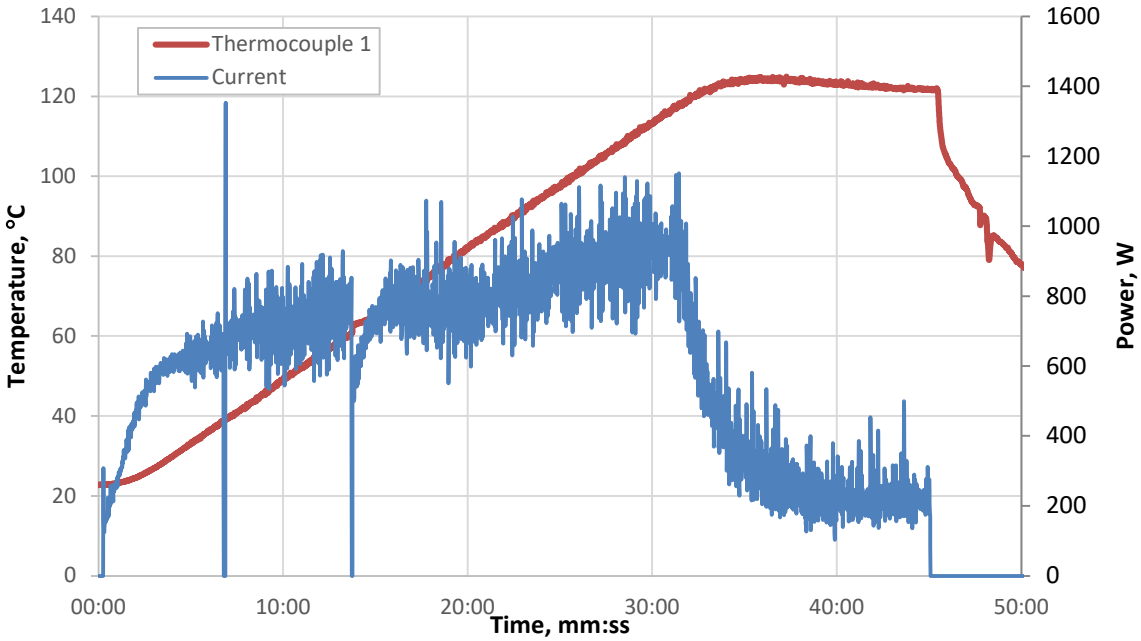

Figure 20: Power and temperature traces for a shortened cure cycle using heated tooling with complex geometry.

The total power usage for this cure cycle is 0.455 kWhr, which has then been normalised to per hour of cure to enable comparison with other novel cure methods, such as DEC and oven cure. Examples of normalised energy per cure can be seen in Table 3. It is noted that the oven used for comparison is 3 x 3 meter and can fit multiple equivalent tools of this size, and the DEC are for different size and geometry components (2-meter-long leading-edge section).

Table 3: Comparison of Joule heated tooling energy consumption to other cure methods.

Cure method	Normalised energy per cure hour per hour, kW/hr^2
Oven Cure (180 °C)	66.58
DEC VARTM (140 °C)	0.64
DEC Pre-preg (120 °C)	0.56
Joule heated tooling (120 °C)	0.61
Joule heated tooling component scaled (120 °C)	1.01

The component cured here is roughly 40 % smaller than the DEC examples, so when adjusted for this scale, it is slightly less energy efficient. However it is still significantly more efficient than oven or autoclave curing. The increased energy efficiency combined with the lower labour cost to implement this system are likely to make it attractive in a manufacturing situation if the required quality and reliability can be achieved.

Three thermocouples were placed on the surface of the component being cured to understand the heat distribution. They were placed along the centre line of the component layup, one at each end of the layup and one in the centre of the component. The range of the thermocouples, indicating temperature distribution, was calculated and can be seen in Figure 21.

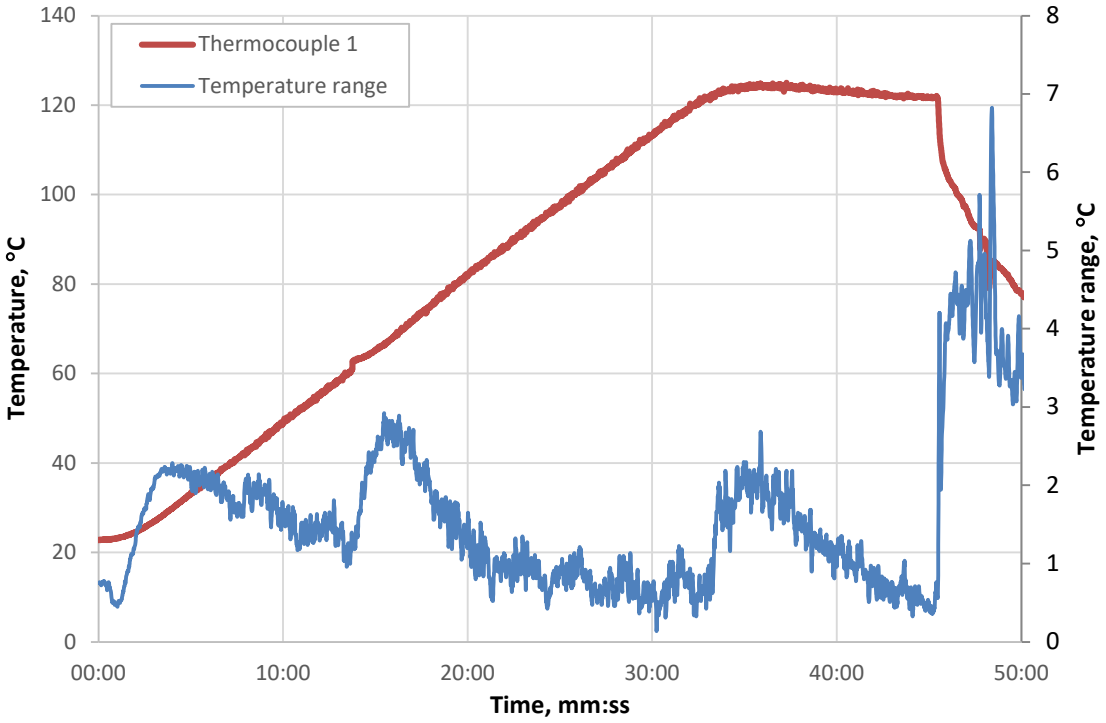

Figure 21: Range of thermocouples compared to the cure temperature of the tool during a 120 °C cure.

During the ramp stage the range does not reach higher than 3 °C, and during the dwell settles to under 1 °C. This is a significant improvement over previous DEC cures, where the range increased significantly during the ramp, above 60 °C, and was at minimum 20 °C difference by the end of the cure.

7.2.6. Discussion and conclusion

In this experimental work, the concept of using DEC principles in composite tooling to develop Joule heated composite tooling was demonstrated with promising results. Small- and large-scale components were tested, with their heating and energy efficiency performance compared to oven cured components. The DSC testing of the smaller flat plate showed that heating through the thickness of the tooling layup was possible and resulted in comparable DOC to oven cured components.

When scaling up the tooling size, energy efficiency could be compared to previous DEC and oven cures. It was found to be less efficient that DEC, but still significantly more efficient than oven curing. Initial

temperature mapping showed significant improvements in heating uniformity compared to DEC, which would be within aerospace specifications for curing. This improvement is likely due to the use of UD plies as the heating elements, however other improvements such as being able to apply insulation closer to the part (no additional tooling required) would also assist with this.

Future work should concentrate on verifying these initial results, by DSC testing components cured on the larger tooling. Additional heater plies can be applied to the complex geometry example, which would allow for the whole tool to be cured using Joule heating, including the flanges/support structure, which would then fully remove the requirement of an oven for curing. If this could be achieved, then tooling and components that are larger than common oven or autoclave sizes could be manufactured. This could lead to components such as wing skins or spars being manufactured without the requirement for heating chambers to be manufactured beyond this size.

7.3. Cure optimisation for rapid and low energy processing of thermosetting composite systems

The following paper on a cure optimisation for rapid curing, considers the exothermic heat generated in the component during curing, and heat loss to the environment, in order to enable shorter curing cycles that use less energy. This has been included to show the potential of the technology if other aspects of composite manufacturing, such as cure cycles, were updated to be compatible with the technology.

The project was conceptualised, and cure optimisation code was developed by Tim Swait. The use of the cure optimisation setup, adaptation to a heater plate and experimentation was completed by Matthew Collinson with experimental assistance from Matthew Bower. The paper was authored by Matthew Collinson, with supervision and reviewing from Tim Swait and Betime Nuhiji.

7.3.1. Abstract

The cure kinetics of a commercially available epoxy resin system were modelled, then cured using the models' predicted outputs, taking into account the curing environment, for reductions in time and power usage. The model was derived from first principles with kinetic cure constants generated by Differential Scanning Calorimetry (DSC) traces. The model calculates exothermic energy and energy transferred to the environment and tooling, depending on the time temperature profile inputted. Optimised cure cycles were completed using a heated tooling plate, resulting in an 87 % shorter cure cycle, whilst achieving the target degree of cure (only 0.14 % lower than baseline), with no runaway exothermic reaction. These optimisations resulted in an estimated 95 % energy saving compared to an equivalent oven cure. This study demonstrates when a resin system is coupled with an optimised cure cycle, significant manufacturing and sustainably improvements can be made over cure cycles provided by manufacturers.

7.3.2. Introduction

Time-temperature cure schedules for thermosetting resin systems are currently specified based on the assumption that the component will be cured by a wide range of convection-based curing methods, typically oven or autoclave [22]. These conventional curing methods result in high quality parts, however, are expensive to acquire and run, and have in many cases, unnecessarily long cure cycles. They are unable to apply rapid changes in thermal energy to the component due to their large thermal masses. This is reflected in cure schedules designed to assume a worst case in terms of part thickness and equipment heating performance. This results in conservative schedules with slow, constant rate heat up ramps and long isothermal dwells, which reduces component throughput and increases energy usage. Novel rapid curing methods such as microwave [23,24], induction [25], direct electric [26] or heated tooling [16,27] can apply and reduce energy input far more rapidly to the part [28]. Some of these methods have the capability to heat at 10 °C/min or higher in a controlled manner [3], however there are few materials for which these heating rates are recommended. Accordingly, these novel methods are currently restricted to following the same cure schedules as the convective methods, meaning that the potential benefits offered by these advanced curing methods cannot be realised.

Control algorithms for these novel curing methods are shared with the convective methods, proportional, integral, differential (PID) based controllers. The underlying assumptions behind these

control algorithms aren't ideally suited to heating [29], therefore additional levels of complexity such as gain scheduling, autotuning or multiple "cascade" PID are used to improve heating performance [30,31]. With appropriate tuning and set up these can provide acceptable results and are used in industrial settings. However, this process is complex, and users are often unaware of how to set up these functions effectively due to tuning being dependent on the complete system of part, tool and curing equipment.

Cure optimisation through the use of kinetic models has been investigated previously. Karkanas et al [32] investigated the use of an autocatalytic model to predict the kinetic response of Hexcel RTM6 resin. This was built using data from Differential Scanning Calorimetry (DSC), providing good correlation to experimental cures. P. Hubert [33] characterised parameters of Hexcel 8552 resin for a modified empirical model, allowing for predictions in glass transition temperature (T_g) and viscosity. A similar method was used Kratz et al [34] to produce thermal, viscosity and T_g models for two commercial out-of-autoclave resins, which were verified by curing thick ply composites.

J. Lopez-Becerio et al [35] defined a non-Arrhenius reaction order model, which was accurate in specific use cases. Accuracy would reduce at higher temperatures not accounted for in the model. It was observed that adding more complex parameters to improve accuracy in these cases compromises the physical significance of the original inputs to the model. The models described all accurately manage to predict physical parameters such as degree of cure (DoC), T_g or viscosity, and in some cases have been verified with experimental trials.

The authors were unable to find any studies that have applied these predictive models to a manufacturing environment to make improvements to a cure, such as reducing energy usage and cure cycle time. The model in this study is not as complex as the ones reviewed, however, it is time and temperature dependent, considering the heating method and heat loss to the environment.

The objective of this study was to create and test a model of the full curing system environment, comprising the Carbon Fibre Reinforced Polymer (CFRP) component, tooling, and the curing equipment. This serves two important purposes. The first is that the model may be used predict the outcomes of cure schedules to achieve an optimal solution for a given system of component, material, and heating equipment. Secondly, the model could form the basis of a more advanced algorithm to control the cure process in real time, further increasing the potential of advanced curing equipment. This study does not cover running the models in real time, allowing for feedback to be introduced, however, the methodology allows for it in the future. This allows for future potential application of modern machine learning and artificial intelligence algorithms beyond estimations and assumptions made in this study.

7.3.3. Cure kinetics in composite manufacturing

Curing of epoxy thermoset materials is driven by the crosslinking mechanism, which is exothermic [36]. This effect is particularly evident when large quantities are mixed for a manufacturing process, the reaction starts as soon as the constituents interact. Depending on the resin type, the epoxy can heat rapidly if the heat cannot be dissipated as quickly as it is generated. If not monitored, or used shortly after mixing, this can evolve into a dangerous runaway exothermic reaction, as the heat generated increases the speed of the reaction further [37].

Figure 22 demonstrates this graphically with energy release measurements using a DSC, which measures the thermal outputs of a resin sample as it cures. Increasing the heating rate of the test results in a higher peak thermal output and heat flow rate from the resin. The area under the curve shows the increased energy output that the epoxy is generating if the heating rates are too high.

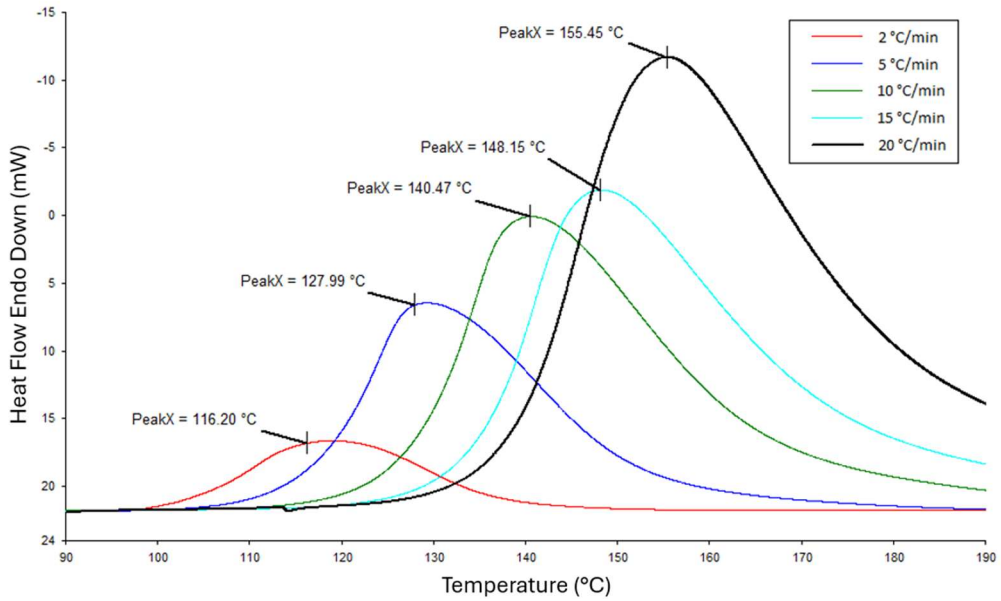

Figure 22: DSC curves of an epoxy resin at different heating rates, showing the higher heating rates increases the peak heat output.

If uncontrolled, it can lead to a runaway exothermic reaction, which can be a fire risk and cause significant damage within composites, requiring the whole part to be scrapped. Common damage due to a runaway reaction on a composite part are reduction in strength [38,39] and discoloured or burnt areas.

An aim of this study is to manipulate this curing reaction so that the heat generated during a cure can be harnessed to assist heating of the panel. This would reduce the time and energy input of the cure whilst increasing safety by predicting peak temperature during the cure.

7.3.4. Cure kinetics for predictive cure

The thermal reaction of epoxy resin is described by a set of equations that define the cure kinetics and the resulting properties. These equations will be used in this study to define a model, allowing cure cycles to be reduced in length, whilst ensuring similar degree of cure compared to the manufacturers cure cycle.

(Equation 1) [36] defines the degree of cure. This ratio defines the crosslinking that has occurred within a resin, compared to the amount of free reactive groups remaining unreacted in the epoxy crosslinking network. In an uncured system that has been mixed at time=0, this will be at its maximum possible value, as no reactions will have occurred. Once a sample has started reacting and crosslinking, the number of reactive groups start to reduce to a point at the end of the cure where very few reactive groups remain.

$$\alpha = \frac{x_0 - x_{tc}}{x_0} \qquad \textit{(Equation 1)}$$

where α is the extent of reaction, x_0 and x_{tc} being the amount of reactive epoxide groups available at the start of the reaction and at the final cure time, tc.

A post cure leads to an almost 100 % cure where there are very few remaining reactive groups, and the properties of the material can no longer change. Depending on the final property requirements of a resin, a cure cycle is usually designed to only react up to 85-98 % of the available reactive groups. An example of this can be seen in the cure percentages in Table 4, with a resin after a post cure reaching 97.80 % DoC.

The degree of cure is found in practice using a DSC, which is a technique that measures the total energy output of an exothermic reaction of a sample as it is heated. Cure percentage compares the energy available in an uncured sample to a cured sample with the same mass [40]. To determine the degree of cure at any point in the cure cycle, a kinetic model must be applied which relates time and temperature to degree of cure. Epoxy resins are commonly considered to cure according to an autocatalytic model equation [33,36,41,42]. This model is based upon two equations. The first is the Arrhenius Equation, (Equation 2), which allows the effect of temperature of reaction rates to be calculated, also defined as the rate constant, k.

$$k = Ae^{\left(\frac{-E}{RT}\right)} \qquad \textit{(Equation 2)}$$

where A is a pre-exponential or frequency factor, which is experimentally defined, E is the activation energy, R is the universal gas constant, and T is the temperature in Kelvin.

The second is the rate equation [33,36], (Equation 3), which defines the change of degree of cure over time.

$$\frac{d\alpha}{dt} = k\alpha^m(1-\alpha)^n \qquad \textit{(Equation 3)}$$

where m and n are the concentration of the reactive groups in the reactants and products of a reaction, respectively.

Equations 1-3 form the basis of the kinetic model developed in this study; however, it is noted that the autocatalytic model is a simplification of most epoxy resins in practice. In reality, there may be a mixture of reactive species present, and some (for example latent hardeners) may not react to temperature in the manner described by the Arrhenius equation [43]. These additional secondary species' cure constants were calculated in practice using curve fitting. Parameters such as T_g and viscosity may also be modelled as a function of time, temperature, and degree of cure. The exothermic heat generated is taken to be proportional to the rate of change of degree of cure as given in (Equation 4).

$$\frac{dH}{dt} = H_r \frac{d\alpha}{dt} \qquad \textit{(Equation 4)}$$

where *dH/dt* is the rate of heat flow in W and H_r is the total heat of reaction in J/kg.

A Kissinger plot is one method that allows for the pre-exponential constant, A, and the activation energy, E, from (Equation 2) to be calculated from multiple DSC plots. This method is used to measure the heat of reaction of a thermosetting system, commonly at a constant rate of 10 °C/min [33].

The temperature at the peak of the DSC trace is related logarithmically to the rate of heating, which is summarised in (Equation 5), [33,36].

$$ln\left(\frac{\beta}{T_p^2}\right) = ln\left(\frac{AR}{E_a}\right) - \frac{E_a}{RT_p} \qquad \textit{(Equation 5)}$$

where β is the heating rate of the DSC trace and T_p is the temperature peak of the reaction at the specified heating rate. This equation is derived by the derivative of the Equations 3-4, and assuming the reaction rate is maximum at T_p which can be seen in the DSC trace to be true. Therefore, if DSC traces are taken at varying heating rates, β plotted against T_p, then the resulting cure constants can be determined, as seen in Figure 23.

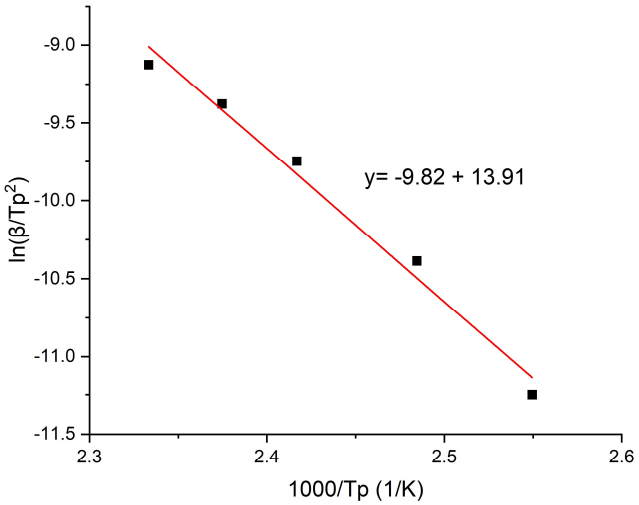

Figure 23: Kissinger plot of values from Figure 22 giving the cure constants for an example resin.

7.3.5. Experiment methodology and model development

This section covers how the cure kinetic equations described in section 7.3.4 were used to create a model written in Python. The model can predict the kinetic response of certain mass of resin when a heating profile is applied, as well properties such as DoC. This needs to be linked to a representative heating condition, therefore heat loss and heat capacity for a basic heated tooling plate was calculated. The assumptions used within these calculations are also detailed.

Curing techniques and materials

The heated tooling plate used a RS Pro 400W 240V heater mat, measuring 200mm x 300mm, bonded to a 2 mm thick aluminium plate of the same size. This was controlled using pulse width modulation with a solid-state relay in LabVIEW. It was assumed that all the power inputted was converted to heat to the composite without losses, however a proportion of this heat will be lost to the environment. A

K type thermocouple was embedded in the heater mat to monitor part temperature, and another was mounted away from the equipment to monitor the ambient temperature of the environment. This ambient temperature was used to calculate heat loss coefficients of the heater plate.

The pre-preg used was SHD LTC210, a plain weave carbon fibre used for tooling applications. It is characterised by a low activation energy and long cure cycle, so that it can be cured at low temperatures in medium to thick sections. This was chosen so that a large exothermic response could be achieved with low energy input. It has multiple cure cycle options, from 45 °C for 24 to 40 hours, to 70 °C curing in 4 hours. For this study the following cycle was used for the oven cure comparison: Initial cure of 1 °C/min up to 60 °C for 8 hours and a post-cure of 0.3 °C/min up to 200 °C for 8 hours.

Determination of thermo-kinetic parameters

Thermal analysis of the epoxy thermosetting systems was conducted using a Perkin Elmer DSC 4000 with a cryogenic chiller unit for thermal stability. The parameters required for the thermo-kinetic model are derived from fitting to a set of DSC traces conducted at various constant heating rates in a 3 dimensional space. Using a constant heating rate for each trace, the traces can then be plotted onto a 3D surface using the three dimensions of time, temperature and heat flow as per Figure 24 A. To ensure that a consistent surface could be created without gaps, a range of heating rate trials were required, so 1 °C/min to 20 °C/min at 1 °C/min intervals were used which can be seen in Figure 24 B. This range was also chosen as it was within the range of heating rates the heater mat could achieve. The materials were tested from 30 °C up to 300 °C, which is within the range of the activation energy of the resin system.

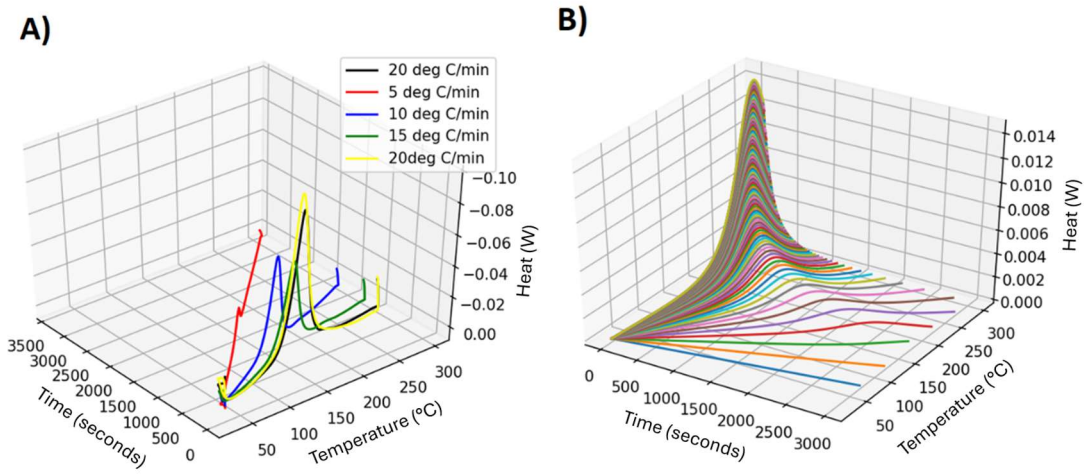

Figure 24: A) DSC traces of different heating rates plotted on a 3D graph, B) Results extrapolated for full range of heating rates using 3D curve fitting.

Determining the cure kinetic constants accurately using a Kissinger plot is not possible when there are multiple undefined components such as latent hardeners [44] within the resin. This is due to having more than one peak in the DSC trace, which are activated at different temperatures. Therefore, 3D curve fitting was used as a more accurate way to determine the multiple kinetic constants. By plotting the multiple curves at different heating generated through DSC, then applying a 3D curve fit, the parameters can be more accurately determined. Curve fitting was then used to generate a surface of which the model can refer to at any point, not being restrained to using the DSC data available. Using a 3D plot additional parameters can be programmatically derived allowing this method to be used regardless of resin type or formulation.

Determination of exothermic energy generation

The rate constant is first calculated at each discrete time interval, 1/s, using a predetermined temperature profile, of which two are used in this study. Each temperature point is first referenced on the Kissinger surface plot to determine the cure constants, which then allow for calculation of the cure constants at those conditions.

The following parameters are then calculated iteratively at each time interval. The rate of reaction is calculated (Equation 3, using estimates of m=1.06 and n=1.57), assuming at the beginning of the cure, DoC and rate of reaction are 0. The DoC can then be calculated by summing the previous iteration's DoC and rate change between intervals. The heat generated at each time interval can be estimated using the total heat of reaction of the resin, multiplied by the rate of reaction.

Determination of environmental tooling parameters

As the power input control was directly to the heater mat using a LabVIEW program, the temperature response to power input could be recorded. The heat capacity and thermal loss coefficient of the tool, including bagging and breather material was determined experimentally. By running a simple stepped power output profile to the heater mat and monitoring the temperature in relation to the environment temperature, the tool heat loss coefficient and heat capacity was determined, as lumped masses. These can then be used to predict the heat capacity and loss of the tooling and environment at discrete time intervals during a cure profile.

Model development and testing

To determine the total power output of the system, the following inputs need to be summed at each time interval: Power output of the heater mat + Exothermic power – Heat loss to the environment – Power required to heat tool at current rate.

The resulting power output is the required power input to the system via the heater mat, to reach the desired temperature profile. In the current iteration of the model's code, the temperature profile is inputted through a graphical user interface, which allows for the final power requirements and DoC to be tuned to requirements. This power output profile is then followed by the LabVIEW program to output to the heater mat in an open loop configuration.

For example, a negative total power output from the model means that the desired temperature cannot be achieved without forced cooling, therefore an uncontrolled temperature rise will occur. The cure cycle can be designed to be near this limit, to minimise energy input from the heater mat, reducing cure energy. This can also be used to heat a thin component at a high heating rate or find the heating rate limits for a thick component without experiencing an uncontrolled exothermic reaction.

In the example given in the right of Figure 25 it can be seen the rapid heating rate results the exothermic power peaking at around 200 W, indicated as a negative required input by the model. The required total power output to the heated tool (blue line) drops significantly in order to maintain the temperature profile. If the power to raise the temperature wasn't adjusted for the energy generated in the composite, the temperature would deviate significantly, and a runaway exotherm could occur. It is also not possible to cool the part to room temperature as rapidly as demanded, seen as a large negative energy requirement at the end of the cure.

7.3.6. Results

Two custom cure cycles were modelled, tested, and analysed using the heater mat and the LTC210 pre-preg system. The first cure cycle invoked a conservative exothermic reaction, to evaluate if the model could predict the timing and amplitude of the reaction. The second cure cycle was to optimise the cure time, DoC and energy usage, by using high heating rates to reach 100 % DoC whilst running close to the exothermic runaway conditions. The two cure cycles can be seen in Figure 25, showing the temperature cycle, power generated by the component and total power output to the heater mat.

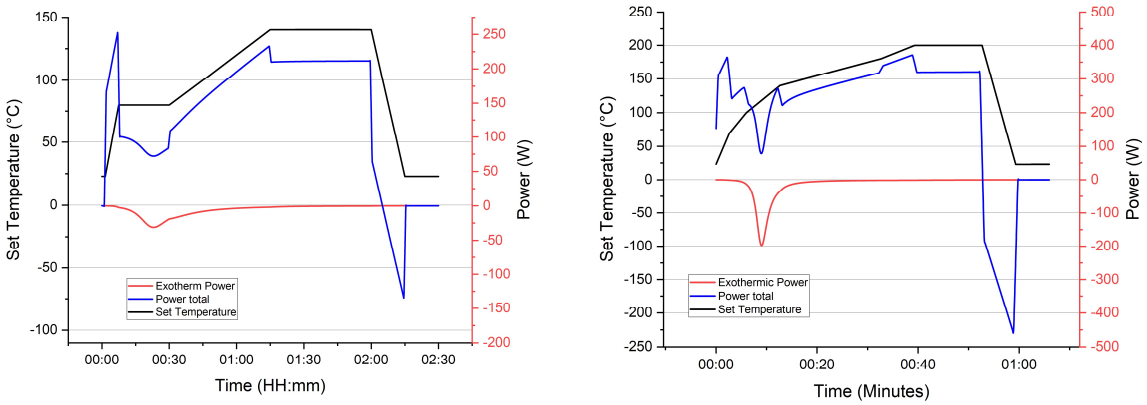

Figure 25: Left: Low ramp rate cure cycle, generating an exotherm around 20 minutes after the start. Right: The higher rate custom cure cycle, designed to have a large exothermic reaction at around 10 minutes.

The time-power outputs from these two cure cycles were then used to power the heater mat, in open loop power control. The resulting temperature profile of the first cure can be seen in Figure 26.

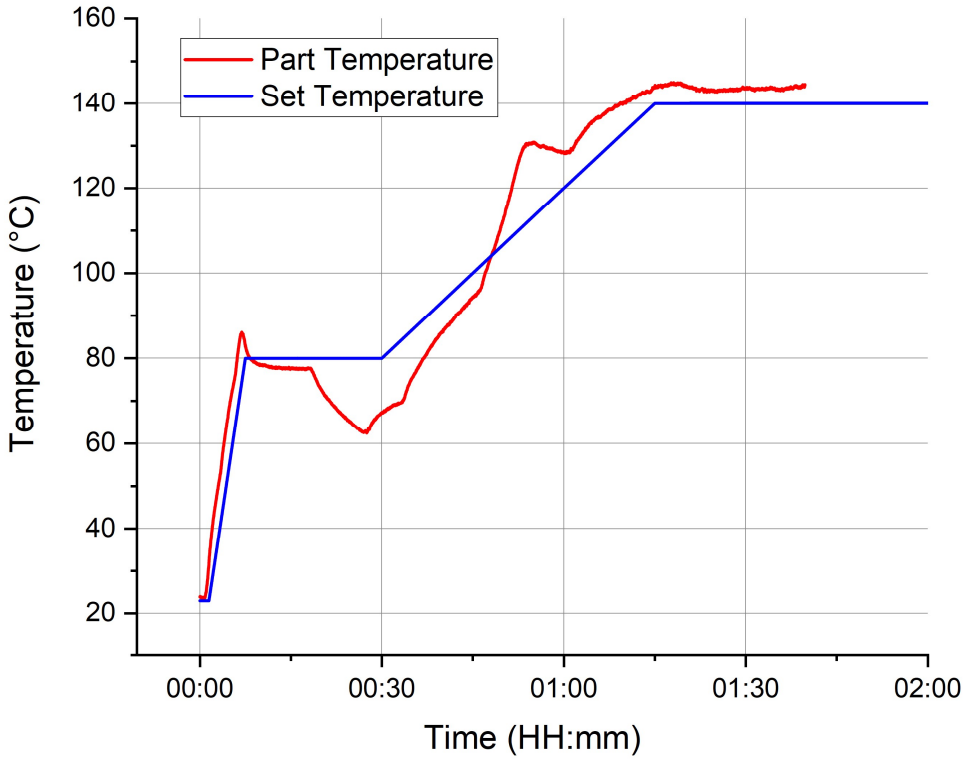

Figure 26: Part temperature against predicted part temperature during the first heater mat cure.

The cure was unintentionally reduced in duration due to technical difficulties with the LabVIEW code. However, the key part of the cure in the first hour of the cure, showing the exothermic reaction was recorded. The temperature profile of the second cure can be seen in Figure 27.

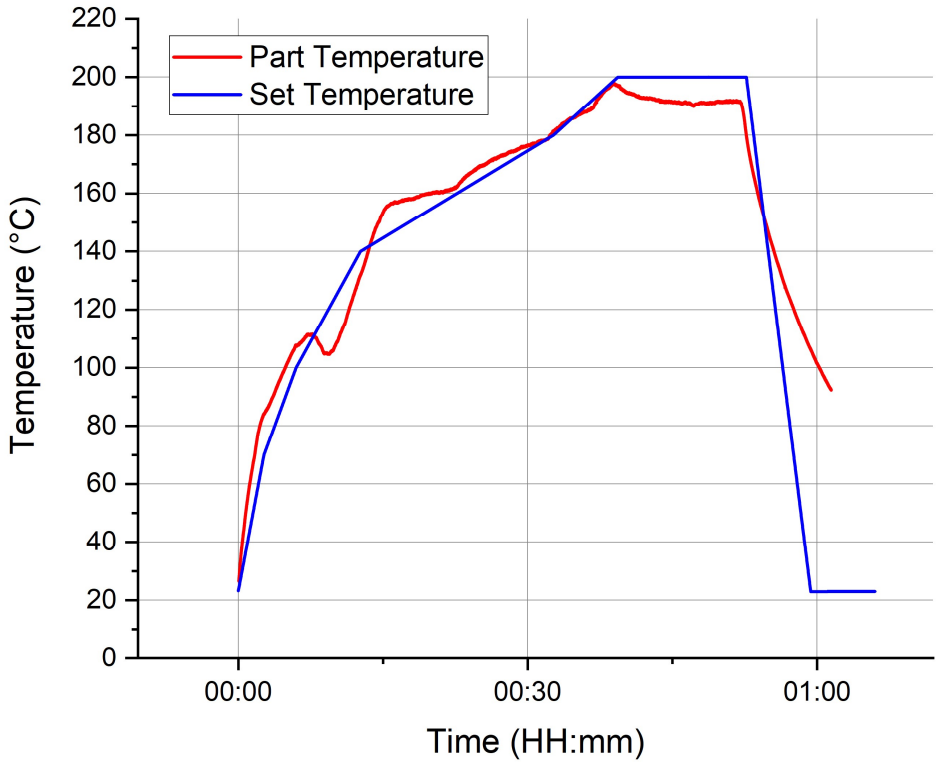

Figure 27: Part temperature against predicted part temperature during the second heater mat cure.

7.3.7. Discussion

The model that has been developed was run as an open loop system, which predicts the temperature of the composite from the amount of energy that is being placed in from the heater mat. This means there was no temperature feedback loop to correct for any temperature deviation. It does this whilst also endeavouring to predict the heat loss to the surroundings and the heat generated in the composite from the exothermic reaction as the composite cures. To identify how effectively the model can predict sample temperature, a direct comparison of the expected set temperature to the part temperature during the cure can be made. These comparisons can be seen in Figure 26 and Figure 27. The differences between these temperatures were calculated, seen in Figure 28 for both optimised cures.

For most of the time of both cures, the difference was less than 10°C, with a peak of 20°C during the ramp where the main exothermic reaction occurred. These figures suggest that the assumptions in the model are broadly correct, as it follows the cure cycle closely, and accounts for significant exothermic reactions at the correct time.

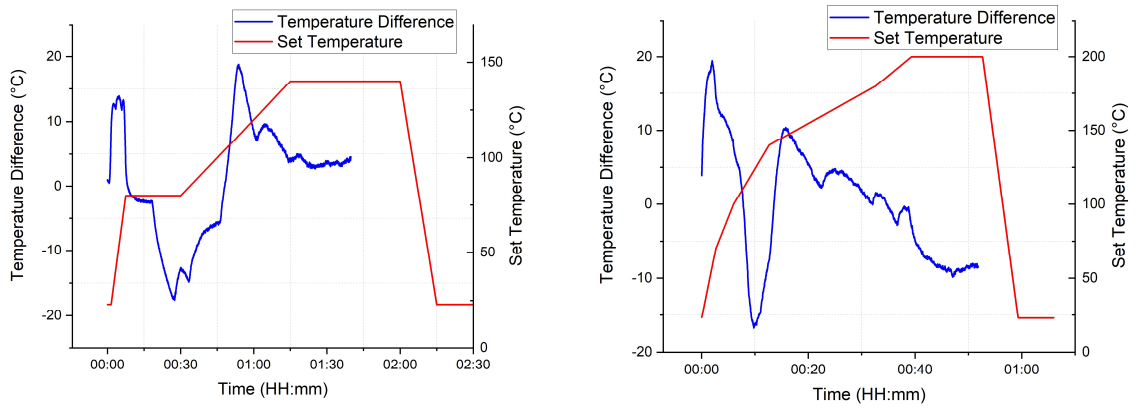

Figure 28: Graphs showing the temperature difference between the set temperature and part temperature for cure 1 (left) and cure 2 (right).

For the first cure, a large temperature difference is seen before and after the exothermic reaction, which peaks at about 30 minutes and 60 minutes into the cure. This large swing from under temperature to over temperature suggests the exotherm happens later than the kinetic model predicts. This could be due to the ramp rates used here being much quicker than the model was characterised with, and not reaching the expected temperature. After these fluctuations, it settles to a 5 °C overshoot during the second dwell.

The second cure cycle with higher ramp rates also has a large temperature differential at the beginning of the cure, as well as during the expected peak of the exothermic reaction. In both cases, the model has overestimated the initial heat up phase, which is significant as at this stage there are no external factors to influence this. The ramp rates during the initial phases are both high, at 7.5 °C/min and 17.3 °C/min, which starts instantly as the cure starts. This gives little time for the model to account for the heating lag of the curing system. During these phases, the power into the system from the model is at its highest and in the case of the second cure cycle, is near the 400 W maximum output of the heater mat. Future cures could provide a short room temperature dwell so that the control system can account for this better.

Aerospace standards for composite curing ovens [45] require commonly ± 6 °C temperature tolerance, however in some cases can be as tight as ± 3 °C. During the temperature ramps and peak points during the exothermic reaction, both were outside the ± 6 °C specification.

DSC tests were conducted on the heater mat cured panels and two oven cured baseline samples to allow for comparison of different cure stages. The first oven cured sample was cured at 70 °C for 4 hours with no post cure, then the second was cured at 60 °C for 8 hours, then post cured at 200 °C which can be seen in Table 4. T_g is taken from the exothermic peak of the DSC traces for oven cured and heater mat samples.

Table 4: Summary of DSC results and cure times of oven cure, post cure and heater mat cure.

Sample Name	DSC Glass transition temperature, T_g °C	Predicted DoC	DoC %	Cure length, minutes	kW.hr
Oven with no post cure average	125.13		61.32	300	0.582
Oven with post cure average	212.02		97.80	1180	24.278
Heater mat cure 1	164.63	95.12%	91.28	135	0.345
Heater mat cure 2	209.52	97.27%	97.66	52	0.252
Datasheet values	210		N/A	1180	N/A

The second heater mat cure closely matches the DoC of the post cured sample, being only 0.14 % lower. It achieves this whilst reducing the time to cure to 5 % of time for the oven cured sample. It also reduces the energy consumption to 1 % of the oven cured sample. It is noted that a lot of the efficiency gains will be due to the change from oven cure to heater mat cure. As a full cure cycle wasn't completed on the heater mat, an estimation was made with existing data, which would be ~ 5 kW.hr, therefore using this model results in a 95% reduction in energy usage. Future implementations of the code will look at directly controlling the power output of an oven, so a direct power consumption comparison can be made of an established cure process. A reduction in cure time of 87 % compared to the recommended cure cycle is significant for production where takt time is a key factor.

7.3.8. Conclusion

The objective of this study was to develop and implement a kinetic model that could be used to predict the kinetic response of a composite cure system. Data input to the model was collected using DSC testing of composite materials and monitoring the heating response of the curing system. Using a heater mat setup, the concept was proven successful, with the kinetic variations such as exothermic energy and convective cooling being predicted accurately, through low temperature differences seen during short cure cycles. In the shortest cure tested, over 200 W of excess exothermic energy was accounted for, whilst maintaining the temperature to within 15 °C of the predicated set point in an open loop setup. The model predicts the cure kinetics well, and external disturbances could be accounted for with temperature feedback in future work. It may not be necessary to remove these however, as they may further modify the calculated DoC. Future models could consider these transient heat transfer coefficients to ensure the correct amount of kinetic energy is going into the composite.

The work described here is the foundation for allowing custom cure cycles on a variety of heating methods, to the maximum of their capability. With simple characterisation of the heating method and the material, cure cycles can be shortened without compromising DoC or T_g. This will allow for improvements with existing convective cure methods and improving adoption of newer methods such as microwave or direct electric cure.

The existing model does provide useful use cases, for example safely reducing the length cure cycle of a reactive pre-preg resin system as seen in this study. Other uses for the existing model could be to predict the maximum safe cure cycle for thick laminates.

A limitation of this model currently is the ability to predict other important parameters such as

viscosity and Tg, as well as the accuracy of more complex resin formulations and heating methods. Adding these features to this model to account for more factors would allow it to be more accurate in some situations. However, this increases complexity of the setup and would have an increase in unknown factors to ensure the model produces accurate results. These types of blind adjustments are common in a manufacturing environment, where this is likely to be deployed. To develop this concept, further process data could be processed by a machine learning algorithm that can account for all these unknown factors, without having to fully understand the physical properties of the process itself.

7.4. References

[1] Zhang J, Lin G, Vaidya U, Wang H. Past, present and future prospective of global carbon fibre composite developments and applications. Compos B Eng 2023;250. https://doi.org/10.1016/j.compositesb.2022.110463.

[2] Adu-Gyamfi BA, Good C. Electric aviation: A review of concepts and enabling technologies. Transportation Engineering 2022;9. https://doi.org/10.1016/j.treng.2022.100134.

[3] Collinson MG, Swait TJ, Bower MP, Nuhiji B, Hayes SA. Development and implementation of direct electric cure of plain weave CFRP composites for aerospace. Compos Part A Appl Sci Manuf 2023;172:107615. https://doi.org/10.1016/j.compositesa.2023.107615.

[4] Oleskiw MM. A Review of 65 Years of Aircraft In-Flight Icing Research at NRC. Canadian Aeronautics and Space Journal 2001;47.

[5] Yang L, Li Y, Huan D, Yang Y, Wang J, Zhu C. An icephobic coating for aircraft anti-icing system. J Mater Sci 2023. https://doi.org/10.1007/s10853-023-09055-5.

[6] Riley JT. Investigations of Performance of Pneumatic Deicing Boots, Surface Ice Detectors, and Scaling of Intercycle Ice. 2006.

[7] Newton Dennis. Severe Weather Flying : Increase your knowledge and skill to avoid thunderstorms, icing and severe weather. Aviation Supplies & Academics, Inc; 2018.

[8] Ostermann M, Schodl J, Lieberzeit PA, Bilotto P, Valtiner M. Lightning Strike Protection: Current Challenges and Future Possibilities. Materials 2023;16. https://doi.org/10.3390/ma16041743.

[9] Xia Q, Zhang Z, Liu Y, Leng J. Buckypaper and its composites for aeronautic applications. Compos B Eng 2020;199. https://doi.org/10.1016/j.compositesb.2020.108231.

[10] Jała J, Nowacki B, Mistewicz K, Gradoń P. Graphite-epoxy composite systems for Joule heating based de-icing. Cold Reg Sci Technol 2023;216:104024. https://doi.org/10.1016/J.COLDREGIONS.2023.104024.

[11] Vertuccio L, Foglia F, Pantani R, Romero-Sánchez MD, Calderón B, Guadagno L. Carbon nanotubes and expanded graphite based bulk nanocomposites for de-icing applications. Compos B Eng 2021;207. https://doi.org/10.1016/j.compositesb.2020.108583.

[12] Prolongo SG, Moriche R, Del Rosario G, Jiménez-Suárez A, Prolongo MG, Ureña A. Joule effect self-heating of epoxy composites reinforced with graphitic nanofillers. Journal of Polymer Research 2016;23:189. https://doi.org/10.1007/s10965-016-1092-4.

[13] Redondo O, Prolongo SG, Campo M, Sbarufatti C, Giglio M. Anti-icing and de-icing coatings based Joule's heating of graphene nanoplatelets. Compos Sci Technol 2018;164:65–73. https://doi.org/10.1016/j.compscitech.2018.05.031.

[14] Martinez-Diaz D, Espeute E, Jiménez-Suárez A, Prolongo SG. Electrical and Joule Heating Capabilities of Multifunctional Coatings based on Recycled Carbon Fiber from Prepreg Scrap. ACS Omega 2023. https://doi.org/10.1021/acsomega.3c05413.

[15] Idris MK, Qiu J, Melenka GW, Grau G. Printing electronics directly onto carbon fiber composites: unmanned aerial vehicle (UAV) wings with integrated heater for de-icing. Engineering Research Express 2020;2:025022. https://doi.org/10.1088/2631-8695/AB8E24.

[16] Grove SM, Progoulakis I, Searle T, Summerscales J, Healey P. Heated tooling for aerospace composites manufacture. SAMPE Journal 2005;41:36–45.

[17] Athanasopoulos N, Koutsoukis G, Vlachos D, Kostopoulos V. Temperature uniformity analysis and development of open lightweight composite molds using carbon fibers as heating elements. Compos B Eng 2013;50:279–89. https://doi.org/10.1016/j.compositesb.2013.02.038.

[18] Weiland JS, Hartmann MP, Hinterhölzl RM. Cure simulation with resistively in situ heated CFRP molds: Implementation and validation. Compos Part A Appl Sci Manuf 2016;80:171–81. https://doi.org/10.1016/j.compositesa.2015.10.020.

[19] Industrialisation of self heated composite tooling based on Tailored Fibre Placement Technology | GREEN-TOOLING | Project | Fact sheet | FP7 | CORDIS | European Commission n.d. https://cordis.europa.eu/project/id/605853 (accessed September 28, 2023).

[20] Athanasopoulos N, Koutsoukis G, Vlachos D, Kostopoulos V. Temperature uniformity analysis and development of open lightweight composite molds using carbon fibers as heating elements. Compos B Eng 2013;50:279–89. https://doi.org/10.1016/j.compositesb.2013.02.038.

[21] Liu S, Li Y, Shen Y, Goh YM. A Multi-Zoned Self-Resistance Electric Heating Method for Curing Irregular Fiber Reinforced Composite Parts. vol. 0, 2021, p. 1–6. https://doi.org/10.3233/ATDE210028.

[22] Hull D, Clyne TW. Thermal behaviour of composites. An Introduction to Composite Materials, Cambridge University Press; 1996, p. 237–70. https://doi.org/10.1017/CBO9781139170130.012.

[23] Green JE, Nuhiji B, Zivtins K, Bower MP, Grainger R V., Day RJ, et al. Internal Model Control of a Domestic Microwave for Carbon Composite Curing. IEEE Trans Microw Theory Tech 2017;65:4335–46. https://doi.org/10.1109/TMTT.2017.2693145.

[24] Nuhiji B, Bower MP, Swait T, Phadnis V, Day RJ, Scaife RJ. Simulation of carbon fibre composites in an industrial microwave. Mater Today Proc 2021;34:82–92. https://doi.org/10.1016/j.matpr.2020.01.284.

[25] Kim M, Kim H, Lee W. Repair of aircraft structures using composite patches bonded through induction heating. Advanced Composite Materials 2015;24:307–23. https://doi.org/10.1080/09243046.2014.899553.

[26] Hayes SA, Lafferty AD, Altinkurt G, Wilson PR, Collinson M, Duchene P. Direct electrical cure of carbon fiber composites. Advanced Manufacturing: Polymer & Composites Science 2015;1:112–9. https://doi.org/10.1179/2055035915Y.0000000001.

[27] Li Y, Xiao Y, Yu L, Ji K, Li D. A review on the tooling technologies for composites manufacturing of aerospace structures: materials, structures and processes. Compos Part A Appl Sci Manuf 2022;154. https://doi.org/10.1016/J.COMPOSITESA.2021.106762.

[28] Collinson M, Bower M, Swait TJ, Atkins C, Hayes S, Nuhiji B. Novel composite curing methods for sustainable manufacture: A review. Composites Part C: Open Access 2022;9:100293. https://doi.org/10.1016/j.jcomc.2022.100293.

[29] Bennett S. The Past of PID Controllers. IFAC Proceedings Volumes 2000;33:1–11. https://doi.org/10.1016/s1474-6670(17)38214-9.

[30] Andersson C, Lindberg M. Autotuning of a PID-controller 2004.

[31] Veselý V, Ilka A. Gain-scheduled PID controller design. J Process Control 2013;23:1141–8. https://doi.org/10.1016/j.jprocont.2013.07.002.

[32] Karkanas P, Partridge K, Attwood D. Modelling the Cure of a Commercial Epoxy Resin for Applications in Resin Transfer Moulding. Polym Int 1996;41:183–91. https://doi.org/https://doi.org/10.1002/(SICI)1097-0126(199610)41:2%3C183::AID-PI621%3E3.0.CO;2-F.

[33] Hubert P, Johnston A, Poursartip A, Nelson K. Cure kinetics and viscosity models for Hexcel 8552 epoxy resin. International SAMPE Symposium and Exhibition 2001:2341–54.

[34] Kratz J, Hsiao K, Fernlund G, Hubert P. Thermal models for MTM45-1 and Cycom 5320 out-of-autoclave prepreg resins. J Compos Mater 2013;47:341–52. https://doi.org/10.1177/0021998312440131.

[35] López-Beceiro J, Fontenot SA, Gracia-Fernández C, Artiaga R, Chartoff R. A logistic kinetic model for isothermal and nonisothermal cure reactions of thermosetting polymers. J Appl Polym Sci 2014;131:n/a-n/a. https://doi.org/10.1002/app.40670.

[36] Ellis B, Ashcroft WR, Shaw SJ, Cantwell WJ, Kausch HH, Johari GP, et al. Chemistry and Technology of Epoxy Resins. Dordrecht: Springer Netherlands; 1993. https://doi.org/10.1007/978-94-011-2932-9.

[37] Chairat A, Joulia X, Floquet P, Vergnes H, Ablitzer C, Fiquet O, et al. Thermal degradation kinetics of a commercial epoxy resin - Comparative analysis of parameter estimation methods. J Appl Polym Sci 2015;132:6–9. https://doi.org/10.1002/app.42201.

[38] Antonucci V, Giordano M, Hsiao K-T, Advani SG. A methodology to reduce thermal gradients due to the exothermic reactions in composites processing. Int J Heat Mass Transf 2002;45:1675–84. https://doi.org/10.1016/S0017-9310(01)00266-6.

[39] Esposito L, Sorrentino L, Penta F, Bellini C. Effect of curing overheating on interlaminar shear strength and its modelling in thick FRP laminates. International Journal of Advanced Manufacturing Technology 2016;87:2213–20. https://doi.org/10.1007/s00170-016-8613-5.

[40] W.J. Sichina. Characterization of Epoxy Resins Using DSC. 2022.

[41] Dr. R. Bruce Prime. Thermoset Cure Kinetics Part 1: Introduction to Kinetics - Polymer Innovation Blog. Polymer Innovation Blog 2014. https://polymerinnovationblog.com/thermoset-cure-kinetics-part-1-introduction-kinetics/ (accessed July 23, 2018).

[42] Lakho DA, Yao D, Cho K, Ishaq M, Wang Y. Study of the Curing Kinetics toward Development of Fast-Curing Epoxy Resins. Polymer - Plastics Technology and Engineering 2017;56:161–70. https://doi.org/10.1080/03602559.2016.1185623.

[43] Zhang P, Ali Shah SA, Gao F, Sun H, Cui Z, Cheng J, et al. Latent curing epoxy systems with reduced curing temperature and improved stability. Thermochim Acta 2019;676:130–8. https://doi.org/10.1016/j.tca.2019.03.022.

[44] Wu F, Zhou X, Yu X. Reaction mechanism, cure behavior and properties of a multifunctional epoxy resin, TGDDM, with latent curing agent dicyandiamide. RSC Adv 2018;8:8248–58. https://doi.org/10.1039/C7RA13233F.

[45] SAE International. AMS2750F - Aerospace Material Specification - Pyrometry. 2020. https://doi.org/https://doi.org/10.4271/AMS2750F.

8. Development of large scale electrical self-sensing of CFRP composites

This chapter is a paper in preparation on the development of electrical response-based impact detection methods within CFRP composites, also known as self-sensing. This was developed over a 3-year period alongside the DEC work.

It is an experimental paper on scaling up existing and newly developed self-sensing methodologies to detect barely visible impact damage on larger components. It covers review and experimental work on a variety of previously published techniques, and establishes new and complementary methods, so that method can be scaled up for practical implementation in representative manufacturing environments.

Experimental work, authorship and editing by Matthew Collinson, with sample manufacturing assisted by Matthew Bower. Reviewing and supervision was completed by Simon Hayes, Tim Swait and Betime Nuhiji.

8.1. Abstract

This study investigates the scale-up of the electrical self-sensing method, for damage detection through electrical resistance monitoring of carbon fibre-reinforced plastic (CFRP) samples. The resistance increases locally to the impact location due to both fibre breakage and the piezoresistive effect. Electrodes were embedded during the manufacturing of CFRP to enable a scalable resistance monitoring method, whilst adding minimal weight and complexity to the component. Damage detection was possible for some configurations, however, it was inconsistent in its detection of impact position and intensity. It was possible to locate barely visible impact damage (BVID) in some samples, whilst in others, there was no response or false positives were encountered. The scale was increased to a detection area of 560 x 400 mm, with no significant reductions in sensing sensitivity. Whilst it wasn't always possible to identify the impact location, in the majority of samples it was possible to detect that a change had occurred because of an impact. Recommendations have been given on potential fundamental improvements to this process to enhance detection capability and repeatability.

8.2. Introduction

Use of composite materials in the aerospace sector is increasing as the requirement for lower emissions and electrification drives light weighting [1]. However, there remains an absence of reliable and accurate methods for structural health monitoring and damage detection for these composites [2]. The brittle nature of the epoxy results in barely visible impact damage (BVID) [3], which can lead to catastrophic failure of the structure [4].

When an impact occurs on a composite, the surface impacted undergoes compression, commonly with little surface damage, whereas the opposite surface undergoes significant strain. This can cause, in order of increasing severity of resulting damage; matrix cracking, fibre pull out, fibre breakage and delamination between plies [5,6]. It can be difficult to visually inspect for BVID in aerospace structures without disassembly, for example a wing skin. Methods available for detection of these impacts are

C-Scan or acoustic emission (AE). However, respectively, these require highly skilled operators or complex solving algorithms for effective detection [7,8].

This study investigates self-sensing, a method that monitors the electrical resistivity of plain weave (PW) composites to detect changes resulting from impact damage. It builds on previously established methods as described in the following section, however in this study it is developed to be more manufacturable and establishes newly developed detection strategies. Previous studies have developed different techniques used to detect damage, all requiring different electrode positioning or current injection patterns on the surface or within a laminate. These previous attempts have been successful at detecting impact damage, but have been on a small scale, so are not suitable for aerospace structures.

To increase the scale, a multiple-mode flexible printed circuit board (PCB) was designed to integrate into the composite easily during the manufacture, allowing the damage area to be increased significantly from previous attempts. It also allowed for different layouts of electrodes and current injection patterns, to determine the most effective method for electrical self-sensing. The knowledge gained was used to develop a modular flexible PCB, which was integrated into larger components, to enable a detection area of 560 x 400 mm. Investigations were on aerospace pre-preg components and composites manufactured with vacuum-assisted resin transfer moulding (VARTM).

8.3. Electrical self-sensing concepts

Carbon fibres are highly conductive, and therefore a CFRP composite can be considered as a network of conductive paths. If conductivity is monitored along the fibre direction, when an impact occurs resulting in fibre breakage, a change in resistance will occur. If the conductivity is measured in different segments or different axis of a woven or Quasi-Isotropic (QI) composite surface, then the damage can be located on a surface.

There are two methodologies for measuring electrical resistance of materials, 2-point and 4-point. The 2-point method applies current between two electrodes and monitors voltage from the same electrodes, which is then used to calculate resistance. As it uses two electrodes, it is easy to implement, however it includes the contact resistance of the electrodes and wires of the whole monitoring system. For composites, this can lead to reliability issues due to the insulating matrix [9–11]. 4-point resistance testing is a more reliable, repeatable testing method. It applies current at separate locations outside to the electrodes where voltage is measured (or voltage can be applied and voltage measured). This method has been used successfully in measuring composite resistance [12,13], as well as measuring resistance change when damage has occurred [14]. It has been found that the inconsistencies with the 2-point method is primarily due to the contact resistance between the composite [15]. Wang et al [12] investigated the setup requirements for the 4-point resistance technique, finding that the 4-point technique was much more sensitive to damage, giving a larger proportional change to resistance than the 2-point method.

Research has covered the piezoresistive and damage detection properties of carbon fibres [16], carbon fibre composites [17] and nanocomposites [18]. However, there is limited research at the component scale, which is needed to make the technique usable for in-service or industrial applications [19]. Swait et al [20] manufactured flexible PCBs with paired electrodes and embedded them into unidirectional (UD) composites. Resistance was monitored using the 2-point technique [21],

which was accurate enough to provide data on an impact's position within the laminate surface, however limited the sensitivity of the system. This study was limited by size (110 mm x 110 mm) and damage detection was only demonstrated with UD composites.

A. Alsaadi et al [22,23] used the 4-point resistivity method with a flexible PCB bonded to woven CFRP with high-conductivity silver adhesive. The 4-point method approach enabled truer conductivity values of the composite to be recorded, providing damage detection with an repeatability of 85%.

Electrical impedance tomography (EIT) has been used by S.Nonn et al [24], R. Schueler et al [25], A. and Baltopoulos et al [26,27]; taking electrical conductivity measurements across a panel at the panel edges and using electrical tomography to post-process the data. It was found possible to locate the damage on panels up to 250 x 250 mm, locating the damage more accurately due to the larger range of measurements taken from the panel. EIT has higher demands in computational and hardware requirements, but it has the potential to be highly accurate in damage detection.

This study develops the methods from these previous studies for self-sensing damage detection on a larger scale, so that they can be used more readily in composite components. Methods were tested on a development panel setup with an interleave flexible PCB, which provided considerable setup flexibility. The results then informed the design and methods adopted for a modular PCB system, to seek to increase scale whilst maintaining detection accuracy. This study concentrated on PW composites, to represent an industry standard layup and to have controllable and repeatable results. It is more challenging to monitor the electrical resistivity of a PW than the UD composites that previous studies have concentrated on. It is expected that if the sensing system is shown to be effective for PW, the concepts are to be likely also applicable to UD composites. The authors didn't want to limit the sensing system based on the layup or the material types used.

8.4. Experimental setup

Materials

Two types of CFRP laminates were manufactured. For pre-preg experiments, PW Cycom 5320-1 was used, and for VARTM, Huntsman Araldite CY 179/ Aradur 917 resin system with Chomarat C-Weave 3K PW carbon fibre was used. The manufacturers recommended cure cycle was used for both. For all initial experiments, 4 plies were used. The difference in the two laminate types were expected to influence the results of the sensitivity of the method. VARTM samples are expected to have closer contact with the fibres, whereas pre-preg will have an insulating epoxy barrier during their layup. This may result in lower contact resistance values for VARTM samples, and therefore improved sensitivity.

A flexible Kapton-Copper PCB (DuPont) was designed and manufactured so that it could be integrated into the composite during the manufacture, see Figure 1. It had a copper thickness of 35 μm and a Kapton thickness of 25μm. Using a PCB ensured that the electrode material and positioning were consistent between samples. The PCBs were cleaned with an isopropyl alcohol wipe before being laminated into the composite.

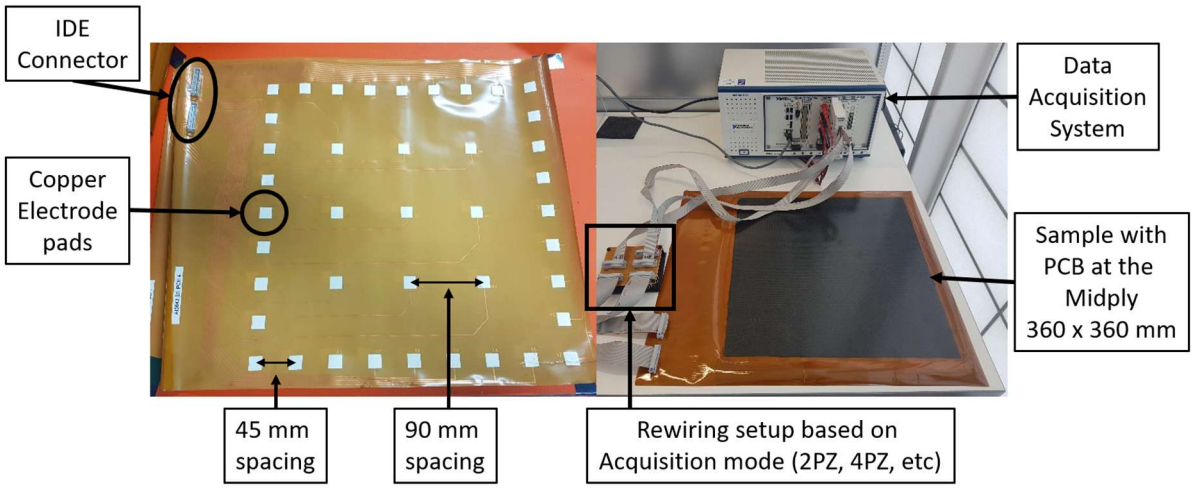

Figure 1: Left, Flexible PCB design, showing electrode positions, right, Test setup, showing PCB integrated into a CFRP panel, connected to the data acquisition system.

The electrode pads were 15 by 15 mm and were spaced 45 mm apart centre to centre around the edge, with 9 centre electrodes spaced 90 mm apart centre to centre, in the PCB's central area. The results from this PCB layout are detailed in their own section, referred to as panel PCB samples in the remainder of this study. Based upon the results from the panel PCB samples, for the scale up of the method, a modular PCB was designed and used, as seen in Figure 2.

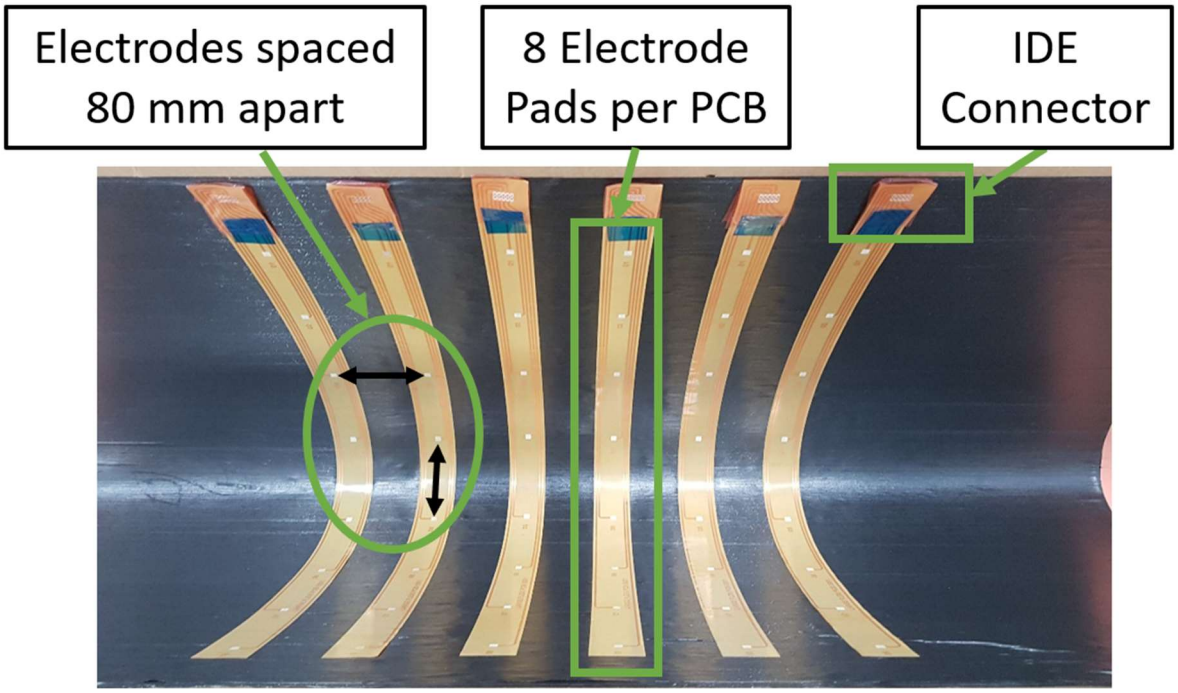

Figure 2: Example of the modular PCB's laid up in a leading-edge component.

The modular arrangement allows many PCB's to be placed side by side, meaning the sensing zone can be increased in increments by adding PCBs, as well as enabling monitoring of more complex geometries such as a wing leading edge. The electrodes on these were smaller, 5 mm by 5 mm, and were 80 mm apart, centre to centre, however the distance between electrodes was the same as the panel PCB, due to the reduction in electrode area. The PCBs were laid up to ensure that the electrodes between separate PCBs were 80 mm apart. Where the PCBs were bonded to the surface, they were

bonded with a high conductivity silver loaded epoxy resin. 6 modular PCBs were integrated into larger components, resulting in a detection area of 560 x 400 mm.

Data acquisition

A National Instruments (NI) PXIe data acquisition (DAQ) chassis (NI PXIe 1078) was equipped with a high accuracy digital multimeter (DMM, NI PXI 4080) and a matrix module (NI PXI 2530B). For resistance monitoring of loads lower than 100 Ω, a test current of 1 mA is used, resulting in µV responses from the lowest resistance composite samples. This may result in the introduction of noise from the environment due to the low voltages involved. However, it isn't practical to change this without the development of custom equipment. This has been detailed further in the future research section.

This data acquisition arrangement enabled resistance monitoring of the composite between 32 electrodes, in both 2-point and 4-point modes. For the "panel" PCB, this allowed full scanning of the component with dual 20-pin IDE connectors. For the modular PCBs data had to be collected progressively by moving 1 of 4 connectors over the length of the component at a time and scanning at each section. After this, the data was compiled to appear as one set of data.

Damage induction

BVID and high energy impacts to puncture holes in the panel were induced by Imatek IM1C impact tower machine, with a 16mm hemispherical impactor head. An example of the impactor inducing BVID can be seen in images in Figure 3, taken from slow motion footage of an impact.

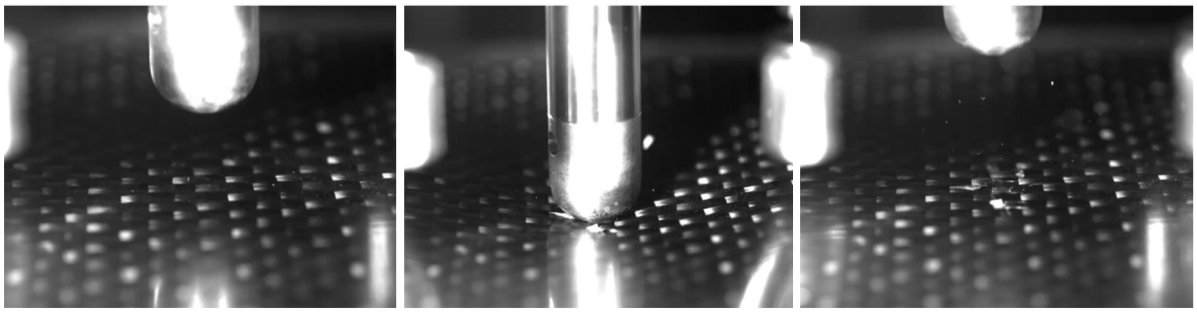

Figure 3: Impact testing showing the induction of BVID, from left to right: Undamaged panel before impact, panel at the peak of deflection, panel after the impact showing the surface damage of the BVID.

It is noted that the integration of a thermoplastic interleave ply (such as Kapton flexible PCB) in a composite can affect its impact resistance [28], however as the PCB interleave is in all samples, its effect can be considered negated. Thermoplastics are commonly used as toughening agents within epoxies and laminates, therefore flexible PCBs could be engineered to achieve this effect.

The energy of impact to cause BVID was determined on a separate set of baseline panels of the same layup, by increasing the energy of the impact until impact damage was visible on the impacted surface, after close inspection. This was verified using an Olympus Omniscan MX with a phased array C-Scan module, generating the output seen in Figure 4.

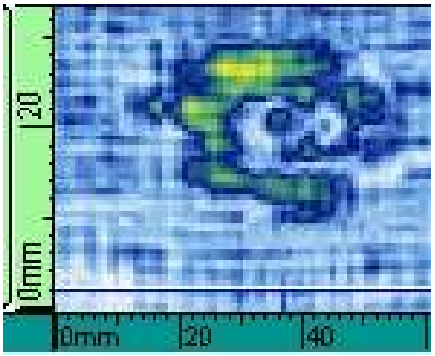

Figure 4: C-Scan image of example BVID induced in samples. The impactor position induces small matrix damage on the surface, however the reverse side to the impact induces delamination, seen in green and yellow on the C-Scan image.

After BVID was induced and analysed on the baseline panels, an impact energy of 5 Joules was selected for use on the panels with integrated PCBs. To induce puncture damage, 15 Joules was used to ensure significant damage so the system was most likely to detect the damage.

8.5. Experimental methodology

In the first set of experiments, the PCBs were integrated into the layup with no conductive adhesive, to minimise the impact on manufacturing. In later experiments with the modular PCBs, conductive adhesive was used to seek improvements in contact resistance. In all cases, the electrodes were applied towards the face where the impact occurred.

The panel PCBs were designed to investigate different types of scan patterns, with a repeatable electrode material and environment. This method ensured that multiple scan types could be examined from the same impact on the same panel, reducing experimental variables. This provided an understanding of what variables were important for damage detection such as electrode spacing and scan pattern types, which were then integrated into the modular PCB design.

A summary of the samples tested in this study, including material, plies, PCB type and position are listed in Table 1.

Table 1: A summary of the samples manufactured with panel PCB's and the modular PCB's and their properties.

Panel PCB Samples				Sample reference
Material	Plies	Electrode interface	PCB Position	
Cycom 5320-1	8	None	Mid ply	Panel-Prepreg-Midply
			Bottom ply	Panel-Prepreg-Botply
Araldite CY 179/ Aradur 917 VARTM	8	None	Bottom ply	Panel-VARTM-Botply
Modular PCB Samples				
Cycom 5320-1	8	None	Mid ply	Modular-Prepreg-Midply
		Silver loaded epoxy	Bottom ply	Modular-Prepreg-Silver
Araldite CY 179/ Aradur 917 VARTM	16	None	Mid ply	Modular-VARTM-Midply
		Silver loaded epoxy	Bottom ply	Modular-VARTM-Silver

With these PCBs, and the grid of electrodes they provide, it is possible to test a range of resistance testing patterns, or "scan" types over the composite components. These scans were completed after manufacturing of the panel to get baseline readings and then after impact damage, to get the damaged resistance readings.

X-Y Scan

This method monitors resistance across the whole width of the panel at set intervals, along the 0° orientation of the fibres, and then repeating in the 90° direction. When damage is induced, the electrodes will monitor for an increase in resistance in 0° & 90° directions, providing X & Y coordinates (hence the X-Y scan name), seen in Figure 5. It uses the 2-point resistance monitoring method, which minimizes the number of electrodes required. This method is similar to that used by Swait et al [20], however the scale is increased, and PW fabric is used.

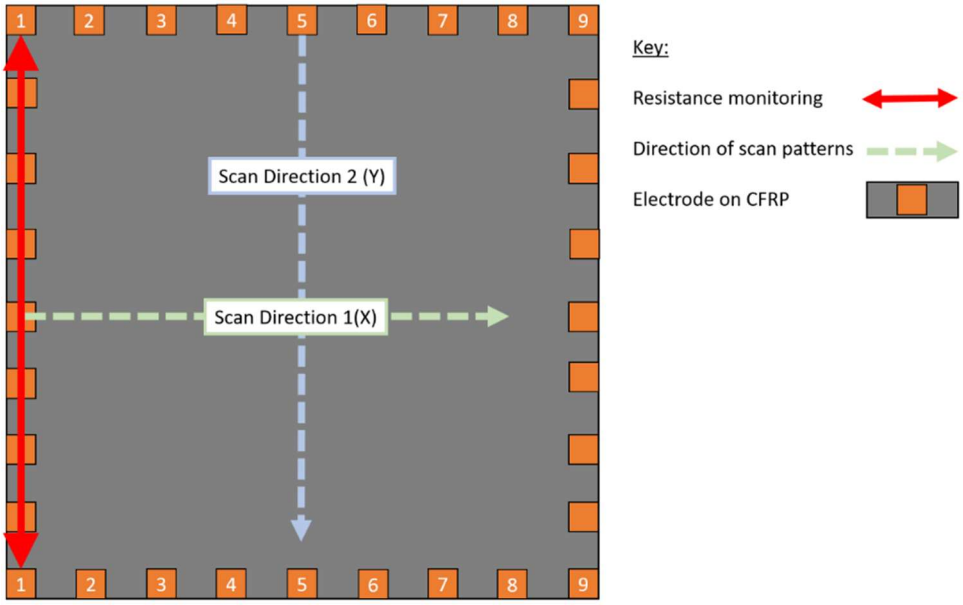

Figure 5: Diagrams showing the "XY" resistance monitoring scan pattern. Resistance is monitored between the electrodes indicated by the red arrows, then is tested on the next set of electrodes in scan direction 1. This is then repeated in the other direction, indicated by scan direction 2.

4-Point zone scan

This method monitors resistance between electrodes in the centre of a panel using the 4-point method. This was completed in X & Y directions over the panel, where a resistance map was built up to locate the damage. As can be seen in Figure 6, 4-point resistance monitoring requires fewer electrodes to monitor from, whilst monitoring the same area. Despite this, the scanning pattern is more complex and leaves areas at the corners and of the panel that cannot be monitored. This is similar to the methods used Alsaadi et al [22,23], though the size of panel and number of electrodes used has been increased.

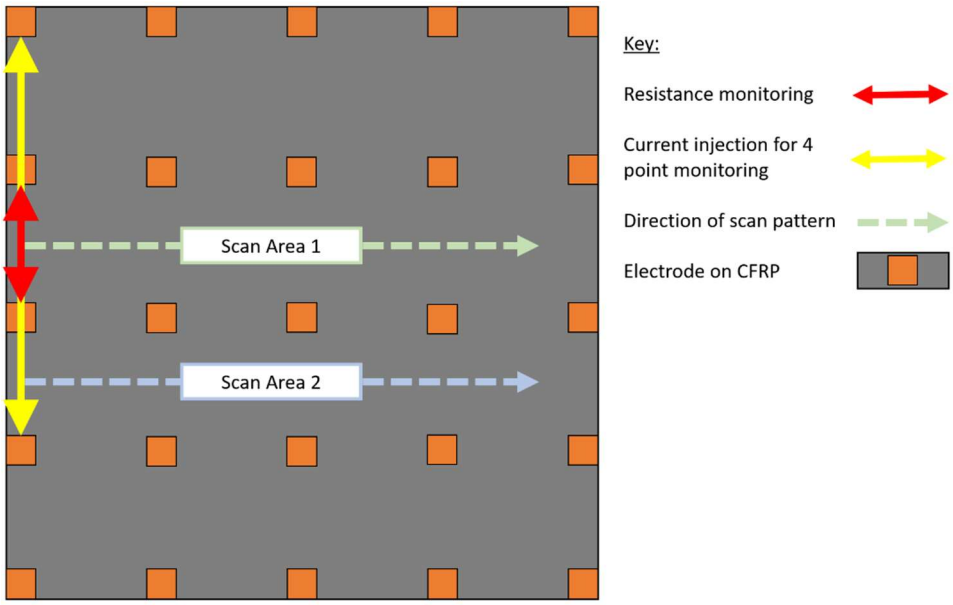

Figure 6: Diagram showing the "4-Point zone" resistance monitoring scan pattern. Voltage is monitored between the electrodes indicated by the red arrows from which resistance is calculated using the known current applied across the yellow arrows, then monitors electrodes along scan area 1 and scan area 2. This is then repeated at 90 ° to cover a larger area.

2-Point zone scan

This method uses the 2-point measurement method to measure between pairs of electrodes on an equally spaced grid of electrodes on a panel. Unit cells are made up of 4 electrodes in a square, where conductivity between every pair of electrodes is tested, including the 45 ° between the opposite corners, 6 measurements in total in each square, seen in Figure 7. Results for the average of the unit cell are then compared before and after. Once all unit cells are measured, a map of the resistance change can be generated to locate impact damage.

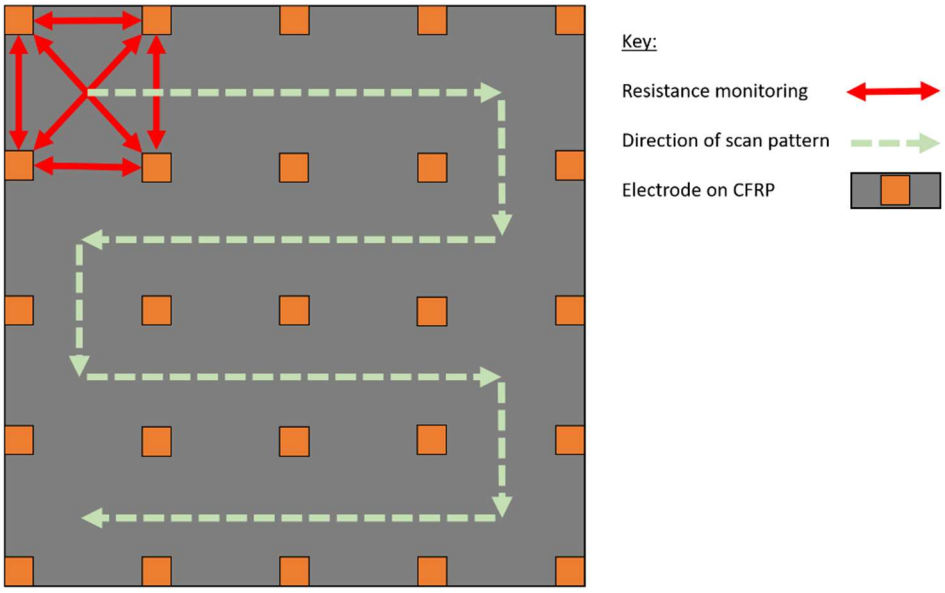

Figure 7: Diagram showing the "2-Point area" resistance monitoring scan pattern. Resistance is monitored between the electrodes indicated by the red arrows. This is then repeated for each unit cell in the direction of the scan pattern to acquire data for the full area of the panel.

8.6. Panel PCB results

This section considers the results of the electrical testing of the panel PCB samples, before and after the impact testing. The effectiveness of each technique can be evaluated by looking at the repeatability of the resistance values before impact. Contact resistance can be estimated by comparing results from 2-point and 4-point for the same area. Post impact data is reviewed from a statistical viewpoint (average and standard deviation) and then locally to see if impact damage can be detected, located and its energy can be determined.

Analysis before impact

Analysis of the resistance before impact was undertaken to evaluate the contact resistance, reliability of the damage detection and differences in resistance monitoring methods used. First, the averages and standard deviations were calculated which can be seen in Table 2. For the 2-point zone values, 45 ° measurements are taken out to avoid artificially increasing the standard deviations (SD) due to the longer distance measured.

Table 2: Statistical analysis of baseline resistance values for the X-Y, 4-point zone and 2-point zone results before damage has occurred for the Panel PCB samples.

Panel	Average XY, Ω	SD %	Average 4PZ, Ω	SD %	Average 2PZ, Ω	SD %
Pre-preg PCB MID	3.715	15.92	0.033	33.500	3.454	9.936
Pre-preg PCB Bot	3.503	11.86	0.015	33.381	3.330	11.116
VARTM PCB Bot	10.107	26.12	0.053	29.776	9.526	22.257

The values that have been recorded with the 2 point method exhibit significantly higher resistances, compared to the ones with the 4 point method, being from 100-200 times larger. The pre-preg samples have a lower average resistance, compared to a VARTM cured sample. For the 4-point measurement where contact resistance is removed, the resistance is still higher for VARTM manufactured panels, however the standard deviation is similar for all sample types.

Standard deviation of all the sample sets are all above 10 %, with the 4 point zone samples reaching 30%. This suggests that there is significant variation between measurements that should be all the same, as they are measuring the same material of the same length. This variation doesn't necessarily mean that the resistance changes will be lost in the noise of the variation, it means that the assumption of using PCBs to improve consistency of results hasn't been as successful as expected, or there is significantly more systemic variation in the monitoring of CFRP. The standard deviations for the VARTM panel using 2-point measurement are significantly higher than pre-preg, suggesting the implementation of the contacts is less consistent.

There is a large difference between the 4-point averages from the two pre-preg manufactured panels, with the PCB on the bottom ply having less than half the resistance. This could be accounted for by the increased volume of conductive carbon the bottom ply PCB can transfer current through. This may explain why Swait and Alsaadi [20,22] had increased response by applying the PCBs on the bottom face of the composite.

Contact resistance can be estimated by subtracting the 4-point measurements from the 2-point measurements, of which an average can be seen in Table 3.

Table 3: Estimates of contact resistance for the Panel PCB samples.

Panel	Contact resistance, Ω	Percentage of total, %
Pre-preg PCB MID	3.367	90.62
Pre-preg PCB Bot	3.155	90.06
VARTM PCB Bot	9.759	96.55

These results suggest that contact resistance accounts for a large percentage of the recorded resistance response. This means that there is a 90% systematic error of true resistance for the 2-point measurement, which reduces the sensitivity of this method significantly. The estimated contact resistance for the VARTM samples are higher than the pre-preg samples, this could be due to the reduced control over the resin introduced ply to ply with VARTM, compared to pre-preg where the resin volume is tightly controlled.

As later results will show, the lower the contact resistance, and percentage this is of 2-point readings, the better the results for the sample will be. This is clear from the 2-point results, where the pre-preg samples with a lower contact resistance percentage perform better than the VARTM sample.

Post-Impact analysis of Panel PCB samples

XY Scan Analysis

The response to damage for the XY scan samples was very poor, with very few samples providing a response that was linked to the location of the induced damage. It was only in the VARTM BVID results where location was indicated in the X direction, which can be seen in Figure 8. In this case, there was a decrease in resistance around the damaged area after BVID, whereas for puncture damage, this pattern was then reversed. In most cases, there was a slight increase in resistance in all measurements, however with no indication of location.

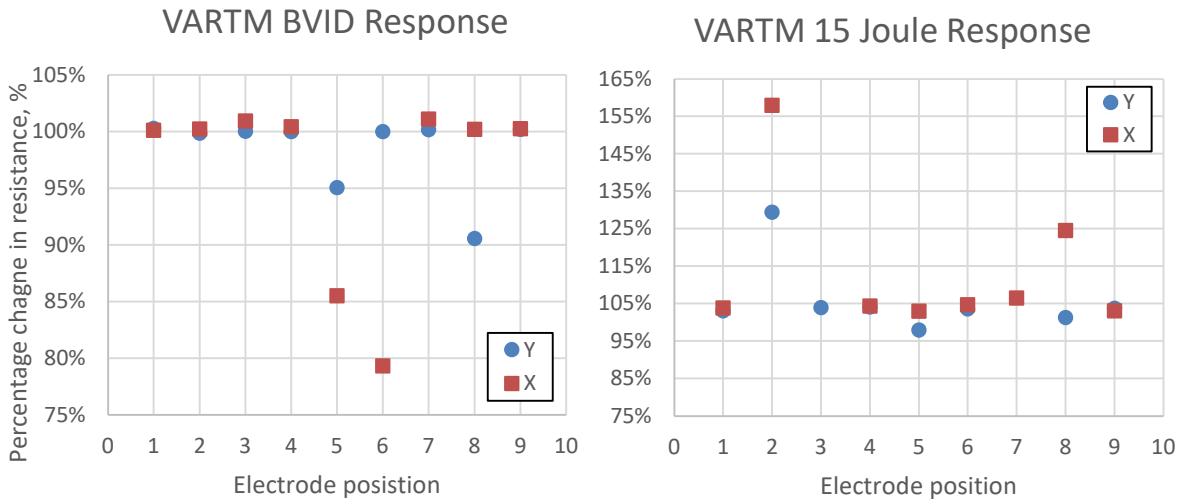

Figure 8: VARTM XY results in the Y direction after BVID (left) and puncture (right), with the damage occurring in the centre of the panel.

As the VARTM values showed the highest contact resistance of all samples, it is unusual that these samples provide the only interpretable data. Because of this, it could be considered that the impacts are inducing strain around the electrode and changing the contact resistance. The increase in distance between electrodes is expected to negatively impact the effectiveness and sensitivity of this method

compared to previous studies. Previous studies also suggest the use of PW would limit the sensitivity compared to UD, as it gives other pathways for current to travel once resistance increases locally. A summary of the percentage changes and range of resistances between BVID and puncture can be seen in Figure 9.

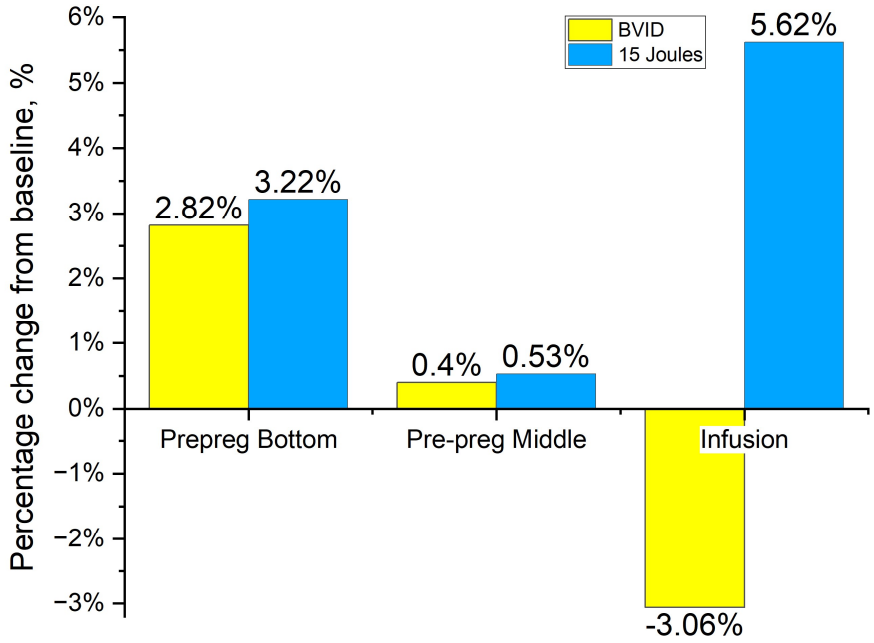

Figure 9: Bar chart showing percentage resistance changes in response to damage for the XY scan method.

Whilst it isn't possible to locate the damage consistently, for the pre-preg samples there is an resistance increase between the two impacts. This indicates that the 2-point method has the potential to be used to evaluate the severity of damage.

2-point zone analysis

To analyse the resistance data collected with electrodes in the centre of the PCB, a heat map visualisation was produced in LabVIEW to indicate where resistance increases on the panel occurred, as seen in Table 4. The scale is from black where there is no change, to white is the largest change, relative to the resistance range during that test.

Table 4: Intensity charts showing the resistance response using the 2-point zone method. Note that the impact was in the centre of these samples, indicated by the cross.

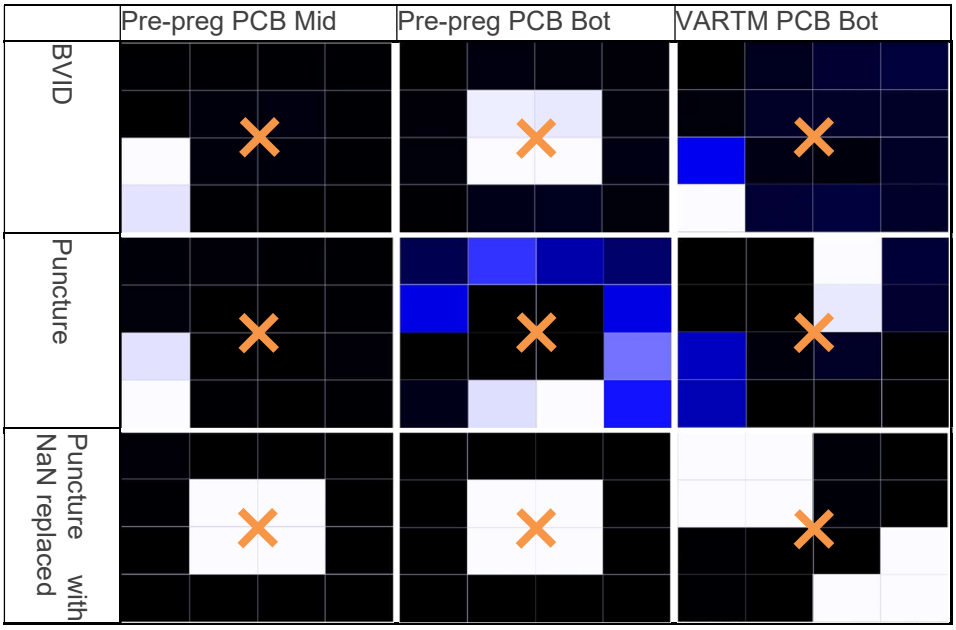

In a few of the puncture cases, electrodes were damaged leading to "Not A Number" (NaN) readings from the LabVIEW software. This would indicate that the electrode had debonded from the composite and a reading couldn't be made. As these were due to extreme damage, the values were replaced with a resistance at the level of the maximum resistance recorded in the panel's dataset. This would represent a relative response to the damage, which scaled to the response seen in the panel. These were compared to the baseline values, of which the percentage difference can be seen in Figure 10.

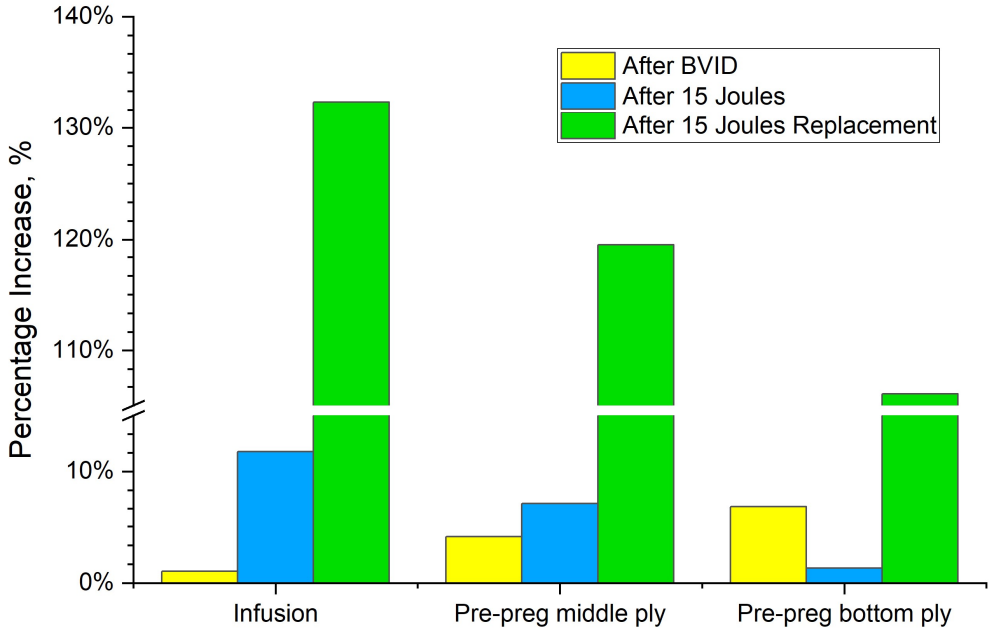

Figure 10: Bar chart showing the percentage increase in resistance between impact energies to the baseline readings for the 3 panel PCB samples, using the 2-point method.

The strongest response to BVID is seen in the pre-preg samples, with the PCB positioned on the bottom ply resulting in the strongest response and locating the damage accurately (Middle top of Table 4). The VARTM sample had the strongest response to higher impact energies, maybe suggesting the change in manufacturing method ensured the electrodes were less likely to dis-bond compared to the pre-preg samples.

4-point zone analysis

A heatmap of the data was produced in LabVIEW, where linear interpolation was used due to the uneven spacing of the data points. Table 5 shows the resulting heatmaps, where noise dominates the results for all the BVID results. An anomaly was that in some of the punctured samples, the DMM was producing negative resistance values, which was likely due to the damage of some of the electrodes. These negative results were replaced with zeros to produce the heatmaps in the 3rd row of results in Table 5. For the pre-preg results, this made the damage location clearer on the heatmap.

Table 5: Interpolated intensity charts of the resistance response using the 4-point zone method. Note that the impact was in the centre of these samples, indicated by the cross.

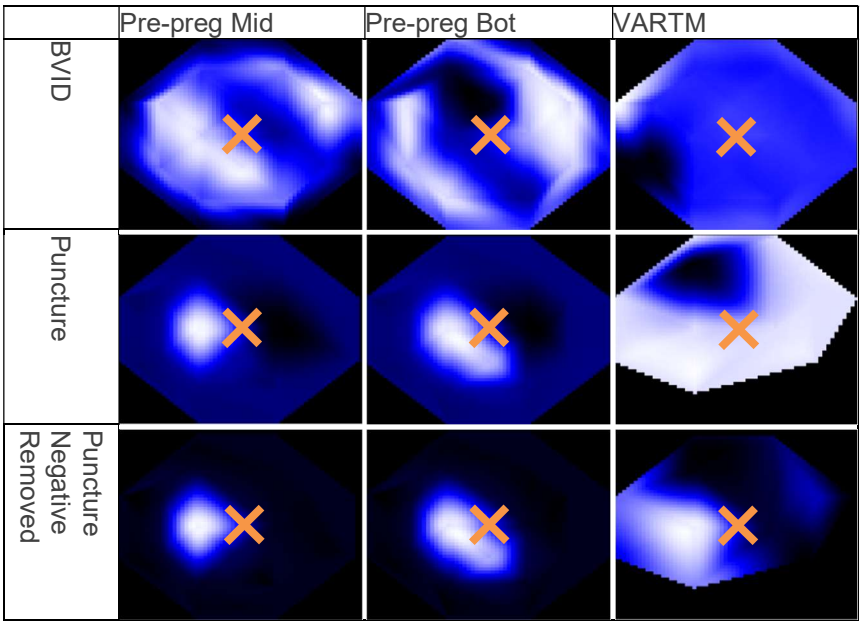

There was a stronger response for the punctured samples, where damage was located with reasonable accuracy for the pre-preg materials. The VARTM manufactured samples provided no indication as to the location of the induced damage. There was little percentage increase in average values between BVID and puncture damage for the pre-preg samples, however more NaN's were produced. The VARTM which showed an increase of 3.25 % for BVID and 54.44 % increase for puncture damage.

8.7. Panel PCB conclusion

From the initial statistical analysis, there was evidence that the PCB on the bottom pre-preg ply had the highest potential to record the true resistance values of the carbon fibres. It had the lowest resistance values recorded in both 2-point and 4-point as well as having the lowest calculated contact resistance. It had the highest sensitivity in the 2-point tests for BVID, accurately locating and indicating the severity of the damage. The X-Y scan mode wasn't successful in indicating damage in woven laminates, and as the scale of the methodology is increased, it is likely to be less effective, therefore

the method won't be used on the larger samples in the remaining samples tested. The 4-point zone was ineffective at detecting BVID, however was able to detect larger impact energies so will be included going forward. VARTM manufactured samples were poor at damage detection in all cases, however, will be included in the modular PCB testing, given the trend towards the manufacture of large aerospace structures in this manner [29].

The calculations of the contact resistance were a good indicator of which samples would have sensing systems that were sensitive to damage. With the modular PCB, there is an opportunity to reduce contact resistance between the electrode and the sample through the use of conductive adhesive. There is also an opportunity to change the design, in order to make it more sensitive to damage. A brief study was completed on the effectiveness of damage detection using different sized silver adhesive based electrodes. Multiple samples with electrodes of 25 mm^2, 100 mm^2 and 225 mm^2 were prepared onto 8 plies of pre-preg CFRP, with all electrodes 100 mm apart. They were impacted with BVID and puncture damage as per the previous panel PCB samples, and it was found that the smaller electrode size provided significantly stronger response to impact damage, despite having higher overall resistance. This is the reasoning for the reduction in electrode size from the panel PCB samples to the modular PCB samples, from 225 mm^2 to 25 mm^2.

8.8. Modular PCB results

The modular PCBs were used with both VARTM and pre-preg manufactured samples, of which an example can be seen in Figure 2. After the analysis showing that contact resistance for 2 point measurements was still high comparatively to the composite measurement, a method was introduced where the PCBs were bonded to the composite surface using silver adhesive to seek a reduction in contact resistance. For the silver adhesive, the surface was prepared using abrasive tools to expose the carbon fibres to the surface, to which the adhesive was applied and was oven cured at 65 °C for 2 hours. In some cases, embedded and silver bonded PCBs were used on the same sample to allow for comparison with fewer variables, as seen in Table 1. Whilst the samples were large in scale (2000 x 700 mm) the sensing area was smaller, resulting in an area of 560 x 400 mm being sensed. Due to the increase in the size of the components, it was no longer possible to impact the components using an impact tower. The samples were manually impacted with a ball bearing of same diameter of the impactor head, impacted from set heights. Therefore, it wasn't possible to test BVID, dent or puncture in all cases, due to the inaccuracies introduced with this new method.

Statistical analysis before impact

The average resistance values and standard deviation were calculated for the 2-point zone and 4-point zone method, which can be seen in Table 6.

Table 6: Average resistance values and standard deviations of the 2PZ and 4PZ.

Panel	Average 2PZ, Ω	SD %	Average 4PZ, Ω	SD %
VARTM modular	0.0104	123.7	0.85455	376.2
VARTM with silver modular	0.0128	32.0	0.00018	266.1
Pre-preg modular	0.0053	12.2	0.00001	50.5
Pre-preg silver modular	0.0061	19.7	0.15715	616.0

Resistance values for both methods are lower than the panel PCB manufactured values. There is a significant increase in SD for almost all cases. The variability could be due to the placement of the PCBs being completed by hand, rather than the PCB providing the positioning. The geometry is more complex, which could introduce opportunities for variation in the layup also. As per the panel PCB samples, this standard deviation is representative of the variation between samples, and not necessarily representative of the reliability of the measurement method. Contact resistance was also estimated, Table 7, which is significantly lower than the Panel PCB samples.

Table 7: Contact resistance estimations for the modular PCB samples.

Panel	Contact resistance, Ω	Percentage of total, %
VARTM modular	0.0078	73.66%
VARTM with silver modular	0.0126	98.58%
Pre-preg modular	0.0050	99.71%
Pre-preg silver modular	0.0061	78.64%

These results are very mixed, however following the panel PCB results, the higher percentage of the total is the contact resistance, the poorer they will perform. It is expected that the VARTM and pre-preg with silver will be most sensitive to damage, however this may be skewed as the 4-point resistances are significantly higher than the previous examples. This may be due to variations in contact resistance leading to higher recorded values.

The silver modified samples all have higher estimated contact resistance compared to the unmodified samples. This may be due to the variations introduced with modifying the surface to obtain contact with the fibres, opposed to being consistent as part of the curing process. This may lead to more inconsistent results from the silver modified samples.

Post impact results VARTM modular

The 4-point zone values resulted with very little location information, however there were indications of damage levels, similar to the panel PCB results, which can be seen in Figure 11.

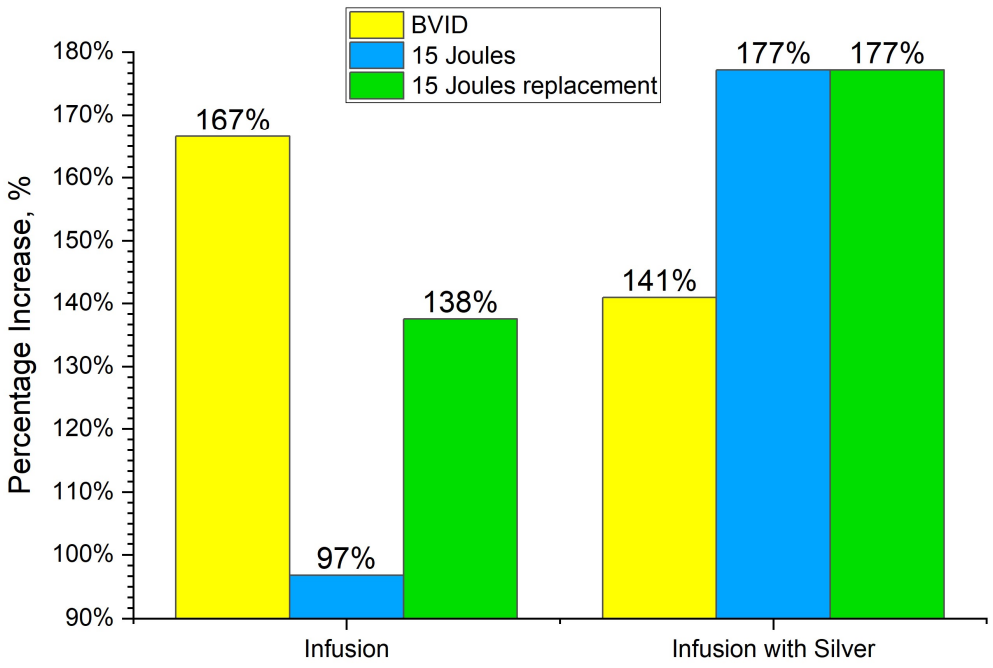

Figure 11: Average percentage increases over the baseline of electrical resistance of the VARTM results

There was a strong indication for BVID in the VARTM only sample, with an increase to 167 % of the baseline, however this was reduced to 97 % after a 15 J impact, and 138 % after the NaN values had been replaced. This inconsistency between significant impact energies suggests that this method is unreliable. The silver modified samples showed a strong progression of resistance increase with increased impact energy.

The heatmaps in Table 8 show the predicted damage position for the 2-point zone VARTM modular PCB samples. The damage was induced in the left of the centre, indicated by the orange cross.

Table 8: VARTM self-sensing heatmaps of BVID 15 Joule and 30 Joule energy impacts using 2-point resistance monitoring. Note that the impact was in the left side of these samples, indicated by the cross.

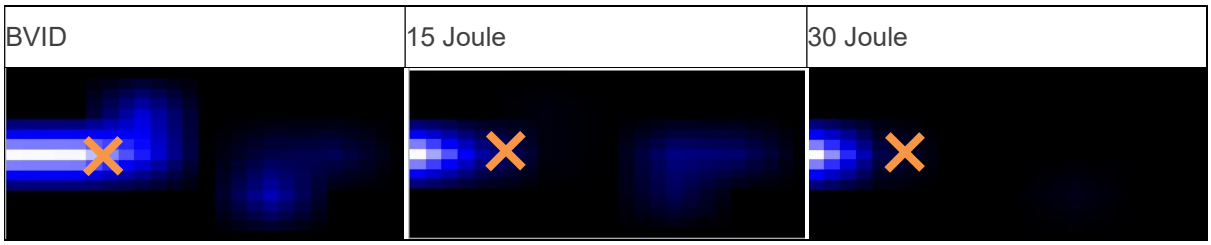

In the BVID heatmap, the area is spread over a larger area and has a low maximum change in resistance, 0.00012 Ω. As the damage increases for the 15 Joule impact, the zone size decreases as the resistance difference increases to 0.00028 Ω. For the 30 Joule impact, the resistance change does not increase, however the area becomes more concentrated. The average values before and after impact can be seen in Figure 12.

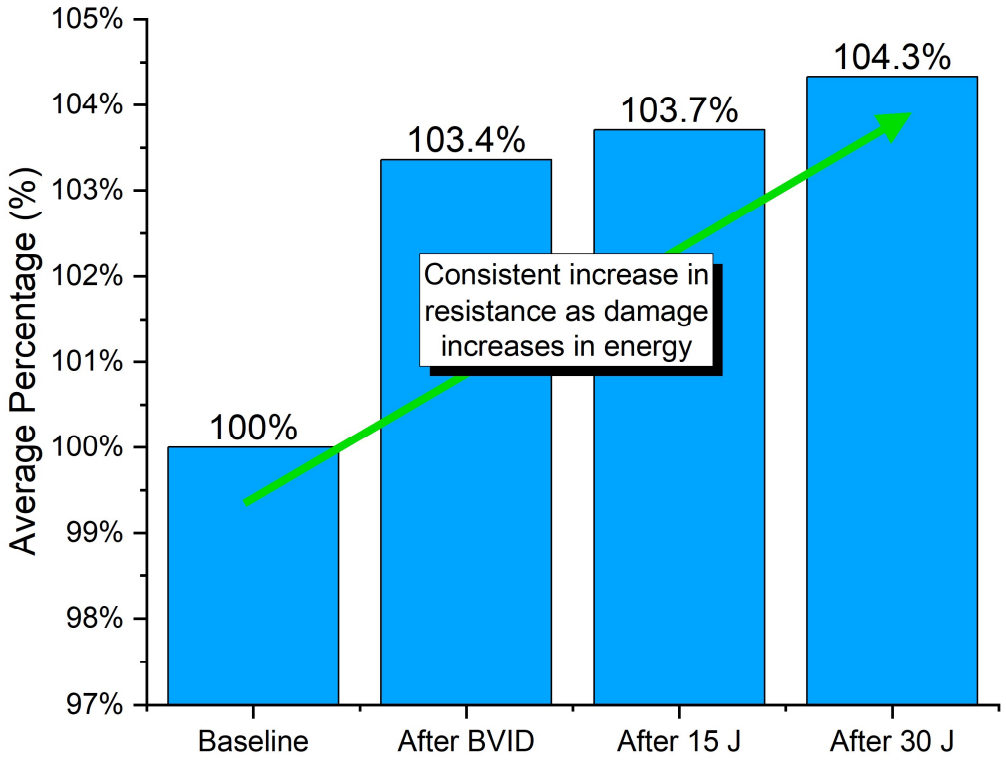

Figure 12: Table of average resistance values and standard deviations from different scans of damage.

One of the main results seen in the averages is that it increases as the level of damage increases, most significantly after BVID, however slightly more as the level of damage increases. This is a strong indicator that this method can be used to indicate that damage has occurred.

Post impact results pre-preg modular

Modular PCB testing was completed on pre-preg with the embedded and silver electrodes. The average values for BVID and higher impact energies for both 2-point and 4-point do not provide clear patterns in order to detect impact damage. Figure 13 shows the increases between the baseline and BVID and 15 Joule impacts, highlighting the changes when NaN values are replaced.

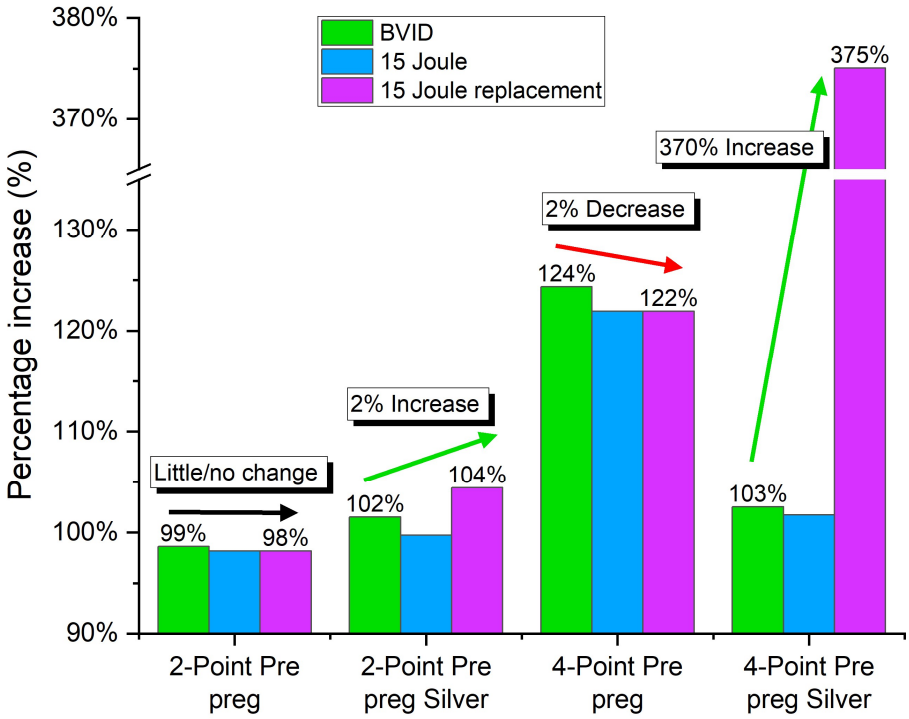

Figure 13: Average percentage increases for all pre-preg samples, for 2-point and 4-point testing.

As expected from the contact resistance estimates, the silver pre-preg samples are showing larger increases in resistance, whereas the pre-preg only samples have more variable responses. The consistent positive response to damage from the silver modified samples suggests that it is having a positive impact on the detecting capability of the system.

Heatmaps for both 4-point zone and 2-point zone can be seen in Table 9 and Table 10, and provide clearer information on the damage location.

Table 9: Pre-preg silver conductive resin bonded self-sensing heatmap results. Damage position is indicated by the cross.

Damage location: Far right section	
Silver BVID 2-point zone	Silver BVID 4-point zone
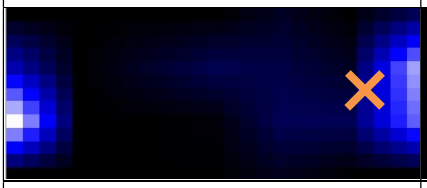	
Silver Puncture 2-point zone	Silver Puncture 4-point zone
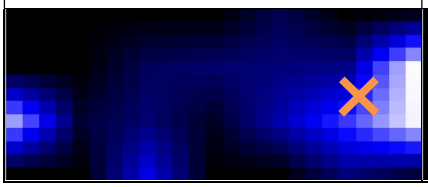	

The silver bonded results in Table 9 provide a very strong response for BVID and puncture for 4-point zone, indicating damage in the correct area of the panel. These results line up with the responses

summarised in Figure 13. The 2-point zone silver bonded heatmaps in Table 10 indicated damage in the correct zone, however they were less accurate and spread out.

Table 10: Pre-preg embedded electrode self-sensing heatmap results. Damage position is indicated by the cross.

Damage location: Centre left	
Embedded BVID 2-point zone	Embedded BVID 4-point zone
	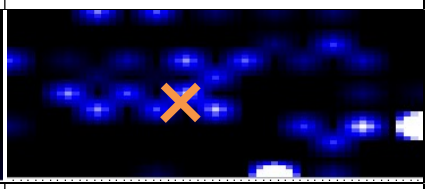
Embedded Puncture 2-point zone	Embedded Puncture 4-point zone
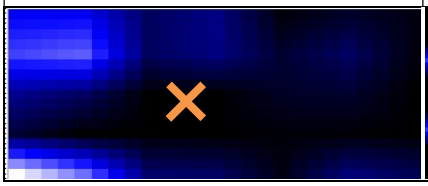	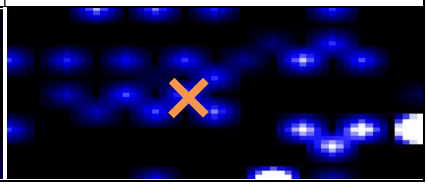

The embedded electrode heatmaps provide inaccurate damage indication and seemingly random responses. The 2-point zone embedded electrodes have a response from the left side, however the heatmap is inconclusive.

8.9. Conclusion

This study has shown the possibility of scaling up a self-sensing system based on the monitoring of the electrical resistance of carbon fibres in CFRP components. It was scaled up to large scale (560 x 400 mm) components where it was possible to detect BVID and puncture damage with certain detection modes and material setups. The method allowed for simple integration of the electrodes during manufacture, ensuring there was minimal impact to the properties of the component, and a robust electrical connection to the testing system. Throughout the study, there were issues with the effectiveness of the method, which was linked to the contact resistance between the electrodes and the CFRP. It was clear that where contact resistance was low, both 4-point and 2-point methods were more sensitive and provided accurate location of the damage and indications of its severity. Efforts were made to decrease the contact resistance of the samples through the use of silver adhesive to the composite as seen in previous studies, however as per earlier samples, the contact resistance had significant variance between samples. Despite these difficulties with the electrode contact resistance, in the majority of cases there was an increase in resistance in almost all samples, and in the majority of cases this was after BVID damage, which is most important to detect for in-service applications. Improvements to allow for more accurate and consistent detection have been made, with varying levels of success. The process is now better understood, has shown its potential value in some use cases and has provided a pathway for future development in this area.

8.10. Future recommendations

For electrical self-sensing to more reliably detect BVID, the following recommendations have been made:

- Understanding of the electrode-carbon interface: An investigation on the performance of different electrode types, including micrographs of the electrode-carbon interface to provide insight into the surface area in contact, as well the differences between pre-preg, VARTM and bonded electrodes.
- Material format changes: Previous studies indicated that UD provided improved change in resistance in response to damage. Potentially the whole component doesn't need to be made of UD to enable this method. A PCB-UD prepreg plies could be used within any layup to provide structural rigidity and damage detection. Similarly, this could be applied to non-crimp fabrics, which contain bidirectional UD fibres.
- Application in other manufacturing methods: Electrical self-sensing could be applied to methods such as filament winding (FW), where there are long tows of UD used to layup parts. A hoop wound section of a FW part could be split into sections, and be used to monitor piezoresistive strain, or responses to impact damage.
- Reduced contact resistance: Currently the PCB method doesn't provide low contact resistance with the fibres. Further research on electrode types, surface preparation and adhesive types should be completed. With VARTM systems it may be an option to bond the electrode directly to the dry fibres themselves.
- Evaluation methods: Currently the review of the performance is very subjective, which is to be expected for this type of development at this early stage, however a more systematic evaluation system needs to be determined, to evaluate changes with the system.
- Custom build of 4-point resistance measuring equipment with a tuneable excitation current. This could increase the sensitivity with less noise when measuring very low resistances, under 1 Ω, of which are the majority of resistance measurements seen in this study.

8.11. References

[1] Irving P, Soutis C. Polymer Composites in the Aerospace Industry. Second Edition. Woodhead Publishing; 2020.

[2] Diamanti K, Soutis C. Structural health monitoring techniques for aircraft composite structures. Progress in Aerospace Sciences 2010;46:342–52. https://doi.org/10.1016/j.paerosci.2010.05.001.

[3] Polimeno U, Meo M. Detecting barely visible impact damage detection on aircraft composites structures. Compos Struct 2009. https://doi.org/10.1016/j.compstruct.2009.04.014.

[4] Mitrovic M. Effect of loading parameters on the fatigue behavior of impact damaged composite laminates. Compos Sci Technol 1999;59:2059–78. https://doi.org/10.1016/S0266-3538(99)00061-5.

[5] Tsigkourakos G, Silberschmidt V V., Ashcroft IA. Damage assessment in CFRP laminates exposed to impact fatigue loading. J Phys Conf Ser 2011;305:12047. https://doi.org/10.1088/1742-6596/305/1/012047.

[6] Kumar P, Rai B. Delaminations of barely visible impact damage in CFRP laminates. Compos Struct 1993;23:313–8. https://doi.org/10.1016/0263-8223(93)90231-E.

[7] Dubinskii S, Fedulov B, Feygenbaum Y, Gvozdev S, Metelkin E. Experimental evaluation of surface damage relaxation effect in carbon-fiber reinforced epoxy panels impacted into stringer. Compos B Eng 2019. https://doi.org/10.1016/j.compositesb.2019.107258.

[8] Duchene P, Chaki S, Ayadi A, Krawczak P. A review of non-destructive techniques used for mechanical damage assessment in polymer composites. J Mater Sci 2018;53:7915–38. https://doi.org/10.1007/s10853-018-2045-6.

[9] De Baere I, Van Paepegem W, Degrieck J. The use of rivets for electrical resistance measurement on carbon fibre-reinforced thermoplastics. Smart Mater Struct 2007;16:1821–8. https://doi.org/10.1088/0964-1726/16/5/037.

[10] Hou L, Hayes SA. A resistance-based damage location sensor for carbon-fibre composites. Smart Mater Struct 2002;11:966. https://doi.org/10.1088/0964-1726/11/6/401.

[11] Abry JC, Bochard S, Chateauminois A, Salvia M, Giraud G. In situ detection of damage in CFRP laminates by electrical resistance measurements. Compos Sci Technol 1999;59:925–35. https://doi.org/10.1016/S0266-3538(98)00132-8.

[12] Wang S, Wang D, Chung DDL, Chung JH. Method of sensing impact damage in carbon fiber polymer-matrix composite by electrical resistance measurement. J Mater Sci 2006;41:2281–9. https://doi.org/10.1007/s10853-006-7172-9.

[13] Mecklenburg M, Mizushima D, Ohtake N, Bauhofer W, Fiedler B, Schulte K. On the manufacturing and electrical and mechanical properties of ultra-high wt.% fraction aligned MWCNT and randomly oriented CNT epoxy composites. Carbon N Y 2015;91:275–90. https://doi.org/10.1016/j.carbon.2015.04.085.

[14] Wang X, Chung DDL. Self-monitoring of fatigue damage and dynamic strain in carbon fiber polymer-matrix composite. Compos B Eng 1998;29:63–73. https://doi.org/10.1016/S1359-8368(97)00014-0.

[15] TODOROKI A, UEDA M, HIRANO Y. Strain and Damage Monitoring of CFRP Laminates by Means of Electrical Resistance Measurement. Journal of Solid Mechanics and Materials Engineering 2007;1:947–74. https://doi.org/10.1299/jmmp.1.947.

[16] Blazewicz S, Patalita B, Touzain Ph. Study of piezoresistance effect in carbon fibers. Carbon N Y 1997;35:1613–8. https://doi.org/10.1016/S0008-6223(97)00120-6.

[17] Chung DDL. A review of multifunctional polymer-matrix structural composites. Compos B Eng 2019;160:644–60. https://doi.org/10.1016/j.compositesb.2018.12.117.

[18] Obitayo W, Liu T. A Review: Carbon Nanotube-Based Piezoresistive Strain Sensors. J Sens 2012;2012:15. https://doi.org/10.1155/2012/652438.

[19] Chung DDL. Damage detection using self-sensing concepts. Proc Inst Mech Eng G J Aerosp Eng 2007;221:509–20. https://doi.org/10.1243/09544100JAERO203.

[20] Swait TJ, Jones FR, Hayes SA. A practical structural health monitoring system for carbon fibre reinforced composite based on electrical resistance. Compos Sci Technol 2012;72:1515–23. https://doi.org/10.1016/j.compscitech.2012.05.022.

[21] Webster JG. Electrical Conductivity and Resistivity. In: Webster JG, editor. Electrical measurement, signal processing, and displays, CRC Press; 2003, p. 1–14. https://doi.org/10.1201/9780203009406.

[22] Alsaadi A, Meredith J, Swait T, Curiel-Sosa JL, Hayes S. Damage detection and location in woven fabric CFRP laminate panels. Compos Struct 2019;220:168–78. https://doi.org/10.1016/j.compstruct.2019.03.087.

[23] Alsaadi A, Meredith J, Swait T, Curiel-Sosa JL, Jia Y, Hayes S. Structural health monitoring for woven fabric CFRP laminates. Compos B Eng 2019;174:107048. https://doi.org/10.1016/j.compositesb.2019.107048.

[24] Nonn S, Schagerl M, Zhao Y, Gschossmann S, Kralovec C. Application of electrical impedance tomography to an anisotropic carbon fiber-reinforced polymer composite laminate for damage localization. Compos Sci Technol 2018;160:231–6. https://doi.org/10.1016/j.compscitech.2018.03.031.

[25] Schueler R, Joshi SP, Schulte K. Damage detection in CFRP by electrical conductivity mapping. Compos Sci Technol 2001;61:921–30. https://doi.org/10.1016/S0266-3538(00)00178-0.

[26] Baltopoulos A, Polydorides N, Pambaguian L, Vavouliotis A, Kostopoulos V. Exploiting carbon nanotube networks for damage assessment of fiber reinforced composites. Compos B Eng 2015;76:149–58. https://doi.org/10.1016/j.compositesb.2015.02.022.

[27] Baltopoulos A, Polydorides N, Pambaguian L, Vavouliotis A, Kostopoulos V. Damage identification in carbon fiber reinforced polymer plates using electrical resistance tomography mapping. J Compos Mater 2012;47:3285–301. https://doi.org/10.1177/0021998312464079.

[28] Walker L, Sohn MS, Hu XZ. Improving impact resistance of carbon-fibre composites through interlaminar reinforcement. Compos Part A Appl Sci Manuf 2002;33:893–902. https://doi.org/10.1016/S1359-835X(02)00010-6.

[29] One-piece, one-shot, 17-meter wing spar for high-rate aircraft manufacture | CompositesWorld n.d. https://www.compositesworld.com/articles/one-piece-one-shot-17-meter-wing-spar-for-high-rate-aircraft-manufacture (accessed July 20, 2023).

9. Conclusions and Recommendations for Further Work

This thesis has investigated novel multifunctional composites, in particular DEC and self-sensing, and their applicability to, and benefits for, aerospace applications. It has sought to bridge the gap between lab-based concepts and practical application for manufacturing, by studying use cases with real world potential. It recognises the challenges of applying and adapting wholly new functionalities to materials already in use, to enable self-sensing, direct electrical cure, and self-de-icing.

The experimental work started with investigating the issue of low conductivity in epoxy resins, and the possibility of improving conductivity further increase the performance of multifunctional composites. Industrial scale mixing methods were tested for their ability to disperse CNT's and graphite into epoxy effectively. Whilst the main objective was achieved, which was to increase the conductivity of the resin, there were other issues that weren't possible to overcome for manufacturing larger components. The quick agglomeration of the resulting CNT-epoxy resins led to unsustainable processing times between mixing and infusion. It also wasn't possible to manufacture a composite with an even distribution of particles over the panel. It wasn't possible to engineer a way around this without significant waste, therefore these nano-composite weren't used as bulk materials within the multifunctional composites being developed. There were opportunities for them to be used as conductive adhesives within the de-icing and self-sensing applications, however their addition had a negligible or in some cases a negative impact on performance. This was particularly the case for de-icing, where the uneven conductivity caused overheating and burning in some cases.

Chapter 6 covered the development of Direct Electric Cure, an alternative low-power curing method, which uses the Joule effect to directly heat up the carbon fibre composite. This was scaled up from 200 x 300 mm panels up to 2000 x 700 mm panels (leading edge) using up to 16 plies during a single cure for pre-preg and 8 plies with VARTM. DoC for VARTM matched oven curing well, whilst pre-preg had issues with temperature uniformity and reaching the cure temperature. Similar results were achieved with the void content, VARTM components cured with DEC had slightly lower void content, whereas the pre-preg components could not match oven cured ones. Therefore with VARTM it matched the curing performance of existing cure methods, in this case oven cure. It is likely with more work, this can also be achieved with pre-preg components. For energy usage, in all cases it outperformed oven curing, consistently 95-99 % less energy used over a cure.

There are still some issues remaining for DEC, such as higher heating rates not being achieved, and excessive local heating in some scenarios. One significant issue, particularly for deployment in industry was the ease of manufacture compared to oven curing. The additional requirement of specific electrodes, and the knowledge on where to put them adds additional cost and time to the manufacture of components, which are unlikely to be offset by energy savings.

This disadvantage of the DEC method was only affected by its specific use case. When applied on a leading edge for the purposes of anti-icing or within a composite tool to enable heated tooling, the electrodes get used multiple times, not only once during manufacture.

When adapting the DEC heating for de-icing, it was set up to only heat 1 ply of unidirectional carbon, laid up near the surface of the demonstrators, which minimised weight impact and layup complexity. It was tested in an environmental chamber at -10 °C, with a build-up of rime ice, that was deemed representative for TRL5. When powered, it provided a very even heating distribution, and provided enough power density to remove the build-up of ice. The more uniform heating response supports the theory and evidence that UD plies would also provide benefits for heated tooling, and self-sensing purposes. Whilst it is difficult to directly compare performance against existing aerospace de-icing solutions, it was possible to compare the power density output of the system, which exceeded performance of existing systems. This was despite having to be run in a low power mode, due to extreme localised heating due to CNT epoxy used at the electrode-CFRP interfaces. The results here show that it has potential as an alternative de-icing method, however it is likely that a weight-cost analysis would need to be completed to see if it is commercially viable for it to be developed further. Due to its low complexity, it appears likely that it would adapt well to further industrialisation.

The DEC and de-icing developments also enabled opportunities for the Joule heating of composites in other areas, such as heated tooling. A single UD ply was laid up into the mid ply of a 1-8-1 tooling layup and heated in order to raise the tool surface up to cure temperature. This was implemented on a small flat panel and subsequently on a more complex aerospace style tool. Cured components on the flat panel tool matched the degree of cure of oven cured samples on equivalent tooling. One of the main concerns and limiting factors of DEC was the time needed to connect the electrodes into the plies, and the requirement to trim and dispose of them after the manufacture. Embedding them removes this concern and reduces investment required to implement this technology. Enhancing the heating uniformity performance means that future efforts can be made in increasing scale and further refining the usability of these tools, which is currently being explored in the EcoTool grant funded project.

To further enhance the performance and efficiency of novel curing methods, the effectiveness of the cure cycles was investigated. Cure kinetics of epoxy resins are well understood, however there have been few instances where they have been modelled and tested to reduce time and cure energy. In Chapter 7.3 a prototype curing algorithm was tested on high heating rate heater mats with tooling pre-preg, resulting in up to an 87 % cycle time reduction and 95 % reduction in energy usage.

To achieve this DSC data was taken from the resin system being cured to calculate the exothermic energy generated depending on the inputted cure cycle. Coupled with the heat loss from the tooling, it enabled the generation of cure cycles with high heating rates that could run near the run-away exothermic limit. It was designed to be adaptable and be easily applied to various heating methods, including novel methods such as DEC and microwave curing. Its future challenges will include improving accuracy through the addition of closed loop feedback, as well as proving that laminates match other thermal properties, such as Tg and viscosity. If more confidence was built in the models outputs, then manufacturers could apply this to existing cure methods and still obtain time and energy savings.

In Chapter 8, an experimental damage detection system was developed and scaled up, based on the electrical resistance monitoring of carbon fibres. Specific equipment and software were setup and developed for the purpose, including data acquisition, bespoke flexible printed circuit boards and custom data visualisation software.

The scaling up of the self-sensing method made improvements to the process, however the system was not able to consistently detect impact damages throughout the testing. It was scaled up to 560 x 400 mm and was possible to detect BVID and other impact damages with certain detection modes and material setups. Flexible PCBs were developed to enable sensing on a larger scale, and with more modularity and scalability than previously capable. Resistance of the panels increased in the majority of the cases after BVID and all cases after larger impact energies. The precise location of the damage was less consistent in its detection, frequently providing noisy images and location data.

Previous studies results were difficult to replicate, therefore completing fundamental testing to understand key parameters would have been beneficial to understanding key parameters. Using alternative materials such as unidirectional carbon was previously demonstrated to increase the performance and repeatability and is suggested to be used in future studies. The use of dry fibre formats such as bi-axial NCF could enable bi-directional sensing on unidirectional plies.

This thesis provided a lot of important learning on the challenges and practical implementation of scaling up multifunctional composite systems from lab scale to component scale. It showed almost all aspects need to be considered, from equipment, tooling, materials and post processing of the data. These considerations ensured that the TRL target objectives were reached in most of the developments. These considerations at scale are what makes this information useful for future researchers, and industrial integrators of these technologies, meaning the research will have a wide impact across sectors.